Characterisation of the major porins OmpU and OmpT of *Vibrio cholerae*

Monisha Pathania

A thesis submitted for the degree of Doctor of Philosophy

December 2017

Institute for Cell and Molecular Biosciences

Faculty of Medical Sciences

Newcastle University

Abstract

The asymmetric outer membrane (OM) of a Gram-negative bacterium has many proteins embedded as β-barrel structures in it called outer membrane proteins (OMPs). The majority of these OMPs (porins) form non-selective channels across the OM to allow passive uptake of substrates. The treatment for infections caused by such bacteria mostly involves the administration of drugs/antibiotics, for which these porins play a very crucial role by providing an efficient (although not yet fully understood) route through their channel. The goal of this study is to study small-molecule permeation through the major porins, OmpU and OmpT, of *Vibrio cholerae* (the causative agent of cholera) for potential use of these proteins as the target for designing antibiotics or vaccines. Towards this project, we have succeeded in solving the 3D X-ray crystal structures of OmpU and OmpT as well as the structures of the major porins from *Klebsiella pneumoniae* (OmpK36) and *Enterobacter cloacae* (OmpE36, OmpE35).

The proteins (OmpU/T, OmpE35/E36 and OmpK36) show the typical arrangement of porins with three β-barrel monomers arranged into a trimer. Each monomer displays 16 antiparallel β-strands forming the hollow β-barrel formed by 8 long extracellular loops and 8 short periplasmic turns. The latching loop L2 stabilises the trimer while loop L3 departs from the β-barrel fold and constricts the pore half-way through the channel. An unusual feature is observed in the channels of OmpU and OmpT that distinguishes them from other typical porins. In OmpU, the first 10 residues of N-terminus insert into the barrel and constrict the pore. In contrast, the structure of OmpT reveals that the extracellular loop L8 folds inwards to constrict the lumen of the channel. Such constriction elements not only reduce the pore sizes of OmpU and OmpT but may also dramatically affect the internal electrostatics of these channels, which is very important for small-molecule permeation. In addition, we also performed single channel electrophysiology experiments with OmpU and OmpT which revealed interesting features with the addition of carbapenems.

Acknowledgements

I would first like to thank my supervisor Bert van den Berg for his excellent advice and continuous support throughout the last three years. The success of this project would not have been possible without Bert's supervision, patience, motivation, and immense knowledge. I could not have imagined having a better advisor and mentor for my Ph.D study.

I would also like to acknowledge all members of the lab, past and present, for their helpful ideas and discussions during the course of my PhD. Their advice and support has been crucial therefore I would like to thank, in no particular order, Anne Doble, Michael Zahn, Javier Abellon-Ruiz, Dave Bulmer and Amy J Glenwright. This project includes several X-ray crystal structures therefore I would like to thank Dr Arnaud Baslé for collecting the datatsets at the DLS.

The study was conducted as a part of 'Translocation' consortium (project number 607694) and is supported by Innovative Medicines Initiatives Joint Undertaking under Grant Agreement 115525, resources that are composed of financial contributions from the European Union's Seventh Framework Programme (FP7/2007–2013) and European Federation of Pharmaceutical Industries and Associations companies in kind contribution. Therefore, a very special gratitude goes out to all down to EU Marie Curie network (ITN) for funding my PhD. Without the financial support of the Foundation this research would not have been possible. I would also like to thank all my fellows from the ITN group for their contribution in exchange of useful comments and ideas, necessary for my research. I would also like to acknowledge the members of Mathias Winterhalter's lab (Jacob's University, Bremen) in particular Satya Prathyusha Bhamidimarri, for the help in performing lipid bilayer experiments and analysing the electrophysiology data.

Finally very big thanks to my husband, family and friends for their love and support over the last four years. Thanks for all your encouragement!

Contents

List of Figures

Chapter 1 Introduction

Chapter 3 Recombinant Expression of OMPs in *E. coli*

Chapter 4. Crystallisation and structure determination of OMPs using X-ray crystallography

Chapter 5. Analysis of antibiotic uptake using in vitro assays

Chapter 6. Final Discussion

Appendix

List of Tables

Chapter 2 Materials and Methods

Chapter 4 Crystallisation and structure determination of OMPs using X-ray crystallography

Chapter 5 Analysis of antibiotic uptake using in vitro assays

Appendix

List of Abbreviations

6X His-tag	Histidine tag of six residues
AA	Amino acid
ATCC	American Type Culture Collection
BCA	Bicinchoninic acid assay
BSA	Bovine serum albumin
C_8E_4	Tetraethylene Glycol Monooctyl Ether
$CHCl_3$	Chloroform
CR	Constriction region
CT	Cholera Toxin
CV	Column volume
DAO	Lauric acid
DDM	n-Dodecyl β-D-maltoside
DLS	Diamond Light Source
DM	n-Decyl-β-D-Maltopyranoside
DPHPC	Dipalmitoylphosphatidylcholine
E. cloacae	*Enterobacter cloacae*
E. coli	*Escherichia coli*
EDTA	Ethylenediaminetetraacetic acid
ESBL	Extended-spectrum β-lactamase
FTT	3-hydroxytetradecanoic acid
GF	Gel filtration
$GlcN_I$	2-amino-2-deoxy-α-D-glucopyranose (reducing)
$GlcN_{II}$	2-amino-2-deoxy-α-D-glucopyranose (non-reducing)
GMH	L-glycero-alpha-D-manno-heptopyranose
HA	Heavy atom
HEPES	4-(2-hydroxyethyl)-1-piperazineethanesulfonic acid
IB	Inclusion body
IEX	Anion-exchange chromatography
IM	Inner Membrane

IMAC	Immobilised Metal Affinity Chromatography
IMI	Innovative Medicines Initiative
IPTG	Isopropyl β-D-1-thiogalactopyranoside
K. pneumoniae	*Klebsiella pneumoniae*
Kdo	3-deoxy-alpha-D-manno-oct-2-ulosonic acid
laciq	gene encoding LacIq (a mutant lac repressor that binds the lac operator more tightly than wild-type LacI)
LB	Lura-Bertani Media
LDAO	Lauryldimethylamine-N-oxide
LLG	Log-likelihood gain
LPS	Lipopolysaccharide
LR	LeMasters-Richards Media
LSA	Liposome swelling assay
MDR	Multidrug resistance
MM	Minimal Media
MQ	MilliQ
MR	Molecular replacement
MW	Molecular Weight
MYR	Myristic acid
NEB	New England Biolabs
OD	Optical Density
OG	n-Octyl-β-D-Glucopyranoside
OM	Outer Membrane
OMPs	Outer Membrane Proteins
PAGE	Polyacrylamide Gel Electrophoresis
PCR	Polymerase Chain Reaction
PDB	Protein Data Bank
PEG	Polyethylene glycol
PG	Prep grade
PL	Phospholipid

RT	Room Temperature
SAD	Single-wavelength Anomalous Diffraction
Sarkosyl	Sodium Lauroyl Sarcosine
SDM	Site Directed Mutagenesis
SDS-PAGE	Sodium Dodecyl Sulfate Polyacrylamide Gel Electrophoresis
SEC	Size Exclusion Chromatography
SeMet	Seleno-methionine
SSC	Single step closures
TAE	Tris-acetate EDTA
TBDT	TonB Dependent Transporter
V. cholerae	*V. cholerae*
WT	Wild-type
YT	Yeast Tryptone

Chapter 1. Introduction

1.1. Gram-negative bacteria

Bacteria are microscopic single-celled prokaryotes. These diverse microorganisms are ubiquitous in soil, freshwater, marine and as well as in extreme environments. The ability of bacteria to survive such harsh environmental conditions is owed in part to the rigid and multilayered structure of the bacterial cell envelope. The primary classification of bacteria into Gram-positive and Gram-negative organisms is based on the nature of this complex cell envelope.

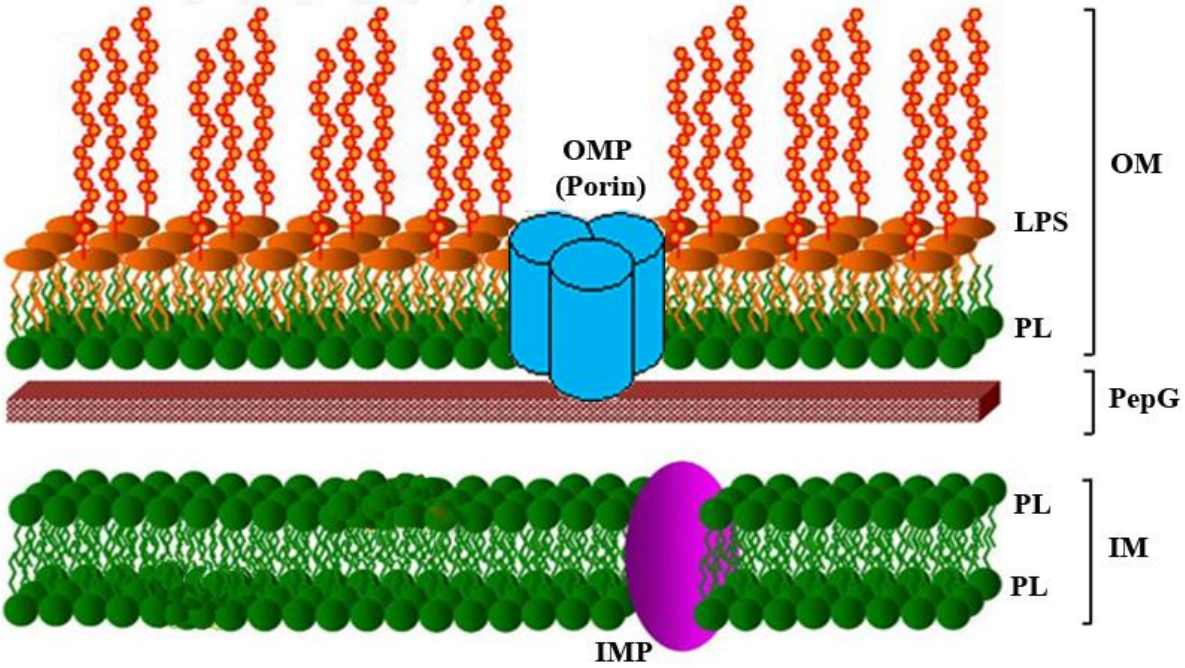

Figure 1.1. Cell wall of Gram-negative bacteria.
The schematic representation of cell wall architecture of Gram-negative bacteria, comprising an inner membrane (IM) of phospholipid (PL) bilayer, a peptidoglycan layer (PepG) in the middle and an asymmetric outer membrane (OM) composed of PL as the inner leaflet and lipopolysaccharide (LPS) in the outer leaflet. OMP; outer membrane protein, IMP; inner membrane protein.

The simplest architecture of the bacterial cell wall is composed of a cell membrane and a peptidoglycan layer. Peptidoglycan (PepG) is composed of a carbohydrate backbone of alternating units of N-acetylglucosamine (GlcNAc) and N-acetylmuramic acid, that are crosslinked by pentapeptide side chains. Gram-negative bacteria possess a significantly thinner peptidoglycan layer than the multilayered thickened peptidoglycan of Gram-positive bacteria.

Gram staining is one of the simple diagnostic tools to differentiate between the two classes of bacteria and is based on the principle of intensive staining of the thickened peptidoglycan layer of Gram-positive bacteria. Gram-negative bacteria, on the other hand, because of thin peptidoglycan layer do not stain as much. However, the thickness of the peptidoglycan layer is not the only factor that differentiates the two primary classes of bacteria. One other major difference between these two is the presence of an outer membrane (OM) in Gram-negative bacteria. The cell wall of Gram-negative cells is thus composed of an inner membrane phospholipid bilayer, a thin PepG layer and an outer membrane, which is absent in the Gram-positive bacteria (Figure 1.1).

1.1.1. *The outer membrane*

The outer membrane is a crucial component of a Gram-negative bacterial cell that helps it to survive the harsh conditions of the environment. The loss of mechanical strength and durability to survive in hostile environments due to the absence of thickened peptidoglycan layer is compensated by presence of the OM in Gram-negative bacteria. The exclusive presence of the OM in Gram-negative bacterial walls allows the exchange of nutrients with the cell environment and disseminates the waste products into the external medium. At the same time, the OM also imparts restricted permeability to toxic compounds and thus serves as a protective barrier. The reason for being such a remarkable and efficient barrier lies in the composition of the OM.

Like other biological membranes, the OM is also a lipid bilayer but is not entirely composed of phospholipids. The phospholipids are confined to the inner leaflet while glycolipids, widely known as lipopolysaccharide (LPS), are present in the outer leaflet of the OM. LPS, also known as endotoxin, is a complex biological entity of Gram-negative bacteria and contributes towards the asymmetric nature of the OM. The complex macromolecular structure of LPS present in the outermost region of Gram-negative cell wall plays a critical role in the barrier function of the OM (also see Section 1.1.2). The outer membrane proteins (OMPs) form channels across the membrane that allow the transport of solutes and hence make the OM selectively permeable. Each OMP spans the OM and its transmembrane segments either form specific or non-specific channels. These transmembrane channels serve as pathways between the interior of the cell and its environment, thereby helping the bacteria to function by allowing exchange of nutrients and waste in and out of the cell (also see section 1.2). Thus, the OM not only separates the external environment from a bacterial cell but also serves as an essential organelle for bacterial survival

by providing solute transport (through OMPs) while at the same time serving as a defence system against toxic compounds (via LPS).

1.1.2. *Lipopolysaccharide structure*

Lipopolysaccharide (LPS) covers 90% surface of a Gram-negative bacterium cell (Rosenfeld and Shai 2006). It has been a subject of intense research for more than three decades that started with the characterisation of LPS (Luderitz et al., 1984, Wu and Health 1973) and identifying its location in the OM (Nikaido 2003, Kamio and Nikaido 1976). To date, several reviews exist that comprehensively describe the structure and biosynthesis of LPS (Raetz and Whitfield 2002, Wilkinson 1996). A typical LPS molecule essentially consists of three components, a hydrophobic **lipid A**, a hydrophilic **core oligosaccharide chain** and hydrophilic **O antigen** repeats forming a long polysaccharide chain (Figure 1.2).

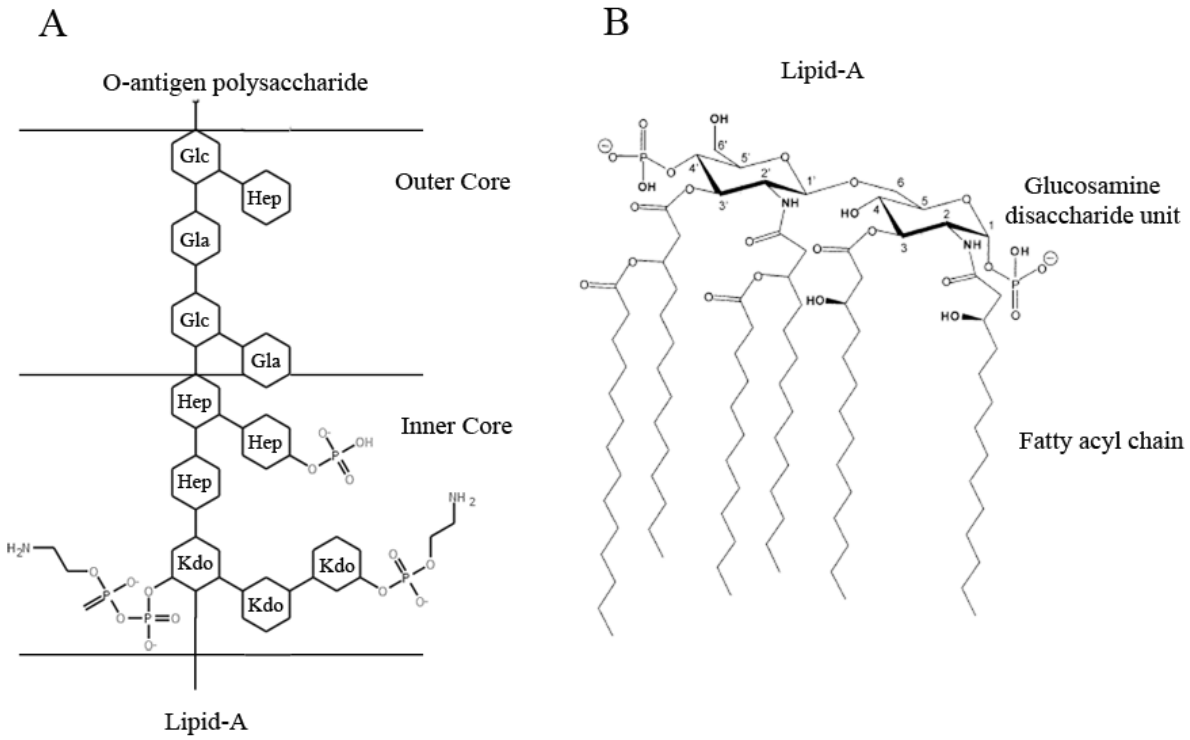

Figure 1.2. Bacterial Lipopolysaccharide (LPS).
(A) The chemical composition of LPS involves a membrane-anchored lipid A moiety, a core oligosaccharide unit (structurally classified into an inner and outer core) and an outermost O-antigen polysaccharide. (B) The lipid A subunit is composed of glucosamine disaccharide sugars acylated by 3-hydroxymyristic acid chains.

Lipid A is the only lipophilic component of LPS which is embedded in the outer leaflet of the OM and is a dimer of phosphorylated N-acetylglucosamine sugars. The disaccharide backbone, composed of β-1',6-linked glucosamine sugar moiety, is attached to four primary 3-hydroxyacyl chains at positions 2, 3, 2' and 3'; and two phosphates at both sugar ends at positions 1 and 4' (Figure 1.2 B). In *Escherichia coli*, two of these fatty acyl chains (on the 1' sugar) are further acylated on their hydroxyl groups by secondary acyl chains (like lauric acid or myristic acid) via forming 'acyloxylacyl' bonds. As a result, *E. coli* LPS is considered to contain mainly hexa-acylated lipid A. Lipid A is the most conserved component of LPS but the acylation pattern of the lipid A moiety of LPS varies among different Gram-negative bacteria. For instance, *Yersinia pestis* has been shown to synthesise tetra-acylated and hexa-acylated lipid-A based on the temperature of the external environment (Montminy et al., 2006). Likewise, tetra- and penta-acylated lipid A has been reported for *Porphyromonas gingivalis,* another Gram-negative pathogen (Herath et al., 2013).

The oligosaccharides of the core region are located on the surface of bacterial cells and are sub-divided into two domains: an inner core and an outer core (Figure 1.2 A). Typically composed of short chains of Kdo (3-deoxy-D-manno-oct-2-ulosonic acid) and Hep (L-glycero-D-manno-heptose) sugars, the inner core oligosaccharide connects to the lipid A disaccharide unit. Kdo is the highly conserved entity of the LPS core region (Wang and Quinn 2010). Structurally more diverse than the inner core, the outer core oligosaccharide mostly contains heptose and hexose (D-glucose and D-galactose) sugars and makes a link with the O-antigenic repeats of LPS.

The outermost and least conserved component of LPS is the O-antigen polysaccharide unit. The repeating oligosaccharide unit of O-antigen is generally composed of two to six sugars (mostly heptoses and hexoses). The length of O-antigen may vary from species to species among Gram-negative bacteria, up to a maximum of 40 repeat units forming smooth-type LPS (S-LPS; Lerouge and Vanderleyden 2002). The rough-type (R-LPS) LPS is devoid of O-antigen chain, for instance *E. coli* K-12 strain is unable to synthesise the O-chain and produces R-LPS (Stevenson et al., 1994).

LPS forms a large macromolecule and the weight of an average LPS monomer is around 10 kDa – 20 kDa (Magalhaes et al., 2007), but depending on the number of O-chain repeating units, the molar mass may vary from 2.5 kDa (lacking O-Ag repeats) to 70 kDa (extremely long

O-Ag repeats). LPS possess a few other crucial features (Nikaido 2003) that contribute in providing defence against the influx of hydrophilic and hydrophobic compounds. These features include; a) rigid lipid interior of LPS layer due to the low fluid texture of its fatty acyl component, b) thermal stabilisation of LPS molecules by mediating strong ionic interactions between the negatively charged phosphates (of LPS) and the divalent cations (Mg^{+2} and Ca^{+2}) in the OM, and c) chemical structure stabilisation mediated through strong lateral interactions between the fatty acid chains within one LPS molecule or among neighbouring LPS molecules.

LPS is also known as endotoxin because it acts as a strong stimulator of innate immunity in eukaryotic species including humans (Beutler and Rietshcel 2003). Lipid A, the most conserved unit of LPS, is responsible for triggering the endotoxin response in human cells (Loppnow et al., 1989 and Alexander and Ritschel 2001).

1.2. Outer membrane proteins (OMPs)

The proteins embedded in the inner membrane as well as outer membrane are collectively referred to as integral membrane proteins. Depending on their location in the membrane (OM or IM), integral membrane proteins are divided into outer membrane proteins (OMPs) and inner membrane proteins. Majority of the OMPs form membrane spanning anti-parallel β-stranded entities that are arranged into cylinder-like closed barrels across the OM. The transmembrane β-strands of the barrel are connected by long loops present in the extracellular space and short turns facing the periplasmic region (Figure 1.3). In contrast to the OMPs, the inner membrane proteins of Gram-negative bacteria are present as transmembrane α-helical bundles in the IM (Dalbey et al., 2011). The transmembrane β-barrel motif is a characteristic architecture adopted by the OMPs, as has been demonstrated by numerous structures available in the protein data bank (PDB) since ≥ 25 years. However, there are few exceptions to the canonical trend seen in the β-barrel structures of OMPs. For example, PorB in *Corynebacterium glutamicum* is an α-helical porin (Ziegler et al., 2008) and Wza, an OMP in *E. coli*, forms an α-helical barrel in the transmembrane region of OM (Dong et al., 2006).

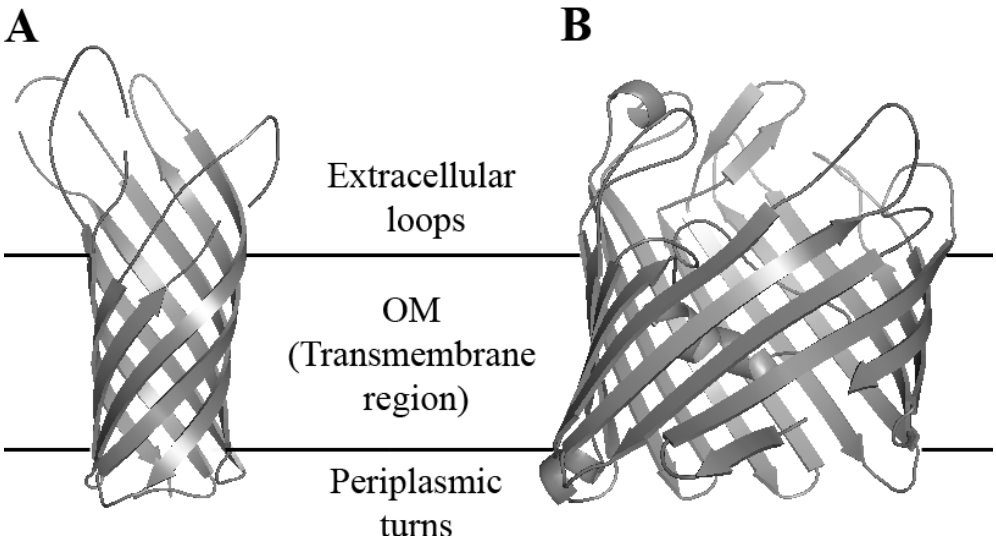

Figure 1.3. General architecture of β-barrel OMPs.
Schematic representation of the protein fold in OMPs showing (A) 8-stranded β-barrel for *E. coli* OmpA and (B) 16-stranded β-barrel for *E. coli* OmpF. The cartoon figures were made using PyMol (Schrodinger 2010) with the PDB codes 1BXW (OmpA; Pautsch and Schulz 1998) and 2OMF (OmpF; Cowan et al., 1992).

1.3. Import channels

The OM of Gram-negative bacteria possess β-barrel channels acting as molecular filters for the influx of compounds. Although OMPs share a common secondary structural β-barrel motif, they vary depending on their functional roles in the membrane and show diversity in the oligomerised states and topology.

1.3.1. *Passive channels: Non-specific Porins*

OMPs forming channels for the passive uptake of substrates are abundantly found in the OM. The outer membrane channels that allow passive uptake of ions or substrates are classified into two types depending on the specificity of the channel. The first category of passive channels are **substrate-specific proteins** that form channels that show specificity for the passage of substrate through the presence of a binding site (also see section 1.3.2). The second class of passive channels are known as **general diffusion porins** that do not discriminate between the substrates and allow the non-specific uptake of water-soluble, small solutes like nutrients and ions.

The general porins are the major outer membrane proteins found in the OM of many Gram-negative bacteria, with ~10^5 copies present per cell (Nikaido and Vaara 1985). The word

porin was proposed to indicate the non-specific nature of these channels (Nikaido 2003) and will continue to denote the same throughout this thesis. These non-specific diffusion channels exist as trimers in the OM and have a molecular weight of around 30-40 kDa per monomer. The porins form a molecular sieve for the access of small hydrophilic solutes with the size exclusion limit of ~600 Da. Although classified as non-specific channels, porins do show some preference for either cations or anions.

1.3.1.1. *Porin regulation*

The major porins of *E. coli*, OmpF and OmpC, have been extensively investigated for their expression and regulation in response to external stimuli. As a result, most of our understanding of porin regulation, expression and function comes from the information available for OmpF/C. Some examples of porin ortholog pairs from different Gram-negative species are OmpE35/OmpE36 (*Enterobacter cloacae*), OmpK35/OmpK36 (*Klebsiella pneumoniae*), Omp35/Omp36 (*Enterobacter aerogenes*), OmpS1/S2 (*Salmonella enetrica*), OmpF/OmpC (*Yersinia pestis*), PorA (*Neisseria meningitidis*), Omp32 (*Comamonas acidovorans*), OmpL/OmpH (*Photobacterium profundum*) and OmpU/OmpT (*Vibrio cholerae*). In a bacterial cell, porin regulation is controlled by various external stimuli including osmolarity, temperature, pH, oxygen starvation or stress. The environmental factors that play influential roles in the expression and regulation of porins are osmolarity, temperature, oxidative stress and pH.

Osmolarity

Bacteria, in general, employ a 'two-component' phosphotransfer signalling system for gene regulation in an adaptive response to external environment. The mechanism of this signalling system is based on the phosphate transfer from histidine (His) to aspartate (Asp) between its two components; a sensor kinase and response regulator (Pratt et al., 1996). Under osmotic pressure, the porin pair of E. coli (OmpF/C) is strictly regulated at the transcription level by the 'two-component phosphorelay system' which includes EnvZ as the 'sensor' and OmpR as the 'response regulator' (Mizuno 1998 and Pratt et al., 1996). In hyperosmotic medium, the osmosensor EnvZ gets autophosphorylated and phosphorylates OmpR. The phosphorylated OmpR binds to the *ompC* promoter region and increases OmpC expression. In contrast, hypo-osmotic media induces binding of OmpR to *ompF* promoter which increases OmpF expression. Thus, the osmoregulation in *E. coli* involves reciprocal expression of its major porins; OmpF during low osmolarity and OmpC during high osmolarity. Like *E. coli*, the reciprocal regulation

of porins in response to the osmolarity levels has also been seen in OmpF/C orthologs of *E. aerogenes* Omp35/36 (Bornet et al., 2004), *K. pneumoniae* OmpK35/K36 (Tsai et al., 2011) and OmpF/C of *Salmonella marcescens* (Begic and Worobec 2006) where the OmpF orthologs show increased expressions in hypo-osmotic environment and vice versa for OmpC orthologs.

1.3.1.2. *Porin structure*

The initial X-ray crystallographic structures of general porins (in 1990s) were determined for a porin from *Rhodobacter capsulatus* (Weiss et al., 1991) and the major porin OmpF from *E. coli* (Cowan et al., 1992). The structure of another major porin from *E. coli*, OmpC, was solved much later (Basle et al., 2006), but its homolog OmpK36 from *K. pneumoniae* (Dutzler et al., 1999) was solved only a few years after OmpF. Since then, there has been quite an increase in the number of porin structures available in the PDB. However, despite their prevalence in the OM, the protein database still lacks structural information on some of the major porins of several other Gram-negative pathogens.

The two major porins of *E. coli*, OmpF and OmpC, are the designated archetypical members of the general porin family of Gram-negative bacteria. As elucidated by the architectural β-barrel fold of OmpF/C, porin structure is characterised by the following typical features:

- **β-barrel**

OmpF and OmpC channel is an 'hour-glass' shaped β-barrel formed by 16 antiparallel strands (Figure 1.4). The β-strands (β1 - β16) vary in their respective lengths, ranging from 5 residues in β6 of OmpF (8 in β7 of OmpC) to 16 residues in β16 of OmpF (and OmpC). The β-strands of the enclosed barrel are connected at their ends in the periplasmic and extracellular spaces. The residues bridging the β-strands at the periplasmic end are referred as 'turns' whereas those that connect at the extracellular end are termed as 'loops'. The 16 stranded β-barrel is thus composed of 8 extracellular loops (L1-L8) and 8 periplasmic turns (T1-T8). The periplasmic turns are short and are typically composed of 2-4 residues, however the longest turn (T4) in OmpF/C structures contains 10 residues. The loops of extracellular space are comparatively very long and except L3, all are exposed (L1, L2, L4-L8) to the outside of the cell. The ones that are exposed to the cell exterior show a large variation in length. In OmpF/C structures, the length of the β-barrel along the channel axis is ~ 30 Å and the diameters of the elliptic cross-section of the barrel are 25 × 38 Å (Rostovtseva et al., 2002).

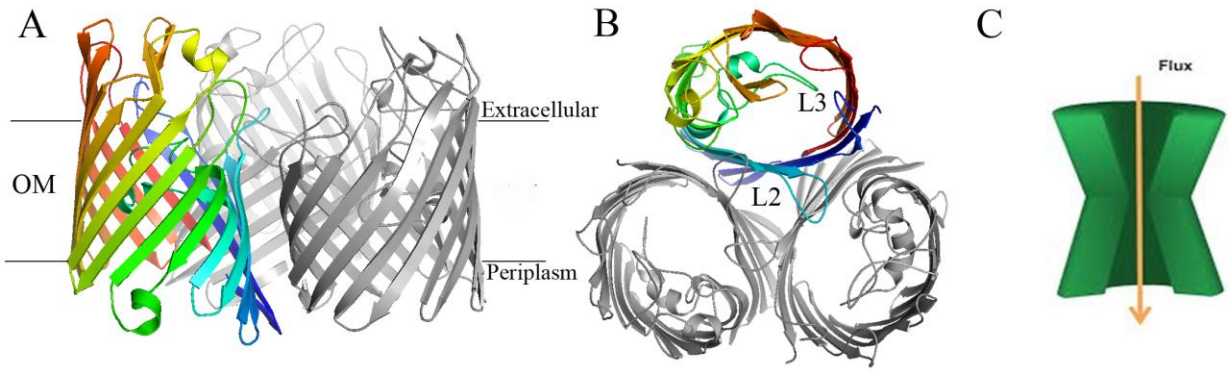

Figure 1.4. Structure of OmpF.

The figure displays the cartoon view from the OM plane (A) and extracellular side (B) for the homotrimer of *E. coli* OmpF. One of the monomers is shown in rainbow (N-terminus in blue to C-terminus in red) and other two in gray. (A) Each monomer is a 16-stranded β-barrel formed by 8 extracellular loops and 8 periplasmic turns. (B) L3 loop folds inside the barrel and the latching loop L2 stabilises the trimer. (C) Schematic representation to show the 'hour-glass' shape of the channel. The cartoon shown is a crystallographic trimer, made using the PDB code 2OMF (OmpF; Cowan et al., 1992).

- **Salt bridged N- and C- termini**

Although the average length of transmembrane β-strands of OmpF/C lies between 11-12, strand β-16 includes 16 amino acids and stands out as the longest strand of the barrel. In addition, β-16 strand is formed of N- and C- terminal ends of the protein. The mature sequences of porins often initiate with alanine at the N-terminus and end with an aromatic residue at the C-terminus, with most common being phenylalanine (Phe) but in some cases tryptophan (Trp) may also be present. . In OmpF/C, the carboxylate oxygen of the terminal Phe makes ionic interaction (~ 2.6 Å) with the α-amino nitrogen of Ala1 (Figure 1.5). The formation of a salt-bridge pair between the terminating ends of N- and C- termini is one of the characteristic features of porin structure (Nikaido 2003).

- **Amphipathic nature**

Any OM channel that transverses the lipid bilayer must maintain an amphipathic character in the membrane. In a porin channel, the extracellular loops and periplasmic turns contain hydrophilic residues but the β-strands show a significant amphipathicity. The transmembrane β-strands contain alternating hydrophobic and hydrophilic residues. The hydrophobic residues

protrude outside the barrel into the hydrophobic core of the lipid bilayer. The hydrophilic residues of the β-strands, on the other hand, orient towards the interior of the channel where they interact with numerous water molecules, present inside the channel. Although the water-filled channels of porins contain abundant water molecules that are highly mobile, some of the waters remain fixed owing to their intricate connection with the polar residues via strong hydrogen bonding. One characteristic feature observed in porins is the presence of a ring of aromatic residues circling the barrel outside at two primary interfaces of the OM. The β-strands at the interfaces between the hydrophobic and polar parts of the OM are marked by either phenylalanine or tyrosine or tryptophan that form two 'aromatic girdles' outside the barrel (Galdiero et al., 2012). In fact, the terminal salt-linked aromatic residue of the C-terminus forms a part of the aromatic girdle at the OM-periplasm interface. The presence of aromatic girdles is not only limited to porins but have been observed in other OMPs as well.

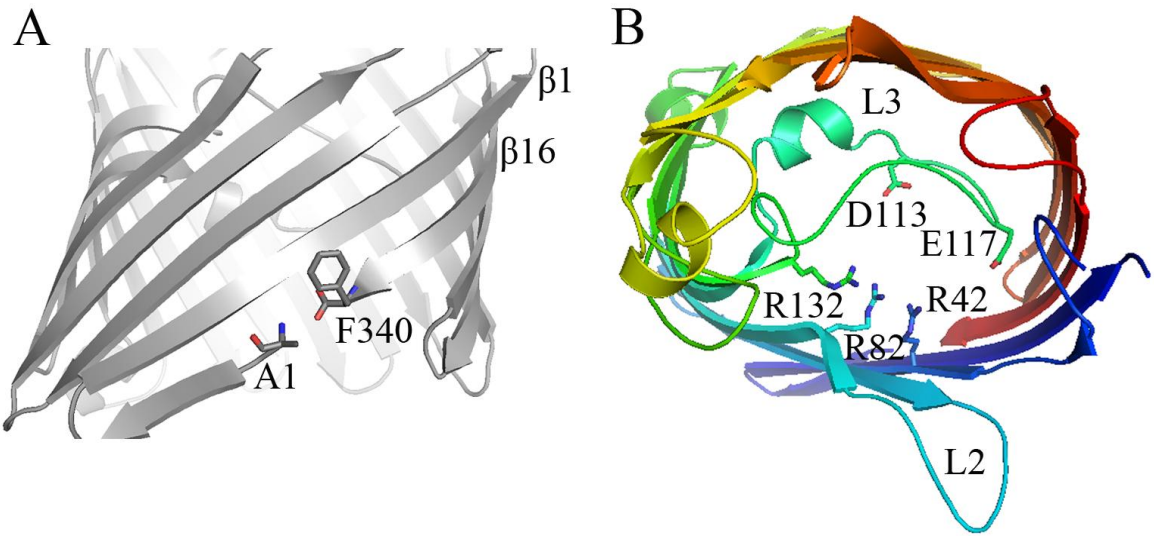

Figure 1.5. OmpF structural features.
(A) The first residue, alanine (at N-terminus), and the terminal residue, phenylalanine (at C-terminus), are salt bridged in the β-16 strand. (B) The eyelet region of OmpF monomer (extracellular view) is constricted by loop L3 that harbours negatively charged residues (Asp113 and Glu117), placed opposite the positive charged residues of the barrel wall (Arg42, Arg82 and Arg132).

- **<u>Pore-constriction: Loop L3</u>**

One of the extracellular loops does not protrude out in the external medium but instead folds back inside the barrel to cause a constriction of the pore. Bridged between transmembrane strands β5 and β6, loop L3 is composed of more than 30 residues, making it the longest loop of all. Loop

L3 folds inside the barrel such that the pore constriction is created almost in the middle of the barrel axis (Figure 1.5). The pore constriction by L3 is generally termed the 'constriction region (CR)' which forms a narrow elliptically shaped selectivity filter in OmpF with dimensions of 7 × 13 Å (Yamashita et al., 2008) and solvent accessible area of 30–40 $Å^2$ (Cowan et al, 1992; Varma et al, 2006).

L3 is a hallmark for all porin channels and a crucial determinant of solute translocation. In OmpF, the two negatively charged residues of L3, Asp113 and Glu117, are placed opposite the positively charged residues of the barrel wall, Arg42, Arg82 and Arg132 (Figure 1.5). Such an organisation of the charged residues of the constriction region (CR) produces a local transverse electric field that, in the light of past and recent studies, is strongly believed to create the barrier that the permeating molecule has to overcome to translocate (Karshikoff et al., 1994, Acosta-Gutierrez et al., 2016, also see section 1.4.3.).

- **<u>Oligomerisation: Loop L2</u>**

The porins exist as trimeric assemblies in the OM. Each of the three β-barrels of the porin trimer are tilted at an angle of 30°-60° and arranged around a central axis in the OM (Schulz 2002). In the trimer, the extracellular loop L2 of one monomer latches over to the groove of an adjacent monomer and is involved in maintaining and stabilising the trimeric state of the porin. The latching loop L2 is negatively charged whereas the surface of the groove contains positive charged residues. As a result, L2 of one monomer makes several electrostatic interactions with the groove of an adjacent monomer and hence aids in stabilising the trimer. In OmpF, the oligomerised state is strongly stabilised by an inter-subunit salt bridge involving 4 H-bonds between Glu71 (of L2 in one monomer) and the guanidium head groups of Arg132* and Arg100* (groove residues of the adjacent monomer indicated by asterisks), and an intra-subunit H-bond between Asp74 and Ser70 (Phale et al., 1998).

1.3.1.3. *Porin function: Solute transport*

The stress-induced activation of OmpC (and repression of OmpF) during increased extracellular osmolarity is explained by the channel size difference between the channels of two major porins of *E. coli*. The early diffusion studies of different compounds indicated that OmpC produced smaller-sized channels than OmpF (Nikaido and Rosenburg 1983). This was later

confirmed through their 3D X-ray crystal structures that revealed a slightly larger channel size for OmpF than OmpC (Cowan et al., 1992 and Basle et al., 2006), providing an explanation for the increased expression of OmpC under hypersmotic conditions. Because of its small channel size, OmpC minimises the influx of toxic products under hostile conditions or ions in high-osmolarity media.

The liposome swelling assay (LSA) has proven to be a significant tool for determining the diffusion rates along with the selectivity of the porin channel (Figure 1.6). For the assay, multilamellar proteoliposomes are prepared in the presence of a non-permeating sugar (e.g. stachyose), of size above the exclusion limit of porins (≥ 600 Da). The molecule of interest is rapidly added to the liposome in an isotonic solution and the optical density of the mixture is measured to assess the permeability of the molecule (Figure 1.6). The assay provides a comparative rate for the diffusion of different sized solutes through one porin or different porin channels. The LSA diffusion studies with *E. coli* OmpF/C not only determined the size-exclusion limit of solutes but also demonstrated the preference of the channels for cationic molecules over the anionic counterparts (Nikaido and Rosenberg 1981 and Nikaido and Rosenberg 1983).

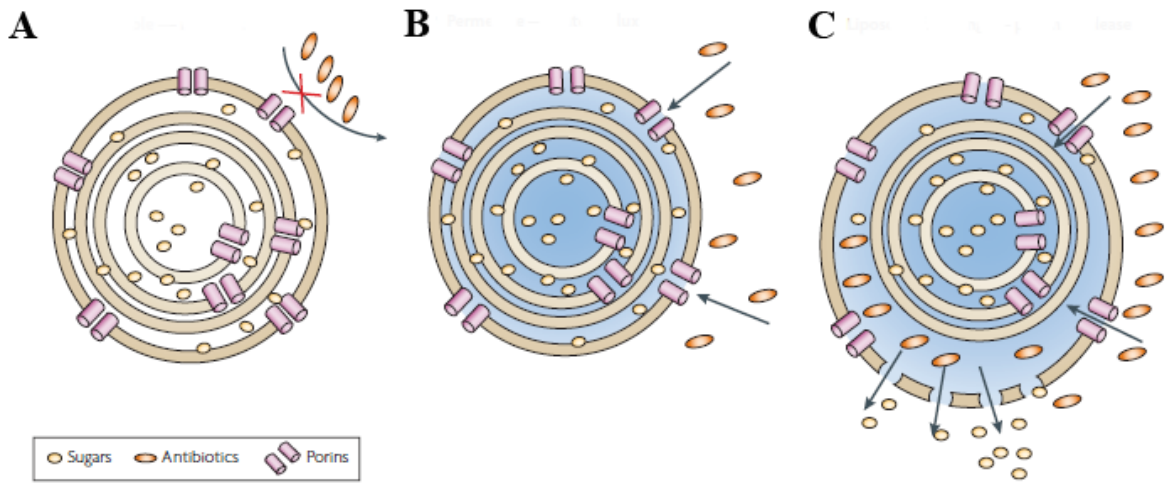

Figure 1.6. Schematic representation of the liposome swelling assay.
The substrate (or molecule) of interest is added to multilamellar liposomes (prepared in the presence of stachyose sugar; yellow circle). (A) If the molecule is unable to permeate through the porin channels, the optical density remains unchanged. (B) Upon permeation of the molecule, an osmotic gradient is created resulting in the influx of water molecules and swelling of the liposome. (C) Ultimately, water influx bursts the liposome and releases the sugar (stachyose), hence decreases the optical density. From Pages et al., 2008.

Electrophysiological techniques have been used for more than 30-40 years to study the functional aspects of pore-forming outer membrane proteins. Its contribution to understanding the nature of structure-function relationship in porins has been particularly significant. In lipid bilayer electrophysiology, the current traces through porins exhibit an open state allowing the passage of ions through their channels and may show the closing of the channel in three steps, also known as trimeric gating, where each step represents the closure of a monomer in the trimer. An important functional feature associated with their ion current traces as established by the initial lipid-bilayer studies of OmpF/C porins is the ohmic dependence, according to which the channel conductance is directly proportional to the applied voltage (Delcour 1997). Electrophysiology provided the first direct evidence of solute interaction with the channel in the form of discreet downward transitions in ion current traces. The zwitterionic molecules of various compounds induced current blocking events in the ion current traces of OmpF, implying the presence of low-affinity binding sites that may (or may not) result in the translocation through the porin channel (Danelon et al., 2006 and Mahendran et al., 2010).

The characteristic folding of loop L3 inside the barrels of OmpF/C inspired several studies to determine the role played by L3 charged residues in solute translocation (also see section 1.5.1). The loop L3 certainly imposes the size exclusion limit on the solute for its translocation through porins, but its charged residues also contribute towards the effective charge inside the channel. Molecular dynamics simulations in combination with electrophysiology studies have also shown that the negatively charged residues of L3 along with the positively charged barrel wall create a transverse electric field at the constriction region which is strong enough to orient water molecules (Im and Roux 2002a, b) and charged dipolar molecules inside the channel (Bajaj et al., 2017 and Acosta-Gutierrez et al., 2015). The data from multiple single channel studies showed the mutants of key charged residues of the eyelet region affected the influx of solutes (Lou et al., 2011 and Bajaj et al., 2016). A report recently showed that the mutations of the charged residues inside the OmpC pore, apart from the CR, affected the permeation profiles of zwitterionic carbapenems (Bajaj et al., 2016). These OmpC mutants with similar pore size (or ion-conductivity) posed altered internal electric fields which resulted in quite drastic variations in the flux of meropenem and imipenem molecules (Lou et al., 2011 and Bajaj et al., 2016).

The preference for the permeation of cations (over anions) is another factor that comes into play during ion diffusion through the porin channels. The selectivity of a channel is a measure of anion-cation permeability ratios as calculated by the Goldman-Hodgkin-Katz (GHK) equation (Hille 2001; see section 2.10.1.1) such that cation selectivity for a channel implies an effective anionic surface charge of the channel interior and vice versa for an anion selective channel (Alcaraz 2009). The intrinsic properties of the ions or the hydrophilic solute like the shape, size, charge and electromobility also play an important role during its diffusion through the channel. For example, in KCl solutions (when K^+ and Cl^- have equal ion permeabilities in solution) OmpF channel shows weak selectivity for the monovalent cations (K^+) that changes to anionic selectivity in solutions of multivalent cations (Alcaraz 2009). The observed anionic selectivity in the latter case may be due to the negative charge (over) compensation of the OmpF channel or the difference in the ionic mobilities of the counter-ions of the electrolyte (Alcaraz 2009). Another factor determining the ion-diffusion process is the charged environment in the channel which is liable to be affected by the external pH. Low pH can cause protonation of acidic residues (in loop L3) of the OmpF channel that may result into an anion-selective channel (Nestorovich et al., 2003 and Aguilella-Arzo et al., 2007).

Thus, solute translocation through a channel is not only dependent on its pore size but may be defined as interplay between the pore size, ionic selectivity and electrostatic properties of the channel. In addition, the overall electrostatic properties of the diffusing ion and the channel, collectively enact to achieve translocation.

1.3.2. *Passive channels: Substrate-specific*

The substrate-specific channels, as the name indicates, shows specificity for the passive uptake of a particular substrate. Such passive uptake of the substrate is facilitated through the process of diffusion that in turn is dependent on concentration differences across the OM. The substrate specific channels possess binding sites which aid the influx of a particular substrate that is not abundant in the cell exterior. As a result, substrate-specific channels can efficiently drive the diffusion of substrates which maintain low concentration gradients across the OM.

In Enterobacteriaceae, LamB (or maltoporin) is an excellent example of a substrate-specific protein from *E. coli* that was initially reported to transport disaccharide (maltose) or as polysaccharide (maltodextrin) sugars (Nikaido and Vaara 1985) but following structural evidence

of LamB bound to sucrose (Wang et al., 1997), it is since established as a carbohydrate-specific channel (Nikaido 2003). ScrY (or sucrose channel) in *Salmonella typhimurium* is a LamB ortholog and a specific channel for many sugars (Forst et al., 1998). Except for few differences (Nikaido 2003), the two sugar-specific channels (LamB and ScrY) exhibit similar structural features. Both LamB and ScrY exist as trimers in the OM where each monomer is an 18-stranded β-barrel (Schirmer et al., 1995 and Forst et al., 1998). Both channels show characteristic folding of loop L3 inside the barrel that constricts the pore mid-way (Figure 1.7). The 'greasy slide' along the channel wall is created by 6 aromatic residues and forms binding sites for the pyranose rings of sugar to allow its passage (through hydrophobic and polar interactions) across the OM (Schirmer et al., 1995 and Forst et al., 1998).

The OM channel devoted to uptake phosphates or phosphate bearing compounds in Enterobacteriaceae is PhoE. The phosphate-specific channels of PhoE from *E. coli* (Cowan et al., 1992) function as trimers of 16-stranded β-barrels, with each barrel constricted inside by folding of loop L3. The specific-channels that are employed for the uptake of nucleosides and deoxynucleosides utilise the Tsx family of proteins in Gram-negative bacteria. Tsx is a monomeric 12-stranded β-barrel with a 'key-shaped' pore lined by 5 aromatic residues important for the substrate binding (Ye and Van den Berg 2004).

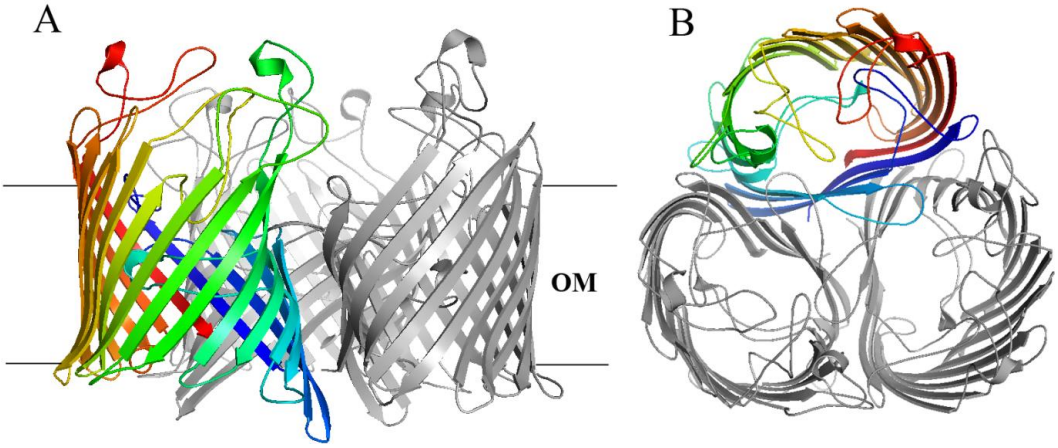

Figure 1.7. Structure of LamB.
The cartoon of a carbohydrate-specific channel of *E. coli*, LamB, forming a homotrimer in the OM. Each monomer is an 18-stranded β-barrel with loop L3 folded inside, constricting the channel.

1.3.3. *Active OM transporters*

The high-molecular weight OMPs that utilise energy to translocate the substrates across the OM are classified as active OM transporters. TonB-dependent transporters (TBTDs) form

gated channels to mediate active transport of very large substrates like iron-siderophore complexes, vitamins etc. The interior of TBTDs β-barrel is capped with an N-terminal plug and the transport of compounds through TBTDs is dependent on a complex of three inner membrane proteins (TonB-ExbB-ExdD) and derives its energy from the proton-motive force (Gumbart et al., 2007 and Schauer et al., 2008). The iron uptake is the most-studied system in *E. coli* for which FhuA (Ferguson et al., 1998 and Locher et al., 1998) and FepA (Buchanan et al., 1999) serve as classic examples of TBTDs by forming dedicated pathways for the transport of iron-siderophore complex (FhuA: ferrichrome, FepA: entrobactin). As shown through crystallography, these two proteins form 22-stranded β-barrel with a globular N-terminal plug domain and exemplify the architectural fold of TBTDs (Figure 1.8). TBTDs solved to date show this same architectural domain (Noinaj et al., 2010). The most common mechanism believed to cause the translocation of the substrate involves a 'pulling' effect, exerted by the periplasmic domain, of TonB protein (anchored to the IM) on the TonB box of the plug domain (Devanathan and Postle 2007 and Shultis et al., 2006). It is speculated that TonB mediated pull somehow delocalises the plug causing its release from the barrel (Ma et al., 2007) or possibly a conformational change (Pawelek et al., 2006) that facilitates the substrate-transport. Apart from the ones involved in iron-transport, other TBTDs that function for the uptake of nickel (Schauer et al., 2007), Vitamin B_{12} (Cherezov et al., 2006), disaccharides (sucrose: Blanvillain et al., 2007) or polysaccharides (SusC: Reeves et al., 1996), colicins (Buchanan et al., 2007 and Devanathan at al., 2007) have also been identified.

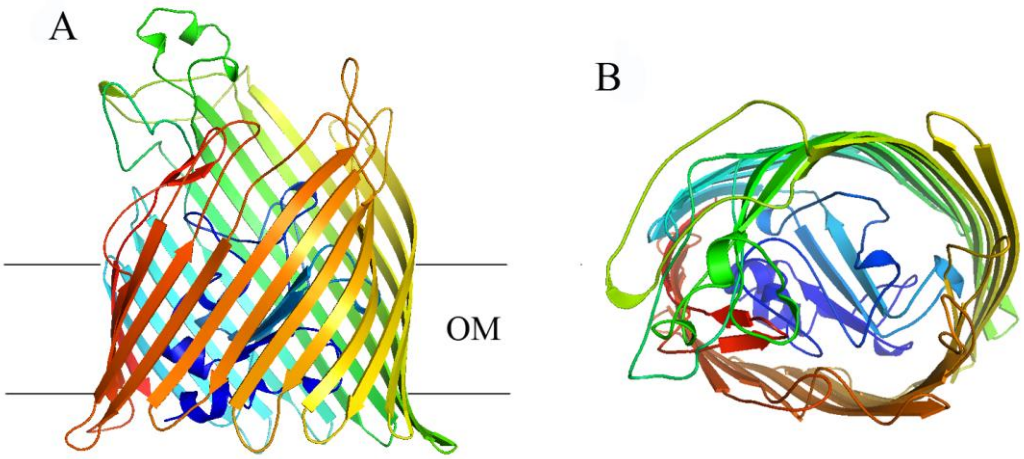

Figure 1.8. Structure of FhuA.
The X-ray structure of FhuA in *E. coli* is shown as a rainbow cartoon (N-terminus in blue to C-terminus in red). It is formed by 22 antiparallel β-strands forming the transmembrane barrel while the first 160 residues of N-terminus function as the plug domain inside the barrel. The cartoon figures were made using PyMol (Schrodinger 2010) with the PDB codes 1BY3.

1.4. Export channels

The impermeable bilayer of Gram-negative bacteria must provide a route for the expulsion of toxic or waste compounds, a task that is well accomplished by outer-membrane export channels as a part of the efflux pumps. Efflux pumps enact as a defence weapon for Gram-negative pathogens against toxic compounds such as antibiotics and thus are one of the major causes of multi-drug antibiotic resistance. Of all multi-drug efflux systems, RND (Resistance-Nodulation-Division) family of transporters form tripartite complexes across the cell wall of Gram-negatives, traversing the OM and the inner membrane. RND transporters utilise the electrochemical potential of protons, i.e., the proton motive force (PMF), to drive the substrate-transport processes (Yamaguchi et al. 2015). RNDs are composed of three essential components: an ABC-type transporter (ABC) in the inner membrane, a Membrane Fusion Protein (MFP) spanning the periplasmic region and an Outer Membrane Factor (OMF) localised in the OM (Zgurskaya et al., 2011). The proteins of OM that are involved in the efflux systems belong to Outer membrane Efflux Protein (OEP) family. TolC protein is one such OEP in *E. coli* that functions as an OMF channel in complex with different types of efflux systems (Federici et al., 2005). TolC presents a unique 140 Å long structure that extends from the OM to the periplasm and contrasts with the typical β-barrels of OMPs (Koronakis et al., 2000). The first domain of TolC is a trimer of 12-stranded β-barrel, constituted by the oligomerisation of three protomers, each contributing $1/3^{rd}$ of the β-barrel domain. The second and third domains of TolC, comprising α-helical and mixed α/β motifs respectively, extend into the periplasmic space. OprM in *Pseudomonas aeruginosa* (Koronakis et al., 2000) and VceE in *Vibrio cholerae* (Akama et al., 2004) are TolC-like OEPs that form OM channels (or OMF) for multi-drug efflux systems in other bacteria.

1.5. Exploitation of porins for antibiotic permeation

Multidrug resistance in Gram-negative pathogenesis is an impending global threat. The Gram-negative pathogens from the extended-spectrum β-lactamase (ESBL) producing Enterobacteriaceae family account for an enormous subset of multi-drug resistance, a majority of which include *E. coli*, *Vibrio cholerae*, *Salmonella spp.*, *Shigella spp.*, *Enterobacter spp.*, *Enterococcus spp.* and *Klebsiella spp.* (Paterson et al., 2005). The efficiency of multi-drug-resistance in Gram-negative bacteria is particularly owed to three main factors (Pages et al., 2008) : a) *Influx:* the inability of the drug to efficiently and quickly cross the OM, b) *Periplasmic enzymes*, the presence of bacterial β-lactamases that immediately degrade the antibiotic

molecules that reach the periplasm and render them inactive before traversing the IM, and c) *Efflux*, the export of drug molecules via multidrug efflux pumps.

The first line of defence in Gram-negative bacteria is provided by its asymmetric outer membrane bilayer which restricts the influx of antibiotics. For an antibiotic to be effective, it must cross the OM efficiently. Hydrophobic antibiotics like macrolides and rifamycins utilise the lipid-mediated pathway whereas hydrophilic antibiotics like β-lactams are transported inside the cell by the porin channels of the OM (Delcour 2009). Some other compounds like tetracycline and quinolones utilise both lipid-mediated and porin-mediated pathways for the transport across the OM (Delcour 2009).

1.5.1. *Porin-mediated pathway for drug translocation*

The β-lactams and fluoroquinolones are the most commonly used antibacterial agents against the majority of infections. The evidence for the interaction of porin channels with the β-lactams like penicllins (Danelon et al., 2006 and Mahendran et al., 2010), cepahalosporins (Mahendran et al., 2010), carbapenems (Bajaj et al., 2016 and Bodrenko et al., 2015) and fluoroquinolones (Mahendran et al., 2010 and Bodrenko et al., 2015) have been mostly provided through single channel electrophysiology. An early study showed the transient current blocking events in the OmpF ion-traces upon the addition of zwitterionic molecules of ampicillin and amoxicillin but not in the presence of mono-anionic (piperacillin) or di-anionic (carbenicillin) compounds (Danelon et al., 2006). Based on the liposome diffusion data (Yoshimura and Niakido 1985) and molecular simulation studies (Danelon et al., 2006), it was proposed that the zwitterionic molecules produce current blocking events because they are able to interact with the residues of the constriction region (CR) and as a result possess high diffusion rates in comparison to anionic molecules.

Molecular dynamics simulations in combination with electrophysiology and liposome swelling data also provide experimental evidence for the porin-antibiotic interaction. These studies have demonstrated that mutations of the charged residues inside the channel affect the flux of β-lactams (Delcour 2009). The mutated key charged residues of the OmpF constriction eyelet, like D113N (or R132A), were shown to exhibit more channel-closing events with ampicillin than the wild type, implying its high susceptibility for the influx of antibiotic as seen in the liposome assays (Hajjar et al., 2010). Molecular modelling studies have demonstrated

D113A mutants of OmpF to be increasingly susceptible to ampicillin, ceftozidine and ceftazidime (Vidal et al., 2005) because these OmpF mutants will let pass such molecules. In contrast to mutating charged residues, several earlier studies have also shown that mutations of uncharged residues in the channel may also affect the influx of substrates with respect to the wild type (Delcour 2009).

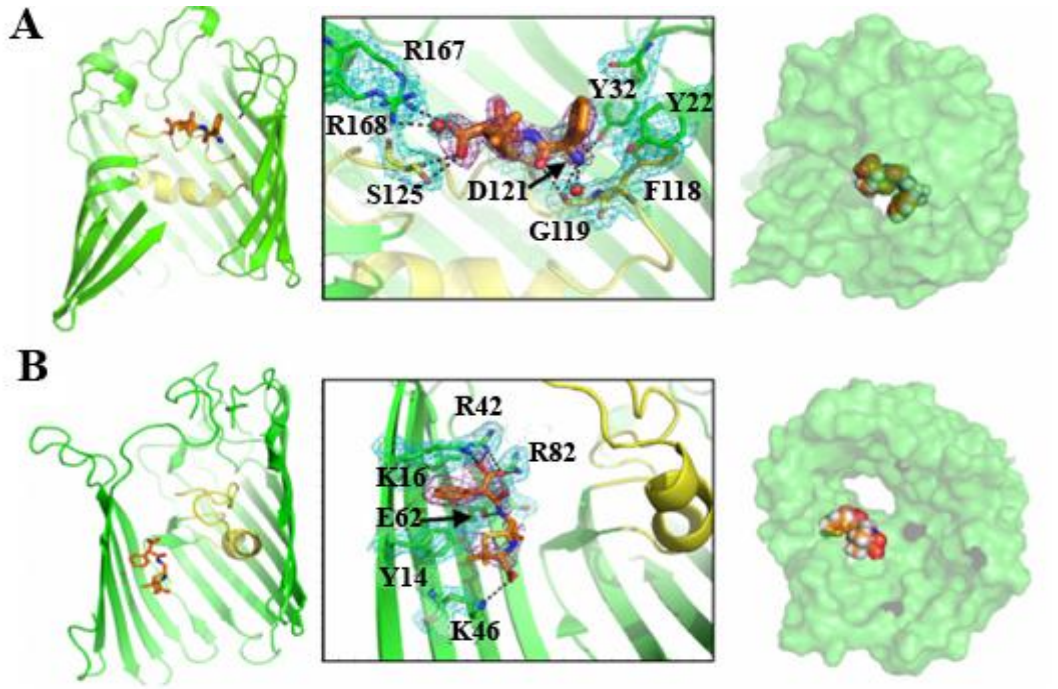

Figure 1.9. OmpF bound to antibiotics.
The crystal structures of OmpF bound to ampicillin (A) and carbenicllin (B) are shown in cartoon (left panels) and surface views (right panels). The middle panels show the OmpF residues making interactions with the bound antibiotic. From Ziervogel and Roux, 2012 (PDB codes 4GCP and 4GCQ).

X-ray crystallography provided the molecular evidence for the porin-mediated pathway for zwitterionic antibiotics. The binding sites of ampicillin, carbenicllin and ertapenem were revealed in recent reported crystal structures of OmpF (Ziervogel and Roux 2013). The ampicillin zwitterion was observed bound just above the constriction zone, aligned perpendicular to the diffusion axis and explaining the reason for causing current blockages in the OmpF channel (Figure 1.9). Carbenicllin was observed close to the barrel wall bound weakly in the periplasmic vestibule region (Figure 1.9) and oriented in a direction parallel to the diffusion axis such that its binding in the channel does not occlude the pore. However, the B-factor values of ampicillin and carbenicllin were ~25% higher than the neighboring protein residues (Ziervogel and Roux 2012),

which suggests low occupation of the bound molecules and possibly, their multiple conformations inside the OmpF channel.

1.5.2. *Porin-mediated antibiotic resistance*

Since many antibiotics utilise a porin-mediated pathway for translocation, the bacterial resistance in multiple cases is linked to the functional modulation or loss of porins. *E. coli*, *Enterobacter spp.* and *Klebsiella spp.* are examples that have shown antibiotic resistance due to the reduced influx of the compounds through porins (Pages et al., 2008). The porin-linked resistance mechanisms in gram-negative bacteria may involve loss of porin function or loss of its copy number due to altered expression (Figure 1.10).

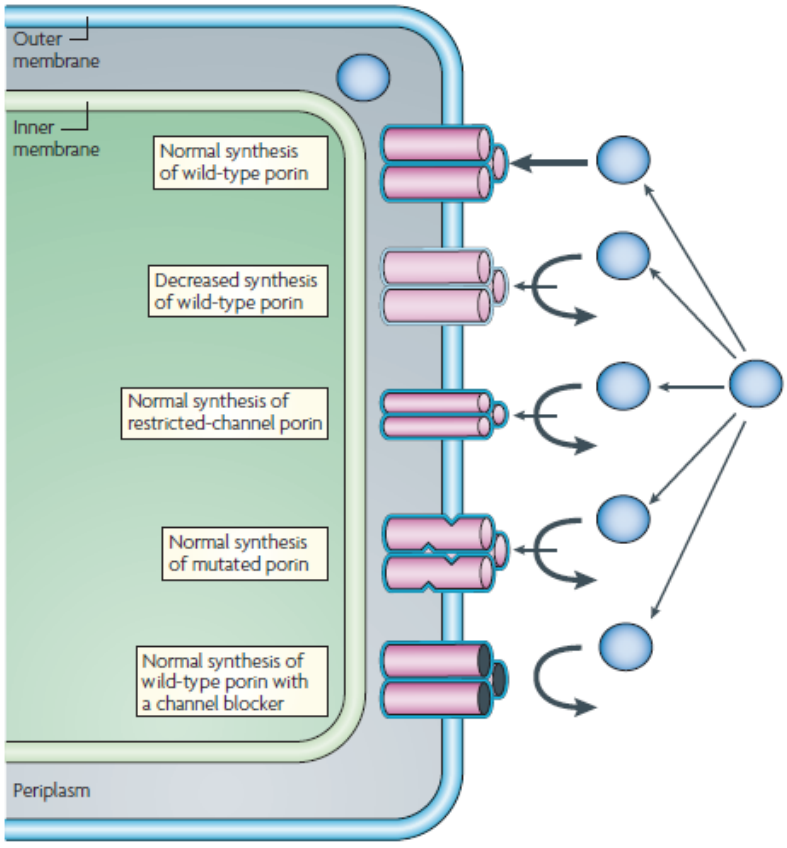

Figure 1.10. Porin-mediated mechanisms of bacterial resistance.
The schematic representation of a Gram-negative cell with β-lactams shown as blue circles and porin trimers as pink cylinders in the OM. The straight arrows represent the uptake of β-lactams; thickness reflecting the level of penetration and curved arrows indicate the failure to permeate the OM through porins. From Pages et al, 2008.

The loss of porin function may involve some mutations that can affect the permeability of the porin channels. For example, clinical isolates of *Enterobacter aerogenes* were characterised

with a G112D mutation in Omp36 porin that provides the bacterium high levels of β-lactam resistance (Domenech-Sanchez et al., 1999). Similarly, the multidrug resistant species of *Neisseria gonorrhoeae* were found to have multiple mutations in the loop L3 of PorA (Domenech-Sanchez et al., 1999).

Porins can alternatively have varied expression profiles during antibiotic attack that may confer resistance. As observed for the altered porin regulation induced by osmotic pressure or acidic pH (also see section 1.4.1), the antibiotic stress may involve transcriptional repression of the porin channels with wide pore sizes and instead activate the expression of narrow-sized porins. For example, tetracycline causes an increase in the *micF* levels that repress OmpR mediated expression of OmpF channel and activates OmpC expression (Viveiros et al., 2007). Likewise, the porin-null strain of *K. pneumoniae* expresses OmpK37 porin and has drastically reduced susceptibility to β-lactams as compared to the wild type strain that expresses OmpK35 and OmpK36 porins (Pages et al., 2008).

1.6. The Gram-negative pathogens of this project

1.6.1. *Vibrio cholerae*

V. cholerae is a motile rod-shaped pathogen from the Vibrionaceae family of Gram-negative bacteria and resides in marine or aquatic environments. The pathogen enters the human gut through ingestion of contaminated food or water resources and colonises the mucosal surface of the small intestine. After colonisation, the pathogen releases cholera toxin that is responsible for causing the severe intestinal infection in humans known as cholera.

1.6.1.1. Overview of Cholera as a disease

Cholera infection involves an acute diarrhoea characterised by profuse watery stool leading to rapid dehydration in the patient. The infection accompanies vomiting and acidosis in the patient. In majority of the cases, the failure of detecting the infection in time results in death. The infection is spread easily and rapidly in areas of poor treatment of sewage, inadequate sanitation facilities, improper hygienic conditions and contaminated water resources (ponds and lakes). According to the Centres for Disease Control and Prevention (CDC), sub-Saharan Africa (Ethiopia, Nigeria, Tanzania, Kenya) is the prime region affected with majority of cholera cases and with outbreaks each year from 2001-2012 (Figure 1.11). Southeast Asia is the foremost

region to have the largest population at risk for cholera, of which the nations with more than 100,000 cases annually include India and Bangladesh (Ali et al., 2015; Figure 1.11). Cholera has very recently (2017) caught the world's attention again through the recent and 'unprecedented' epidemic in Yemen causing more than 100,000 cases according to the WHO and UNICEF.

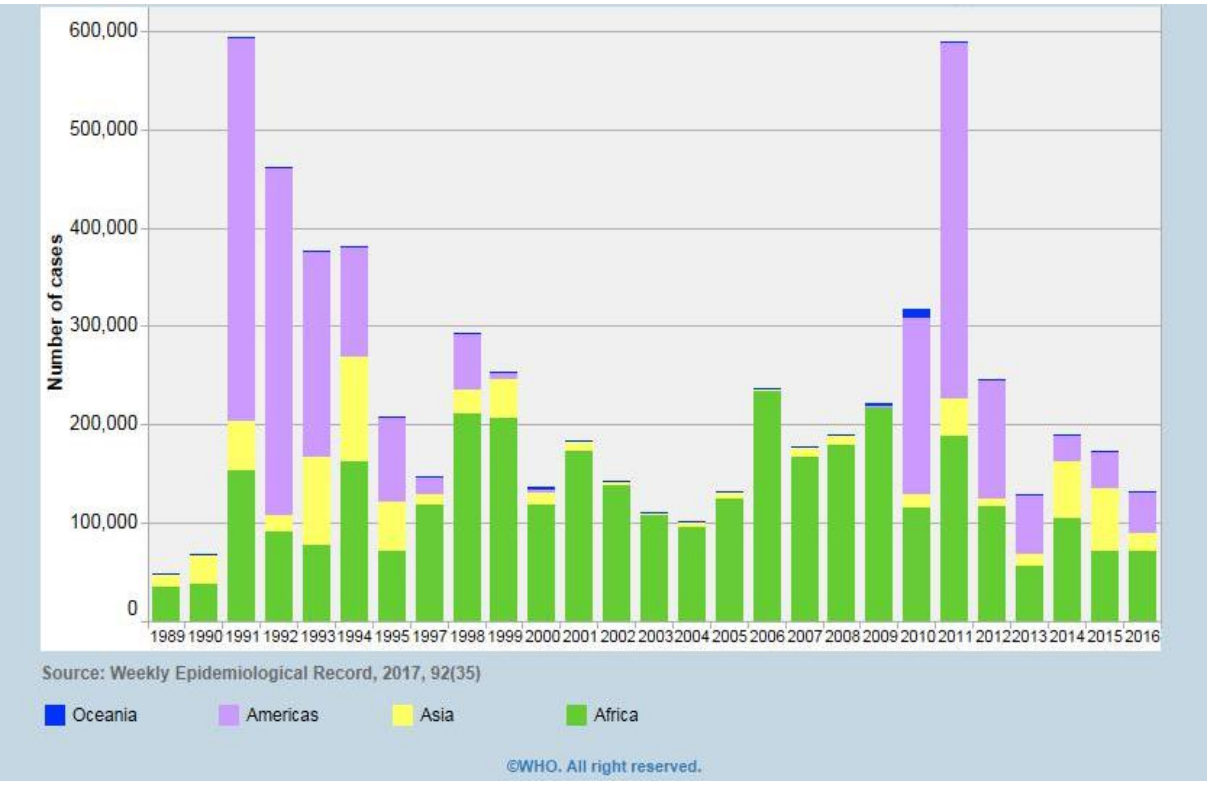

Figure 1.11. Cholera cases reported to WHO by continent from 1989-2016.
From the World Health Organisation (WHO) 2017.

Rehydration and antibiotics are the two primary methods for the treatment of cholera. Rehydration therapy involves extensive intake of fluids and salts to restore the loss of dehydration in the human body. The rehydration is often accompanied by antibiotic therapy to reduce the illness and control the dehydration in the patients. Tetracyclines and quinolones are widely employed during the infection to control the severity of the symptoms. From tetracyclines, doxycycline is most important antibiotic provided to infected adults and azithromycin for pregnant women (or children). According to WHO, the global efforts to control the resurgence of cholera have also included the development of effective oral cholera vaccines that have been successfully used in various outbreaks and humanitarian emergencies.

1.6.1.2. *OMPs of Vibrio cholerae*

Seven major outer membrane proteins have been reported in *V. cholerae* that include the 45 kDa maltoporin OmpS (like LamB of *E. coli*), 25 kDa immunogenic protein OmpV, 35 kDa OmpA-like protein, 27 kDa trypsin-resistant OmpX (Simonet et al., 2003) and 22 kDa heat modifiable OmpW (Nandi et al., 2005). The other two major outer membrane proteins of *V. cholerae*, OmpU and OmpT, form hydrophilic non-specific channels across the OM and are thus classified as porins. The proteins OmpU and OmpT are the most-studied OMPs of *V. cholerae* and the literature investigating their expression, regulation and function dates back more than 30 years. The preliminary characterisation of OmpU/T proteins as non-specific porins was performed using liposome swelling assays (Chakarbarti et al., 1996).

The proteins OmpU/T of *V. cholerae* are regulated by a transmembrane DNA-binding protein, ToxR. Being localised in the inner membrane, ToxR comprises a cytoplasmic domain and a periplasmic domain. The cytoplasmic domains of ToxR and OmpR (of *E. coli*) share 30% homology and thus ToxR belongs to OmpR family of transcriptional factors. ToxR has been shown to activate the expression of OmpU (Crawford et al., 1998) and repress the expression of OmpT (Miller et al., 1988 and Li et al., 2000). The porin regulator acts at the transcription level for the expression (of *ompU*) or repression (of *ompT*) by binding to the upstream regions of their promoters (Crawford et al., 1998 and Li et al., 2000). To activate the *ompU* promoter, ToxR binds to the upstream region and through co-operative binding (protein-protein interaction) interacts with other ToxR proteins (Crawford et al., 1998). For OmpT repression, ToxR binds upstream of the *ompT* promoter and represses its activation by interfering with the interaction between the activator(s) and RNA polymerase (Li et al., 2000). ToxR-mediated reciprocal regulation of OmpU/T porins is thus similar to OmpR-mediated regulation of OmpF/C porins in *E. coli* (also see section 1.4.1) except for the phosphosignalling mechanism which is absent in the porin regulation of *V. cholerae*. Apart from porin regulation, ToxR with the help of other membrane proteins like, ToxS, TcpP and TcpH, activates the expression of a transcriptional activator ToxT (Li et al., 2000). The expression of ToxT is required for the expression of virulence factors of *V. cholerae*: cholera toxin (CT), toxin co-regulated pilus (TCP) and accessory colonisation factor (ACF) (Li et al., 2000 and Klose 2007). Hence, ToxR plays a prime role in the virulence properties of *V. cholerae* by directly regulating porin expression and indirectly regulating the virulence genes expression.

The effect of bile on the *V. cholerae* cells was first demonstrated by Provenzano et al., 2000 who reported reduced growth rates for the *toxR* mutant strains of *V. cholerae* in the presence of the bile component deoxycholate (Provenzano et al., 2000). The study demonstrated bile-induced activation of OmpU implying bile-resistant property of OmpU (in OmpT null background) while OmpT expression (in OmpU null background) proved deleterious for the expression of virulence factors *in vitro* (Provenzano and Klose 2000). Another study showed that the presence of bile did not affect the antibiotic flux in *V. cholerae* cells expressing only OmpU but that flux was reduced (~70%) in cells expressing only OmpT (Wibbenmeyer et al., 2002). These studies indicated different behaviours of OmpU/T channels in response to bile but direct evidence of a bile effect on *V. cholerae* was provided through the single channel studies of OmpU and OmpT with deoxycholate (Duret and Delcour 2006). The deoxycholate clearly induced channel-blocking single-step closures (SSC) in the ion-current traces of OmpT but did not affect the ion current traces of OmpU (Duret and Delcour 2006). This illustrates the interaction of deoxycholate with OmpT which in turn could imply that OmpT allows the permeation of bile components (like deoxycholate). In contrast, bile may not permeate through OmpU porin and as a result, OmpU plays a protective role in the virulence and survival of *V. cholerae* cells in the small intestine of humans where bile is the principal component of the intestinal fluid (Wibbenmeyer et al., 2002).

1.6.1.3. *Antibiotic resistance in Vibrio cholerae*

The past 10-15 years have seen a significant increase in the number of drug-resistant strains of *V. cholerae*, reported worldwide. The resistance against antibacterial compounds is very broad and ranges from penicillins, fluoroquinolones, macrolides, aminoglycosides to tetracyclines (Kitaoka et al., 2011). The antibiotic resistance in *V. cholerae* has been elaborated in a review by Kitaoka et al., 2011 and is linked to several intrinsic mechanisms of the bacteria that involve spontaneous mutations, presence of active multi-drug efflux pumps and through the transmission of mobile genetic elements or conjugative plasmids. However, porin-mediated resistance in *V. cholerae* has not been observed yet.

1.6.2. *Enterobacter cloacae* and *Klebsiella pneumoniae*

The Enterobacteriaceae family of Gram-negative bacteria includes two common nosocomial pathogens, namely *Enterobacter cloacae* and *Klebsiella pneumoniae*. Both are facultative anaerobes that are ubiquitous in nature. *E. cloacae* is present in the intestinal tract of

humans (and animals) and causes opportunistic infections of urinary tract, septic arthritis, respiratory and abdominal systems. *K. pneumoniae* is also an opportunistic pathogen that resides in the human intestine and is responsible for causing pneumonia, meningitis and other infections in blood, urinary tract or wounds. The outbreaks caused by *E. cloacae* and *K. pneumoniae* have also been reported in hospital surgical units and neonatal units (Pages et al., 2008). Most of the multidrug resistant (MDR) clinical isolates of *E. cloacae* and *K. pneumoniae* have been isolated with extended spectrum β-lactamases (ESBL) and carbapenemases. In fact after *E. coli*, *E. cloacae* and *K. pneumoniae* are the two most notorious Enterobacteriaceae species that are responsible for causing nosocomial infections and hence are included in the list of ESKAPE pathogens (*Enterococcus faecium, Staphylococcus aureus, Klebsiella pneumoniae, Acinetobacter baumanii, Pseudomonas aeruginosa, and Enterobacter spp*) (Rice 2009).

The major porins present in *E. cloacae* are OmpE35 and OmpE36 (previously characterised as F and D proteins, Lee et al., 1992) and are considered structural and functional homologs of OmpF and OmpC respectively, of *E. coli*. The porins OmpE35/E36 have been minimally investigated for the effect of antibiotics (Lee et al., 2012) and scarce experimental data exists to show that carbapenem resistant strains of *E. cloacae* lack porins (Raimondi et al., 1991). However, MDR strains of *Enterobacter aerogenes* have been reported in several studies to have altered expression profiles of porins (Omp35 and Omp36; Davin-Regli and Pages 2015).

In *K. pneumoniae*, OmpK35 and OmpK36 are the two major porins present in the OM and are homologs of *E. coli* OmpF and OmpC (Doménech-Sánchez et al., 2003 and Alberti et al., 1995). There have been a significant number of studies linking the antibiotic resistance in *K. pneumoniae* to the deficiency of OmpK35/K36 porins (Zhang et al., 2014, Tsai et al., 2011 and Shin et al., 2011). However, quite recently a report assessed the diffusion properties of OmpK35 and OmpK36 porins with β-lactams (Sugawara et al. 2016). The report concluded that one of resistance mechanisms in *K. pneumoniae* may involve altered porin expression profile (i.e. downregulation of OmpK35 and upregulation of narrow channels of OmpK36 to restrict the drug influx) (Sugawara et al. 2016).

1.7. Aims of the project

The PhD is affiliated to the 'ND4BB' (New Drugs for Bad Bugs) initiative undertaken by the Innovative Medicines Initiative (IMI). IMI is a partnership between the European Union (represented by the European Commission) and the European pharmaceutical industry (represented by EFPIA, the European Federation of Pharmaceutical Industries and Associations). The current PhD project is a part of 'TRANSLOCATION', a component of the ND4BB platform that is aimed to determine the antibiotic influx/efflux mechanisms through outer membrane proteins of Gram-negative pathogens in order to aid in drug discovery strategies.

In order to contribute towards the understanding of antibiotic permeation mechanism through the porins of Gram-negative bacteria, the major porins from three different Gram-negative pathogens were targeted for the study. These include *Vibrio cholerae* porins OmpU and OmpT (and their mutants OmpUΔN and OmpTΔL8), *Enterobacter cloacae* porins OmpE35 and OmpE36 and *Klebsiella pneumoniae* porin OmpK36. The target proteins were recombinantly expressed in *E. coli* and purified in high amounts (**Chapter 3**). The 3D structures of the proteins were determined through crystallisation and X-ray diffraction (**Chapter 4**). In addition, we performed electrophysiological studies to study the effect of antibiotics on OmpU/T porins (**Chapter 5**). For comparing the antibiotic permeation through the diffusion channels, different *in vitro* assays such as the liposome swelling and disc-diffusion assays were conducted with OmpU/T, OmpE35/E36 and OmpK35/K36 proteins in the presence of different antibiotics (**Chapter 5**).

Chapter 2. Materials and Methods

2.1. Molecular Biology Reagents

2.1.1. *Chemical suppliers*

All chemicals and molecular biology reagents were purchased from Sigma Aldrich or Thermo Fischer Scientific, unless stated otherwise. The amino acids were purchased from Formedium, while the antibiotics were purchased from Carbosynth Limited and Melford Laboratories Limited. The detergents used for the research were purchased from Anatrace. The enzymes and DNA/gel extraction kits were purchased from New England Biolabs (NEB) and Qiagen respectively.

2.1.2. *Buffers and solutions*

The buffers of HEPES and Tris were made in deionized water from HEPES acid powder and Trizma base powder respectively. The pH values of the HEPES-based buffers were adjusted using sodium hydroxide (NaOH) or potassium hydroxide (KOH), while Tris-based buffers were pH adjusted with hydrochloric acid (HCl). All the buffers and reagents were made in deionized water.

2.1.3. *Growth media*

All the bacterial cultures were grown in Luria Broth liquid media (LB broth; composition given in Table 2.1) and LB solid media, prepared with 1.5% agar, was used for overnight incubation of bacterial cells. For Selenomethionine-substituted protein expression, LeMasters-Richards (LR) medium (mixture of buffer and salts) was used for the bacterial growth (components of LR buffer and LR salts are listed in Table 2.1). Depending on the type of plasmid construct used, the antibiotic solutions of Ampicillin (100 µg/ml) and Kanamycin (50 µg/ml) were added to growth media whenever required. The stock solutions of antibiotics (Amp: 100 mg/ml and Kan: 50 mg/ml) were stored at -20°C for a month and diluted 1:1000 in the media, whenever required.

2.2. Bacterial strains and vectors

A list of bacterial strains and plasmid vectors used in the study are detailed in Table 2.2 and Table 2.3 respectively.

Table 2.1. Growth media composition and description for use in the study.

Growth Medium	Components (per litre)		Description
Luria-Bertani (LB)	25 g LB granules as supplied (Sigma-Aldrich; Composition: 10 g/L Tryptone, 5 g/L Yeast Extract, 5 g/L NaCl		Rich media for *E. coli*. Dissolved in H2O and pH adjusted to 7.2 with NaOH. Autoclaved before use.
LeMasters-Richards (LR) media	LR salts (100X per litre) LR buffer (per litre) 100X AA stock (filter sterilized and stored at 4°C)	167.5 g $(NH4)_2SO_4$ 30 g $MgSO_4.H_2O$ 300 mg $FeSO_4.7H_2O$ 1 ml conc. H_2SO_4 24 g KH_2PO_4 1 g NaOH 0.25-3 g glycerol (5-6 ml of a 50% w/v solution) 5 g each of: Lys/Phe/Thr 2.5 g each of : Leu/Ile/Val 0.06% w/v seleno-methionine	Minimal media for producing Seleno-methionine-substituted protein by inhibition of the methionine biosynthesis pathway in *E.coli* (Van Duyne et al., 1993) Salts and media autoclaved separately. The Glucose and salts added immediately before inoculation.
2×YT ($MgSO_4$) media	16 g Tryptone 10 g Yeast extract 5 g NaCl 2 mM $MgSO_4$		Nutrient-rich media for *E. coli* growth, containing double the concentration of yeast extract compared to LB media. Magnesium supplemented in the media increases the cell biomass (Webb 1949)

Table 2.2. List of *E.coli* strains used for the study

Bacterial strain	Genotype	Source	Description
DH5α	*fhuA2 Δ(argF-lacZ)*U169 *phoA Φ80Δ (lacZ)M15 gyrA96 recA1 relA1 endA1 thi-1 hsdR17*	New England Biolabs (NEB)	General strain of *E. coli* routinely used for cloning (Hanahan 1983).
Bl21(DE3)	*F^- dcm ompT hsdS(rB- mB-) gal (DE3)*	Van den Berg lab (Newcastle University, UK)	Optimised for protein expression using a T7 promoter. Routinely used to over-express recombinant proteins (Studier and Moffat 1986).

omp8 Bl21 (DE3)	Bl21(DE3), *ΔlamB ompF*: :Tn5 *ΔompA ΔompC*	Lab of Mathias Winterhalter (Jacobs University, Bremen)	Porin deletion strain of *E. coli*. Lacks major porins OmpF and OmpC, in addition to other OMPs like OmpA and LamB (Prilipov et al., 1998)

Table 2.3. List of the plasmids used in the study

Plasmid	Size (kbp)	Supplier	Description
pBAD24	4.5	Van den Berg lab (Newcastle Univeristy, UK)	Bacterial expression vector with pBAD promoter under tight regulation by arabinose operon (araBAD). Ampicillin resistance. (Guzman et al., 1995)
pET28a	5.4	Novagen	T7 promoter, lac operator, *laciq*, multiple cloning site with integrated N- and C- termnial 6×His-tag. Kanamycin resistance.

2.3. Cloning

The targeted protein genes were cloned into pBAD24 plasmid for membrane expression using NcoI and XbaI restriction sites. Nucleotide sequences of target protein without the signal sequences were cloned into pET28a plasmid for inclusion body expression using NcoI and XhoI restriction sites. For cloning in pET28a, an additional glycine (Gly) residue was added between the NcoI restriction site (CCATGG) and the start codon.

2.3.1. *Polymerase Chain Reaction (PCR)*

The nucleotide sequences of the target proteins were amplified using PCR (Mullis et al., 1986). The primers of 20-30 base pair length were designed using the 5' and 3' of the target DNA sequence and manufactured from Eurofins genomics (Wolverhampton, UK). For primer design, the online tool software '*Oligo Calc* (http://biotools.nubic.northwestern.edu/OligoCalc.html)' was used to ensure the proper melting temperature ($T_m \geq 50°C$) and avoid self- or cross -complementarity of the primers. Following the first two steps in PCR, i.e. denaturation and primer annealing, the final step of target DNA amplification was achieved using a thermostable DNA polymerase that synthesises and extends

the new DNA complementary strands based on the source template. The online software of NEB T_m calculator was used to get an estimate of the annealing temperature (T_a) required for the PCR.

2.3.1.1. *Standard PCR*

The standard PCR mixture was prepared on ice and comprised of the reagents listed in Table 2.4. The conditions for a standard PCR reaction used in a thermocycler are described in Table 2.5.

Table 2.4. Reagents used in a standard PCR

Reagents (stock)	Volume used from the stocks (Amount per reaction)
Forward primer (10 µM)	2.5 µl (0.5 µM)
Reverse primer (10 µM)	2.5 µl (0.5 µM)
deoxy nucleotide triphosphates (dNTPs; 10mM)	1 µl (200 µM)
Target DNA template	2 µl (50-100 ng)
PCR Buffer (5×)	10 µl (1×)
Phusion polymerase	0.5 µl (0.5 units)
Autoclaved H_2O	31.5 µl
Total volume	50 µl

Table 2.5. Conditions used for standard PCR

Step	Temperature (^OC)	Duration	Number of cycles
Initial Denaturation	98	5 minutes	1
Denaturation	98	10 seconds	25
Annealing*	55 - 65	30 seconds	25
Amplification[ɪ]	72	40 seconds	25
Final Extension	72	4 minutes	1

*Annealing temperature can be varied depending on the melting point of primers used.

[ɪ] The extension rate for phusion polymerase is 45 seconds per kilo-basepair (kbp). Hence, 40 seconds was used for the amplification of sequences below 1 kbp.

The amplified DNA products from standard PCR were analysed by agarose gel (also see section 2.3.2).

2.3.1.2. *PCR for Site directed mutagenesis (SDM)*

Site directed mutagenesis (SDM) is an *in vitro* technique that uses custom-designed primers to create selected single or multiple amino-acid mutations (insertions or deletions) in a double-stranded DNA plasmid. The Q5 Site-Directed Mutagenesis kit (Q5 kit) from NEB was used to

create deletion or insertion constructs of target sequences via SDM. In this study, site directed mutagenesis was used to create:

- N-terminus deletion construct (Δ10 amino acids) of pBAD24 OmpU (OmpU ΔN)
- Loop deletion construct (Δ16 amino acids) of pBAD OmpT (OmpT ΔL8)

The protocol for Q5 site-directed mutagenesis involved the following two steps.

Step 1 The initial step was to amplify the targeted gene sequence with the custom designed primers (flanking the DNA region to be deleted/inserted). The PCR was done using standard PCR methodology (Table 2.5) with the reagents listed in Table 2.6. Since the amplified regions were approximately around 6 kbp, the amplification time was set to 3.5 minutes based on the extension rate of Q5 Hot Start High-Fidelity DNA polymerase (~20-30 kbp/second).

Table 2.6. PCR reagents for SDM

Reagents (stock)	Volume used from the stock (amount used)
Q5 Hot Start High-Fidelity Master Mix (2×)	12.5 µl (1×)
Forward primer (10 µM)	1.25 µl (0.5 µM)
Reverse primer (10 µM)	1.25 µl (0.5 µM)
Template DNA (25 ng/µl)	1 µl (25 ng)
Autoclaved H_2O	9 µl
Total Volume	25 µl

Step 2 The amplified DNA product was incubated with a unique enzyme mix containing a kinase (K), a ligase (L) and DpnI (D), hence referred to as KLD treatment. These enzymes allow for rapid circularization of the PCR product and removal of the template DNA. **Table 2.7** shows the reagents used for KLD treatment. The KLD mix was kept for incubation at room temperature (RT) for 5 minutes, followed by the transformation of the competent cells.

Table 2.7. KLD treatment for SDM

Reagents	Volume used from the stock
PCR product	1 µl
KLD Reaction Buffer (2×)	5 µl (1×)
KLD enzyme mix (10×)	1 µl (1×)
Autoclaved H_2O	3 µl
Total volume	10 µl

2.3.2. *Agarose gel electrophoresis*

The quality and size of a target polynucleotide (from PCR or DNA isolation and purification methods) was analysed using agarose gel electrophoresis. 1 % (w/v) agarose gels were prepared by mixing DNA-grade agarose powder with 1× TAE (Tris-Acetate-EDTA; 40 mM Tris, 20 mM acetic acid, 1 mM EDTA) buffer and the mixture was boiled until the agarose dissolved completely. Upon cooling, the SYBR Safe DNA stain (1 in 10,000 dilution) was added to the agarose solution to aid in DNA visualisation during electrophoresis. The mixture was poured in a gel mould casting tray and a comb was placed at one end to produce wells for loading DNA samples. For the preparation of DNA samples, 1× DNA loading dye (6× dye stock from NEB) was added to the desired amount (10 ng – 1 µg) of target DNA. To estimate the size of the samples, 1 µl of 1 kb DNA ladder (500 µg/ml, solubilised in sample buffer) was used as the marker and run along the samples. The gel was submerged in 1× TAE buffer and ran at 100 V for 40-50 minutes (depending on the size of DNA).

The DNA samples on the agarose gel was visualised and photographed through a Bio-Rad Gel Doc EZ Imager (Image Lab/ PC Windows software).

2.3.3. *Purification of PCR products from agarose gel*

The PCR products were run on the agarose gel and the amplified DNA was carefully excised from the gel using a sharp scalpel by visualising under a UV transilluminator. The extraction of DNA from the agarose gel slices was performed using QIAquick Gel Extraction Kit (Qiagen) and the steps were followed according to the kit's protocol. The agarose gel slices were initially solubilised in a buffer and incubated at 55^{O}C for 10 minutes. The mixture was then applied to a column with silica membrane that absorbed DNA in high salt conditions. Impurities like primers, enzymes, nucleotides, salts etc. are removed with ethanol wash. The pure DNA was finally eluted in autoclaved MilliQ water (pH 7.0, 20 – 30 µl per PCR reaction) and stored at -20°C until further required.

2.3.4. *Restriction digestion*

The insert (DNA) and vector are digested with selected restriction enzymes. For insert digestion, 1-3 µg of the target DNA was mixed with High-Fidelity restriction enzymes (1 unit per µg of DNA) in the presence of 1× fast digest reaction buffer (ThermoFisher Scientific). Likewise for vector digest, plasmid (~1 µg) was added to the mix containing High-Fidelity restriction

enzymes and 1× fast digest reaction buffer. The reaction mixture volume was made up to 50 µl with autoclaved milliQ (MQ) water and incubated for 1-2 hours at 37°C.

Post-restriction digestion, the plasmid and DNA inserts were purified using the Qiaquick PCR Purification Kit (Qiagen). According to the kit's protocol, the digests were mixed with a binding buffer and subsequently applied to a silica column that entraps the nucleic acids to the silica membrane under high salt conditions of the buffer. The impurities were washed away using ethanol but the DNA was eluted in 20 - 30 µl autoclaved MQ water.

2.3.5. *Ligation of the plasmid and DNA insert*

The plasmid and the DNA insert, digested with compatible endonucleases, were mixed at a molar ratio of 3:1 (insert: vector) using Equation 1 (50 ng of vector was used as the standard amount). For ligation, 1× T4 DNA ligase buffer and T4 DNA ligase enzyme were added to the plasmid and DNA mix. Ligation reactions using reagents from the Rapid DNA Ligation kit (Thermo Fisher Scientific) were mixed in 200 µl PCR tubes. The ligation mixture was made up to a volume of 20 µl and incubated at 22 ^{O}C for 15 – 30 minutes. Post-incubation, 5-7 µl of the ligation mixture was transformed into DH5α *E. coli* competent cells.

$$Insert\ amount = Insert\ size \div Vector\ size \times Vector\ amount \times 3$$

Equation 1: Calculating molar ratio of insert to vector DNA

2.3.6. *DNA Transformation in E. coli competent cells*

For cloning purposes, chemical competent cells of *E. coli* DH5α were transformed with the target DNA.

Preparation of competent cells A single bacterial colony was picked from a LB agar plate to inoculate 3 ml of LB starter culture and incubated at 37^{O}C overnight. A volume of 0.2 % of this culture was used to inoculate 100 ml LB media. The 100 ml preculture was placed in an incubator 37^{O}C and shaken at 150 rpm for 2-3 hours till the optical density (OD) of the bacterial cells (recorded at 600 nm in a UV-Vis spectrophotometer) reached 0.3 – 0.5.

Electrocompetent cells The cells were incubated on ice for 20 minutes. Incubation on ice was followed by harvesting at 4000 rpm for 10 minutes at 4^{O}C. The cell pellet obtained was washed with 50 ml chilled (at 4 ^{O}C) 10 % glycerol. The washed cells were again spun down at 4000 rpm for 10 minutes at 4 ^{O}C. Following washing of the subsequent cell pellet with 25 ml 10 % glycerol (at 4 ^{O}C), the cells were spun down again (as above). Finally, the cell pellet was suspended in 2 ml of chilled 10 % glycerol.

Chemical competent cells The cells were incubated on ice for 10 minutes and centrifuged at 4000 rpm for 10 minutes at 4^{O}C in sterile tubes. The cell pellet was suspended in 20 ml ice-cold 0.1 M $CaCl_2$ followed by incubation on ice for 20 minutes. The cells were again spun down at 4000 rpm for 10 minutes at 4^{O}C and the subsequent cell pellet was finally suspended in 5 ml of ice-cold 0.1 M $CaCl_2$.

The suspended solution of competent bacterial cells was aliquoted (50 – 100 µl) in 1.5 ml eppendorf tubes and flash-frozen with liquid nitrogen before storing in -80^{O}C. DH5α strain of *E. coli* cells were prepared chemically competent and used for transformation in cloning purposes whereas omp8 or BL21 (DE3) strain of *E. coli* cells were prepared electrochemically competent to be used for transformation during expression purposes.

Transformation For transformation, 10-20 ng of DNA (or 5-7 µl from the ligation mix) was added to 25-50 µl of the chemical competent DH5α cells of *E. coli* and placed on ice for 15-20 minutes. The cells were then given a heat shock at 42°C for 45 seconds and placed back on ice for 5 minutes prior to mixing with 900 µl of LB media. The mixture was incubated at 37°C for the revival of the transformed cells. After 45 minutes, the bacterial cells from the suspension were plated on LB agar.

2.3.7. *Plating of bacteria*

For the preparation of LB-agar plates and bacterial plating, the work area was sterilised by cleaning the bench with ethanol and a bunsen flame was kept on throughout. To prepare the agar-medium plates, 1.5 g of LB-agar powder was added per 100 ml water and sterilised by autoclaving. The selected antibiotic solution (also see section 2.1.3) was added to the autoclaved LB-agar media just before pouring into sterile petri dishes. The LB-agar plates were stored at -20°C for 1 month.

The LB-agar plate was incubated at 37°C for 15-20 minutes prior to bacterial plating. A glass rod was moulded into a spreader using the heat flame. Approximately, 150 µl of bacterial suspension was pipetted on the LB-agar plate. For plating, the spreader was dipped into 70% ethanol, passed through the flame for few seconds and then used for spreading the bacterial cells uniformly through the plate. The agar-plate was incubated at 37°C overnight for bacterial cell growth.

2.3.8. *Screening of the recombinant plasmids: Colony PCR*

The colonies obtained next day after bacterial plating were screened for positive clones using colony PCR. Around 10-15 colonies were picked at random, one at a time, using a sterile tip and patched at the inside bottom of a PCR tube. This was followed by streaking a small patch by the tip on a LB-agar plate (Amp^r/Kan^r). The LB-agar plate was incubated at 37°C overnight, to be used later for growing small-scale cultures of the positive clones.

For one PCR reaction, 6.5 µl of 2× EmeraldAmp® PCR Master Mix was added to the PCR tube, along with 0.2 µM of the universal primers (T7 Fwd/Rev for pET28a and pBAD Fwd/Rev for pBAD24b). The reaction volume for each PCR tube was made to 13 µl with sterilised MQ water. The colony patched at the bottom of each PCR tube acted as a DNA template for the synthesis and amplification of the insert DNA. The amplification time for the PCR reaction was set according to the extension rate of Emerald enzyme (1 kb per minute). The conditions for the colony PCR reaction were same as described section 2.3.1.1 and Table 2.4. The results of the cloning were analysed via agarose gel electrophoresis.

2.3.9. *DNA isolation from small-scale cultures*

The recombinant plasmid DNA from the LB-agar plates (streaked during colony PCR; also see section 2.3.7) was isolated from small-scale cultures. Whenever required, the stocks of vectors and recombinant plasmid constructs were prepared by DNA transformation, bacterial plating followed by DNA isolation and purification from small scale cultures.

A sterile tip was used to transfer a single colony from LB-agar plate to 10 ml of LB-media containing 1:1000 dilution of Amp (100 mg/ml) or Kan (50 mg/ml) antibiotic stock. The inoculated media was shaken at 180 rpm overnight (16-18 hours) at 37°C. The cells were spun

down the following day by centrifuging at 4000 rpm for 10 minutes. The supernatant was discarded while the cell pellet was processed to isolate DNA using the QIAprep Spin Miniprep Kit (QIAGEN). The manufacturer's protocol was followed for the plasmid/DNA isolation. Finally, the eluted DNA (in MQ) was stored at -20°C.

2.3.10. *DNA quantification*

DNA estimation was carried out using nanodrop method by NanodropLite Spectrophotometer (Thermo Scientific). 1 µl of autoclaved MQ water was used for blanking before measuring the absorbance of 1 µl target DNA sample at 260 nm.

2.3.11. *Automated DNA Sequencing*

The final confirmation of the recombinant plasmid constructs was carried out through automated DNA sequencing. Two positive DNA clones (100 ng/µl) for each recombinant construct were sent to Eurofins Genomics. The sequencing of each cloned plasmid was carried out in both forward and reverse directions, using universal primers (T7 and pBAD primers for pET28a and pBAD24 constructs respectively).

BLAST was used to check sequencing results by comparing the sequences of the cloned genes with those in KEGG or UniProt databases (Table 2.11).

2.4. Expression and purification of recombinant proteins

The target proteins were expressed in the outer membrane (OM) of the bacterial cells by using *E. coli* cells of Omp8 strain for large-scale growth. Omp8 is a porin deletion strain of *E. coli* (Kan^r) that lacks the major OMPs of the bacterium like OmpA, LamB, OmpF and OmpC. Whenever required, the proteins were also expressed as inclusion bodies (IBs) in Bl21 DE3 cells of *E. coli* to increase the yield.

2.4.1. *Transformation of DNA in electro-competent cells*

For expression purposes, the recombinant plasmid DNA was electroporated into competent cells of *E. coli* expression strain Bl21 (DE3) or Omp8 (also see section 2.3.6). An amount of 1-2 ng of DNA was electroporated into 50 µl electro-competent Omp8 cells (porin deletion strain) or Bl21 DE3 cells of *E. coli* in a Micropulse Electroporator at a pulse of 2500 V voltage, 25 µF capacitance. The electroporated cells were immediately transferred to 750 µl of

pre-warmed LB broth in a sterile eppendorf tube and revived at 37^{O}C. After 1 hour, 150 µl of the cells were plated on LB-agar plates (Amp^{r}/Kan^{r}) and incubated at 37^{O}C overnight (also see section 2.3.7).

2.4.2. *Overexpression of target proteins*

The large-scale overexpression of proteins required 8-10 litres of growth media for an optimum yield (≥ 5-10 mg). The details for the expression and growth conditions of the proteins used in the study are described in Table 2.8.

2.4.2.1. *Standard method for overexpression of proteins*

The single cell colonies of *E. coli* transformed with desired recombinant plasmid were used to inoculate pre-cultures of LB media. Using 1% v/v inoculum size conditions, a starter culture of 10 ml LB broth (Amp^{r}/Kan^{r}), grown at 37^{O}C for 16-18 hours, was used for the inoculation per litre LB media (Amp^{r}/Kan^{r}) in 2-litre conical flasks.

For large-scale expression, the inoculated media was incubated at 37°C whilst continuously shaking at 180 rpm. The cells were allowed to grow past the lag phase until the beginning of exponential phase which was carefully monitored by measuring optical cell density (OD_{600}) using a UV-Vis spectrophotometer (Eppendorf BioSpectrometer kinetic). The amount of time required to achieve the exponential phase varied depending on the *E. coli* strain used for growth (2-3 hours for Bl21 DE3 and 4-5 hours for Omp8). At an OD_{600} of 0.5-0.6, the target proteins were expressed by adding a specific inducer to the growth media. The pBAD24-cloned constructs were induced with 0.1 % w/v arabinose while pET28a cloned constructs were induced with 1 mM Isopropyl β-D-1-thiogalactopyranoside (IPTG). Post-induction, the cells were grown for 3 hours at 37°C or for 5 hours at 30°C. The final cell OD was typically around 1-1.5 (or above) and the bacterial cells were spun down by centrifugation (Avanti J-26 XP Centrifuge, Beckman Coulter Inc.) at 5000 rpm for 20 minutes at 4°C.

2.4.2.2. *Overexpression trials of Seleno-methionine substituted protein*

The method for expressing Seleno-methionine (SeMet) substituted protein is based on the inhibition of the methionine biosynthesis pathway protocol for *E. coli* (Van Duyne et al., 1993). The seleno-methionine substituted protein was expressed using LeMasters-Richards (LR) media that comprises 2 components: LR buffer and LR salts (Table 2.1). A single colony from the LB-

agar plate was used to inoculate 2-3 ml LB media. This starter culture was grown for 6-8 hours at 37°C till the OD reached around 0.8. It was then transferred to 100 ml of LR preculture which was grown at 37°C for 16-18 hours at 200 rpm. For 1 % v/v inoculation, 10 ml of LR preculture was used to inoculate 1 L of LR media (usually required 6-8 L of media for good yield). The LR media was grown at 37°C with continuous shaking at 150 rpm. Anywhere between an OD of 0.5 to 1.0, 0.01% v/v of 100× amino acid stock (100× AA; Table 2.1) was added to the cells to shut down methionine biosynthesis and incorporate seleno-methionine. Half an hour later, the induction step was done using 1 mM IPTG (for pET-cloned constructs) to express the protein overnight at 30°C at 150 rpm.

Table 2.8. Expression conditions of recombinant proteins.
The table enlists the cloning vectors, *E. coli* strains used for expression and growth conditions for all the proteins of this study.

Protein	Expression as (*E. coli* strain)	Plasmid	Antibiotic added	Induction	Temperature (Time post-induction)
OmpE35	OMP (Omp8)	pBAD24	Ampicillin	Arabinose	37°C (3 hours)
OmpE36	OMP (Omp8)	pBAD24	Ampicillin	Arabinose	37°C (3 hours)
OmpK36	OMP (Omp8)	pBAD24	Ampicillin	Arabinose	37°C (3 hours)
OmpU	OMP (Omp8)	pBAD24	Ampicillin	Arabinose	37°C (3 hours)
OmpUΔN	OMP (Omp8)	pBAD24	Ampicillin	Arabinose	30°C (5 hours)
OmpUΔN	IB (Bl21(DE3))	pET28a	Kanamycin	IPTG	37°C (3 hours)
OmpT	OMP (Omp8)	pBAD24	Ampicillin	Arabinose	30°C (5 hours)
OmpT	IB (Bl21(DE3))	pET28a	Kanamycin	IPTG	37°C (3 hours)
OmpT (6×His)	OMP (Omp8)	pBAD24	Ampicillin	Arabinose	37°C (3 hours)
OmpT (Se-Met)	OMP (Omp8)	pET28a	Kanamycin	IPTG	37°C (3 hours)
OmpTΔL8	IB (Bl21(DE3))	pET28a	Kanamycin	IPTG	37°C (3 hours)

2.4.3. *Outer membrane protein extraction*

The following subsections describe the extraction strategies employed for the isolation of proteins expressed in the outer membrane (OM) or expressed as the inclusion bodies (IBs). The list of buffers used during OMP extraction from OM or solubilisation of IBs are listed in Table 2.9.

2.4.3.1. *Extraction of OM-expressed proteins*

The cell pellet was resuspended in Tris-saline buffer (20 mM Tris HCl and 300 mM NaCl, pH 8.0) and lysed with a cell disrupter (0.75 kW; Constant Systems; one pass at 23 kpsi) at 4°C. After lysis, the cells were ultracentrifuged at 42,000 rpm (Beckman Coulter Inc.) using a 45 Ti rotor for 45 min at 4°C. The resulting membrane pellet was extracted twice with 0.5% N-lauroylsarcosine (sarkosyl) detergent (in 20 mM HEPES, pH 7.5; Table 2.9) to solubilise the inner membrane fraction followed by ultracentrifugation (45 Ti rotor) at 42,000 rpm for 30 minutes at 4°C. The inner membrane fraction obtained in the form of supernatant was removed while the cell pellet containing outer membrane (OM) fraction was resuspended in 50 ml of 1% lauryldimethylamine-oxide (LDAO) buffer (10 mM HEPES, 50 mM NaCl, pH 7.5; Table 2.9). The LDAO suspension was kept for constant stirring overnight at 4 °C to solubilise the targeted outer membrane protein. Next day, the LDAO extract was ultracentrifuged using a 70 Ti rotor (Beckman) at 50,000 rpm at 4°C for 30 minutes. The supernatant containing the solubilised outer membrane protein was collected while the pellet was discarded.

2.4.3.2. *Solubilisation of IB-expressed proteins*

The bacterial cells expressing the inclusion bodies (IBs) were harvested by centrifuging at 5000 rpm for 20 minutes and lysed using the cell disrupter (as described in section 2.4.3.1). The inclusion bodies were collected in the form a cell pellet by ultracentrifugation at a low speed of 10,000 rpm for 20 minutes (at room temperature). 1% Triton, solubilised in an Inclusion Body (IB) buffer (50 mM NaCl and 10 mM HEPES, pH 7.5; Table 2.9), was used to remove residual membranes from IB pellet. Following ultracentrifugation at 10,000 rpm for 10 minutes (at RT), residual membrane fraction was removed in the form of supernatant while the IBs were obtained in the form of cell pellet. The pellet was washed twice in the IB buffer to remove any residual Triton, each step followed by centrifuging at 10,000 rpm for 10 minutes. Cells were re-suspended in 8 M Urea (in IB buffer; Table 2.9) and continuously stirred at RT to solubilise and denature the target protein overnight. The urea extract was then subjected to ultracentrifugation at 50,000 for 30 minutes (at RT) and the supernatant containing the denatured protein was added drop-wise to 1% LDAO in IB buffer such that urea concentration was 10-fold diluted in the resulting solution. The protein was allowed to fold *in vitro* by constantly stirring at RT for 2-3 days and was finally applied to an ion-exchange column for purification.

2.4.4. *Purification of recombinant proteins*

Protein purification was carried out using ion-exchange chromatography for tag-less proteins (IEX) and immobilised metal affinity chromatography (IMAC) for his-tagged proteins. In addition, the protein purification steps typically employed two rounds of size exclusion chromatography (SEC). Whenever required, a second IEX followed by SEC was used at the end stages of purification to increase protein purity or for exchange purposes (crystallisation). The list of buffers used during elution and purification are listed in Table 2.9.

2.4.4.1. *Purification by Anion-Exchange chromatography (IEX)*

The isoelectric points (pI) of the proteins, used in the study, ranged between 3.5– 4.5. The use of purification buffers at pH 7.5 rendered negative charge to the proteins and as a result, a positively charged anion-exchanger was applied for protein purification. Elution of tag-less proteins isolated from IBs was performed using gravity-flow anion-exchange columns and proteins isolated from OM were subjected to pre-packed anion-exchangers (from GE Healthcare).

Gravity-flow columns

The LDAO extracts isolated from the inclusion bodies were subjected to gravity-flow columns prepared using 10 ml of Q-Sepharose Fast Flow resin (GE Healthcare). The columns were initially charged with 2-3 CV (column volume) of high salt IEX Buffer B solution and then equilibrated by running 5-10 CV of low salt IEX Buffer A (Table 2.9). The LDAO extract was filtered using a 0.45 µm MF-Millipore membrane filter (Merck) before loading on the equilibrated anion-exchange column. The flow-through was discarded and the column was washed with 10 CV of IEX Buffer A (in 0.1 % LDAO). The elution of the protein was done by passing 2-3 CV of IEX Buffer B (in 0.1% LDAO) through the column and the flow-through was collected in a 15 ml falcon tube.

Pre-packed HiTrap Q columns

To elute the proteins isolated from the membrane fractions, the LDAO extracts were loaded on pre-packed HiTrap-Q HP (5 ml, GE Healthcare) columns and the protein separation was monitored using an AKTA protein purification system (ÄKTA FPLC from GE Healthcare). HiTrap Q equilibration was done by passing 15 CV of IEX Buffer A after charging the column with 5 CV of IEX Buffer B. The column was loaded with filtered LDAO extracts, washed with

10 CV of IEX Buffer A and eluted with a gradual increase in salt gradient (150 mM to 1 M of NaCl over 5 CV).

Pre-packed Resource Q and MonoQ columns

The impure OMP extracts were subjected to another anion exchanger, Resource Q (6 ml volume, GE Healthcare) column. The column was first charged with 2 CV of IEX Buffer B and then equilibrated with 5 CV of IEX Buffer A. After elution through HiTrap-Q HP column, the sample was buffer exchanged (see section 2.4.6) to low salt buffer before applying to Resource Q column. The column was washed with 10 CV IEX Buffer A and target protein was separated with a salt gradient using IEX Buffer B (150 mM to 1 M of NaCl over length of 10 CV).

Some of the protein samples required additional strategies to get rid of stubborn impurities which were not removed through SEC purification columns. For such samples, the protein fractions obtained from the SEC runs, were further subjected to another anion exchange column (Mono Q 10/100 GL; GE Healthcare) using the AKTA system. The column equilibration and protein elution was done as described previously (see section 2.4.4.1) in 0.1% LDAO using IEX Buffers A and B (Table 2.9). The protein eluted in high salt buffer was either subjected to another SEC column (in C_8E_4 buffer) or buffer exchanged (see section 2.4.6) to C_8E_4 buffer (Table 2.9) for crystallisation.

The protein separation and fraction collection was monitored through Unicorn software on an AKTA FPLC. The eluates from the peak fractions of HiTrap Q and Resource Q columns were collected and assessed using SDS-PAGE (see section 2.4.7) to pool the purest fractions for further purification.

2.4.4.2. *Elution by Immobilised Metal Affinity chromatography (IMAC)*

The protein expressed with the histidine-tag (six His residues) was eluted using immobilised metal affinity chromatography (IMAC). The gravity-flow columns were prepared using 10 ml of chelating Sepharose Fast Flow IMAC resin (GE Healthcare). The IMAC media was charged with Ni^{+2} ions by passing 2 CV of 0.1 M $NiCl_2$ solution through the column and equilibrated with 10 CV of IMAC buffer solution (Table 2.9) in 0.1% LDAO. The protein extract isolated from the cell fractions was subjected to Ni^{+2} charged IMAC column. The column was washed with 15 CV of 25 mM imidazole (Imidazole buffer: 50 mM NaCl, 10 mM HEPES, pH

7.5 and 0.1% LDAO; Table 2.9). For protein elution, 3 CV of 250 mM imidazole (in Imidazole buffer; Table 2.9) was passed through the column. The eluates were collected in 50 ml falcon tubes for purification by size-exclusion chromatography (SEC).

Table 2.9. Buffers used during protein extraction, elution and purification.

Buffer Name	Buffer Composition	Use	pH	Detergent
OMP extraction from OM				
Tris-saline buffer	150 mM Tris HCl, 300 mM NaCl	Cell lysis and cell pellet resuspension	8.0	-
Sarkosyl buffer	20 mM HEPES	Solubilise inner membrane proteins	7.5	0.5% Sarkosyl
LDAO buffer	10 mM HEPES, 50 mM NaCl	Solubilise OMP from IB	7.5	1% LDAO
OMP extraction from IB				
Triton-IB buffer	50 mM NaCl,10 mM HEPES	Solubilise membrane proteins (IB wash)	7.5	1% Triton
Anion-exchange chromatography (IEX)				
IEX Buffer A	150 mM NaCl, 10 mM HEPES	Column Equilibration	7.5	0.1% LDAO
IEX Buffer B	1 M NaCl, 10 mM HEPES	Elution	7.5	0.1% LDAO
Immobilised metal affinity chromatography (IMAC)				
IMAC buffer	20 mM Tris, 300 mM NaCl,10 mM HEPES	Column Equilibration	7.5	0.1% LDAO
Imidazole buffer	20 mM Tris, 300 mM NaCl NaCl,10 mM HEPES	Washing/Elution	7.5	25 /250 (mM) imidazole
Size-exclusion chromatography (SEC)				
SEC buffer	100 mM NaCl, 10 mM HEPES	Column Equilibration and Elution	7.5	0.1% LDAO
C_8E_4 buffer	100 mM NaCl, 10 mM HEPES	Final purification (for crystallisation) + exchange	7.5	0.45% C_8E_4

2.4.4.3. *Purification by Size Exclusion chromatography (SEC)*

The protein samples were concentrated by centrifuging (also see section 2.4.5) to an appropriate volume (≤ 5 ml) for purification through size-exclusion chromatography (SEC) columns using FPLC. Depending on the protein amount and molecular weight, three types of SEC prep grade (PG) columns (GE Healthcare) were used for protein purification: HiLoad

16/600 Superdex 200 PG column (120 ml), HiLoad 26/600 Superdex 200 PG column (320 ml) and Superdex 200 PG 10/300 GL analytical column (24 ml). The columns were equilibrated with 0.05 % LDAO in SEC buffer (10 mM HEPES, 100 mM NaCl, pH 7.5; Table 2.9). For 120 ml column, the protein sample in a 5 ml tubing loop was injected into the column using a syringe and the protein fractions were collected in volume of 3 ml in falcon tubes using a fraction collector. A typical purification involved one round of SEC column (mostly in 0.05% LDAO) to isolate the purest fractions of the protein (impure fractions required two rounds of purification through SEC).

The final step of protein purification was done through SEC column equilibrated in C_8E_4 buffer (Table 2.9) containing 0.45% C_8E_4 for crystallisation. The purity of the peak fractions was assessed using SDS-PAGE (see section 2.4.7), following which the purest protein samples were pooled together and typically concentrated to 10-15 mg/ml (see section 2.4.5), flash-frozen in LN2 and stored at -80°C.

2.4.5. *Protein concentration*

The concentration of protein samples was achieved using Amicon Ultra-15 Centrifugal Devices (molecular weight cut-off size of 50 kDa or 100 kDa). The samples were spun at 4000 rpm at 4°C until a required volume was obtained. To inject the samples for SEC, the protein sample was concentrated to less than 5 ml (typically around 3 ml) volume. For C_8E_4 purified fractions, the protein was concentrated down to 10-15 mg/ml and aliquoted in ~100 µl fractions in eppendorf tubes for storage at -80°C.

2.4.6. *Buffer exchange*

The Amicon Ultra-15 Centrifugal Devices (molecular weight cut-off size of 100 KDa) were also used to exchange protein buffer. The sample was centrifuged at 4000 rpm at 4°C until the volume was reduced to 1 ml. The tube was filled with 15 ml of desired buffer and centrifuged again at 4000 rpm till the volume was reduced to 1 ml. The process was repeated at least twice to achieve buffer exchange.

2.4.7. *SDS-PAGE for protein analysis*

The quantity, purity and size of proteins were visualised through sodium-dodecyl sulphate polyacrylamide gel electrophoresis (SDS-PAGE). The apparatus and reagents for SDS-PAGE

were purchased from ThermoFischer Scientific. The protein samples (in the form of LDAO extracts, purified OMP fractions etc.) were loaded on the NuPAGE 4-12% Bis-Tris Plus Gels. Due to heat modifiable nature of OMPs (Beher et al., 1980), the proteins were loaded as boiled (B) and non-boiled (UB) samples on the SDS-PAGE. A volume of 15 µl was used for loading each sample prepared in 4X Bolt™ LDS sample buffer along with prestained protein ladder (10 - 250 kDa). The samples were boiled for 5-10 minutes at 100°C prior to loading. The apparatus was assembled using XCell SureLock™ Mini-Cell Electrophoresis System (ThermoFischer Scientific) the SDS-gels were run at 165 V for 70-80 minutes.

After the run, the gel cassette was disassembled to wash the gels in distilled water by microwaving for 1 minute followed by shaking for 3 minutes. This step was repeated at least three times to get rid of any residual SDS that can inhibit effective staining of the gel. The gel was finally stained in coomassie stain (0.01 % Coomassie Blue R-250, 10% ethanol, 30 mM HCl) for 20 minutes and destained overnight in distilled water. The pictures of the SDS-PAGE gels were taken through a Bio-Rad Gel Doc EZ Imager (Image Lab/ PC Windows software).

2.4.8. *Native PAGE for protein analysis*

The Native PAGE reagents were purchased from ThermoFisher Scientific. The samples for the Native PAGE were made of volume 10 µl (each), prepared with 1% n-Dodecyl β-D-maltoside (DDM), 1× Native PAGE sample buffer and 0.25% Native PAGE G-250 additive. The NativePAGE 4-16% Bis-Tris Protein Gels were used with the Native PAGE Anode Buffer (1×) and Native PAGE Dark Blue Cathode Buffer (1×) which were prepared following the manufacturer's protocol. The samples were run at 165 V for 100 minutes using the XCell SureLock™ Mini-Cell electrophoresis tank.

After the run, the gel was transferred to 100 ml fixing solution (40 % methanol, 10 % acetic acid), microwaved for 45 seconds and incubated on an orbital shaker for 15 minutes. This process was repeated twice before the gel was removed from the fix solution and placed in 100 ml Destain Solution (8 % Acetic acid). The gel was incubated overnight to remove the excess stain and photographed next day using Bio-Rad Gel Doc EZ Imager (Image Lab/ PC Windows software).

2.5. Determination of protein concentration

2.5.1. *Bicinchoninic acid assay (BCA) method*

The Pierce BCA Protein Assay Kit (ThermoFisher Scientific) was used to estimate the protein concentration. The BCA working reagent (WR) was prepared by mixing two reagents of the BCA assay kit in a ratio of 50:1 (Reagent A: Reagent B). 500 µl of WR was added to 10 µl of the protein sample and incubated with a slight shaking at 37°C for 45 minutes. Post-incubation, the samples were measured at 562 nm in the spectrophotometer, since BCA-Cu^{+} complex exhibits strong linear absorbance at this particular wavelength with increasing protein concentrations. BSA protein standards (2 µg, 4 µg and 8 µg) were used to compare and calculate the concentration of the target protein sample.

2.5.2. *UV absorption method*

Another method of protein concentration was via absorption at 280 nm wavelength in the NanoDrop 2000 benchtop spectrophotometer (Thermo Fisher Scientific). The absorbance values ($\varepsilon^{0.1\%}$) of 0.1 % (=1g/L) solutions measured in a 1 cm cuvette were obtained by entering the specific amino acid sequence of the expressed protein into the ProtParam tool (Table 2.11). Equation 2 was used to calculate protein concentration in mg/ml using A_{280} nm.

$$Concentration\ \left(\frac{mg}{ml}\right) = (A/\varepsilon 0.1\%)$$

Equation 2 – Calculating concentration of a protein solution in mg/ml.

A = absorbance at 280 nm,

$\varepsilon^{0.1\%}$= 0.1% extinction coefficient

2.6. Crystallisation

The process of crystallisation completes by achieving a special phase equilibrium between a protein-rich phase (in the form of a well-ordered crystal) and a saturated protein solution.

2.6.1. *Crystal screens*

Frozen aliquots of protein were thawed at room temperature for setting up initial screens by the sitting-drop method. Three commercial membrane crystallisation screens from Molecular Dimensions: MemGold1 (MG1; Newstead et al., 2008), MemGold2 (MG2; Parker and Newstead

2012) and Morpheus (Gorrec et al., 2015) were used for the initial screening. An automated Mosquito crystallisation robot (TTP Labtech) was employed to set up the screens in MRC 96-well crystallisation plates (Molecular Dimensions). 75-80 µl of screen conditions were manually pipetted into the reservoir wells of 96-well plate. The robot was used to dispense 200 nl + 200 nl and 200 nl + 150 nl of protein + reservoir solution in the two sample wells. The screen plates were incubated at 20°C and checked periodically for the growth of protein crystals.

2.6.2. *Optimisation of crystal hits*

The initial crystal hits were manually optimised using two types of vapour diffusion method: sitting-drop and hanging-drop. For crystal optimisation, the original hit condition with required pH was fine screened as follows.

2.6.2.1. *Vapour diffusion using hanging-drop method*

VDX 24-well hanging drop plates (Hampton Research) were used for setting up hanging-drops of the protein sample. The crystallisation cocktail, with varying PEG amount (± 10%), was pipetted into the reservoir wells (500 µl) such that a precipitant gradient was set up across an entire row of the plate for the same condition. For each well, the protein was mixed with its reservoir solution as two drops in volumes of 1 + 1 µl and 1.5 + 1 µl, respectively. The drops were placed on 18 × 0.22 mm or 22 × 0.22 mm siliconised glass cover slides (Hampton Research) and placed upside down by inverting the slides on the top of individual wells. The grease was applied on the raised rims of the wells to seal the drops. The plates were stored at 20°C and checked periodically.

2.6.2.2. *Vapour diffusion using the sitting-drop method*

Intelli-Plate 48-3 well plates from Art Robbins Instruments (Hampton Research) were used to set up sitting drops for crystal optimisation. The crystallisation cocktail, with varying PEG amounts, was pipetted into the reservoir wells (200 µl) similar to as described above (section 2.6.2.1). The protein was mixed with its reservoir solution in volumes of 1 + 1 µl and 1.5 + 1 µl, respectively, in the drop wells. The drops were sealed by applying transparent scotch tape across the rows of 48-well plates. The optimised plates were stored at 20°C and checked periodically.

2.6.2.3. *Co-crystallisation trials with antibiotics*

The antibiotic solutions were prepared using the desired concentration of antibiotic dissolved in buffer solution (in 10 mM HEPES, 100 mM NaCl, pH 7.5). The antibiotic concentration for the co-crystallisation trials were varied from 0.1 M to 0.5 M. Co-crystallisation of proteins with antibiotics was enforced in crystal-optimised conditions via two independent approaches using either hanging-drop or sitting drop method (sections 2.6.2.1 and 2.6.2.2). One method was to incubate protein and the antibiotic solution for an hour at room temperature or 4°C prior to setting up the crystal drops. A second approach adopted was to mix protein sample with the antibiotic solution and dilute to 1 ml (using buffer solution 10 mM HEPES, 100 mM NaCl, pH 7.5). The mixture was incubated at room temperature for 30 minutes and then concentrated together at 4°C (4000 rpm; section 2.4.5) to the original volume. The co-concentrated protein-antibiotic mix was used to set crystal drops and the plates were stored at 20°C. Sometimes, the pre-formed protein crystal (or crystals) were soaked in a 1-2 µl drop of the antibiotic solution for overnight (or a few hours depending on crystal stability) before crystal harvesting.

2.6.2.4. *Heavy-atom incorporation*

Different heavy atoms (HAs) [Platinum (Pt), Lead (Pb), Iridium (Ir) and Osmium (Os)] were procured from Hampton Research in the form of powder [Potassium tetrachloroplatinate- K_2PtCl_4, Lead acetate trihydrate- $Pb(CH_3COO)_2.3H_2O$, Potassium hexachloroiridate- K_2IrCl_6, and Potassium osmate dehydrate- $K_2OsO_4.2H_2O$]. HA was dissolved in the mother liquor to 2-10 mM and 1-2 µl drops of HA solution was mixed with the protein crystal drop. The selected crystals were picked using suitable-sized loops and transferred to HA solution. After few hours of incubation (1-2 hours), the crystals were backsoaked into the mother liquor before harvesting using appropriate cryoprotection (see section 2.7).

2.7. Crystal harvesting

Unless the crystallisation condition contained more than 25% of PEG 400 as the precipitant, the selected crystals were cryoprotected (Teng 1990) prior to harvesting. A default cryoprotectant solution is composed of 200 µl of optimised condition with 20% glycerol and 0.4% C8E4 detergent. The crystals were dipped in 1-2 µl of cryoprotectant solution for a few seconds just before the harvest. The optimum size crystals were harvested using suitably sized loops (Hampton Research). The crystals were immediately flash-frozen by transferring to the

liquid nitrogen and stored in dewars (filled with liquid N_2) prior to shipment to Diamond Light Source (DLS).

2.8. X-ray diffraction and structure determination

X-ray diffraction data of crystals was processed as follows.

2.8.1. *In-house screening of crystals for diffraction*

Protein crystals were first screened through in-house X-ray diffraction. Crystals were mounted on a copper anode Rigaku MSC microfocus generator and data was collected on Raxis IV^{++} image plate detector. Two diffraction images per crystal were collected, at relative phi angles of 0° and 90° and were indexed in iMOSFLM (Leslie, 2006). Crystals were ranked based upon diffraction pattern and resolution, and accordingly, the best ones were sent to DLS.

2.8.2. *Diffraction dataset collection*

Datasets were collected at Diamond Light Source (DLS, Didcot, Oxfordshire, UK) by Dr. Arnaud Baslé. Among the five automated beamlines of Diamond (I02, I03, I04, I04-1 and I24) used for macromolecular crystallography, the available beamline was used for the diffraction of the crystals. For data collection, the crystal was rotated around a single axis by small increments (~ 0.1°) while exposed to X-rays and diffraction images were collected for each increment using fast readout and shutter-less operation of the Pilatus detector (Broennimann et al, 2006).

2.8.2.1. *Single-wavelength anomalous diffraction (SAD)*

Single-wavelength anomalous diffraction (SAD) data was collected for Se-Met substituted protein (Se-Met OmpT) and heavy-atom incorporated protein crystals (HA-incorporated-OmpT). The heavy atoms in the protein crystal act as anomalous scatterers and provide important phase information for structure determination (Hendrickson 2014). A fluorescence scan was performed to determine the maximum wavelength for SAD data collection. The optimal wavelength values for the absorption edges of other heavy atoms was identified online using the Heavy-atom-choices webpage (http://xray0.princeton.edu/~phil/Facility/heavyatompick.html). Based on the fluroscence scan, peak wavelengths chosen for different heavy atoms were: 0.9792 Å for selemium (Se; 12.658 eV

and K absorption edge), 1.072 Å for platinum (Pt; 11.564 eV and L-III absorption edge) and 1.1055 Å for iridium (Ir; 11.2152 eV and L-III absorption edge).

2.8.3. *Data processing*

The data indexing was performed by XDS (Kabsch 2010. For data scaling and reduction, Aimless (Evans and Murshudov 2013) within CCP4 (Winn et al., 2011) was used. Typically, 5% of the data reflections were kept unmerged (as R_{free}; during scaling and merging of the data) for computing statistics during model refinement (Brünger 1992). During scaling, the quality of the data was assessed based on different factors like reliability or R-factor (Rmerge/Rpim), signal to noise ratio ($I/\sigma I$), correlation coefficient ($CC_{1/2}$), and completeness. Whenever required, scaled data from the xia2 pipeline (Winter 2010), an automated system for X-ray data processing, were directly used for molecular replacement.

2.8.3.1. *Phase information by Molecular Replacement (MR)*

Molecular replacement is a phasing technique used only when a search model, with a crystal structure available in the PDB, is structurally similar to the target molecule. As a result, the phases calculated from the search model are used to estimate the phases for the unknown structure of target molecule. In general, the search model should have more than 20-25% of sequence identity with the target molecule in order to be used for molecular replacement.

To solve the structure of target proteins in this study, molecular replacement was done using either MolRep (Vagin and Teplyakov 1997) or PHASER (McCoy et al., 2007) within CCP4i (Winn et al., 2011) or PHENIX (Adams et al., 2010). In MolRep, the potential solutions were monitored by observing the 'contrast score', followed by manual inspection of cell symmetry and packing in COOT (Emsley and Cowtan 2004). In PHASER, the LLG (log-likelihood gain) values of rotation and translation search functions are used to compute the 'Z score' to identify a definite solution, followed by manual inspection of the solution in COOT for any symmetry clashes. Table 2.10 enlists the structures of recombinant proteins solved by molecular replacement method in this study.

2.8.3.2. *Phase information by Experimental phasing*

The anomalous scattering caused by the HA atoms (in OmpT-HA and Se-Met OmpT crystals) was used to derive the phase information required for experimental phasing. SAD data were auto-processed by SHELX C/D/E (Sheldrick 2008) pipeline using a graphical user interface,

hkl2map (Pape and Schneider 2004). SHELX program sets up files and calculates the estimated substructure structure factor amplitude (FA) (*shelxc*), finds heavy atoms (*shelxd*; Sheldrick, 2010) and modifies the density (*shelxe*; Thorn and Sheldrick 2015) to obtain the electron density map. The solution output is judged on the basis of best CFOM value (≥ 35 for a good SAD solution), CC for partial structure against native data (if available) and manual inspection in COOT.

Table 2.10. List of structures solved by molecular replacement with search models and sequence identity to the target.

Structures	Search Model	Sequence identity	MR method
OmpE35	2ZFG (OmpF of *E. coli*)	80%	MolRep
OmpE36	2J1N (OmpC of *E. coli*)	66%	MolRep
OmpK36	2OSM (OmpK36 of *K. pneumoniae*)	94%	MolRep
OmpU	3UPG (OmpF of *S. typhi*)	26%	PHASER
OmpUΔN	OmpU (this study)	99%	MolRep
OmpT-monomer; IB expressed	OmpU (this study)	19%	PHASER
OmpT-trimer; IB expressed	OmpT-monomer; IB expressed (this study)	100%	MolRep
OmpT; OM expressed	OmpT-monomer; IB expressed (this study)	100%	PHASER
OmpTΔL8	OmpT-monomer; IB expressed (this study)	99%	PHASER

Another program applied to determine the phases and build an initial model was by using AutoSol (Terwilliger et al., 2009), an experimental phasing pipeline in PHENIX. The input data files were either provided as premerged .sca or .mtz files (after scaling in Aimless). The SAD data obtained from the diffraction of Se-Met substituted OmpT and HA-incorporated OmpT crystals was used for attempts to solve the structure via experimental phasing.

2.8.4. *Model building, refinement and validation*

The electron density maps obtained from the molecular replacement were improved manually by model building in COOT (Emsley and Cowtan 2004) followed by refinement cycles in Refmac5 (Murshudov et al., 1997) within CCP4i or by Phenix.Refine (Afonine et al., 2012) in PHENIX. Electron density maps for model building are combination of: 2Fo-Fc (density map, weighted towards experimental data) and Fo-Fc (difference map) where Fo are the structure

factors observed from the diffraction pattern and Fc are the structure factors calculated from the model. Simulated annealing was used to generate an omit map in PHENIX (with starting temperature of 1000K). The reliability of the model (R-factor) was assessed by comparing the measured amplitudes with those calculated from the model (R_{free} for unmerged data reflections and R_{work} for the working model). Models were validated using COOT validation parameters and the online validation software program, MOLPROBITY (Chen et al., 2010) to check the geometry and Ramachandran outliers in addition to clashes.

2.9. Antibiotic binding and transport assays

In vitro uptake of antibiotics (see Appendix Figure 4) through the target OMPs was performed using disc-diffusion assays, bacterial growth rates and liposome swelling assays, described below.

2.9.1. *Disc diffusion assay*

The recombinant constructs of the target proteins were electroporated in omp8 competent cells (see section 2.3.6). The single colonies were used to inoculate small-scale LB media cultures (3 ml per target protein) and incubated at 37°C overnight (16-18 hours). For each protein, the bacterial cells were diluted to 0.3-0.4 OD using sterilised LB media. The omp8 cells were transformed with an empty pBAD24 plasmid and used as a negative control for the assay (referred to as pBAD). 200 µl of diluted cell sample was plated on pre-warmed LB-agar plates (Amp^r + 0.01 % Arabinose) using a glass spreader (see section 2.3.7). The plates were incubated at room temperature for 2 hours or for 1 hour at 37°C. For the assay, drops of 25 µl antibiotic solution (8 mg/ml) were pipetted on the filter discs (12 mm size) and left at room temperature to dry for 2-3 hours. Three discs were placed per LB-plate (spread with bacterial cells) and incubated at 37°C. Next day, the plates were assessed to calculate the radii of zone of lysis for each target protein and compare with that of a negative control. The radii were calculated with the help of a ruler for each individual measurement.

2.9.2. *Bacterial growth assay*

The overnight bacterial cultures of target proteins in 3 ml LB-media (see above section 2.9.1) were diluted to 0.3-0.4 OD and aliquoted in wells of a microplate reader. Sterilised LB media (Amp^r), 0.01 % arabinose and desired antibiotic solution (with varying concentration) were added to the wells. Each well (150 µl volume) of the microplate was aliquoted with 75 µl

cells + 65 µl LB-media + 5 µl of arabinose + 5 µl of antibiotic solution. The omp8 cells were also transformed with an empty pBAD24 plasmid and used as a negative control for the assay (referred to as pBAD). The microplate was placed in a plate reader to incubate by continuous shaking 180 rpm for 16 hours at 37°C. The cell OD was measured every 20 min during the incubation by the plate reader. After 16-hour incubation, the growth rates of the cells expressing the target protein were assessed in the presence of different concentrations of antibiotics and compared with the cell growth of negative control.

2.9.3. *Liposome swelling assay (LSA)*

The liposome suspension mixture was prepared by mixing 100 mg egg phosphatidycholine (solubilised in 25 mg/ml in chloroform; Avanti Polar Lipids) and 2.3 mg dihexadecyl phosphate (dissolved in 1 ml of chloroform). For each protein, 100 µl from the liposome suspension was aliquoted in glass tubes and vacuum dried for 2 hours. The thin dried lipid layer was then suspended in 100 µl water along with the addition of protein, such that all proteins have the same millimolar amount in each experiment set-up. This mixture was sonicated for 2 min before leaving for drying overnight in a dessicator. The control liposome mixture was prepared by adding buffer without protein into the liposome suspension. The next day, 200 µl of 12 mM of stachyose solution (in 10mM HEPES, pH 7.5) was added to the overnight dried proteolipid film and pipetted gently before proceeding to the swelling assay. For each assay, 5 µl of proteoliposome mixture was added to 100 µl of substrate solution (8-15 mM depending on the empirical, iso-osmotic concentrations of these substrates that show no change in the optical density values when measured with the control liposomes) and mixed rapidly before measuring the optical density at 400 nm for 60 secs at a 5 sec interval. The swelling assay rate for glycine permeation through OmpF of *E. coli* was taken as 100% (as reference). To ensure equimolar amounts of proteins, 15 µg for a protein with a molecular weight of 25 kDa was set as the standard to calculate the amounts of all proteins needed for the assays.

2.10. Electrophysiology

The biophysical characterisation of proteins was performed using lipid bilayer electrophysiology via single-channel or multi-channel experiments. In this study, the proteins of *Vibrio cholerae* (OmpU, OmpT, OmpUΔN and OmpTΔL8) were characterised through electrophysiology experiments.

2.10.1. *Multichannel bilayer experiments*

The multichannel bilayer experiments were used to compute conductance and ion-selectivity of the target OMPs.

2.10.1.1. *Ion-selectivity experiments*

The ion-selectivity measurements were done as described elsewhere (Benz et al., 1985)**.** The instrumentation consisted of a Teflon cuvette partitioned in the middle by a thin wall containing a 2 mm^2 small hole. The two chambers of the cuvette were each filled with 5 ml of salt solution (mostly buffered in 10 mM HEPES, pH 7.0) and dipped in calomel electrodes (Metrohm, Herisau, Switzerland), one connected to an amplifier and the other to an electrometer (Keithley 427) to monitor current. 10 mg/ml DPhPC (diphytanoylphosphatidylcholine) in n-decane butanol was used for prepainting while 20 mg/ml DPhPC (in chloroform) was used to form the black lipid bilayer across the hole using a teflon loop. At a constant voltage of 20 mV, upon forming stable bilayer, a certain amount of protein was added to increase the conductance up to 100-200-fold so as to allow the insertion of multiple channels (100-200). High molar salt solution (3 M NaCl, 10 mM HEPES, pH 7.0) was then added to create a desired salt gradient and the zero-membrane potentials were measured from the connected electrometer. The study with the low salt gradient involved 0.01 M KCl in bath solution to achieve 10-fold KCl concentration with the stepwise addition of high molar salt. Likewise, the high salt gradient measurement was done by achieving 10-fold concentration of 0.1 M KCl (in bath solution). The resting membrane potential (V_m) was calculated using the Goldmann-Hodgkin-Katz equation (Equation 3).

$$V_m = \frac{RT}{F} \ln \frac{(P_{cation}[cation]_o + P_{anion}[anion]_i)}{(P_{cation}[cation]_i + P_{anion}[anion]_o)}$$

Equation 3 – Goldmann-Hodgkin-Katz equation.

V_m = Resting membrane potential, R = universal gas constant (8.314 $J.K^{-1}.mol^{-1}$)

T = temperature in Kelvin (K = °C + 273.15), F = Faraday's constant (96485 $C.mol^{-1}$)

P_{cation}/P_{anion} = relative membrane permeability of cation/anion

$[cation]_o/[anion]_o$ = concentration of cation/anion in the extracellular medium

$[cation]_i/[anion]_i$ = concentration of cation/anion in the intracellular medium

2.10.1.2. *Conductance measurements*

To compute the conductance of target proteins, the instrumentation for multichannel was set up in a similar manner as described above (section 2.10.1.1). The lipid bilayer experiments

were carried out in 1 M KCl buffer solution (10 mM HEPES. pH 7.5). A certain concentration of protein (5 µl of $10^7/10^8$ dilution of 10 mg/ml protein stock) was added to both sides (cis and trans) of the membrane and 20 mV potential was applied through the attached electrodes. The gradual increase in the channel insertions induced stepwise increase in the conductance which was printed on a chart. The steps indicating the conductance increase were manually counted off the chart and plotted to calculate the average conductance (at least 80-100 channels).

2.10.2. *Single channel experiments*

All single channel measurements were done with a 25 µm thick Teflon film partitioning a cuvette, where each formed chamber contained 10 mM HEPES buffer with 1 M KCl at pH 7.0 (unless stated otherwise). The Teflon film was pierced with a 75 µm wide aperture that was used for forming a lipid bilayer from n-pentane solution of 5 mg/ml diphytanoylphosphatidylcholine (DPhPC, Avanti Polar lipids). The electrodes of Ag/AgCl (World Precision Instruments, Sarasota) were used to measure current, with one electrode grounded (at the cis side of the membrane) and the other electrode (at the trans side of membrane) connected to an amplifier (200B Axopatch, Axon Instruments, CA). To ensure the insertion of a single channel, a very low concentration of protein (1-2 µl of $10^{-6} – 10^{-7}$ dilution of 10 mg/ml protein stock) was added to the cis side of the chamber. The voltages were applied with an Axopatch™ 200B Patch Clamp amplifier and data was captured using Axon Digidata 1440 digitizer. Sampling frequency of 50 kHz was used for all measurements with a low-pass Bessel filter cut-off applied at 10 kHz. Acquisition and analysis of the data was done using Clampex and Clampfit software respectively (Axon Instruments, CA).

2.10.4. *Antibiotic interaction studies*

The instrumentation for studying antibiotic interaction was set up as described for the single channel experiments (section 2.10.2). Antibiotic solutions (with varying concentrations of up to 10 mM) were added at cis- and trans- sides of the membrane to analyse antibiotic-porin interaction.

In order to calculate the binding constant values (K; Equation 3), transient current blocking events were analysed to derive values for k_{on} (association rate constant) and k_{off}

(dissociation rate constant). The number of binding events per second divided by the concentration (of the added substrate) gives k_{on} , while k_{off} is derived from the inverse of the residence time τ, which in turn is calculated by an exponential fit of the dwell time histogram.

$$K = \frac{kon}{koff}$$

Equation 3: Binding constant. Where K=binding constant (M^{-1})
k_{on} (M^{-1} s^{-1}) is association rate constant, k_{off} (s^{-1}) is dissociation rate constant.

2.11. Bioinformatics

Bioinformatics tools used in this study are listed below in Table 2.11.

Table 2.11. List of Bioinformatic tools used for the study.
Provided with the website links and description of use.

Bionformatic tool		Source	Description
Genetic and Proteomic tools	BLAST	https://blast.ncbi.nlm.nih.gov/	Basic Local Alignment Search Tool (BLAST; Altschul et al., 1990). Finds proteins with conserved regions (homologues). The query sequence (protein or nucleotide) is compared to a database of non-redundant sequences.
	KEGG	http://www.genome.jp/kegg/	Kyoto Encyclopedia of Genes and Genomes (KEGG; Kanehisa et al., 2000). Used for searching DNA/protein sequences and organisation of proteins within the genome.
	UniProt	http://www.uniprot.org/	A vast database providing comprehensive sequence and functional information of proteins.
Protein Parameters	ExPASy ProtParam	http://web.expasy.org/protparam/	Calculates *e.g.* molecular weight, isoelectric point and extinction coefficient for the input protein sequence.
	ExPASy Translate	http://web.expasy.org/translate/	Translates the DNA nucleotide sequence to amino acid sequence. Useful for analysing sequencing results for recombinant constructs.
Primer Design	OligoCalc	http://biotools.nubic.northwestern.edu/OligoCalc.html	(Kibbe 2007) Calculates oligonucleotide parameters (melting temp, G/C content etc.) based on DNA sequence. Useful for primer designing.
	NEBcutter V2.0	http://nc2.neb.com/NEBcutter2/	(Vincze et al., 2003) Helps in locating restriction enzyme sites within a DNA sequence, provided as input.

Alignment	Clustal Omega	https://www.ebi.ac.uk/Tools/msa/clustalo/	(Sievers et al., 2011). Tool provided by EMBL-EBI. Used for multiple sequence alignment of protein sequences.
Structural data	Molprobity	http://molprobity.biochem.duke.edu/	Online validation tool for checking the refinement parameters of protein structure models. (Chen et al., 2010)
	Diffraction Anisotropy server	https://services.mbi.ucla.edu/anisoscale/	An online tool for performing ellipsoidal truncation and anisotropic scaling for the diffraction data (Strong et al., 2006)
	CCP4 online	https://www.ccp4.ac.uk/ccp4online/	Collaborative Computational Project No. 4 (CCP4) is a software suite for Macromolecular X-Ray Crystallography. Used for automated molecular replacement (MR) pipelines for data processing.
	RCSB-PDB PDBe	https://www.rcsb.org/pdb/ https://www.ebi.ac.uk/pdbe/	Database of protein structures. Structures from this study were deposited to PDBe.

2.12. Statistical Analysis and Data Presentation

The following statistical analysis has been applied for calculating and presenting the data (as described in Chapter 5):

- Disc-diffusion assay (discussed in section 5.2): For each molecule, three independent measurements were used to calculate the mean and the standard deviation. To present the data, a column-graph (Figure 5.1) was plotted using the mean values and the error bars represent the standard deviation of the data set.
- Liposome swelling assay (discussed in section 5.4): For each substrate, triplicate values were recorded in every experiment. Three such experiments were performed to produce a total of nine values which were then used to calculate the mean and the standard deviation. The mean values were plotted to present the data in a column-graph (Figures 5.5 and 5.18), with the error bars corresponding to the standard deviation.
- Multichannel conductance (discussed in section 5.6): The data presented in the column-graph (Figure 5.8) was plotted using the mean of three values, each recorded from three independent experiments.
- Ion-selectivity (discussed in section 5.7): The data presented in the scatter-graph (Figures 5.9 and 5.10) was plotted using the mean of three values, each recorded from three independent experiments and the error bars represent the standard-deviation of the data set.

Chapter 3 Recombinant expression of OMPs in *E. coli*

3.1 Introduction

OmpF and OmpC in *E. coli* are two typical diffusion porins representing a structural as well as functional paradigm for Gram-negative porins. This chapter describes the isolation and purification of major porins from 3 notorious gram-negative pathogens: OmpE35/E36 (from *Enterobacter cloacae*), OmpK36 (from *Klebsiella pneumoniae*) and OmpU/T (from *Vibrio cholerae*) in *E. coli* as the recombinant host. The other major porin of *Klebsiella pneumoniae*, OmpK35, was structurally characterised by another member of the lab (also see section 5.1). As a result of interesting findings for the structures of OmpU and OmpT (as discussed in section 4.1), two additional mutants; OmpUΔN and OmpTΔL8, were also constructed and expressed in *E. coli*. In order to target these recombinant OMPs (OmpE35/E36/K36, OmpU/UΔN and OmpT) to *E. coli* OM, each of their signal peptides were swapped with the signal sequence of OmpA (OMP in *E. coli*). Since the membrane expression of OmpT and OmpUΔN produced low yields of the sample with poor purity (as discussed in sections 3.4 and 3.5), both OMPs (and OmpTΔL8) were alternatively expressed as IBs. For transformation (of pBAD24 cloned constructs) we have used a porin-deficient strain of *E. coli*, referred to as omp8 (BL21), which lacks *ompF*, *ompC*, *ompA*, *lamB* and *phoE*. The pET28 cloned constructs (designed for IB expression) were electroporated in *E. coli* Bl21 (DE3) cells. To check the expression of an OMP, the overexpression trials were usually done with 2 litres of LB media (unless stated otherwise) prior to large scale harvest (that employed 10-12 litres growth media).

In *E. coli* OmpF/C porins, β-barrel structure is characterised by a salt bridge between α-amino group and the C-terminal carboxylate. This precludes the use of terminal tags for protein purification given the presumed structure similarities between OmpF/C and OMPs of this study. Hence, all tag-less OMPs were purified by anion-exchange chromatography (IEX) and size exclusion chromatography (SEC) (also see sections 2.4.4.1 and 2.4.4.3). Except for histidine tagged OmpT (with a 6× his-tag in one of the predicted loops of OmpT), which was purified by immobilised metal affinity chromatography (IMAC) and SEC (also see sections 2.4.4.2 and 2.4.4.3). To assess the purity and integrity of the purified OMPs, the samples were analysed on SDS-PAGE as boiled (B) and non-boiled (NB) samples.

Detergents (or surfactants) are normally used to extract the membrane proteins from the membrane fraction. Sarkosyl, an anionic detergent, plays a unique role in the separation of the IM and OM fractions. Since in low ionic strength buffer the density of sarkosyl resembles that of the LPS-phospholipid layer, treatment with sarkosyl followed by centrifugation solubilises and removes IM-bound proteins. For the extraction and purification of OMPs, the most common detergent used was lauryldimethylamine N-oxide (LDAO) except for some cases, where milder detergents such as n-decyl-β-*D*-maltopyranoside ***(***DM) and n-dodecyl-β-D-maltopyranoside (DDM) were employed for OM extraction purposes (see section 3.5.3). We have used octyl tetraethylene glycol ether (C_8E_4) for our final protein stocks, since this has been a successful detergent for the crystallisation of β-barrel membrane proteins.

3.2. Overexpression and purification of OmpE35, OmpE36 and OmpK36

The genomic DNA of *Enterobacter cloacae* (ATCC 13047) and *Klebsiella pneumoniae* (ATCC 43816) were obtained from Basilea Pharmaceutica Limited, Basel Switzerland. The genes of OmpE35, OmpE36 and OmpK36 were amplified using the genomic DNA (of *E. cloacae* and *K. pneumoniae*) as the template in the Polymerase Chain Reaction (PCR) (Figure 3.1). Primers designed using the N- and C- terminus of *ompE35*, *ompE36* and *ompK36*, were used to amplify the gene sequences and successfully cloned into pBAD24 plasmid using the restriction sites NcoI and XbaI (Figure 3.1).

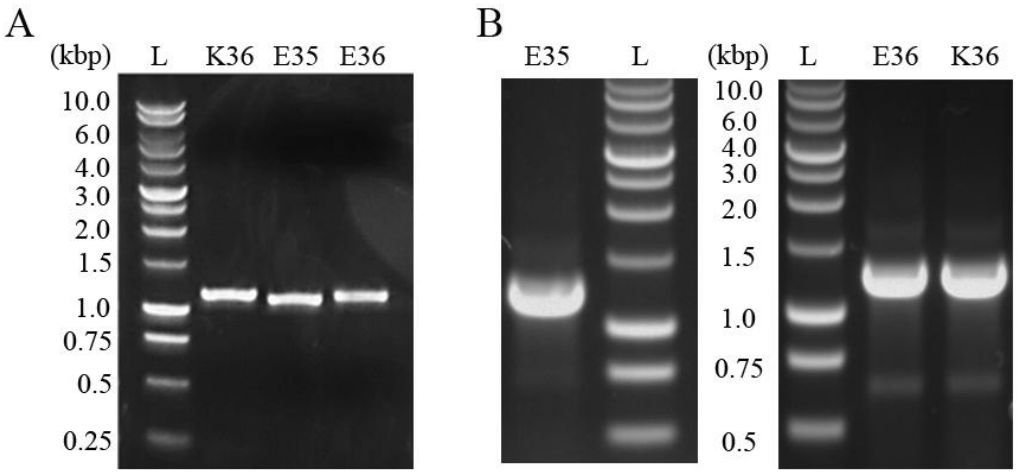

Figure 3.1 PCR and cloning of OmpE35/E36 and OmpK36.
DNA gel image showing (A) PCR amplified genes of OmpE35, OmpE36 and OmpK36 (using genomic DNA as the template) and (B) amplified products of pBAD cloned constructs of OmpE35/E36 and OmpK36 using colony PCR. L represents the molecular weight marker.

The pBAD24-cloned OmpE35/E36/K36 constructs were electroporated in the competent cells of *E. coli* omp8 (Bl21) strain and the OMPs (OmpE35, OmpE36 and OmpK36) were overexpressed (Table 2.8 and section 2.4.2.1) and extracted from the membrane fraction (section 2.4.3.1). The proteins were separated by IEX (section 2.4.4.1) with a salt gradient from 50 mM to 1 M over 20 column volumes (CV) using Resource Q (Figure 3.2 A, B and C).

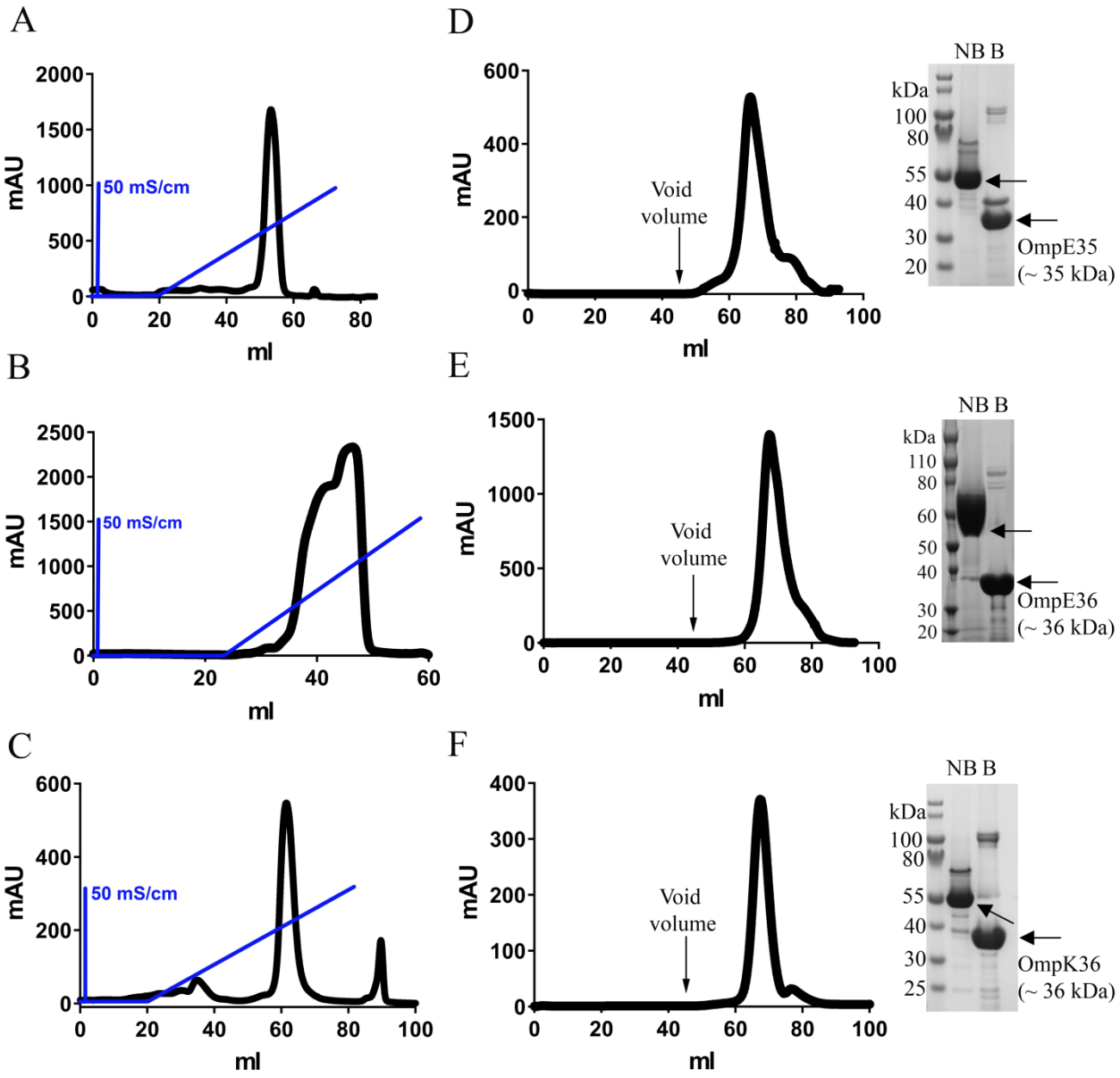

Figure 3.2. Purification of OmpE35, OmpE36 and OmpK36 by IEX and SEC.
The elution of OmpE35 (A), OmpE36 (B) and OmpK36 (C) through Resource Q with the salt gradient (y axis: 50 mM – 1 M NaCl) shown in blue. The GF peak obtained in 0.45% C_8E_4 for OmpE35 (D), OmpE36 (E) and OmpK36 (F) eluted at ~65 ml. For each protein, the peak fractions were pooled and analysed by SDS-PAGE (indicated by arrows) as non-boiled (Lane NB) and boiled (Lane B) samples.

The purification of OmpE35/E36/K36 was done by SEC (section 2.4.4.3) using 120 ml S200 GF (Superdex 200 PG gel-filtration) column in 0.05% LDAO followed by second round of SEC purification in 0.45 % C_8E_4 (Figure 3.2 D, E and F). C_8E_4 peak fractions of OmpE35, OmpE36 and OmpK36 were pooled and analysed by SDS-PAGE to assess the purity of the proteins (Figure 3.2). Post-visualisation of protein bands by Coomassie blue staining, the proteins were subjected the crystallisation trials (section 4.2). The typical yields of OmpE35 and OmpK36 were 4-5 mg of protein per litre of cells, while the yield for OmpE36 was ~12 mg of protein per litre of cells.

3.3. Overexpression and purification of OmpU

A synthetic gene for the mature part *ompU* (*V. cholerae* OmpU Uniprot id K08720) and the signal sequence of *E. coli* OmpA was obtained from Eurofins Genomics and cloned into pBAD24 plasmid using NcoI/XbaI restriction enzymes. The bacterial colonies containing pBAD-OmpU constructs were screened by colony PCR (section 2.3.8 and Figure 3.3) and confirmed by DNA sequencing.

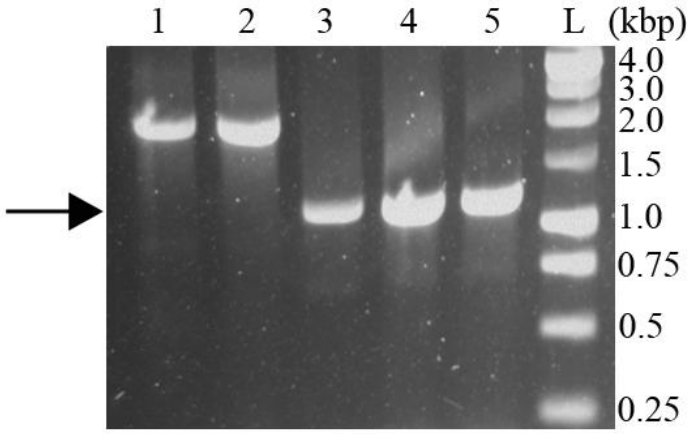

Figure 3.3. Screening of bacterial colonies with pBAD-OmpU plasmid by colony PCR. DNA gel image showing amplification of *ompU* (insert, ~1 kbp) cloned in pBAD24 with 3 positive clones (indicated by arrow in lanes 3, 4 and 5) and 2 negative clones (1 and 2; estimated size is ~1 kbp). L represents the molecular weight marker.

The pBAD24-OmpU construct was transformed into omp8 (Bl21) competent cells and the protein was overexpressed at 37°C for 3 hours after induction with 0.1% arabinose (also described in section 2.4.2.1). OmpU was eluted by IEX using a salt gradient (50 mM – 1 M NaCl over 20 CV) on Resource Q column (Figure 3.4 A). OmpU purification by SEC was first carried

out in 0.05% LDAO and then in 0.45% C_8E_4 (Figure 3.4 B). The chromatogram in Figure 3.4 B shows the main peak of OmpU at ~75 ml (in 120 ml GF column) which indicates the elution of monomer. The quality of purified OmpU was analysed on SDS-PAGE (Figure 3.4 C). The overall yield of OmpU was ~1 mg of protein per litre of cells and the pure protein was concentrated to 10 mg/ml for crystallisation (as described in section 2.4.5).

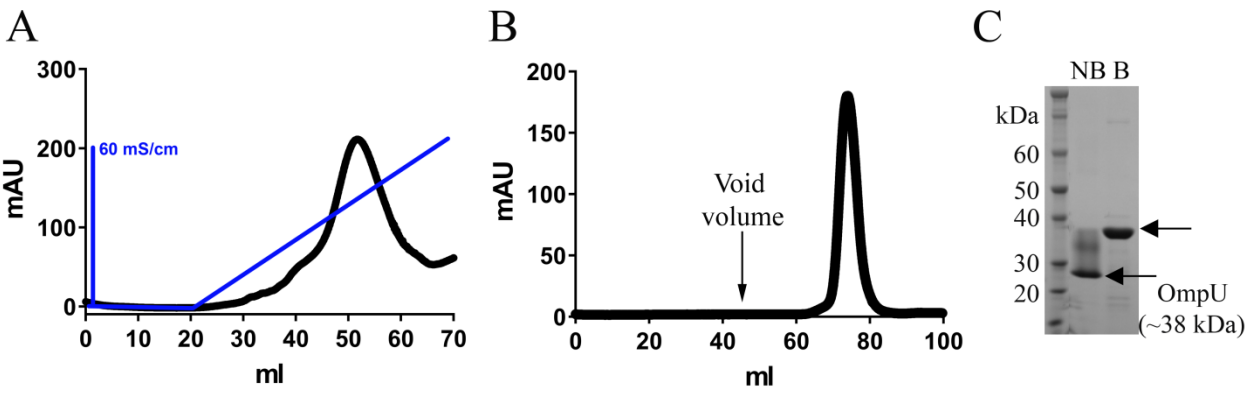

Figure 3.4. Elution and Purification of OmpU.
(A) Resource-Q chromatogram of OmpU showing elution in a high salt gradient as represented by linearly increasing conductance (in blue). (B) GF chromatogram showing the final purification step of OmpU in 0.45% C_8E_4 column with a peak at ~75 ml. (C) Coomassie stained SDS-PAGE gel showing contents of GF peak fractions (Lane NB: non-boiled and Lane B: boiled). The arrows of SDS-PAGE indicate the bands of OmpU (~38 kDa).

3.4. Overexpression and purification of OmpUΔN

The first 30 nucleotides from the N-terminus of the mature *ompU* were deleted by site-directed mutagenesis (SDM; section 2.3.1.2) using OmpU-pBAD24 plasmid as the template. As a result, *ompUΔN* sequence optimised with signal sequence of *E. coli* OmpA was cloned into pBAD24 using NcoI and XbaI restriction sites and omp8 (Bl21) cells were transformed with the recombinant OmpUΔN-pBAD24 construct. Figure 3.5 shows the DNA gel image for the screening of clones containing OmpUΔN-pBAD24.

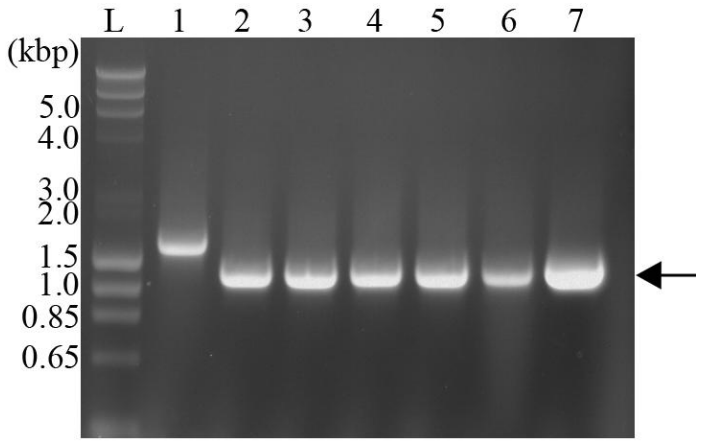

Figure 3.5. Screening of clones with pBAD24-OmpUΔN recombinant plasmid.
DNA gel image showing amplification of *ompUΔN* (insert, ~1.2 kbp) cloned in pBAD24 plasmid. Except for lane 1, the other 6 clones are positive (lane 2- lane 7; indicated by arrow).

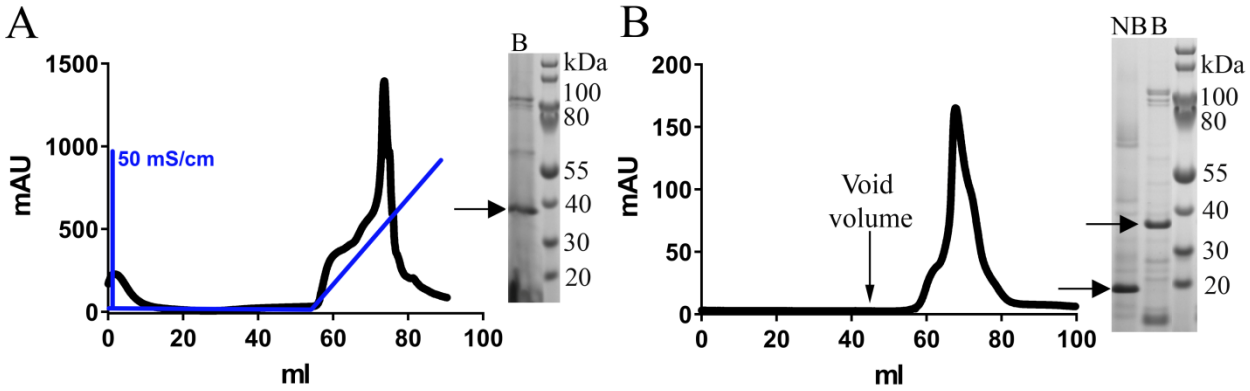

Figure 3.6. Purification of membrane-expressed OmpUΔN
(A) The elution peak of OmpUΔN through HiTrap-Q in high salt gradient (conductance in blue) was analysed on SDS-PAGE (as boiled; B). (B) The S200 chromatogram showing OmpUΔN peak at 70 ml and the peak fractions were loaded as non-boiled (Lane NB) and boiled (Lane B) samples on SDS-PAGE. The arrows of SDS-PAGE indicate the bands of OmpUΔN (~37 kDa).

OmpUΔN was expressed at 37°C for 3 hours post-induction with arabinose and extracted from the OM (as described in sections 2.4.2.1 and 2.4.3.1). A shallow salt gradient (50 mM – 0.5 M NaCl over 10 CV) was applied to purify OmpUΔN by IEX (section 2.4.4.1) using HiTrap-Q (Figure 3.6 A). On SDS-PAGE, the eluted fractions showed low expression of OmpUΔN and high levels of impurities (Figure 3.6. A). To remove the excess impurity, the protein was purified through S200 GF column in 0.05 % LDAO and subsequent fractions of OmpUΔN peak were subjected to MonoQ. OmpUΔN was purified using a salt gradient (50 mM – 0.5 M NaCl over 30 CV) and the peak fractions through MonoQ column were loaded on S200 GF column for the final step of purification in 0.45 % C_8E_4 (Figure 3.6. B). Extensive purification carried out for

OmpUΔN resulted in big losses of the protein and as a result, its final yield was extremely low (~0.2 mg per litre of cells). In addition, the purity levels of purified OM-expressed OmpUΔN were imperfect for crystallisation (Figure 3.6 B). Despite these concerns the protein was used for crystallisation trials (Chapter 4).

The problem of membrane expression of OmpUΔN was solved by expression as IBs. *ompUΔN* was cloned into pET28a plasmid using NcoI and XhoI restriction sites without the signal peptide. Following overexpression trials of OmpUΔN (as described in section 2.4.2.1 and Table 2.8) and protein isolation by solubilisation of IBs, OmpUΔN was folded *in vitro* by continuously stirring in IB buffer containing 1% LDAO (also see section 2.4.3.2) at room temperature (RT). A salt gradient was used to elute OmpUΔN through gravity flow anion-exchange (see section 2.4.4.1). The SDS-PAGE gel of OmpUΔN OM extract (Figure 3.7 B; Lane 1) showed high expression levels of the IB-expressed OmpUΔN as compared to the membrane expressed OmpUΔN (Figure 3.6 A). A two-step purification was performed by SEC, first in 0.05 % LDAO followed by 0.45 % C_8E_4 (Figure 3.7 A). The C_8E_4 GF peak was analysed by SDS-PAGE (Figure 3.7 B; Lanes 2 and 3). Typical yields of IB-expressed OmpUΔN were 5-6 mg of protein per litre of cells.

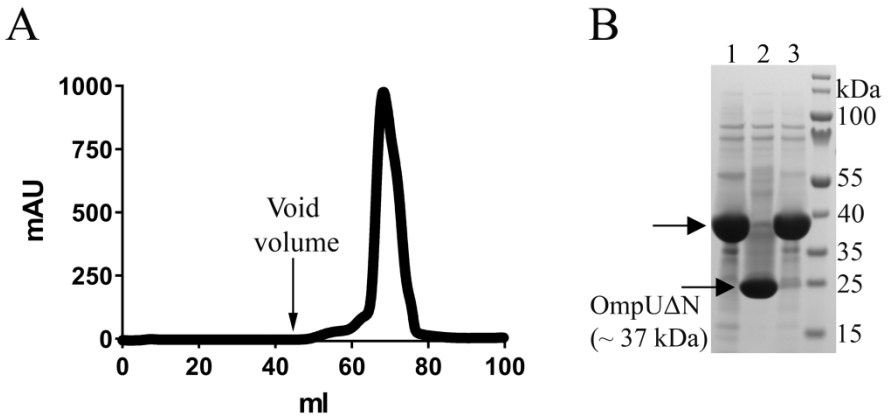

Figure 3.7. Purification of OmpUΔN from Inclusion Bodies.
(A) The S200 GF-chromatogram of OmpUΔN purification in 0.45 % C_8E_4. (B) Coomassie stained SDS-PAGE gel showing the contents of the OM extract (Lane 1) and GF peak fractions (Lane 2: non-boiled and Lane 3: boiled). The arrows indicate the DNA band for OmpUΔN (~37 kDa).

3.5. Overexpression and purification of OmpT

The DNA sequence of *Vibrio cholerae* OmpT (Uniprot id K10940) was synthesised by Eurofins Genomics. *ompT* was directly excised from the obtained plasmid constructs using

restriction digestion and cloned into the desired vector. The overexpression of OmpT was extremely challenging because of very low expression. Thus, for isolating the purest fractions of OmpT, several different methodologies had to be adopted that are detailed in this section.

3.5.1. *Overexpression trials of OmpT*

The *ompT* gene sequence was cloned into pBAD24 plasmid using NcoI/XbaI restriction sites (Figure 3.8).

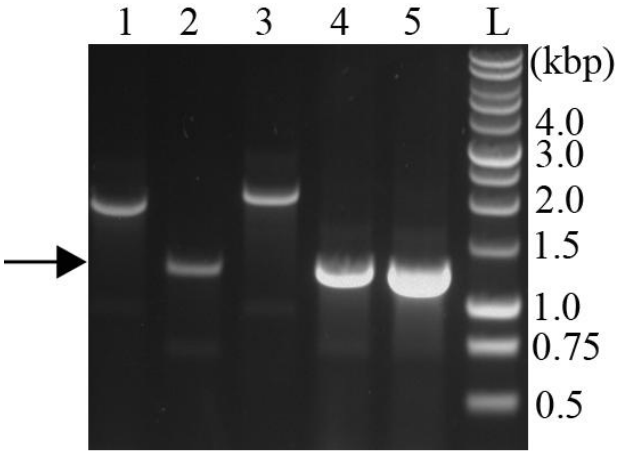

Figure 3.8. Screening of pBAD24-OmpT plasmid constructs.
DNA gel image showing amplification of *ompT* (insert, ~1.1 kbp) cloned in pBAD24. Lanes 2, 4 and 5 display the clones with pBAD24-OmpT recombinant plasmid (indicated by arrow).

The pBAD24-OmpT construct was electroporated into omp8 (Bl21) competent cells and overexpression of OmpT was done in similar manner as described earlier (in section 2.4.2.1 and Table 2.8). OmpT was isolated from the membrane fraction using a high salt gradient (50 mM – 1 M NaCl over 20 CV) through HiTrap Q (Figure 3.9 A). The OmpT peak fractions were subjected to SEC in 0.05 % LDAO for purification (Figure 3.9 B). The GF peak fractions, as assessed by SDS-PAGE, showed strong contamination (Figure 3.9 C). Moreover, since average yield of membrane-expressed OmpT was extremely low (~ 0.1 mg per litre of cells), we varied different growth conditions (like growth media and temperature) to boost the expression of OmpT.

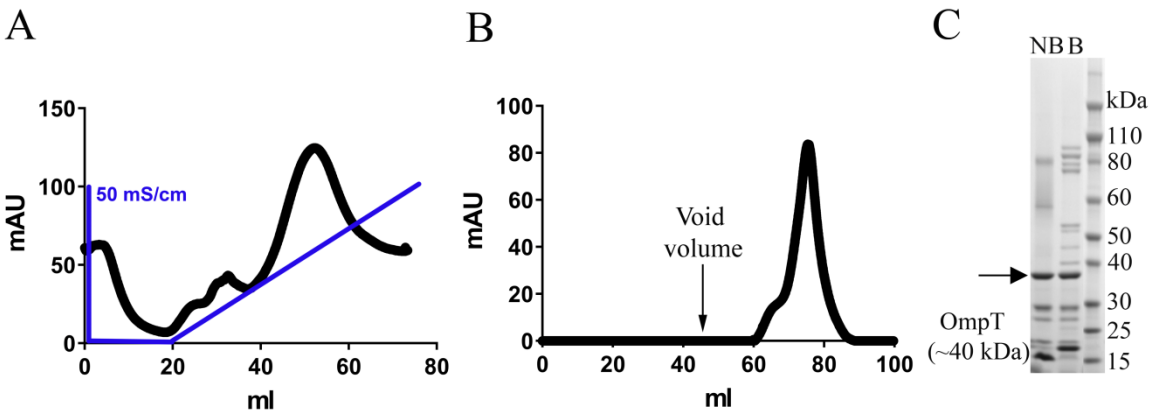

Figure 3.9 Membrane expression of OmpT (cloned in pBAD24 plasmid).
(A) OmpT elution from HiTrap-Q column using high salt gradient. (B) The S200 GF chromatogram showing OmpT peak at ~ 75 ml (in 0.05% LDAO). (C) Coomassie stained SDS-PAGE gel showing contents of GF peak fractions (Lane NB: non-boiled and Lane B: boiled). The arrows of SDS-PAGE indicate the bands of OmpUΔN (~37 kDa).

A particular observation made for the membrane expression of OmpT was low cell OD after 3 hours of induction (0.6 - 0.7) which indicated toxicity. On the other hand, under similar conditions, the membrane expression of OmpU resulted in an OD of 1.0 - 1.2 post-induction. In order to promote the extended growth phase of OmpT-expressed cells, a nutritionally enriched media (2×YT) media was used in combination with $MgSO_4$ (Table 2.1) that enhances the bacterial cell growth. The overexpression trials of OmpT in $MgSO_4$ supplemented 2×YT media were done at 37°C (for 3 hours), 30°C (for 5 hours) and 18°C (for overnight) (Figure 3.10 C). A few reports have implicated the role of environmental conditions such as high osmolarity or minimal media in affecting the expression of OmpT in *V. cholerae* (Li et al., 2002). Subsequent steps were taken to improve the protein expression by varying the composition of growth media. The overexpression trials of OmpT were performed in LR minimal media at two different temperatures (30°C or 37°C) (Figure 3.10 A). In addition, the expression trials were also carried out in high osmolarity conditions using LB media supplemented with different NaCl concentrations; 0.125 M and 0.225 M (Figure 3.10 B). The expression trials with media supplemented with 0.125 M NaCl was done in 3 different batches and cells were harvested at different time-points post induction (1, 2 or 3 hours) to ensure accumulation of healthy cells and avoid toxicity (Figure 3.10 B).

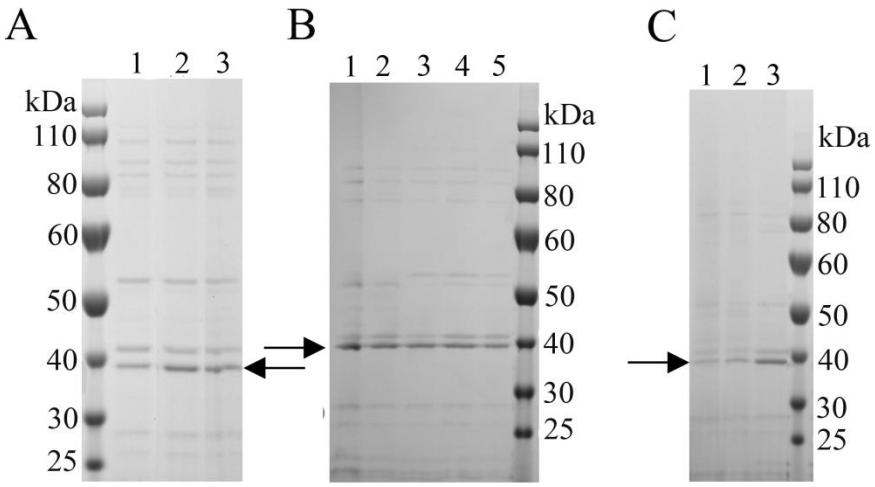

Figure 3.10. Expression checks of OmpT under different growth conditions.
(A) SDS-PAGE of IEX eluates (boiled) of OmpT grown in LR minimal media and expressed at 30°C (Lane 1) and 37°C (Lane 2); OmpT expressed at 37°C in LB media was run as control (Lane 3). (B) SDS-PAGE of boiled OM extracts of OmpT grown in LB media with no supplement (Lane 1; control), supplemented with 0.125 M NaCl [Lane 2; 3 hours induction, Lane 3; 2 hours induction and Lane 4; 1-hour induction) and supplemented with 0.225 M NaCl (Lane 5; 3 hours induction). (C) SDS-PAGE of boiled OM extracts of OmpT grown in 2×YT media (with $MgSO_4$) expressed at 37°C for 3 hours (Lane 1), 30°C for 5 hours (Lane 2) and 18°C for overnight (Lane 3). The arrows indicate the bands of OmpT (~40 kDa).

The SDS-PAGE of the OM extracts from different overexpression trials (Figure 3.10) indicated low membrane expression of OmpT with poor purity levels.

3.5.2. *Large scale expression of OmpT*

Despite the low yield for the membrane expression of OmpT (~0.1 mg of protein per litre of cells), we expressed OmpT on a large scale to obtain sufficient amount of protein for crystallisation. The plasmid construct pBAD24-OmpT was electroporated in omp8 (Bl21) cells and OmpT was expressed in 50 litres LB media (Amp^r) in 5 different batches (10 litres each) at 37°C for 3 hours. For each batch, the OM extracts were subjected to HiTrap-Q chromatography and the protein was further purified by SEC (in 0.05 % LDAO) and Mono-Q (50 mM-0.5 M NaCl over 30 CV). The peak fractions of OmpT of the 5 Mono-Q batches were pooled together prior to the final purification by SEC in 0.45 % C_8E_4 (Figure 3.11 A). A total of 4 mg of OmpT was obtained from the large-scale expression of 50 litres. SDS-PAGE in Figure 3.11 B shows the non-boiled and boiled samples of purified OmpT (from C_8E_4 GF peak) used for crystallisation.

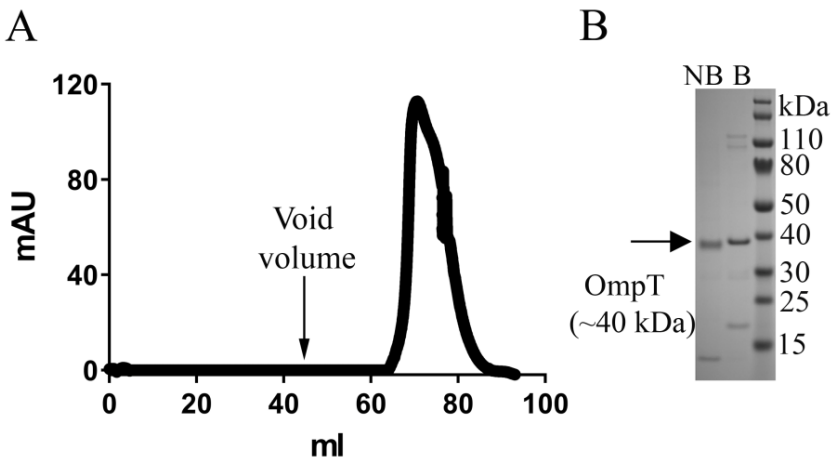

Figure 3.11. Purification of OmpT from large scale expression (50 litres).
(A) OmpT peak at 72 ml through SEC purification in 0.45% C_8E_4. (B) Coomassie stained SDS-PAGE gel showing contents of GF peak fractions (Lane NB: non-boiled and Lane B: boiled). The arrow on SDS-PAGE indicate the bands of OmpT (~40 kDa).

3.5.3. *Overexpression and purification trials of His-tag OmpT*

OmpT produced from the expression of 50 litres allowed us to set up 150-200 screen conditions for crystallisation and optimise some of the hit conditions. One of the screen conditions yielded just one crystal of decent size (further discussed in sections 4.3 and 4.8). The protein crystallisation was perhaps hindered by the persistent presence of impurities in the membrane isolated fractions of OmpT, as seen in the SDS-PAGE gels (Fig. 3.11). To improve the efficiency of OmpT purification, a histidine tag was incorporated in the *ompT* sequence.

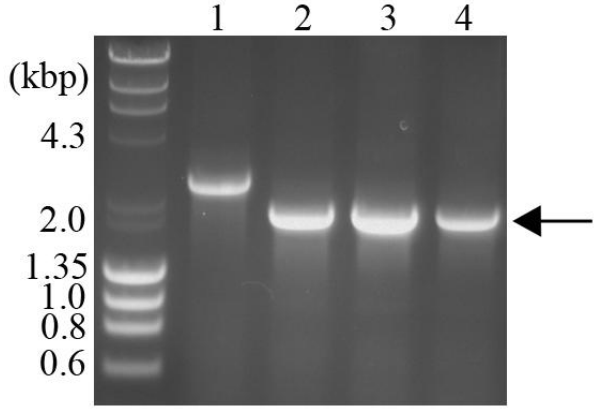

Figure 3.12. Screening of pBAD24 his-OmpT plasmid constructs.
DNA gel image showing amplification of histidine-tagged *ompT* (insert, ~1.2 kbp) cloned in pBAD24. Lanes 2, 3 and 4 display the positive clones with pBAD24 his-OmpT recombinant plasmid (indicated by arrow).

According to OmpT structure prediction (by online software program BOCTOPUS (Hayat and Elofsson 2012), the histidine tag was incorporated in one of its predicted extracellular loops (L6) such that the insertion might not interfere the (expected) trimeric form of OmpT. Thus, histidine-tagged *ompT* was synthesised from Eurofins with the 6× His tag between Thr260 and Gly261 of mature OmpT. His-tag *ompT* was cloned in pBAD24 using NcoI/XbaI restriction sites and His-OmpT pBAD24 constructs were confirmed by colony PCR (Figure 3.12).

His-OmpT pBAD24 construct was transformed in DE3 cells (Bl21) of *E. coli* (healthier strain as compared to slow growing omp8 strain). The overexpression trials for his-OmpT were done similarly to the previous section (section 3.5.2). Histidine-tagged protein was isolated from the membrane fraction by IMAC (section 2.4.4.3). His-OmpT was further purified by SEC in 0.05 % LDAO. During purification, the protein peak was very close to the void volume of the GF column (Figure 3.13 A) suggesting aggregation of his-OmpT. The identity of his-OmpT was assessed by loading the GF fractions of both peaks on SDS-PAGE (Figure 3.13. B).

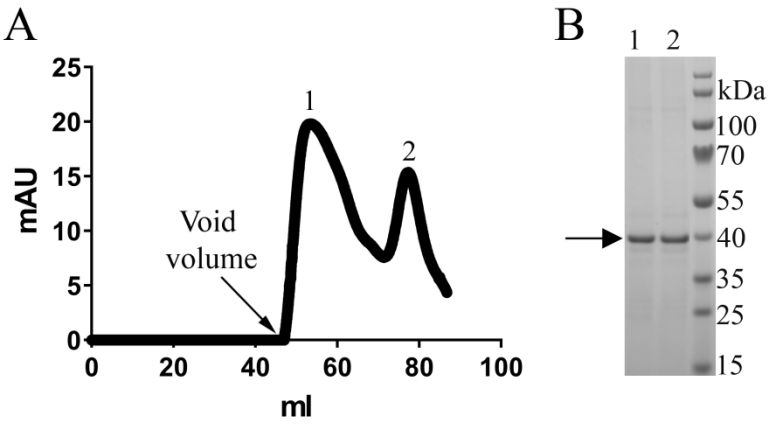

Figure 3.13. Purification of his-OmpT (cloned in pBAD24).
(A) S200 GF (120 ml) chromatogram for the purification of his-tag OmpT shows peak 1 at ~ 55 ml and peak 2 (at ~ 75 ml) implying a monomer. (B) Coomassie stained SDS-PAGE gel showing contents of GF peak fractions of peak 1 (Lane 1) and peak 2 (Lane 2). The arrows in the SDS-PAGE indicate the bands of OmpT (~ 40 kDa).

To solve the aggregation problem, different detergents (other than LDAO) were employed for the extraction and purification of his-OmpT. Towards this, 3 different detergents (1% DM, 1% DDM or 1% OG + 0.5% LDAO) were used for the extraction (section 2.4.3.1). In addition, 0.1% DDM (n-Dodecyl-β-D-Maltoside) was used in the purification buffers (instead of 0.05% LDAO) for the protein elution through Ni^{+2} affinity column and purification through 24 ml

analytical GF column (Superdex 200 PG 10/300 GL). The purification chromatograms in Figure 3.14 show protein elution near the void volume of GF column (~ 9 ml), again suggesting aggregation of his-OmpT.

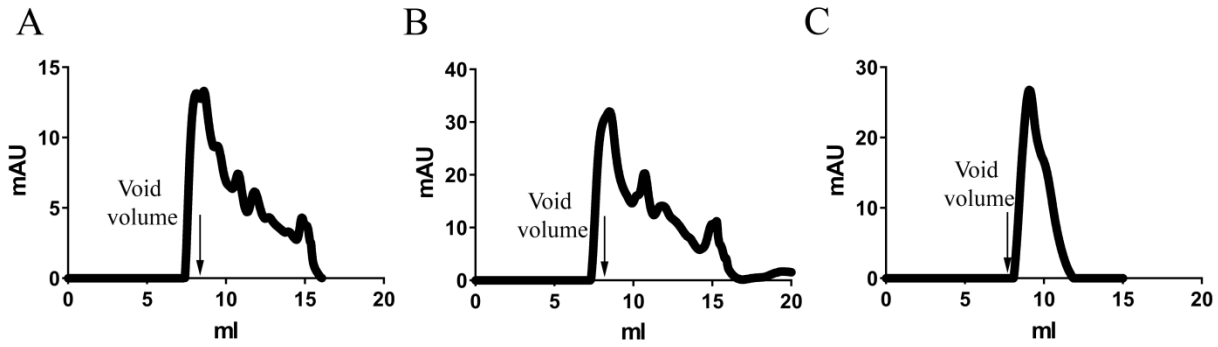

Figure 3.14. Purification of his-OmpT (cloned in pBAD24).
The chromatograms show the elution of his-OmpT in the void volume (~ 9 ml) of analytical GF after IMAC of the membrane fraction extracted in (A) 1% OG + 0.5% LDAO, (B) 1% DDM and (C) 1% DM.

Imidazole (~ 250 mM) used to elute protein from the IMAC column could be a potential factor for the aggregation of his-tagged protein. Towards this, we employed alternate methods for the elution of his-tagged OmpT. One such method adopted the use 100 mM EDTA (instead of imidazole) to chelate the nickel ions of the column and strip off the metal and protein, which was immediately followed by buffer exchange to remove Ni-EDTA from the protein. Another method employed for elution of his-OmpT used low pH buffer (50 mM sodium acetate, 200 mM NaCl, pH 4.5) in order to protonate the histidines of OmpT and disrupt binding with the nickel ions of the column. For both elution strategies, the purification of his-OmpT through 24 ml analytical GF column displayed irregular peaks (Figure 3.15 A and B). Cobalt has a lower affinity for His and requires lower imidazole concentration for the protein elution than nickel. Hence, 50 mM imidazole was used to elute his-OmpT from a cobalt-charged IMAC column. The purification of his-tag OmpT by analytical GF produced a single sharp peak at ~ 13 ml (Figure 3.15 C) and showed no trace of aggregation. However, since the final yield of his-OmpT was very low (0.05 mg protein per litre of cells), it was not pursued for large scale expression.

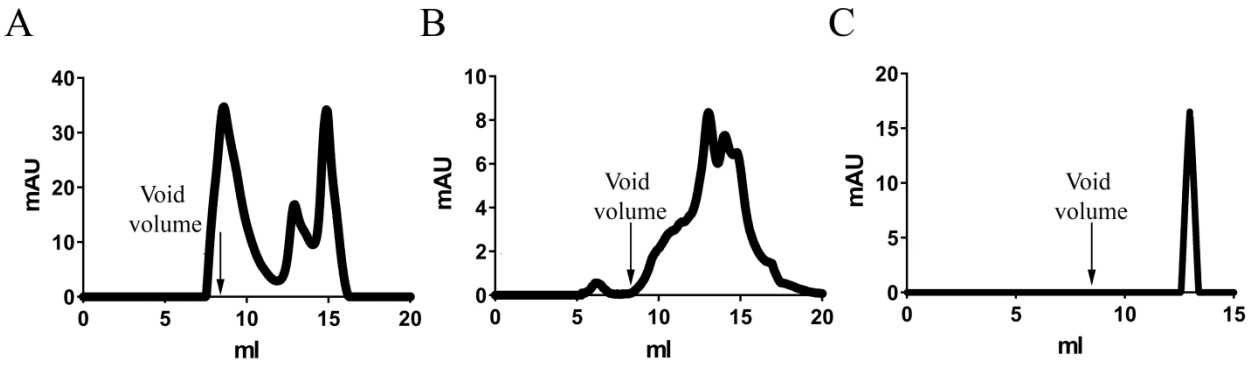

Figure 3.15. Purification of his-OmpT (cloned in pBAD24).
Protein purification through 24 ml analytical GF column for his-tag OmpT, which was eluted using (A) EDTA, (B) low pH and (C) 50 mM imidazole in a Co^{2+} affinity column.

3.5.4. *Inclusion body expression of OmpT*

Since the membrane expression of OmpT (or his-OmpT) produced low yields of purified protein, we approached an alternative strategy of expression by forming inclusion bodies (IBs). *ompT* (without the signal peptide) was PCR amplified and subsequently cloned into pET28a expression vector using NcoI/XhoI restriction sites (Figure 3.16).

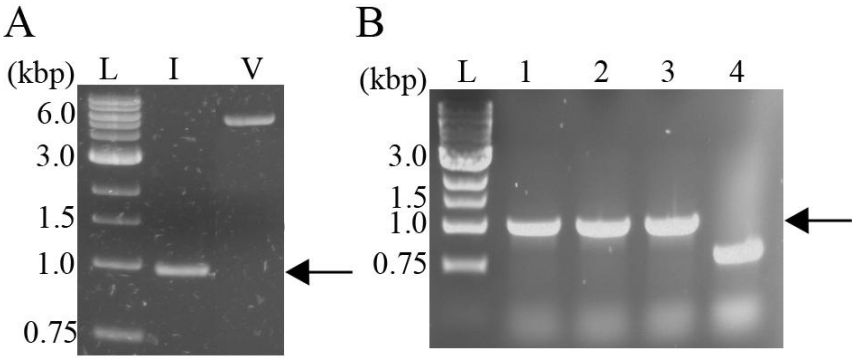

Figure 3.16. Cloning of OmpT-pET28a recombinant plasmid.
(A) DNA gel image showing digests of *ompT* insert (995 bp; Lane I, arrow indicated) and pET28a vector (5.3 kbp; Lane V) using NcoI/XhoI restriction enzymes. (B) DNA gel image for the screening of OmpT-pET28a constructs (positive clones) by colony PCR; Lanes 1-3 show positive clones (indicated by arrow).

The omp8 (Bl21) and DE3 (Bl21) strains of *E. coli* cells were separately transformed with OmpT-pET28 construct. The overexpression trials followed by protein purification were done in a similar manner as described above for the IB expression of OmpUΔN (section 3.4; also see sections 2.4.2.1, 2.4.3.2 and Table 2.8). For the purification of OmpT, isolated from omp8 (Bl21) cells, some of the protein came out as an aggregated mass in the void volume (~ 45 ml) of SEC

(Figure 3.17 A). Surprisingly however, OmpT isolated from DE3 (Bl21) cells was purified as a single sharp peak (at 72 ml) and showed no trace of aggregation (Figure 3.17 B). Hence for large scale expression, IBs of OmpT (cloned in pET28a) were expressed in DE3 (Bl21) cells and the purified protein was obtained by performing two rounds of SEC (first in 0.05% LDAO and final in 0.45% C_8E_4). Typical yields obtained for OmpT (isolated from IBs) were 2-3 mg of protein per litre of cells and was used to set up the crystal drops (section 4.3).

During initial crystallisation and optimisation, one of the crystals obtained for OmpT diffracted to ~2.0 Å. However, the structure of the protein could not be solved because of the unavailability of a good molecular replacement (MR) model for OmpT. Experimental phasing is another method (other than MR) that provides the solution for the phase problem and requires the anomalous scattering by a heavy atom (HA). Hence, OmpT was expressed to incorporate selenomethionine in its sequence and use selenium as the phasing marker (as described in the next section 3.5.5).

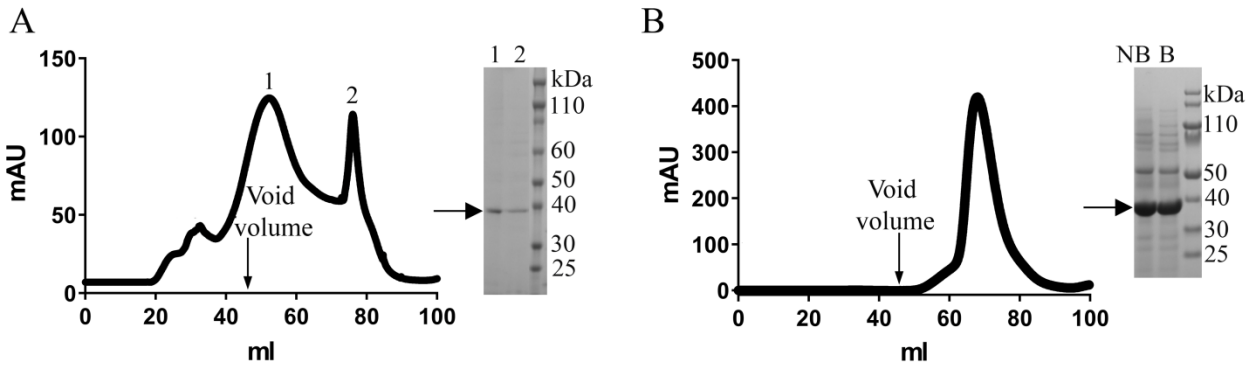

Figure 3.17. Purification of OmpT expressed as inclusion bodies (IBs).
(A) S200 GF chromatogram for purification of OmpT, isolated from IBs in omp8 (Bl21) cells; peak 1 in the void volume of GF column indicates protein aggregation (Lane 1 of SDS-PAGE; boiled) and peak 2 is OmpT monomer (Lane 2 of SDS-PAGE; boiled). (B) S200 GF chromatogram for purification of OmpT, isolated from IBs expressed in DE3 (Bl21) cells. A single sharp peak at 70 ml is present (on SDS-PAGE, Lane NB; non-boiled and Lane B; boiled). The arrows indicate OmpT (~ 40 kDa).

3.5.5. *Overexpression of selenomethionine substituted of OmpT*

The use of selenium (Se; heavy atom) in methionine instead of sulphur forms the basis of anomalous diffraction (required for experimental phasing). In order to use Se as the phasing

marker, we overexpressed and purified SeMet-labelled OmpT (cloned in pET28a) as IBs from Bl21 (DE3) cells of *E. coli* (see section 2.4.2.2 and Table 2.8).

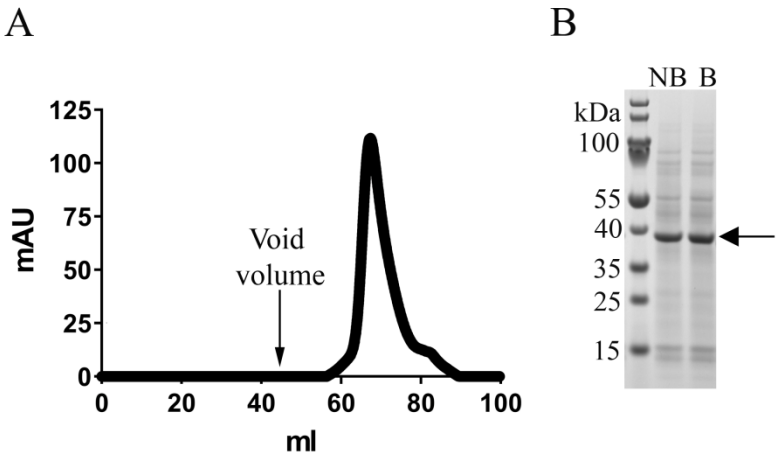

Figure 3.18. Purification of selenomethionine substituted OmpT (SeMet OmpT).
(A) S200 GF chromatogram showing a single sharp peak of SeMet OmpT (at ~ 70 ml). (B) Coomassie stained SDS-PAGE gel showing contents of pooled GF peak fractions (Lane NB: non-boiled and Lane B: boiled). The arrow indicates SeMet OmpT (~ 40 kDa).

SeMet-OmpT (folded in vitro) was purified by IEX using a gravity flow anion-exchange column and further purified by SEC in 0.05% LDAO. A final round of S200 GF purification was done in 0.45% C_8E_4 (Figure 3.18 A). Elution of OmpT at 70 ml (in 120 ml GF column) corresponds to the monomeric form of Se-Met OmpT (Figure 3.18 B). Typical yields of Se-Met OmpT were 2 mg per litre of cells.

3.6. Overexpression and purification of OmpTΔL8

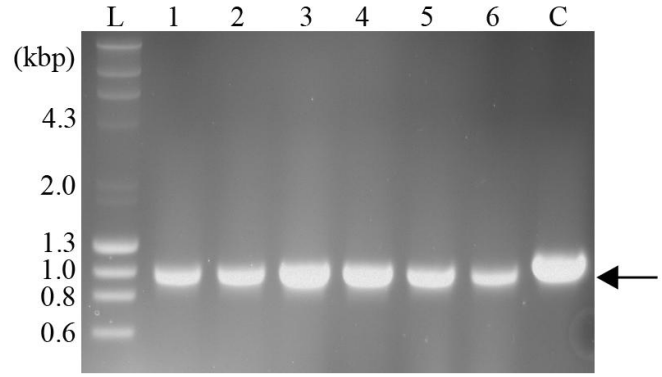

Figure 3.19. Cloning of OmpTΔL8-pET28a recombinant plasmid.
DNA gel image for the screening of OmpTΔL8-pET28a constructs (*ompTΔL8*; ~ 1.0 bp) by colony PCR; Lanes 1-6 show positive clones (indicated by arrow). Lane C is the control showing *ompT* (~ 1.1 kbp).

Sixteen residues from loop L8 of OmpT (Thr294 - Thr309 in mature OmpT sequence) were deleted by Q5 site-directed mutagenesis kit (SDM) and replaced by one glycine residue to connect the strands (section 2.3.1.2). As a result, *ompTΔL8* (L8 deletion mutant of *ompT*) was cloned into pET28a without the signal peptide using NcoI/XhoI restriction sites (Figure 3.19).

OmpTΔL8-pET28a was electroporated into DE3 (Bl21) cells of *E. coli*. The protein overexpression as IBs was followed by isolating OmpTΔL8 through solubilisation of IBs (section 2.4.3.2). Protein purification (section 2.4.4) was done by IEX using gravity flow anion-exchange column and by SEC in 0.05% LDAO and 0.45% C_8E_4 (Figure 3.20). The average yield of OmpTΔL8 was 4 mg of protein per litre of cells.

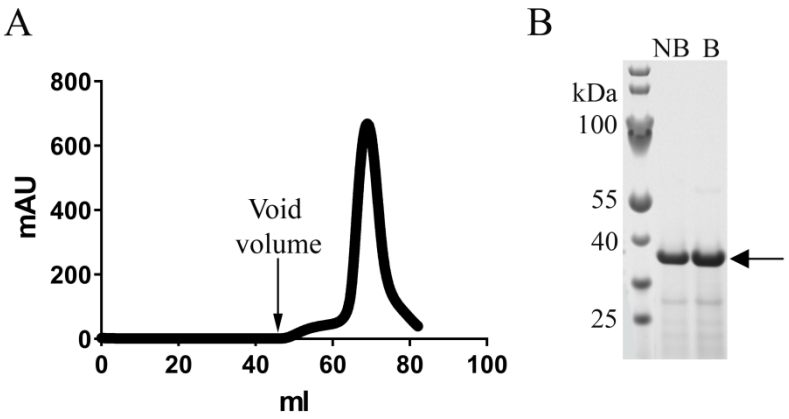

Figure 3.20. Purification of OmpTΔL8.
(A) The purification chromatogram of S200 GF column (120 ml) showing a single sharp peak at 70 ml for OmpTΔL8. (B) Coomassie-stained SDS-PAGE gel showing contents of GF peak fractions (Lane NB: non-boiled and Lane B: boiled). The arrow indicates OmpTΔL8 (~ 38 kDa).

3.7. Discussion

The OmpF/C orthologs of *E. cloacae* (OmpE35, OmpE36) and *K. pneumoniae* (OmpK36) were recombinantly expressed in the OM in the porin deficient omp8 strain of *E. coli*. Despite considerable loss of proteins during the purification steps, the overall high expression levels of OmpE35/E36/K36 enabled us to obtain approximately ~ 2-3 mg of pure proteins per litre of cells which were used for crystallisation. On other hand, the membrane expression of *V. cholerae* porins, OmpU and OmpT was comparatively poor. Average yield of OmpU was approximately 1 mg of protein per litre of cells while the yield for membrane-expressed OmpT was 5-fold less (~ 0.2 mg per litre of cells). In addition, OmpT fractions isolated from the membrane contained

several impurities that were persistent despite multiple rounds of purification. The histidine tag employed to improve the efficiency of OmpT purification and get rid of the impurities instead resulted in protein aggregation due to imidazole. At last, IB-expression of OmpT produced pure protein with typical yield of 4 mg per litre of cells.

The reports for the native expressions of OmpU and OmpT in the wild type strains of *V. cholerae* are available in plenty but data for the recombinant membrane expressions of these proteins is scarce (Khan et al., 2012). To our knowledge, this is the first study to describe the recombinant expression of OmpT in *E. coli*. The reasons for poor membrane expression levels of OmpT compared to OmpU in *E. coli* are not clear.

The isolation of the N-terminal deletion mutant of OmpU, OmpUΔN, from *E. coli* OM was almost as challenging as for OmpT. The purified fractions of OM-expressed OmpUΔN displayed the presence of impurities and yielded an average amount of 0.2 mg of protein per litre of cells which is a little unexpected considering the comparatively high membrane expression levels achieved for OmpU (~ 1 mg/L). This suggests that deletion of the N-terminus may somehow be involved in the export or effective localisation of OmpU and might account for the poor membrane expression levels of OmpUΔN. Unfortunately, the studies providing evidence for the role of N-terminus in the export or localisation of the mature protein in the OM are limited. Nontheless, a few reports demonstrate the significance of N-terminus (Rasmussen and Silhavy 1987 and Bosch et al., 1988) in efficiently exporting the mature protein precursor to the OM. Some other groups have shown the C-terminus to contain motifs that are required for the targeting of the proteins to the OM (Robert et al., 2006, Tommassen 2010 and Rollauer et al., 2015). These studies suggest both N- and C- terminal ends contain essential information for the effective insertion of a protein in the OM. Thus, the deletion of N-terminus might have affected the export or insertion of OmpUΔN causing the decrease in its expression levels compared to wild type OmpU.

Chapter 4. Crystallisation and structure determination of OMPs using X-ray crystallography

4.1. Introduction

The structural paradigm for the typical general porins of Gram-negative bacteria is set by the two major general porins, OmpF (Cowan et al., 1992) and OmpC (Figure 4.1; Basle et al., 2006) of *E. coli* which consist of a 16 stranded β-barrel formed by long extracellular loops and short periplasmic turns (also see section 1.3.1.2). In OmpF (and other porins), N- and C- terminal ends of the protein constitute the β-16 strand (Figure 4.1). Unlike *E. coli* OmpF/C, the structural data for *Enterobacter cloacae* porins (OmpE35 and OmpE36) are not available. The structure of OmpK36 porin of *Klebsiella pneumoniae*, however has been determined previously at a low resolution of 3.2 Å (Dutzler et al., 1999). With 1OSM as the PDB code, the OmpK36 trimer shows a 16 stranded β-barrel constricted by L3 loop for each monomer (Dutzler et al., 1999). In order to perform detailed structural analysis, we attempted to obtain a high resolution structure for OmpK36, in addition to determining the structures for OmpE35 and OmpE36.

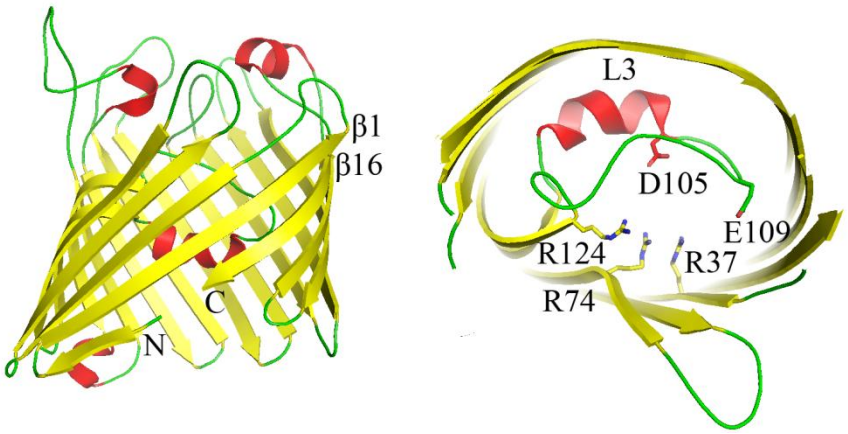

Figure 4.1. Structure of OmpC.
The figure shows cartoon for OmpC monomer from the side (left panel) and extracellular environment (right panel). The constriction zone of OmpC comprises the acidic residues of loop L3 (Asp105 and Glu109) opposite the positive charged residues (Arg37, Arg74 and Arg124). The figures were made using PyMol (Schrödinger 2010) from PDB ID 2J1N (Basle et al., 2006).

Vibrio cholerae OmpU and OmpT have been widely investigated over the past 10-15 years at the genetic level (Crawford et al., 1998 and Li et al., 2000) but no structural data for these two proteins has been reported. Due to the implication of these OMPs in the virulence of *V. cholerae* (Wibbenmeyer et al., 2002, Merrell et al., 2001 and Provenzano and Klose 2000), the

structure determination of these two major porins might provide an insight into the pathogenesis of *V. cholerae*. Based on their homology to OmpF/C proteins, both proteins (OmpU and OmpT) are assumed to form water-filled channels across the OM (Chakrabarti et al., 1996) and based on the structure prediction programs, OmpU is speculated to be a 16-stranded β-barrel while OmpT might form a 14-stranded β-barrel (Duret and Delcour 2010).

In the present study, MemGold and MemGold2 (Molecular Dimensions) are the two main crystal screens used for the crystallisation of the purified OMPs (as described in Chapter 3). Typical protein concentration used for setting up the crystal drops was 10 mg/ml (unless stated otherwise; also see sections 2.6 and 2.7). This chapter describes the high-resolution 3D structures of *E. cloacae* OmpE35 and OmpE36, *K. pneumoniae* OmpK36 and *V. cholerae* OmpU and OmpT (also see Table 2.10 and section 2.8). The structures of OmpU and OmpT revealed interesting constrictions inside their channels that led us to construct deletion mutants, OmpUΔN and OmpTΔL8 respectively. OmpUΔN has a deletion of the first 10 residues of the N-terminus of OmpU whereas in OmpTΔL8, 16 residues of loop L8 of OmpT are deleted (also see sections 3.4 and 3.6).

4.2. Crystallisation trials for OmpE35, OmpE36 and OmpK36

The initial crystal screens of proteins were set up at concentrations of 10 mg/ml (for OmpE35), 24 mg/ml (for OmpE36) and 18 mg/ml (OmpK36) using a Mosquito crystallisation robot. The crystal hits obtained for each protein were optimised (see section 2.6.2) to obtain high quality crystals that were sent to DLS (Figure 4.2). Table 4.1 lists the conditions that generated the crystals diffracting to highest resolution for OmpE35, OmpE36 and OmpK36.

Table 4.1. Optimised crystal conditions.
The optimised conditions of OmpE35/E36, OmpK36, OmpU/UΔN and OmpT/TΔL8 crystals diffracting to highest resolution at the synchrotron.

Protein	Expression	Crystal Screen	Crystal Condition
OmpE35	OM-expressed	MemGold2	0.2 M Ammonium sulfate, 0.05 M ADA, 13% w/v PEG 4000, pH 6.5
OmpE36	OM-expressed	MemGold2	0.4 M Ammonium sulfate, 0.1 M MES, 10% w/v PEG 3350, pH 6.5
OmpK36	OM-expressed	MemGold2	0.08 M Magnesium acetate tetrahydrate, 0.1 M Na citrate, 14% w/v 5000 PEG MME, pH 6.0
OmpU	OM-expressed	MemGold2	0.2 M sodium acetate, 0.1 M MES, 28% w/v 400 PEG, pH 6.5
OmpT	OM-expressed	MemGold	15% PEG 4000, 0.1 M sodium acetate, 0.4 M ammonium thiocyanate, pH4.5
OmpT	IB-expressed	MemGold	0.1 M sodium chloride, 0.1 M MES, 33% v/v PEG 400, 4% v/v ethylene glycol, pH 6.5
OmpUΔN	IB-expressed	MemGold	0.1 M sodium chloride, 0.05 M bicine, 33% PEG 300, pH 9.0
OmpTΔL8	IB-expressed	MemGold2	0.05 magnesium acetate, 0.1 M glycine, 32% PEG 400, pH 9.5

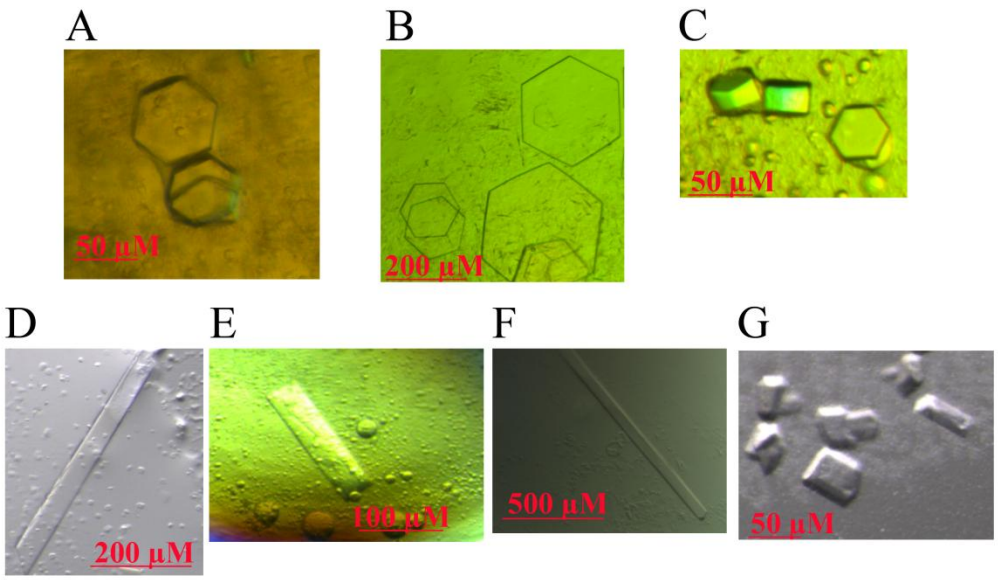

Figure 4.2. Crystals formed by the OMPs.
The figure shows pictures of the crystals for OmpE35 (A), OmpE36 (B), OmpK36 (C), OmpU (D), OmpUΔN (E), OmpT (F) and OmpTΔL8 (G) which were sent to DLS for X-ray diffraction data collection.

4.3. Crystallisation trials for OmpU/UΔN and OmpT/TΔL8

Crystallisation for OmpU (OM-expressed) and OmpUΔN (IB-expressed) was done at 10 mg/ml and the hits were optimised to produce big crystals using vapour diffusion (Figure 4.2). The crystal conditions of OmpU and OmpUΔN that diffracted to the highest resolution are listed in Table 4.1. The crystallisation for OM-expressed OmpUΔN proved difficult and produced no crystal hits primarily because of the poor quality of the purified protein fractions (as discussed in section 3.4). The total amount of protein obtained from large-scale culture of OM-expressed OmpT (see section 3.5.2) was adequate to set up the crystal screens (MG and MG2) at 8 mg/ml. One of the screen conditions (Table 4.1) generated a small crystal (~ 50 µM) which diffracted to 3.2 Å at DLS. Attempts to optimise this condition didn't generate any crystals. On the other hand, crystallisation of IB-expressed OmpT and OmpTΔL8 at 15 mg/ml produced multiple crystals (Figure 4.2), the best ones of which were sent to DLS (Table 4.1).

4.4. Crystal structure of OmpE36 with bound LPS

The structure of OmpE36 was solved by molecular replacement with *E. coli* OmpC as a search model [PDB code 2J1N and 66% sequence identity] using data to 1.45 Å resolution. Table 4.2 lists the statistics of X-ray diffraction data and refinement of OmpE36.

Table 4.2. X-ray diffraction and refinement statistics for OmpE36

Data collection		***Refinement statistics***	
Beamline	DLS I02	Resolution (Å)	48.92-1.45
Wavelength (Å)	0.9796	Reflections (n)	529555
Space group	$P2_1$	R_{work}/R_{free} (%)*	15.2/17.8
Cell dimensions (a,b,c), (α,β,ϒ)	109.75, 123.26, 116.01 90.00, 91.01, 90.00	Atoms (n) Protein/solvent ligand/detergent	16245/1910 1239/231
Molecules/AU	6	B factors ($Å^2$) Protein/solvent ligand/detergent	17/30 37/42
Solvent content (%)	65	Rmsd bond lengths (Å) bond angles (^{O})	0.0095 1.5091
Resolution (Å)	48.92-1.45	Ramachandran plot (%) Most favoured/outliers	95.5/0.6
Completeness	99.6 (100)		
Redundancy	3.7 (3.7)		
I/ σ	8.0 (1.6)		
Rpim (%)	4.9 (46)		
CC (1/2)	0.98 (0.62)		

Values in parentheses refer to the highest resolution shell.
*R_{free} was computed as for R_{work} using a test set (~5%) of randomly selected reflections that were omitted from the refinement

The crystal was obtained in space group $P2_1$ and shows two trimers in the asymmetric unit (AU). Due to the high resolution of the data (higher than 2.0 Å), NCS restraints were not applied applied during refinement. The two trimers are stacked in a double layered head-to-head arrangement, with lattice contacts between the periplasmic ends of the β-barrels in the AU. OmpE36 showed a typical arrangement of 3 β-barrel monomers arranged into a trimer (Figure 4.3 A). Each monomer displays 16 antiparallel strands (β1-β16) forming the hollow β-barrel, with 8 long flexible loops (L1-L8) in the extracellular space and 8 short turns (T1-T8) in the periplasmic region (Figure 4.3 B). N- and C- terminal ends of OmpE36 barrel formed a salt-bridge. The loop L2 of each monomer latches over to the top of adjacent monomer in each OmpE36 trimer. The stability of the trimer is owed to the electrostatic as well as hydrogen-bonding interactions between the L2 loop and the groove of adjacent monomer. The typical CR of porins, caused by the folding of L3 loop inside the channel, is also observed in OmpE36 monomer (Figure 4. 3 C). The loop L3 departs from the β-barrel fold and is extended along the inner side of the barrel wall, constricting the pore half-way through the channel. In addition and as seen for OmpF/C porins, loop L3 in OmpE36 harbours two negatively charged residues (Asp105 and Glu109) that are placed opposite the positively charged residues (Arg37, Arg74 and Arg124) lining the β-barrel wall (Figure 4.3 C).

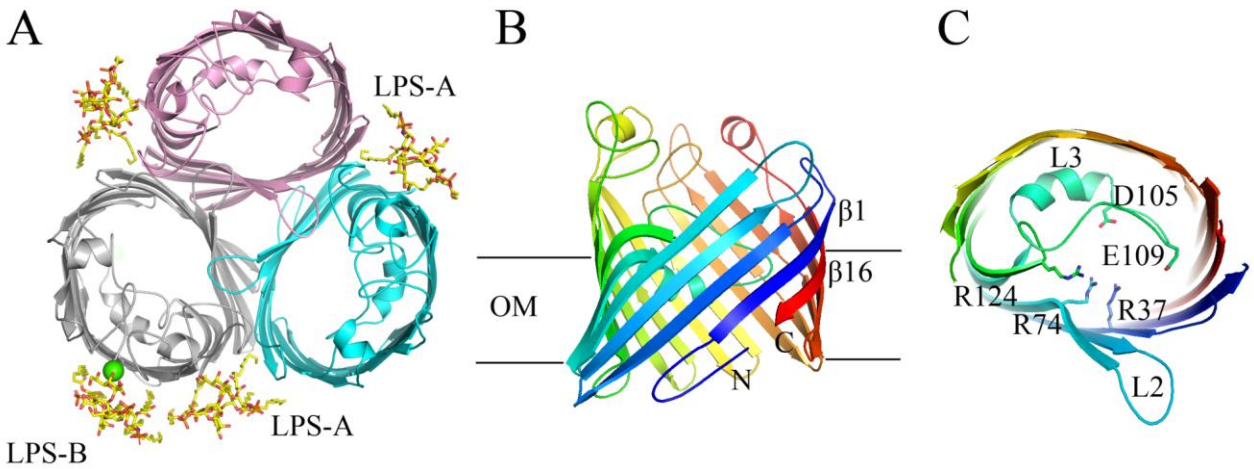

Figure 4.3. Structure of *E. cloacae* OmpE36.
(A) The extracellular view of OmpE36 trimer with 3 β-barrel monomers bound to 4 LPS molecules at site A (LPS-A) and site B (LPS-B), with calcium ion shown as green sphere. (B) The rainbow cartoon of 16-stranded β-barrel of OmpE36 monomer displaying salt-bridged N- (blue) and C-terminus (red). (C) Constriction region of OmpE36 is formed by the charged residues present in loop L3 (Asp105 and Glu105) and the barrel wall (Arg37, Arg74 and Arg124).

The F_o-F_c difference map of refined OmpE36 showed electron density on the outer surface of barrel wall close to L4, L5 and L6 extracellular loops of every protein chain. After careful inspection, the electron density was found to be matching with lipopolysaccharide (LPS) which forms an integral part of the outer leaflet of the OM. So far, there is only one structure in the PDB that has reported LPS bound to an OMP (the siderophore TBDT FhuA of *E. coli*; Ferguson et al., 1998). OmpE36-LPS is thus the second structure to show the interaction of LPS with an OMP but is the first porin to show bound LPS. Each OmpE36 trimer shows the presence of 4 bound LPS molecules and since the AU consisted of 2 trimers, a total of 8 LPS molecules are found for OmpE36 structure (Figure 4.3 A). The crystal structure exhibits two different positions of LPS molecules; LPS-A corresponds to the site where LPS is bound in each groove between two monomers and LPS-B corresponds to an additional site on just one monomer per trimer (Figure 4.3 A). As a result, each trimer contains 3 LPS-A and 1 LPS-B molecule. The LPS molecule at site B (LPS-B) serves as a sandwich between the two symmetry-related protein molecules and explains why only one of the monomers (per trimer) is bound to 2 LPS molecules.

The typical structure of LPS in gram-negative bacteria includes three main components: 1) a hydrophobic lipid A, a short hydrophilic core oligosaccharide and a hydrophilic O-antigen (also see section 1.1.2 and Figure 1.2). In the OmpE36 structure (Figure 4.4), both LPS-A and LPS-B molecules show clear density for the glucosamine disaccharide unit ($GlcN_I$ and $GlcN_{II}$) and the KDO residues (KDO_I and KDO_{II}) of lipid A moiety while in LPS-B (but not in LPS-A) the density extends beyond KDO_{II} to reveal the linked manno-pyranose ring of heptose sugar GMH (L-glycero-D-manno-heptopyranose). The structure of FhuA-LPS complex showed hexaacylated lipid A (Ferguson et al., 1998) but in OmpE36 we observe heptaacylated lipid A for both LPS-A and LPS-B molecules. The two glucopyranose rings of lipid A disaccharide are each acylated at two positions by 3-hydroxymyristic acid residues (FTT), accounting for 4 FTT chains per disaccharide unit. Three of these FTT chains are further acylated on their hydroxyl groups either by lauric acid (DAO) or myristic acid (MYR) residues, generating heptaacylated lipid A for each LPS molecule which is quite interesting because heptaacylated LPS is thought to be uncommon in *E. coli*.

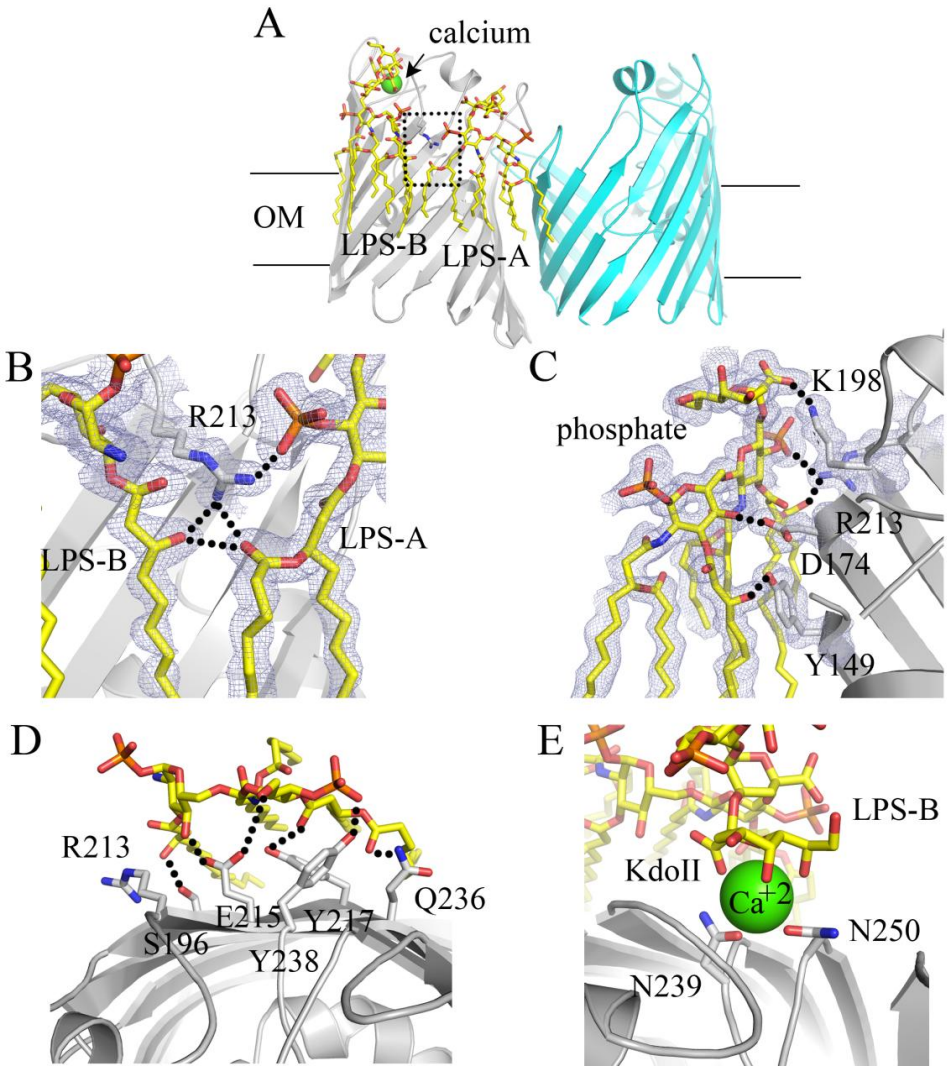

Figure 4.4. LPS bound to OmpE36.
(A) The side view of OmpE36 trimeric structure shows the monomer (in gray) bound to 2 molecules of LPS; LPS-A and LPS-B with one calcium ion (green sphere) between LPS-B and OmpE36. (B) Dotted box in A is zoomed in to show the triad H-bond formed between Arg213, LPS-A and LPS-B. Multiple interactions of OmpE36 residues with (C) LPS-A and (D) LPS-B molecules. (E) The bound calcium ion forms ionic interactions with the OmpE36 residues Asn250 and Asn239, and Kdo_{II} of LPS-B. The panels B and C show 2Fo-Fc map contoured at 1.5σ.

LPS-A and LPS-B are linked to each other via H-bonding between their fatty acyl chains and both molecules show multiple polar (ionic and H-bonds) interactions with OmpE36 residues (Table 4.3). In LPS-A (Figure 4.4 C), $GlcN_I$ forms H-bonds with the carboxylate oxygen of Asp174 while $GlcN_{II}$ shows H-bonding with the basic residues Lys198 and Arg213. The KDO_I of LPS-A forms a single ionic interaction with Lys198 whereas KDO_{II} shows interactions with residues Lys152, Glu159, Arg199 and Ser201. In LPS-B (Figure 4.4 D), Tyr238 H-bonds with

$GlcN_{II}$ and the two carboxylate oxygens of Glu215 interact with both GlcNI and $GlcN_{II}$. Since KDO_I of LPS-B is oriented away from the barrel wall of OmpE36, it does not interact with any protein residue but KDO_{II} of LPS-B shows interactions with 2 asparagines; the side chain of Asn210 and α-carboxyl of Asn250. Interestingly, the crystal structure displays a strong electron density peak consistent with a metal atom between LPS-B and OmpE36 residues. Because of the high-resolution data (1.45 Å), we were able to rule out sodium (Na) and magnesium (Mg) through initial refinement runs by placing each metal atom one at a time. The calcium metal atom fitted perfectly with the evident density (Figure 4.4 E) which was further confirmed by a metal-binding site validation server CheckMyMetal (Zheng et al., 2017). Since calcium ion was neither present in the expression/purification conditions nor in the crystallisation condition, its presence in OmpE36 structure suggests that it must have been co-purified from *E. coli*.

Table 4.3. List of H-bond interactions between OmpE36 residues and LPS (A/B) molecules; and ionic interactions formed by calcium ion with LPS-B and protein residues.

Residue of E36-C chain	LPS atom (moiety)	H-bond distance (Å)
174 Asp, OH	2 $GlcN_I$, O4 (LPS-A)	2.63
174 Asp, OH	3 $GlcN_{II}$, N2 (LPS-A)	2.82
149 Tyr, OH	7 FTT, O3 (LPS-A)	2.69
213 Arg, NH_2	11 MYR, O1 (LPS-A)	3.56
213 Arg, NH_2	9 FTT, O2 (LPS-A)	3.6
213 Arg, NH_2	6 PO_4, O3 (LPS-A)	2.78
198 Lys, NH_2	4 KDO, O1 (LPS-A)	2.84
198 Lys, NH_2	3 $GlcN_{II}$, O4 (LPS-A)	3.6
198 Lys, NH2	6 PO_4, O1 (LPS-A)	2.8
160 Asp, OH	5 KDO, O5 (LPS-A)	2.52
199 Arg, O-	5 KDO, O8 (LPS-A)	2.86
159 Glu, O-	5 KDO, O4 (LPS-A)	2.8
152 Lys, NH_2	5 KDO, O1 (LPS-A)	2.91
152 Lys, NH_2	5 KDO, O6 (LPS-A)	3.2
152 Lys, NH_2	5 KDO, O5 (LPS-A)	2.81
201 Ser, NH	5 KDO, O7 (LPS-A)	2.99
11 MYR, O1 (LPS-A)	7 FTT, O3 (LPS-B)	3.09
213, Arg, NH	7 FTT, O3 (LPS-B)	3.58
196, Ser, OG	7 FTT, O3(LPS-B)	2.9
215, Glu, OH	9 FTT, O2 (LPS-B)	3.23
215, Glu, OH	2 $GlcN_I$, O4 (LPS-B)	2.41
250, Asn, OH	5 KDO, O5 (LPS-B)	3.11
217, Tyr, OH	9 FTT, O2 (LPS-B)	3.54
239, Asn, NH	5 KDO, O1A (LPS-B)	2.79
210, Asn, OH	5 KDO, O5 (LPS-B)	2.94
215, Glu, OH	3 $GlcN_{II}$, N2 (LPS-B)	3.14

236, Gln, NH	12 DAO, O1 (LPS-B)	3.31
238, Tyr, OH	6 PO_4, O3 (LPS-B)	2.64
238, Tyr, OH	3 $GlcN_{II}$, O4 (LPS-B)	3.58
251, Lys, NH	6 PO_4, O3 (LPS-B)	3.43
Residue/LPS molecule	**Metal ion**	**Ionic bond distance (Å)**
250, Asn, O-	Calcium	2.36
239, Asn, O-	Calcium	2.49
210, Asn, O-	Calcium	2.35
5, KDO, O7- (LPS-B)	Calcium	2.59
5, KDO, O1- (LPS-B)	Calcium	2.46
5, KDO, O5- (LPS-B)	Calcium	2.45
5, KDO, O6- (LPS-B)	Calcium	2.59

*Abbreviations for the components in the molecules of LPS-A and LPS-B are listed in the Abbreviation Table.

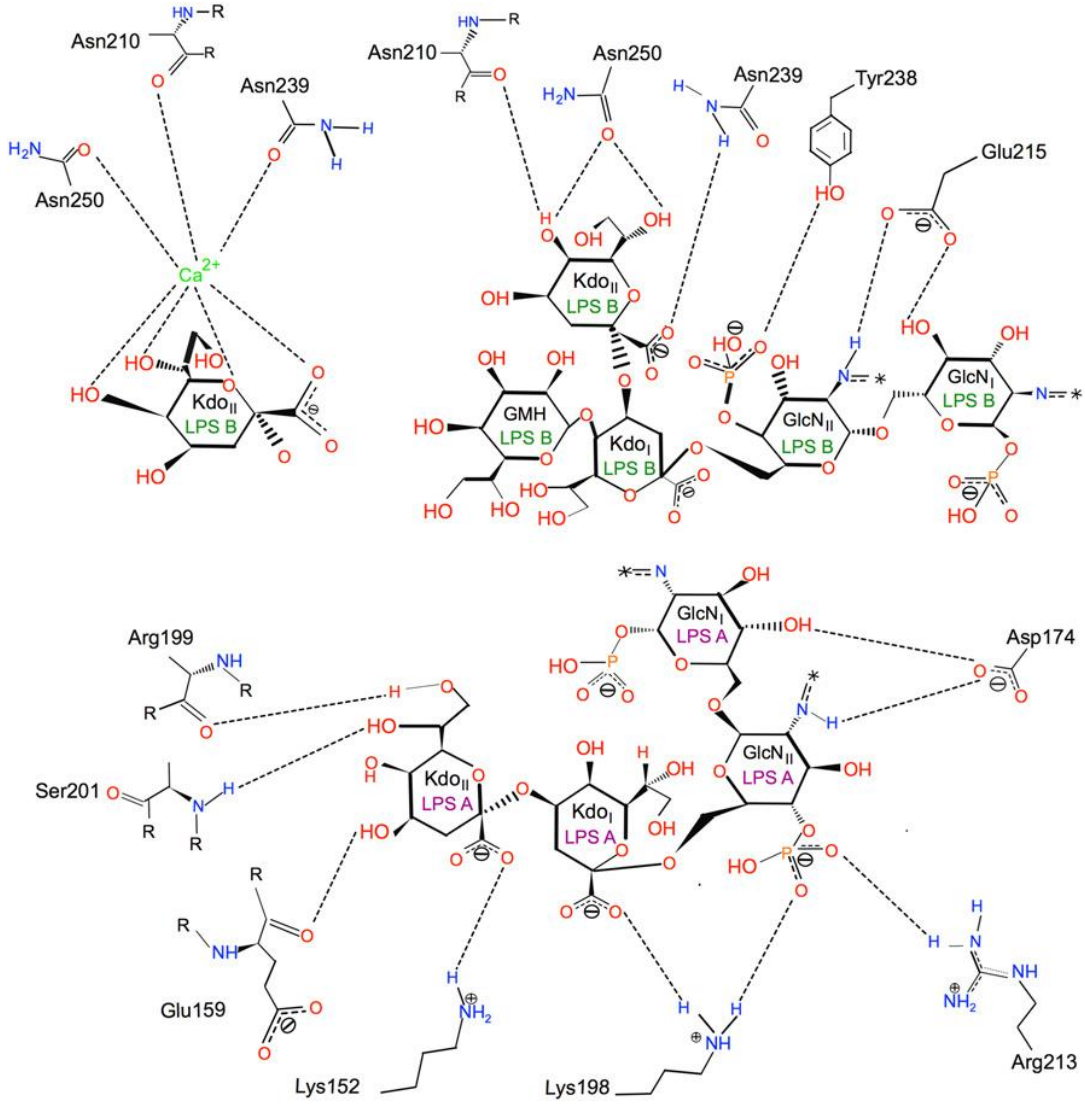

Figure 4.5. 2D diagram of LPS interactions with OmpE36 resdiues.
The diagram depicts the interactions of LPS-A and LPS-B molecules with the protein residues and was generated using the online software program PoseView (Stierand and Rarey 2010). For the abbreviation of the LPS components, see the List of Abbreviations.

The ligands of the calcium ion are the side chains of Asn239 and Asn250 as well as the backbone carbonyl of Asn210 (Table 4.3). In addition, four functional groups on Kdo_{II} provide ligands to the calcium ion (Table 4.3). In this structure, the presence of calcium ion shows the important role played by metal ions in maintaining the binding of LPS to protein. An overview of the interactions between LPS-A/B and OmpE36 residues is presented in Figure 4.5 as a 2D-structure diagram generated by PoseView (Stierand and Rarey 2010).

The structure of the complex of OmpE36-LPS has been published recently in PNAS (Arunamanee et al., 2016). This paper discusses the high-affinity LPS binding sites in Gram-negative bacterial porins (like OmpF). The paper not only shows the importance of the LPS-binding site (LPS-B) in stabilising the OmpF trimer but also sheds a light on its essential role in the OM biogenesis of porins.

4.5. Crystal structure of OmpE35

Table 4.4. X-ray diffraction and refinement statistics for OmpE35.

Data collection		***Refinement statistics***	
Beamline	DLS I04-1	Resolution (Å)	45.8-2.3
Wavelength (Å)	0.9282	Reflections (n)	70510
Space group	$C222_1$	R_{work}/R_{free} (%)*	20.6/24.6
Cell dimensions	137.55, 187.25, 122.96	Atoms (n) Protein/solvent	7736/188
(a,b,c), (α,β,ϒ)	90.00, 90.00, 90.00	ligand/detergent	35/79
Molecules/AU	3	B factors ($Å^2$) Protein/solvent	53/46
		ligand/detergent	67/61
Solvent content (%)	65	Rmsd bond lengths (Å)	0.015
		bond angles (^{O})	1.405
Resolution (Å)	46.81-2.30	Ramachandran plot(%) Most favoured/outliers	95.2/0.1
Completeness	100 (99.9)		
Redundancy	7.6 (7.5)		
I/ σ	16 (1.4)		
Rpim (%)	3 (56)		
CC (1/2)	0.99 (0.63)		

Values in the parentheses refer to the highest resolution shell.
*R_{free} was computed as for R_{work} using a test set (~5%) of randomly selected reflections that were omitted from the refinement.

The crystals produced from the purified OmpE35 in this study diffracted to low resolution (≥ 3.0 Å). However, one of the colleagues from the lab was able to get good quality diffraction for OmpE35 crystals for a different batch of purified protein. The resolution achieved for the best diffracting crystal of OmpE35 was 2.3 Å with the space group $C222_1$. The phase problem for OmpE35 was solved by molecular replacement using *E. coli* OmpF (PDB accession code 2ZFG; sequence identity 80%) as a search model. The X-ray diffraction data collection and refinement statistics are mentioned in Table 4.4.

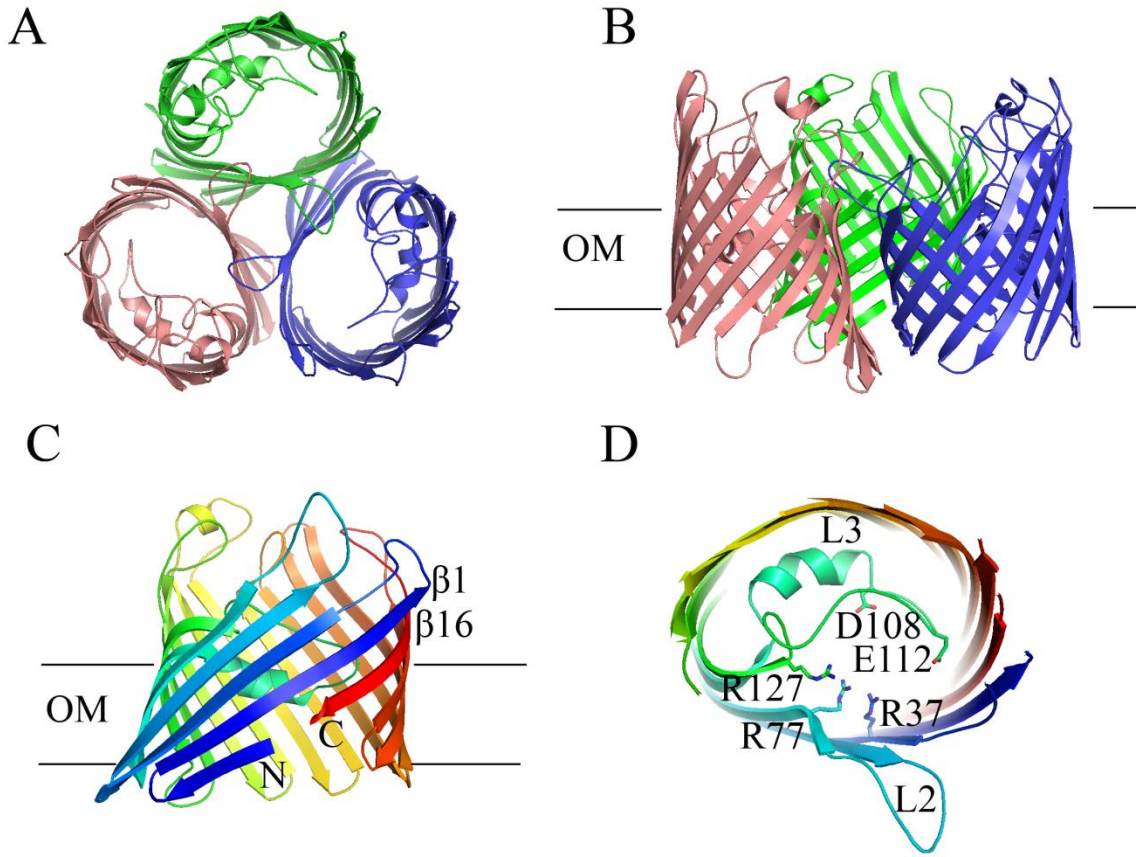

Figure 4.6. Structure of *E. cloacae* OmpE35.
The cartoon views from the (A) extracellular side and (B) OM plane display the 3 β-barrel monomers arranged into a trimer of OmpE35. (C) Each monomer is a 16 β-stranded barrel (rainbow) forming a salt-bridged N- and C-terminus. (D) The constriction region is formed by the charged residues of loop L3 (Asp108 and Glu112) and the barrel wall (Arg37, Arg77 and Arg127).

The crystal of OmpE35 reveals one trimer in the AU (Figure 4.6 A). Like OmpE36, 16 antiparallel β-strands of each OmpE35 monomer form 8 extracellular loops (L1-L8) and short periplasmic turns (T1-T8) (Figure 4.6 C). The negative charged loop L2 latchs over from one monomer to the positive charged groove of the adjacent monomer and stabilises the OmpE35

trimer. The β-16 strand shows N- and C- termini linked through a salt bridge. The asymmetric charge distribution across the channel is mediated by the loop L3 folded inside causing the constriction of OmpE35 pore. The negative charged residues Asp108 and Glu112 of loop L3 are faced opposite the positive ladder of Arg37, Arg77 and Arg127 in the β-barrel wall (Figure 4.6 D).

4.6. Crystallographic structure of OmpK36

The best crystal of OmpK36 diffracted to ~ 1.65 Å resolution at the synchrotron and the phase problem was solved using the low-resolution structure of previous deposited OmpK36 (with PDB code 1OSM) as the molecular replacement model. The crystallographic data and refinement statistics are summarised in Table 4.5.

Table 4.5. X-ray diffraction and refinement statistics for OmpK36.

Data collection		*Refinement statistics*	
Beamline	DLS I04	Resolution (Å)	107.57-1.65
Wavelength (Å)	0.9793	Reflections (n)	161366
Space group	C2	R_{work}/R_{free} (%)*	14.6/18.9
Cell dimensions (a,b,c), (α,β,ϒ)	232.31, 74.51, 90.81 90.00, 112.17, 90.00	Atoms (n) Protein/solvent ligand/detergent	8032/635 -/54
Molecules/AU	3	B factors ($Å^2$) Protein/solvent ligand/detergent	28.8/39.2 -/49.6
Solvent content (%)	63	Rmsd bond lengths (Å) bond angles (^{O})	0.0136 1.5878
Resolution (Å)	45.4-1.65	Ramachandran plot (%) Most favoured/outliers	95.5-0.6
Completeness	98.5 (97.3)		
Redundancy	3.8 (3.9)		
I/ σ	11.6 (1.6)		
Rpim (%)	3.9 (60)		
CC (1/2)	0.99 (0.68)		

Values in the parentheses refer to the highest resolution shell.
*R_{free} was computed as for R_{work} using a test set (~5%) of randomly selected reflections that were omitted from the refinement.

With the space group of C2, the OmpK36 structure shows the arrangement of three β barrel monomers arranged into a homotrimer in the AU of the crystal (Figure 4.7 A, B). OmpK36

monomer displays a similar protein fold as seen for its orthologs (OmpE35/E36 and OmpF/C). Each monomer is a 16-stranded β-barrel formed by 8 long flexible loops (L1-L8) in the extracellular space and 8 short periplasmic turns (T1-T8). The OmpK36 barrel also shows N- and C-terminal ends linked through a salt bridge, another typical feature of general porins. Loop L3 is folded inside to constrict the barrel and loop L2 latchs over to the grooves of adjacent monomer to stabilise the trimer (Figure 4.7 A). Like other porins, the constriction region (CR) of OmpK36 comprises five charged residues Asp106, Glu110, Arg37, Arg75 and Arg125 (Figure 4.7 D).

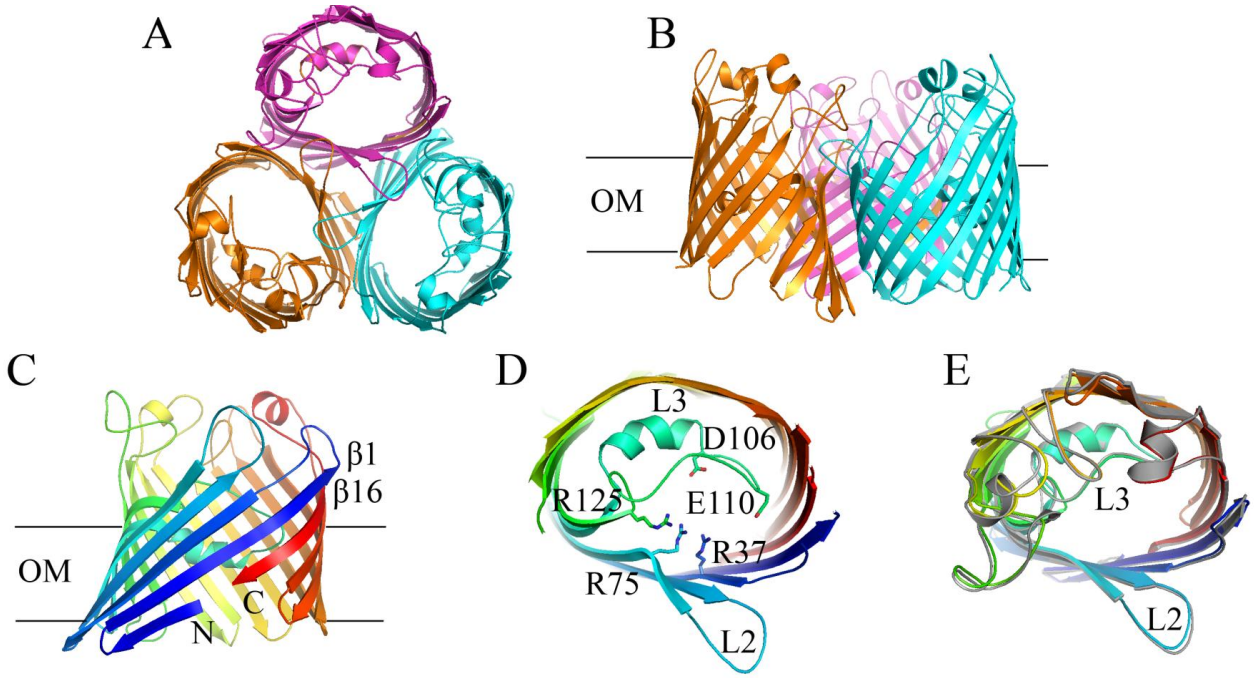

Figure 4.7. Structure of *K. pneumoniae* OmpK36.
The cartoon views from the (A) extracellular side and (B) OM plane display the 3 β-barrels arranged into a trimer of OmpK36. (C) Each 16 β-stranded monomer (rainbow) forms a salt-bridged N- and C-terminus and (D) is constricted in the middle by the positive charged residues of loop L3 (Asp106 and Glu110) and negative charged residues of the barrel wall (Arg37, Arg75 and Arg125). (E) Structural superposition of OmpK36 (in rainbow) and 1OSM (in gray).

The structural superposition of 1OSM (OmpK36, Dutzler et al., 1999) and OmpK36 from our study (Figure 4.7 E), exhibit similar lengths and orientations of the β-strands as well as extracellular loops and periplasmic turns (except turn T4). Unexpectedly however, OmpK36 when superposed on 1OSM gives a Cα core rmsd of 0.7 Å, which is slightly higher than expected considering both are the same proteins. This can be explained by the fact that the proteins are derived from two different strains of *K. pneumoniae* and have a sequence identity of 94% (Figure 4.8). OmpK36 (1OSM), published earlier was obtained from the *K. pneumoniae* strain KT793

(Dutzler et al., 1999) while the protein used in our study is from the *K. pneumoniae* strain ATCC 43816 (GenBank Assembly GCA_000742755.1). Thus, 1OSM and OmpK36 have the same protein fold but the difference in the two proteins sequences accounts for the somewhat high core r.m.s.d. value after superposition (Figure 4.7 E).

```
OmpK36          1 AEIYNKDGNKLDLYGKIDGLHYFSDDKSVDGDQTYMRVGVKGETQINDQL     50
1OSM            1 AEIYNKDGNKLDLYGKIDGLHYFSDDKDVDGDQTYMRLGVKGETQINDQL     50

OmpK36         51 TGYGQWEYNVQANNTESSSDQAWTRLAFAGLKFGDAGSFDYGRNYGVVYD     100
1OSM           51 TGYGQWEYNVQANNTESSSDQAWTRLAFAGLKFGDAGSFDYGRNYGVVYD     100

OmpK36        101 VTSWTDVLPEFGGDTYGSDNFLQSRANGVATYRNSDFFGLVDGLNFALQY     150
1OSM          101 VTSWTDVLPEFGGDTYGSDNFLQSRANGVATYRNSDFFGLVDGLNFALQY     150

OmpK36        151 QGKNGSVSGEGATNNGRGWSKQNGDGFGTSLTYDIWDGISAGFAYSHSKR     200
1OSM          151 QGKNGSVSGEGATNNGRGALKQNGDGFGTSVTYDIFDGISAGFAYANSKR     200

OmpK36        201 TDEQNSVPALGRGDNAETYTGGLKYDANNIYLASRYTQTYNATRAGSLGF     250
1OSM          201 TDDQNQL-LLGEGDHAETYTGGLKYDANNIYLATQYTQTYNATRAGSLGF     249

OmpK36        251 ANKAQNFEVVAQYQFDFGLRPSVAYLQSKGKDLERGYGDQDILKYVDVGA     300
1OSM          250 ANKAQNFEVAAQYQFDFGLRPSVAYLQSKGKDL-NGYGDQDILKYVDVGA     298

OmpK36        301 TYYFNKNMSTYVDYKINLLDDNSFTRNAGISTDDVVALGLVYQF         344
1OSM          299 TYYFNKNMSTYVDYKINLLDDNSFTRSAGISTDDVVALGLVYQF         342
```

Figure 4.8. Sequence alignment of 1OSM and OmpK36 from the present study.
The differences in the two aligned sequences are coloured in red and these residues are mostly correspond to the extracellular loops (except few located in the β-strand regions and are indictaed by black dots in the figure).

4.7. Structural comparison of porin orthologs

The sequence homology studies have classified porins OmpE36/OmpK36 and OmpE35 as orthologs of *E. coli* OmpC and OmpF respectively. Thus, in this section we draw a structural comparison between the three ortholog pairs; OmpE36/OmpC, OmpK36/OmpC and OmpE35/OmpF (OmpC PDB code 2J1N and OmpF PDB code 2ZFG). The low Cα core r.m.s.d. values obtained for the superposition (Table 4.6) imply strong resemblance between the structures of OmpF/C and their respective ortholog (s) that extends from adopting a similar β-barrel fold to displaying a striking similarity in the orientations of the charged residues of the constriction region (CR).

Table 4.6. Structural comparison of OmpF/C orthologs.
The structural superimpositions (using COOT; Emsley and Cowtan 2004) of OmpE35, OmpE36 and OmpK36 on OmpF and OmpC reveal the backbone core Cα r.m.s.d values (in Å) with the sequence identities mentioned in parenthesis (for alignment of ≥ 320 Cα-atoms) .

Protein	OmpF	OmpC	OmpE35	OmpE36	OmpK36
OmpE35	0.6 (80%)	0.8 (66%)	-	0.8 (67%)	1.0 (66%)
OmpE36	0.8 (65%)	0.5 (89%)	0.8 (67%)	-	0.6 (82%)
OmpK36	1.0 (63%)	0.7 (80%)	0.9 (65%)	0.6 (82%)	-

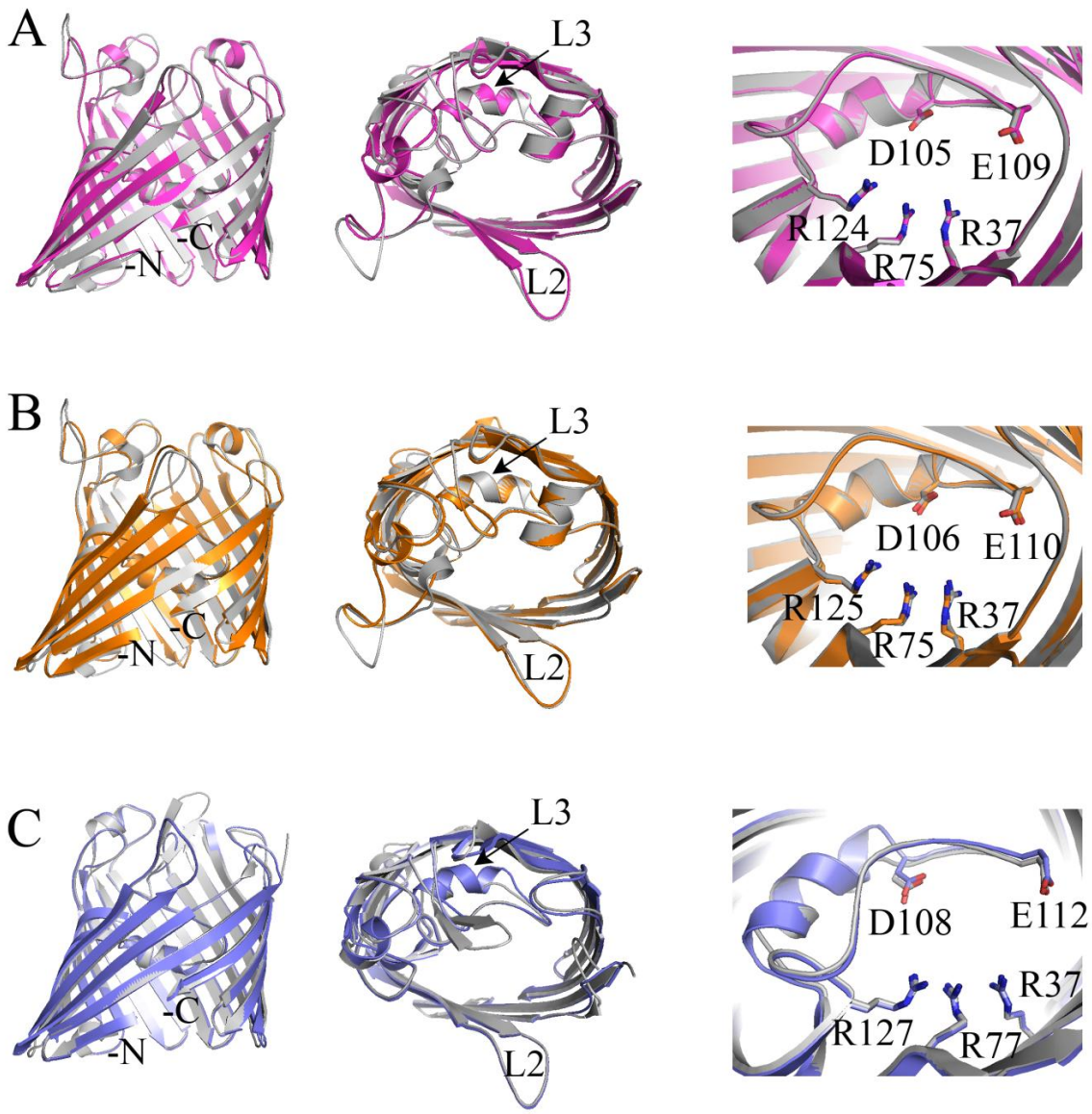

Figure 4.9. Structural superposition of OmpF/C orthologs.
The structures of (A) OmpE36 (magenta), and (B) OmpK36 (orange) are superposed on OmpC (gray in A and B), whereas in (C) the OmpE35 structure (light blue) is superposed on OmpF (gray in C). The left and middle panels show side and extracellular views respectively. The right panels display the charged residues in the CR of OmpE35/E36/K36 to compare their positions with the corresponding CR residues of OmpF/C.

In Figure 4.9, the charged CR residues of OmpC (Arg37, Arg74, Arg124, Asp105 and Glu109) and OmpF (Arg42, Arg82, Arg132, Asp113 and Glu117) are displayed for comparison with their counterparts in OmpE36/K36 and OmpE35 respectively. OmpE36 (Arg37, Arg74, Arg124, Asp05 and Glu105) and OmpK36 (Arg37, Arg75, Arg125, Asp106 and Glu110) exhibit almost identical orientations of the CR residues in comparison to those of OmpC (Figure 4.9 A, B). Likewise, OmpE35 (Asp108, Glu112, Arg37, Arg77 and Arg127) displays similar orientations of the charged residues in the CR as observed for its ortholog OmpF (Figure 4.9 C).

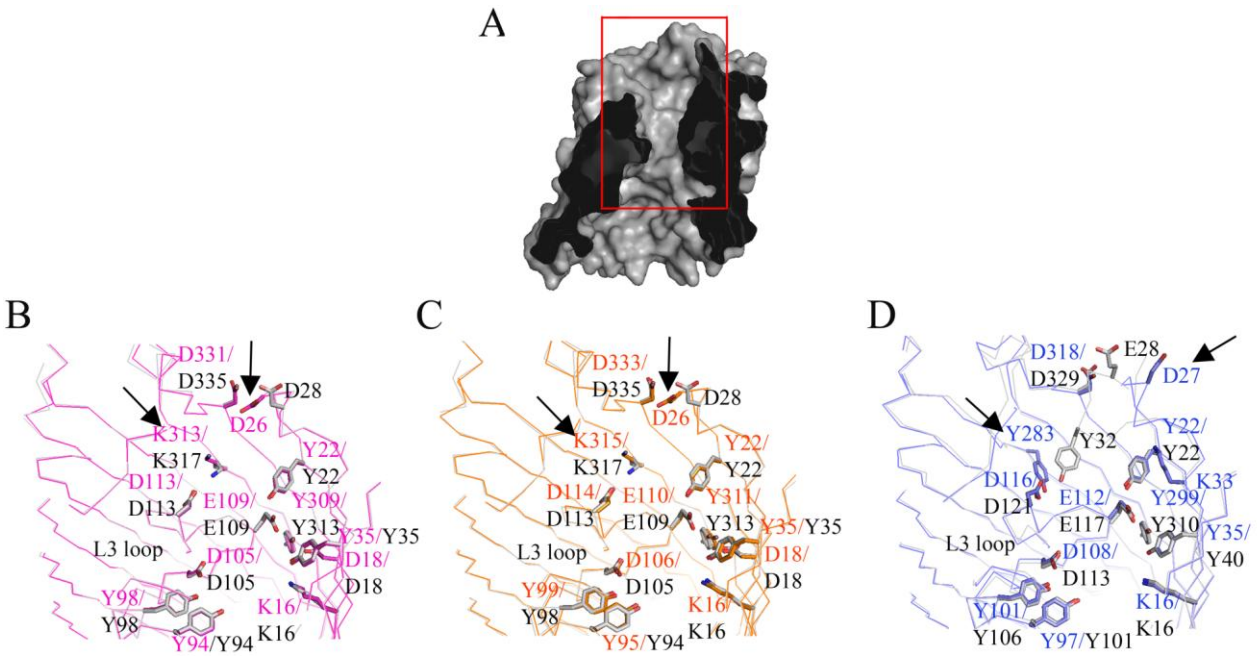

Figure 4.10. Pore-lining residues of OmpF/C orthologs.
(A) Surface view of OmpF from the side to show the pore (boxed in red) and illustrate the structural differences between the ionisable residues lining the pores of (B) OmpE36/OmpC (pink/gray), (C) OmpK36/OmpC (orange/gray) and (D) OmpE35/OmpF (blue/gray). The labelled residues are colour-coded for each protein and residues in black correspond to OmpF/C.

The channels (of OmpE35/E36/K36) display the archetypical strong segregation of positive and negative charges of porins. Although the ionisable residues lining the pore constriction are identical for each ortholog pair, the residues at the vestibule opening at the extracellular surface reveal subtle variations (Figure 4.10). The lysine residue of OmpE36 (Lys313) and OmpK36 (Lys315) show similar orientations but differ from Lys317 of OmpC (marked with arrows in Figure 4.10 A, B). The aspartate residues of OmpE36 (Asp26) and OmpK36 (Asp26) at the vestibule top are located in a different position than the corresponding residue in OmpC (Asp28). In comparison to OmpF, OmpE35 has Asp27 (instead of Glu28 in

OmpF) and has an additional Lys33 oriented towards the vestibule region (marked with arrows in Figure 4.10 C). The counterpart for Y32 of OmpF is missing in OmpE35 and is replaced by Y283, located just above loop L3.

In spite of the significant similarity between the orthologs and OmpF/C, a marked difference is revealed on the comparison of their electrostatic surfaces (Figure 4.11). Asp171 of OmpC does not have a counterpart in OmpE36 and OmpK36 that accounts for an increased positive charged region in their grooves compared to OmpC. This may affect the electrostatics involved between L2 loop-groove interfaces to stabilise the oligomerisation state of porins. In addition, the extracellular view of OmpE36 electrostatics exhibit high negative charged region due to the presence of acidic residues Glu159 (in loop L4) and Asp205 (in loop L5) (Figure 4.11 C). Quite contrary, OmpK36 displays a dominant positive-charged region on its extracellular surface which is owed to the presence of Arg285 (in loop L7) and Arg326 (in loop L8) (Figure 4.11 E). Likewise, OmpE35 shows a pre-dominant negatively charged region in its extracellular surface as compared to OmpF, that arises due to the two subsequent aspartates of loop L8, Asp309 and Asp310 (Figure 4.11 D).

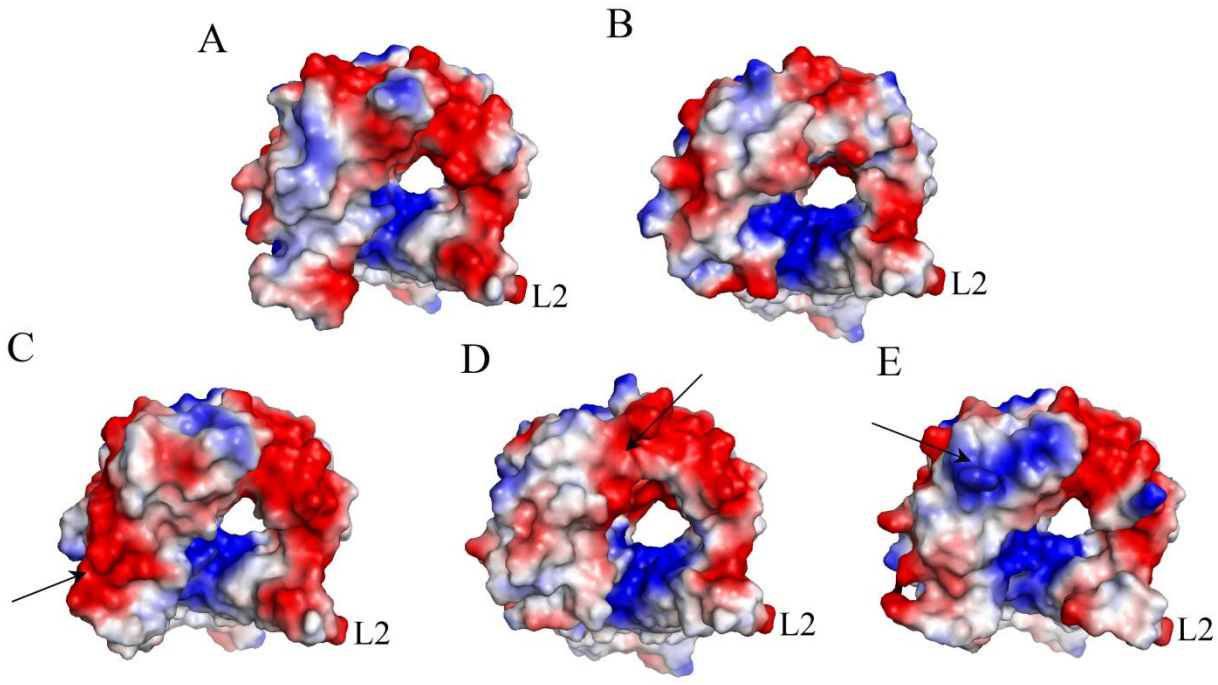

Figure 4.11. Electrostatics of OmpF/C orthologs.
The extracelluar views for the electrostatic surfaces of (A) OmpC (-67.4 kT/e to +67.4 kT/e), (B) OmpF (-62.5 kT/e to +62.5 kT/e), (C) OmpE36 (-72.1 kT/e to +72.1 kT/e), (D) OmpE35 (-67.6 kT/e to +67.6 kT/e) and (E) OmpK36 (-68.1 kT/e to +68.1 kT/e). Arrows indicate the positive or negative charge regions in comparison to the surfaces of OmpF/C. The figures for the electrostatic surface potentials were made using PymoL (Schrödinger 2010).

One of the main goals to determine these porin structures (OmpE35/E36/K36) is not only to analyse the structural differences but understand the effect of these differences on the uptake of different types of compounds. We are working on a paper that describes permeability prediction of different molecules through Gram-negative bacterial porins. The paper is under final stages of completion for submission (also see section 5.1) and is a collaboration of 3-4 labs from the European Innovative Medicines Initiative (IMI) consortium.

4.8. Crystal structure of OmpU shows an N terminal constriction element

The structure of OmpU was solved via molecular replacement using data to 1.55 Å resolution (Table 4.7), with the structure of the *Salmonella typhi* OmpC loop deletion mutant as the search model (PDB accession code 3UPG; sequence identity ~ 26%).

Table 4.7. X-ray data collection and refinement statistics for OmpU

Data collection		***Refinement statistics***	
Beamline	DLS I03	Resolution (Å)	49.49 – 1.55
Wavelength (Å)	0.97949	Reflections (n)	171689
Space group	$P2_1$	R_{work}/R_{free} (%)*	17/19.9
Cell dimensions	62.7, 153.8, 66.2	Atoms (n) Protein/solvent	7325/674
(a,b,c), (α,β,ϒ)	90, 102, 90	ligand/detergent	0/99
Molecules/AU	3	B factors ($Å^2$) Protein/solvent	23.0/32.2
		ligand/detergent	-/38.4
Solvent content (%)	58.3	Rmsd bond lengths (Å)	0.023
		bond angles (^{O})	2.14
Resolution (Å)	49.49 – 1.55	Ramachandran plot (%) Most favoured/outliers	94.55/0.64
Completeness	97 (95)		
Redundancy	3.9 (4.0)		
I/ σ	9.8 (1.4)		
Rpim (%)	3.7 (55.5)		
CC (1/2)	0.9 (0.5)		

Values in the parentheses refer to the highest resolution shell.
*R_{free} was computed as for R_{work} using a test set (~5%) of randomly selected reflections that were omitted from the refinement.

The OmpU structure showed a trimer in the AU and each monomer with 16-stranded β-barrel displays typical features of the porin (Figure 4.12 A). Like other porins, the L2 loop latches into the groove of the adjacent monomer and forms hydrogen bonding as well as electrostatic interactions that stabilise the trimer, while the long L3 loop is folded inwards and constricts the

channel (Figure 4.12 A, B). An unusual feature is observed in the structure of OmpU distinguishing it from other typical porins. In OmpU, the α-amino group does not interact with the C-terminus; instead, the first ~11 residues of the N-terminus fold inwards to constrict the lumen of the channel (Figure 4.12 C). Ser12 takes over the role of the N-terminus in OmpF/C, with its side chain hydroxyl interacting with the C-terminal carboxyl group (Figure 4.12 B).

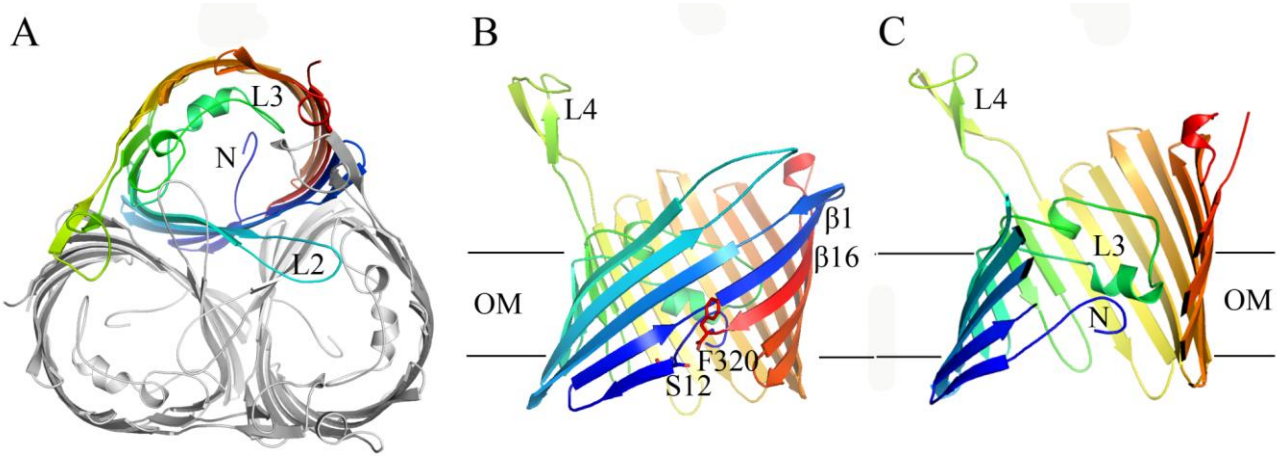

Figure 4.12. Structure of *V. cholerae* OmpU.
(A) Extracellular view of OmpU trimer with one monomer presented as a rainbow cartoon and adjacent two monomers shown in gray. (B) Side view of the monomer in rainbow shows the 16 β-strands of the barrel with loop L4 in extracellular space. (C) Side-cut view displays the N-terminal constriction of OmpU just below loop L3.

The N-terminus forms several interactions with the OmpU residues from the barrel wall and loop L3 (Figure 4.13). The side chain of Asp8 interacts with the side chains of Arg27 and Arg46 in the barrel wall, whereas Asn4 forms a strong hydrogen bond with the backbone of Asp113 and Asp116 in loop L3. The N-terminus masks three basic residues Arg288, Arg317 and Arg27 and one acidic residue Asp319 from the periplasmic space to the inside of the OmpU channel. The presence of the N-terminus and the occurrence of a basic residue in loop L3 (Lys128) makes the archetypal asymmetric charge distribution across the pore seen in OmpF and OmpC orthologs (loop L3 negative, barrel wall positive) less pronounced in OmpU. This probably suggests that the electric field across the pore will be less strong in OmpU compared to Enterobacterial porins. In terms of pore size, the OmpU constriction has a diameter of ~ 5.5 Å, comparable to that of *E. coli* OmpC. To our knowledge, the presence of N-terminus inside the lumen of OmpU marks a novel feature that is observed for the first time in the structure of general diffusion porins.

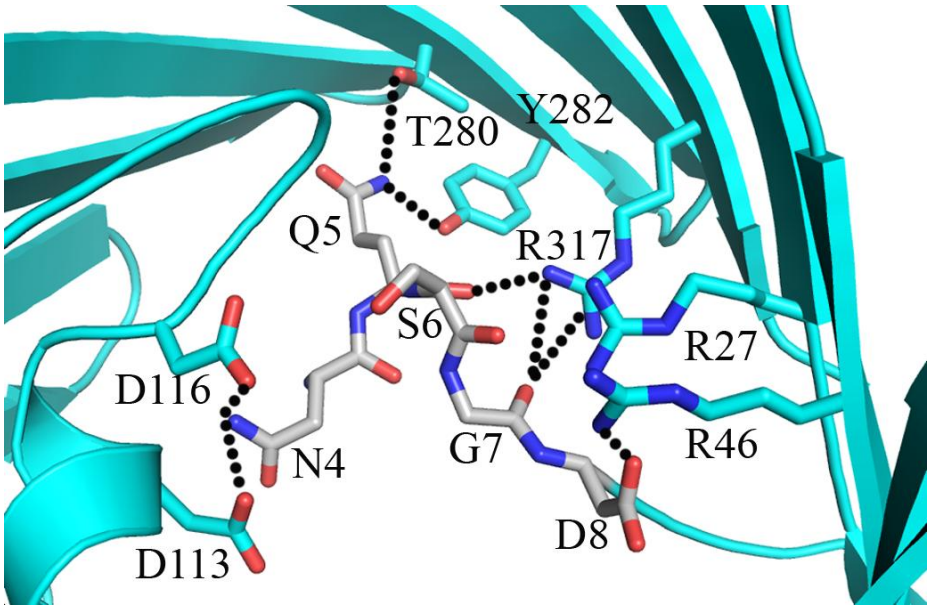

Figure 4.13. Interactions of N-terminus with OmpU residues in the CR.
The residues of the N-terminus (in gray sticks) form hydrogen bonds with the residues of OmpU in loop L3 (D113 and D116) and the barrel wall (R27, R46, T280, Y282 and R317).

The DALI (Holm and Laakso 2016) comparison of OmpU with the PDB structures mapped three proteins with top Z-scores of ~30 and r.m.s.d values of 2.0 Å over ~280 residues. These three proteins are porin 2 from *Providencia stuartii* (PDB code 4D65), phosphoporin PhoE of *E. coli* (PDB code 1PHO) and OmpE36 from *E. cloacae* (PDB code 5FVN). These proteins therefore show more similarity to OmpU than *E. coli* OmpF and OmpC (Table 4.8).

Table 4.8. DALI structural alignment of OmpU.
The table lists the top three proteins of PDB with greatest structural similarity to OmpU, as revealed by DALI, followed by the comparison with the porins OmpF/C and OmpT.

Proteins aligned against OmpU	PDB	Z-score	rmsd	Sequence identity (%)	Aligned residues
Omp-Pst2 (*P. stuartii*)	4D65	30.1	2	28	279
Phosphoporin (*E. coli*)	1PHO	30.1	2.1	25	283
OmpE36 (*Enterobacter cloacae*)	5FVN	30	2.4	25	283
OmpC (*E. coli*)	2J1N	29.6	2.6	24	288
OmpF (*E. coli*)	2ZFG	29.5	2.4	25	281
OmpT (*V. cholerae*)	6EHd	26.5	2.1	19	267

4.9. Crystal structure of OmpT shows that loop L8 constricts the pore

The diffraction datasets of 2.0 Å from the crystals of IB-expressed OmpT (see section 3.5.4) were unsuccessful in generating a good solution during molecular replacement (MR) because of the unavailability of a good MR search model. The attempts with different search models (with PDB accession codes 3UPG, 3VYS, 3PRM, 3RPK etc.) including OmpU by using automated MR pipelines like BALBES (Long et al., 2008) and Mr. BUMP (Keegan and Winn 2007) were not successful to solve the phase problem. However later, one crystal of OmpT (IB-expressed) diffracted to a higher resolution yielding a dataset in space group C2 with one molecule in the AU. For this dataset the phase problem was solved via molecular replacement with OmpU and the OmpT structure was refined using data to 1.66 Å (Table 4.9). In addition, yet another crystal of OmpT from a different condition (0.05 M calcium chloride dihydrate, 0.05 M barium chloride, 0.1 M tris, 32% PEG 400, pH 8.2) yielded one molecule in the AU with space group I432 and the data was refined to 2.7 Å resolution (MR was performed with OmpT as the search model; Table 4.9).

The models generated from both datasets were very similar with one notable difference. Only the I432 crystals showed a trimeric arrangement of OmpT (generated by crystallographic symmetry), with gross features consistent with that of OmpU and other porins (Figure 4.14 A). The monomer of OmpT is a 16-stranded β-barrel (Figure 4.14 B) with the typical porin architecture of the negatively charged L3 loop folded inside the pore and arranged opposite the positively charged residues of the β-barrel wall. The loop L2 is disordered in the crystal structure of OmpT and hence is missing a few residues in the cartoon (Figure 4.14 B). The α-amino group of OmpT interacts with the C-terminal carboxyl group, showing another typical feature of Enterobacterial porins (Figure 4.14 B). However similar to OmpU, the OmpT structure reveals an additional constriction besides loop L3 inside the lumen of its channel. This constriction is caused by extracellular loop L8 that forms a sharp bend in the extracellular space, bringing its tip into the constriction region to interact with and pack against the tip of loop L3 (Figure 4.14 C).

Table 4.9. X-ray data collection and refinement statistics for OmpT (OM and IB expressed).

	monomeric OmpT (IB-expressed)	OmpT (OM-expressed)	trimeric OmpT (IB-expressed)
Data collection			
Beamline	DLS I04	DLS I02	DLS I04
Wavelength (Å)	0.9282	0.979	0.9762
Space group	C2	C2	I432
Cell dimensions (a,b,c), (α,β,ϒ)	143.8, 75.8, 49.6 90, 92.06, 90	144.6, 74.3, 62.3 90, 96.74, 90	200.91, 200.91, 200.91 90, 90, 90
Molecules/AU	1	1	1
Solvent content (%)	64.8	72.2	72.3
Resolution (Å)	49.64 - 1.66	46.41 – 3.2	71.03 - 2.72
Completeness	99 (98)	98 (96)	99 (98)
Redundancy	3.4 (2.5)	3.6 (3.5)	42.2 (43.7)
I/ σ	14.5 (1.1)	5.0 (1.5)	22.1 (1.2)
Rpim (%)	2.2 (61)	8.8 (84.7)	2.5 (67.9)
CC (1/2)	0.9 (0.5)	0.9 (0.5)	1.0 (0.6)
Refinement			
Resolution (Å)	49.64 – 1.66	46.41 – 3.2	71.03 – 2.72
Reflections (n)	62456	6527	18714
R_{work}/R_{free} (%)*	18.6/ 21.4	21.2/24.4	23.9/28.3
Atoms (n)	2521/141	2479/0	2453/12
Protein/solvent ligand/detergent	12/137	0/0	0/0
B factors ($Å^2$)	38.7/45.5	64.2/22.3	99.1/84.8
Protein/solvent ligand/detergent	60.0/57.7	-/-	-/-
Rmsd			
bond lengths (Å)	0.024	0.011	0.016
bond angles (^{O})	2.185	1.528	1.881
Ramachandran plot (%)			
Most favoured/ outliers	94.87/1.28	84.8/2.2	89.5/2.2

Values in the parentheses refer to the highest resolution shell.

*R_{free} was computed as for R_{work} using a test set (~5%) of randomly selected reflections that were omitted from the refinement.

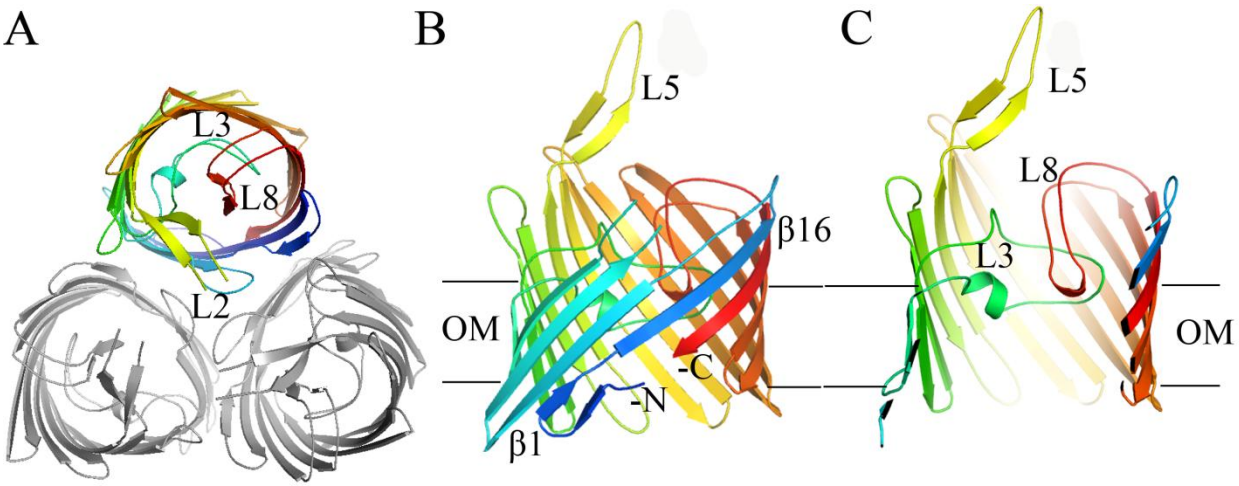

Figure 4.14. 3D cartoon for OmpT structure.
(A) Extracellular and (B) side views of 16 stranded β-barrel of OmpT monomer (in rainbow), constricted in the lumen by loops L3 and L8. (C) The slabbed side view of monomer presents a better illustration for the L8 constriction of OmpT channel.

The loop L8 makes several interactions with the neighbouring residues lining the barrel wall and loop L3 (Figure 4.15). Gly301 in L8 interacts strongly with two arginines (Arg18 and Arg322) in the barrel wall while Asn299 in L8 forms interactions with multiple residues of L3; Asp98, Ser100, Phe102 and Phe103. The constriction is lined by Arg69 in the barrel wall, Trp88, Asp92 and Asp115 in loop L3, and Thr298, Lys300, Asp303 and Glu305 in L8. This configuration of residues is clearly non-typical, and especially the presence of Trp88 (and to a lesser extent Thr298) will likely make the OmpT constriction region much less polar than that of other porins. The presence of L8 makes the channel constriction very small, with a diameter of ~ 4 Å. As a result to date, OmpT has probably the narrowest pore size among the other porins of Gram-negative bacteria.

The DALI (Holm and Laakso 2016) analysis for OmpT protein revealed its greatest structural similarity to the anion-selective porin Omp32 from *Comamonas acidovorans* (Z = 26, 2.1 Å r.m.s.d. over 270 residues), but with a sequence identity of only 15% (Table 4.10) followed by PorB from *Neisseria Meningitidis* (PDB code 3VZT) and OmpE36 from *E. cloacae* (PDB code 5FVN). Similarly to OmpU, these proteins showed higher structural similarity to OmpT than OmpF/C from *E. coli* (Table 4.10).

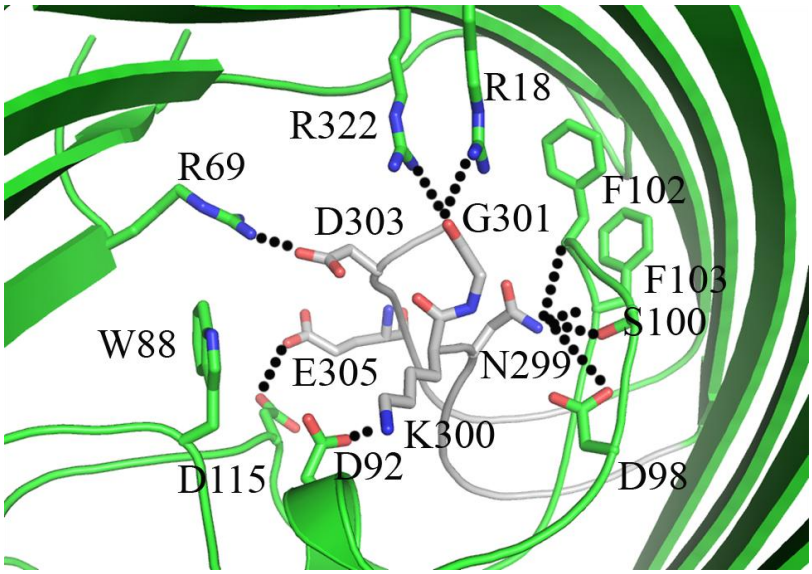

Figure 4.15. Interactions of loop L8 with OmpT residues.
The residues of loop L8 (in gray sticks) form multiple H-bonds and salt bridges with the OmpT residues of the barrel wall (R69, R322, R18) and loop L3 (D115, D92, D98, S100, F103 and F102).

Table 4.10. DALI structural alignments of OmpT.
The table lists the top three proteins of PDB with greater structural similarity to OmpT, as revealed by DALI, followed by the comparison with the porins OmpF/C and OmpU.

Proteins aligned against OmpT	PDB	Z-score	rmsd	Sequence identity (%)	Aligned residues
Omp32 (*Comamonas acidovorans*)	1E54	27.3	2.1	14	283
PorB (*Neisseria Meningitidis*)	3VZT	25.6	2.4	14	280
OmpE36 (*Enterobacter cloacae*)	5FVN	25.5	2.7	16	280
OmpC (*E. coli*)	2J1N	25.5	2.8	16	282
OmpF (*E. coli*)	2ZFG	25.2	2.8	14	279
OmpU (*V. cholerae*)	6EHB	26.5	2.1	19	267

An interesting feature in the OmpT structure is the presence of clear density for a bound ligand at the pore constriction (Figure 4.16). The density fitted well with 2-(N-morpholino)ethanesulfonic acid (MES), used at a concentration of 100 mM in the crystallisation condition. The morpholine ring of MES is pointed towards the extracellular side and sandwiched between Asp 92 (of L3 loop) and Asp 303 (of L8 loop) in one direction and between the side chain of Trp88 and Lys300 in the other. The sulphonate group of MES is oriented towards the periplasmic side and interacts with Arg 37 and Arg 69 in the barrel wall, with Trp88 in L3 and

with Asp303 in loop L8 (Figure 4.16). The antibiotic binding sites in OmpF pore, published earlier (Ziervogel and Roux 2013), were compared with MES binding site inside the OmpT pore. While ampicillin and carbenicillin bound more closely to the extracellular and periplasmic regions respectively of the OmpF pore (Ziervogel and Roux 2013), the binding site of MES was located nearly in the mid-region of the OmpT pore.

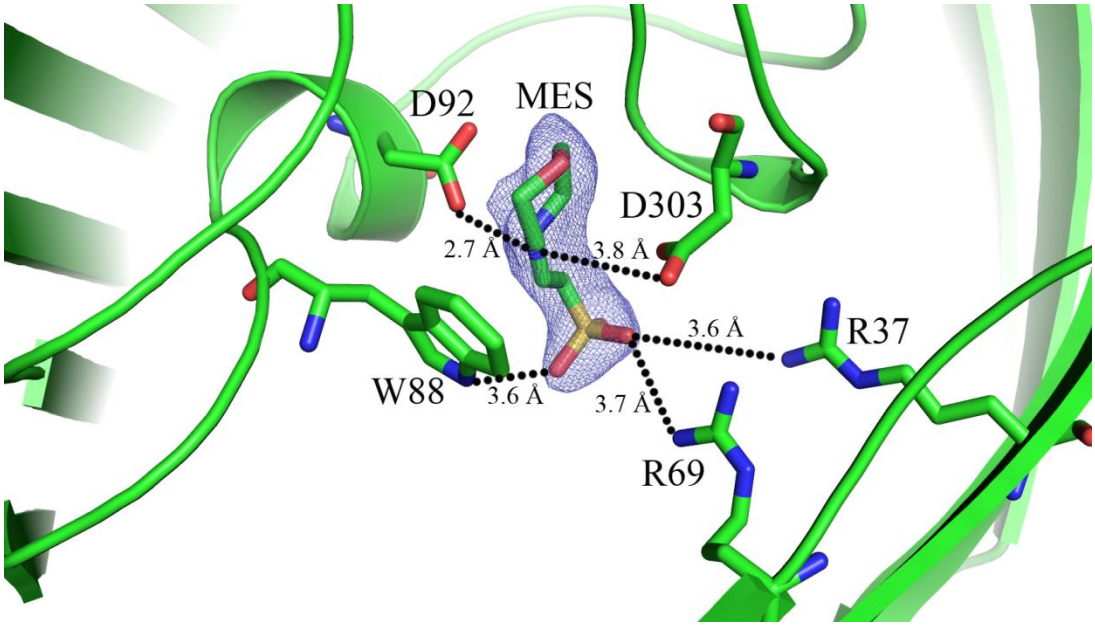

Figure 4.16. MES bound in OmpT constriction region.
2Fo-Fc electron density map (contoured at 2σ) for MES bound in the CR. MES forms multiple interactions through its morpholine ring and the sulphonate group with the surrounding pore constriction residues of OmpT (R69 and R37 from barrel wall; W88 and D92 from loop L3; D303 from loop L8).

Crystal structure from membrane-expressed OmpT

The crystal obtained for OM-expressed OmpT (see section 3.5.2) diffracted to a low resolution of 3.2 Å. Due to the absence of the good molecular replacement model initially, the phase problem for the data could not be solved. But after obtaining the structure of *in vitro*-folded OmpT, we re-analysed the diffraction data obtained from OM-expressed OmpT to exclude the possibility that the unusual conformation of the L8 loop is caused by the *in vitro* folding of the protein. Molecular replacement with *in vitro* folded OmpT gave a clear solution with PHASER (McCoy et al., 2007) yielding LLG and TFZ scores of 1393 and 26.3 respectively and the AU showed one molecule with the space group C2 (Table 4.9). As expected, the protein fold of OM-expressed OmpT is very similar to the one obtained from *in vitro* folding. In addition, subsequent

refinement clearly shows the electron density supporting a similar conformation of the L8 loop as observed for *in vitro* folded OmpT, making it likely that the conformation of loop L8 is physiological. Figure 4.17 shows the 2Fo-Fc electron density map as well as the 2Fo-Fc omit electron map including simulated annealing for loop L8 of the final refined model of OmpT.

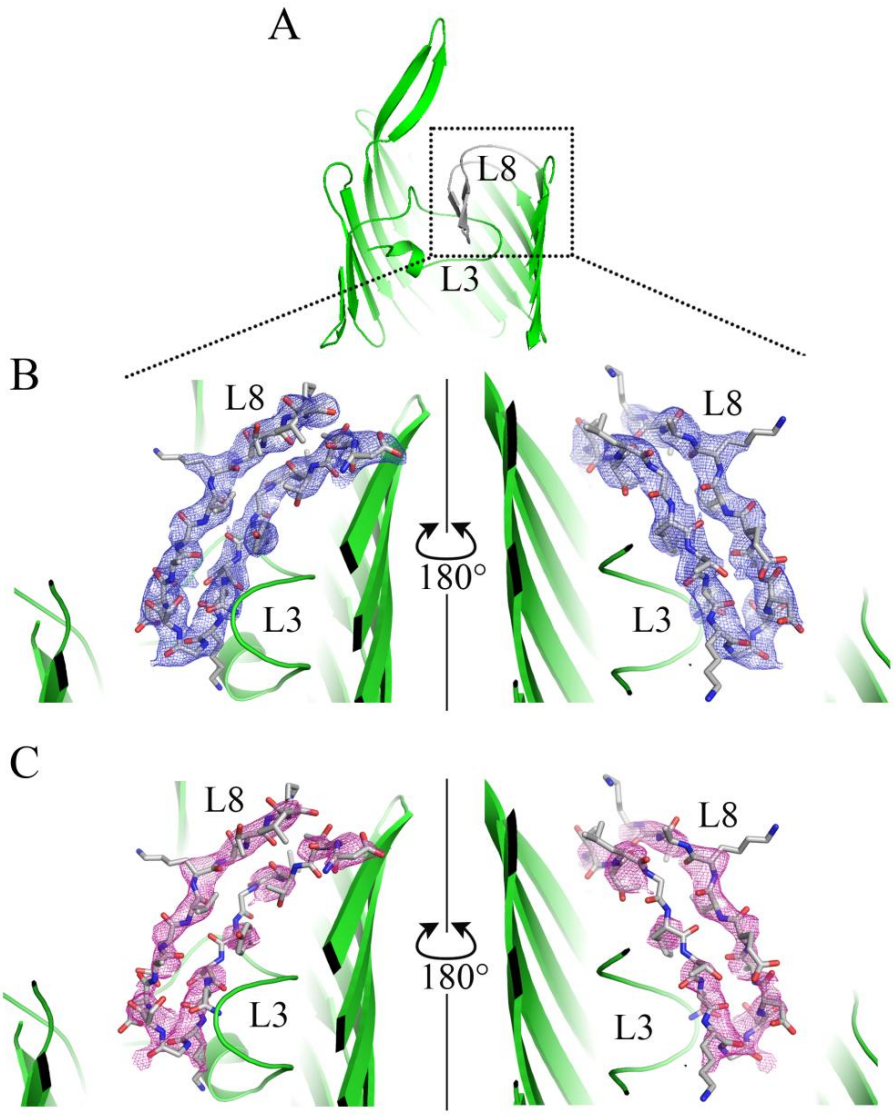

Figure 4.17. Electron density for loop L8 in OM-expressed OmpT.
(A) Cartoon showing side-cut view of OM-expressed OmpT with L8 in gray. (B) Final 2Fo-Fc electron density map contoured at 2σ, for loop L8 residues (gray sticks). (C) Simulated annealing omit Fo-Fc map contoured at 1.5σ, for loop L8 residues.

4.10. Anomalous diffraction of OmpT crystals

Prior to solving the OmpT structure (also discussed in section 4.8), the *in vitro* folded protein was used to produce crystals of selenomethionine substituted (SeMet) OmpT or crystals incorporated with a heavy atom (HA).

For HA incorporation (see section 2.6.2.4), the OmpT crystals (from the condition 0.5 M $CaCl_2$, 0.05 M $BaCl_2$, 0.1 M Tris, 32% w/v PEG400 and pH 8.2) were soaked for few hours or overnight (depending on crystal stability) in solutions of 4 different heavy atoms (see section 2.6.2.4): Platinum (Pt, K_2PtO_4), Lead (Pb), Iridium (Ir) and Osmium (Os). A total of 70 crystals, soaked in different HA solutions, were analysed for X-ray diffraction. Of these, two crystals, Ir-OmpT and Pt-OmpT diffracted to ~ 3.5 Å. A complete set of 360° data was collected for an Ir-OmpT crystal while two sets of 360° data was collected for a Pt-OmpT crystal. The two OmpT crystals (Pt- and Ir- derived) yielded datasets in space group I432 with almost identical unit cell dimensions (Pt-derived crystal a=201.07, b=201.70, c=201.70, α=90, β=90, γ=90; Ir-derived crystal a=200.30, b=200.30, c=200.30, α=90, β=90, γ =90). The scaled reflections for both datasets were analysed using *AutoSol* (Terwilliger et al., 2009), an automated experimental phasing pipeline in PHENIX (Adams et al., 2010). Due to the high symmetry space group ($P6_3$) obtained for the OmpT crystals (Pt- and Ir- derived), the high redundancy (70) of the data aided in generating a solution. Interestingly, after density modification in RESOLVE, the map revealed clear electron density for a porin trimer (Figure 4.18) but the FOM (figure of merit) was somewhat low (~ 0.28). As a result of the low resolution, AutoSol failed to build an acceptable model.

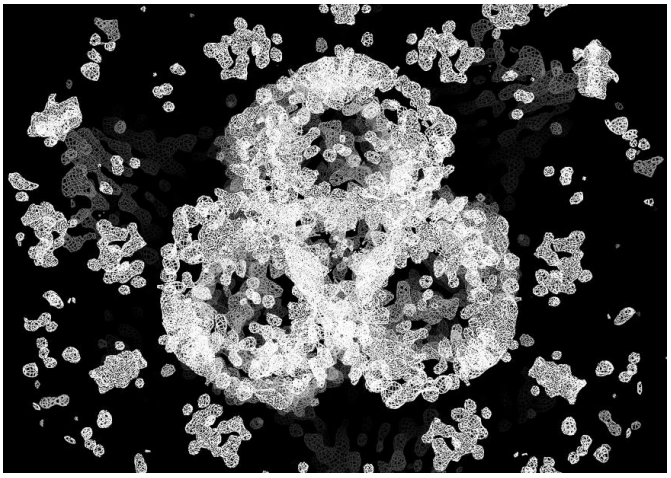

Figure 4.18. Electron density map of in-vitro folded OmpT from SAD data.
The anomalous diffraction data from Ir-derived crystal generated a density-modified map by RESOLVE, showing the density for 3 β-barrel monomers arranged into a porin trimer.

The best SeMet OmpT crystal diffracted to a resolution of 2.4 Å (C2 space group, 1 molecule in the AU) and 7 datasets were collected for the same crystal. In PHENIX, 7 isomorphous datasets were merged using *AutoSol* that yielded a good FOM scoring value (~ 0.5) for 6 substructure HA sites but the experimental electron maps obtained were of poor quality.

This could be either due to the poor data quality or because OmpT contains only two methionines in its sequence (insufficient HA atoms for successful phasing).

4.11. Crystal structures of OmpUΔN and OmpTΔL8

The structure of the truncation mutant of OmpU with the first 10 N-terminal residues removed (OmpUΔN) was solved using data to 2.0 Å resolution (Table 4.11).

Table 4.11. X-ray diffraction and refinement statistics for OmpUΔN.

Data collection		***Refinement statistics***	
Beamline	DLS I04-1	Resolution (Å)	66.17 – 2.02
Wavelength (Å)	0.9282	Reflections (n)	48646
Space group	$P6_3$	R_{work}/R_{free} (%)*	19.7/ 24.9
Cell dimensions	81.3, 81.3, 198.5	Atoms (n) Protein/solvent	4714/248
(a,b,c), (α,β,ϒ)	90, 90, 120	ligand/detergent	0/24
Molecules/AU	2	B factors ($Å^2$) Protein/solvent	40.4/46.6
Solvent content (%)	54.5	ligand/detergent	-/57.1
Resolution (Å)	66.17 – 2.02	Rmsd bond lengths (Å)	0.017
Completeness	100 (100)	bond angles (^{O})	1.64
Redundancy	11.5 (11.4)	Ramachandran plot (%) Most favoured/outliers	94.88/0.33
I/ σ	12.3 (1.3)		
Rpim (%)	4.4 (62.8)		
CC (1/2)	0.9 (0.6)		

Values in the parentheses refer to the highest resolution shell.
*R_{free} was computed as for R_{work} using a test set (~5%) of randomly selected reflections that were omitted from the refinement.

The OmpUΔN crystal shows a trimer of 16 antiparallel β-stranded monomeric barrels, as seen for other porins (Figure 4.19 A). The structure of OmpUΔN and its Cα r.m.s.d. of 0.6 Å with native OmpU suggests that the deletion of the N-terminal 10 residues did not affect the protein fold. The remaining segment of the N-terminus (residues 11-19) extends into the periplasmic space in OmpUΔN (Figure 4.19 B). As a result, the C-terminal carboxyl group does not interact with any other residue in the OmpUΔN barrel. In addition and as expected, the comparison of CRs between OmpU and OmpUΔN showed large differences (Figure 4.19 D, E). The pore dimension of OmpUΔN (~ 10 × 15 Å) was considerably larger than that of WT OmpU (~ 9 × 10 Å).

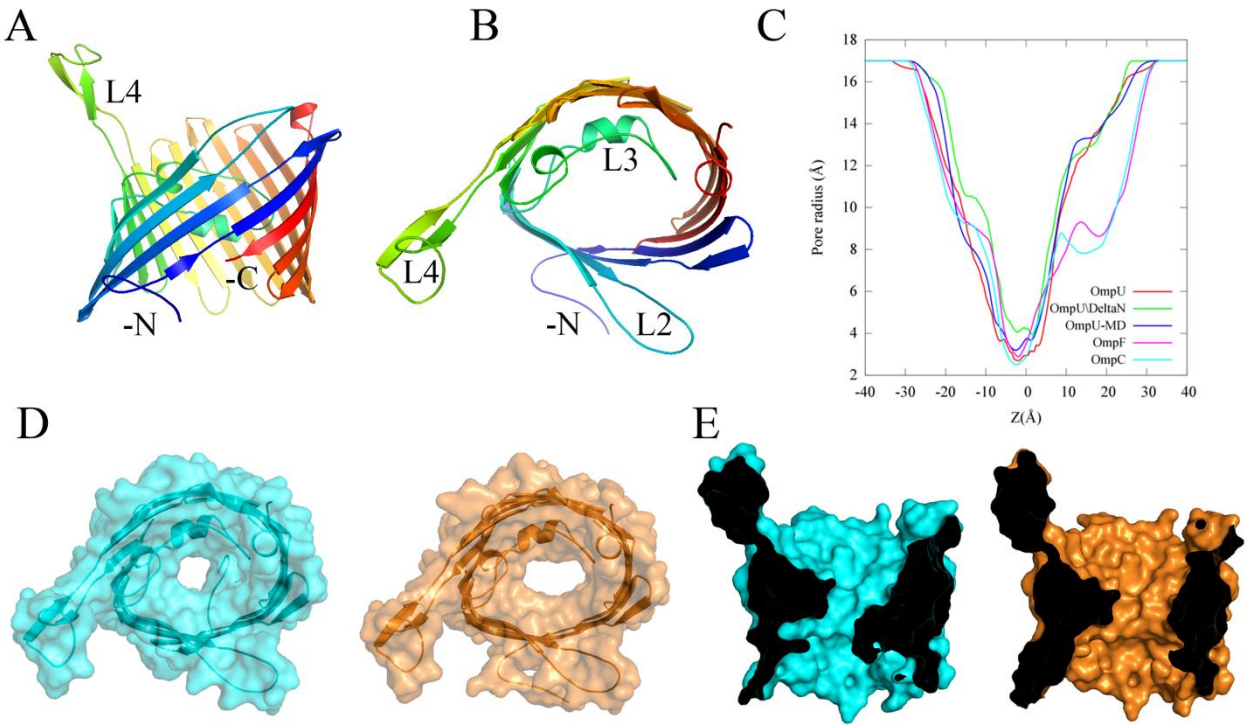

Figure 4.19. Structure of OmpUΔN.
(A) Extracellular side and (B) OM plane views for the monomer cartoon of OmpUΔN. (C) HOLE (Smart et al., 1993) comparison between OmpU, OmpUΔN, OmpF and OmpC (OmpU-MD corresponds to the pore size calculated from MD simulations)*. The surface views from the OM plane (D) and extracellular side (E) show the difference in pore sizes for OmpU (cyan) and OmpUΔN (orange).
*The HOLE figure was obtained from Matteo Ceccarelli (Univeristy of Cagliari).

The structure of the loop deletion mutant OmpTΔL8 was solved using data to 2.3 Å resolution (Table 4.12). Similar to OmpUΔN, the structure of OmpTΔL8 displayed a 16-stranded β-barrel protein fold with only one molecule in the AU (Figure 4.20 A, B), as observed for the structure of (IB-expressed) OmpT.

Table 4.12. X-ray diffraction and refinement statistics for OmpTΔL8.

Data collection		*Refinement statistics*	
Beamline	DLS I24	Resolution (Å)	85.84 – 2.3
Wavelength (Å)	0.96861	Reflections (n)	18688
Space group	I222	R_{work}/R_{free} (%)*	22.4/27.3
Cell dimensions	43.4, 128.4,171.6	Atoms (n) Protein/solvent	2343/39
(a,b,c), (α,β,ϒ)	90, 90, 90	ligand/detergent	0/77
Molecules/AU	1	B factors ($Å^2$) Protein/solvent	47.10/44.61
		ligand/detergent	-/55.04
Solvent content (%)	60.5	Rmsd bond lengths (Å)	0.011
		bond angles (^{O})	1.113
Resolution (Å)	85.84 – 2.3	Ramachandran plot (%) Most favoured/outliers	95.9/1.7
Completeness	99 (98)		
Redundancy	6.9 (5.1)		
I/ σ	13.1 (1.5)		
Rpim (%)	3.4 (51)		
CC (1/2)	0.9 (0.6)		

Values in the parentheses refer to the highest resolution shell.
*R_{free} was computed as for R_{work} using a test set (~5%) of randomly selected reflections that were omitted from the refinement.

The superposition of OmpTΔL8 on OmpT gave a Cα r.m.s.d. of ~ 1.0 Å demonstrating that both structures are similar and that L8 deletion did not affect the protein fold. The pore sizes of OmpT and OmpTΔL8 were also compared to evaluate the difference in the constriction zones resulting from removal of loop L8 (Figure 4.20 D, E). The OmpTΔL8 channel was very large, with pore size dimensions of ~ 7.4 × 10 Å but in OmpT due to the L8 loop, the pore size decreases substantially to ~ 4 × 5 Å (Figure 4.20 C).

Quite recently, we submitted a paper (to Structure; Pathania et al., 2017) that reports the 3D X-ray structures of *V. cholerae* porins, OmpU and OmpT (and their deletion mutants) and is currently under revision. The paper describes the effect of the constriction elements on the size and electrostatics of these porins. In addition, the paper discusses the electrophysiology and molecular dynamics simulations that were used to analyse the functional aspects of OmpU/T porins.

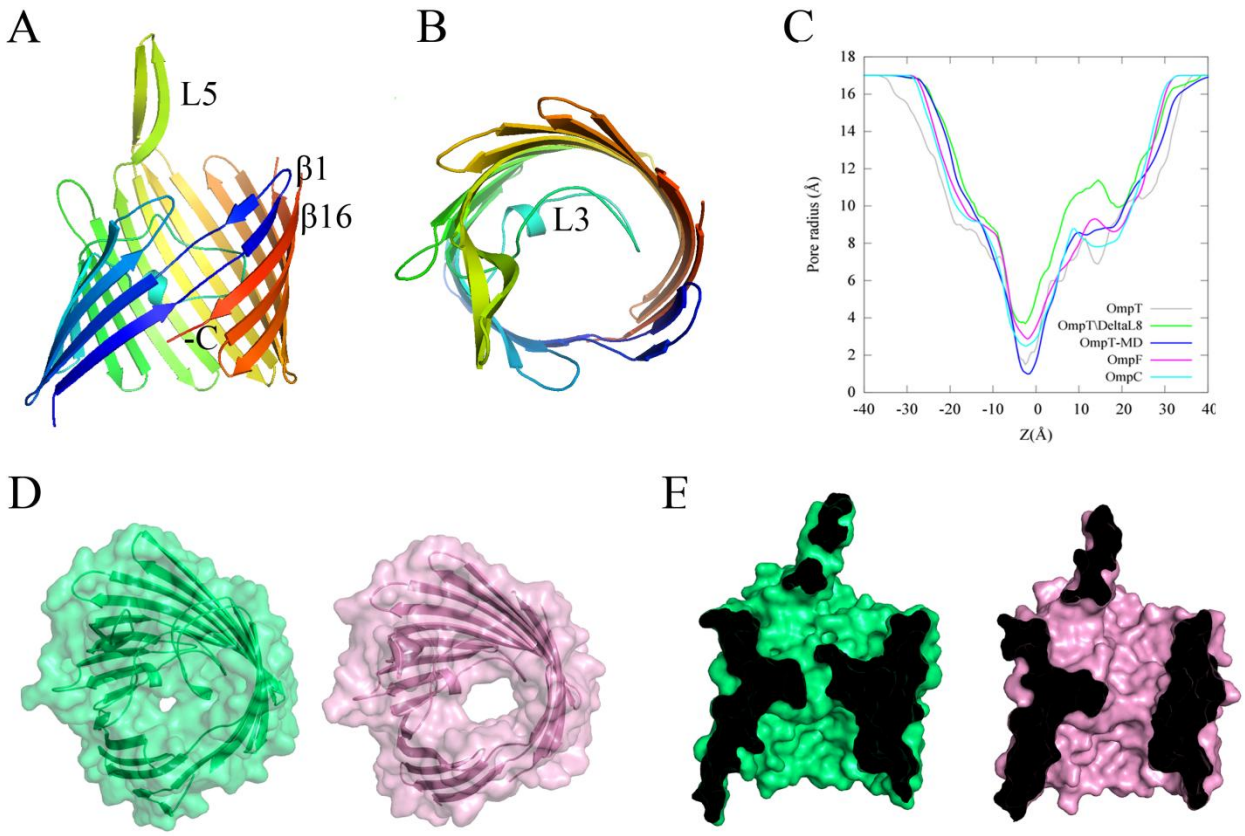

Figure 4.20. Structure of OmpTΔL8.
Monomer cartoon of OmpTΔL8 shows the 16-stranded β-barrel from the OM plane (A) and from the extracellular side (B) with loop L3 constriction inside the lumen (N- terminus being disordered could not be build in the structure). (C) HOLE (Smart et al., 1993) comparison of constriction zones for OmpT, OmpTΔL8, OmpF and OmpC (OmpT-MD corresponds to the pore size calculated from MD-simulations)*. The surface views from the OM plane (D) and extracellular side (E) compare the constriction zones of OmpT (green) and OmpTΔL8 (purple).
*The HOLE figure was obtained from Matteo Ceccarelli (Univeristy of Cagliari).

4.12. Co-crystallisation trials with antibiotics and OmpT/OmpTΔL8

In vitro antibiotic permeation assays and electrophysiology experiments with *V. cholerae* porins revealed interactions with meropenem and imipenem (discussed in Chapter 5). Based on this information, we tried to obtain the co-crystal structures of these antibiotics with OmpU/T porins (and OmpUΔN/OmpTΔL8) to probe the protein residues that interact with the substrate (see section 2.6.2.3). Due to limited solubilities [meropenem (HMDB0014898) - 5.63 g/L; imipenem (HMDB0015536) - 0.78 g/L], the maximum concentration used to prepare stock solutions for co-crystallisation was 0.4 M for meropenem and 0.25 M for imipenem.

The antibiotic-soaked crystals of OmpU, OmpUΔN and OmpTΔL8 did not reveal the presence of the substrate inside the channel. However, one of the meropenem-soaked OmpTΔL8 crystals diffracted to a resolution of 2.4 Å with one molecule in the AU in I222 space group and showed electron density for a bound ligand at the constriction region (Figure 4.21). The components like MES from the crystal condition or HEPES from the purification buffer were ruled out based on the output of negative electron density after refinement. The β-lactam ring-opened hydrolysed form (MER-1; Figure 4.22) of meropenem was fitted manually into the ligand density using COOT. On inspection of the $2F_o$-F_c electron map, post-refinement, the hydrolysed meropenem proved to be a poor fit because of the inadequate density obtained for its pyrrolidine moiety (Figure 4.21 C). Since meropenem has a natural tendency to degrade at room-temperature owing to its low stability (Joseph and Rodvold 2008), the ligand density was fitted with the thiazolidine ring (bearing a hydroxyethyl side chain) of degraded meropenem (MER-2; Figure 4.22). However post-refinement, the 2Fo-Fc electron map was still not fully consistent with the fitted ligand (Figure 4.21 D). A ligand-fitting approach in PHENIX, LigandFit, resulted in CC values of 0.63 (ideal fit requires CC value of ≥ 0.7), implying meropenem is not a good fit for the density.

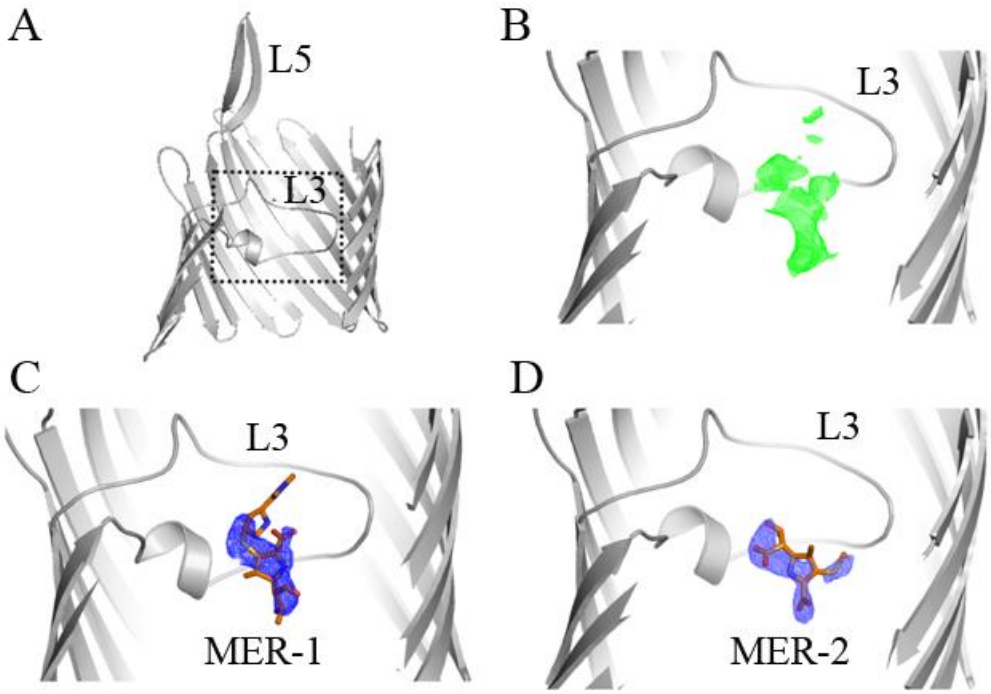

Figure 4.21. Electron density evident for meropenem bound to the CR of OmpTΔL8.
(A) The boxed region shown in the side cut view of OmpTΔL8 (in gray) is zoomed in the next panels. (B) The Fo-Fc difference map (green) contoured at 1.5σ (carve = 1.6), displays electron density for a ligand bound at the CR. (C, D) The 2Fo-Fc maps contoured at 1.5σ show the electron density for meropenem.

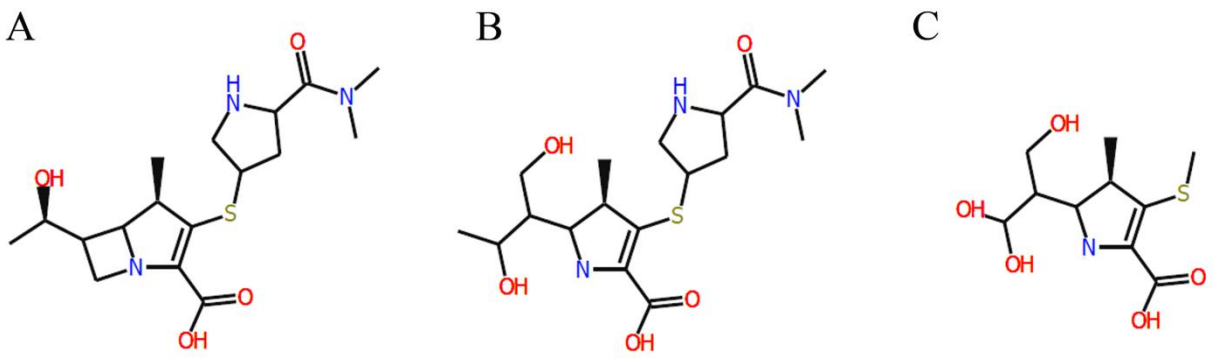

Figure 4.22. Meropenem structure.
The figure shows the chemical representations of (A) intact meropenem, (B) hydrolysed β-lactam ring opened form of meropenem (MER-1) and (C) degraded meropenem containing the thiazolidine ring (MER-2).

4.13. Discussion

The general diffusion porins of *E. cloacae* (OmpE35/E36) and *K. pneumoniae* (OmpK36) not only share high percentage of sequence identities with OmpF/C orthologs of *E. coli* but our structural studies show that these channels are also very similar in the architecture of the β-barrel folds. The β-barrels of OmpE35/E36/K36 display the characteristic pattern of charge segregation across the pore with charged residues of the constriction zone overlapping with the identical residues of OmpF/C channels. Recent studies have shown that the charged residues of the constriction region (CR) apart from creating a transversal electric field across the eyelet also involve electrostatics that play a crucial role in facilitating the permeation of solute (Im and Roux 2002a, b, Bajaj et al., 2017 and Acosta-Gutierrez et al., 2015). Thus the similarity of the charged residues in the CR of the orthologs suggests that OmpE35 and OmpE36/K36 channels might involve electric fields of similar strengths as in OmpF and OmpC respectively, to facilitate the translocation of solute. Moreover, the conservation between the pore-lining ionisable residues of the orthologs and OmpF/C porins imply that the channels may employ similar electrostatic forces for the transport of solute from the vestibule opening to the periplasmic end.

The determination of the OmpE36–LPS structure is the first porin with attached lipopolysaccharide and this allowed us to make the comparison with FhuA–LPS complex (Ferguson et al., 1998). For FhuA (with 11 coordinate files present in the PDB showing one LPS molecule bound to the same site), basic residues dominate the polar interactions with the bound

LPS but in OmpE36, the dominance of basic residues in LPS binding is much less pronounced. Moreover, the calcium-mediated interaction in OmpE36–LPS was not present in the FhuA–LPS structure. The original FhuA–LPS complex structure [PDB ID code 2FCP (Ferguson et al., 1998)] contained a putative nickel metal ion bound to one of the phosphates of LPS that did not contribute to the binding to FhuA. The major difference in LPS binding between the two OMPs lies in the role of the Kdo_{II} moieties. In FhuA–LPS, Kdo_{II} points away from the protein and contributes just one interaction to the binding to FhuA (a salt bridge between Arg384 and the Kdo_{II} carboxylate). In sharp contrast, the Kdo_{II} forms the interaction hub (metal-mediated and direct interactions) with OmpE36 in both LPS A and LPS B (Figure 4.4). It is therefore clear that OMPs can interact with LPS in different ways, and an expanded database incorporating the LPS–OmpE36 data should enable a better prediction of LPS binding sites on OMPs (Arunmanee et al., 2016).

The structures of *V. cholerae* porins OmpU and OmpT, despite being OmpF/C orthologs, exhibit an unusual feature inside their channels. Both channels reveal additional constriction elements (other than loop L3) that have not been reported before for any general diffusion porin of Gram-negative bacteria. The channels of OmpU and OmpT are constricted inside by the folding of N-terminus and L8 loop, respectively. We suspect these additional constrictions might be caused due to the external conditions like osmolarity, temperature or pH that are faced by the bacterium in aquatic or marine environments. These constrictions of OmpU/T porins cause a further reduction in the pore sizes of the channels as compared to OmpF/C porins (Figure 4.23). A HOLE comparison (Figure 4.19 C and 4.20 C) illustrates the differences of the pore sizes between OmpU/T and OmpF/C structures along the length of the diffusion axis. In addition to the differences in the pore constrictions of OmpU and OmpF/C porins, the channels exhibit some variations in the regions exposed to the hydrophilic environments *in vivo*. In contrast to the loops of OmpF/C porins, OmpU extracellular loops are comparatively short except loop L4 which comprises ~30 residues (Figure 4.23 A, B). As a result, the OmpU channel exhibits an increased surface area in the vestibule opening in comparison to OmpF/C channels (Figure 4.23 D). However in OmpT, L8 constricts the channel in such a way that the pore is absolutely occluded when viewed in a direction perpendicular to the diffusion axis (Figure 4.23 E). The OmpT pore becomes visible after tilted at an angle (~10°) with respect to the membrane normal (Figure 4.20 D) and is restricted at the extracellular surface by loop L5 (~20 residues; Figure 4.20 E).

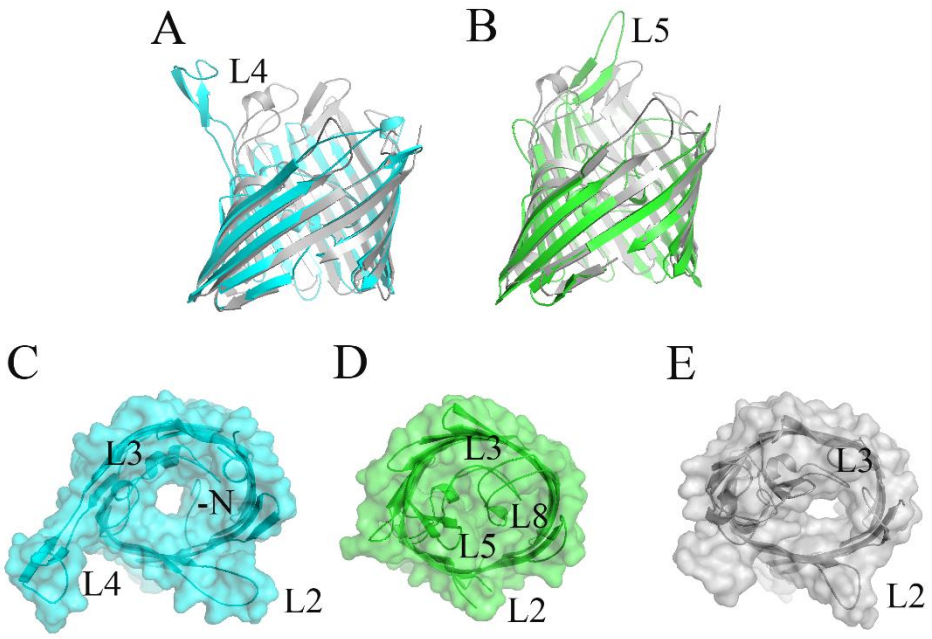

Figure 4.23. Structural comparison of OmpU/T channels with OmpF.
The side views for the channels of OmpU (A; cyan) and OmpT (B; green) superposed on OmpF (in gray). Extracellular surface and cartoon views of OmpU (C), OmpT (D) and OmpF (E) porins.

Chapter 5. *In vitro* antibiotic uptake assays and single channel electrophysiology

5.1 Introduction

The lack of new drug development since 1987 and misuse of the drugs/medicines has led to the rapid emergence of multi-drug resistant (MDR) bacteria worldwide. One of the three main factors (see section 1.5) that are attributed to the cause of MDR is the inability of antibiotics to cross the OM interface of Gram-negative bacteria. The water-filled porin channels provide a porin-mediated pathway (detailed in section 1.5.1) for the transport of hydrophilic drug molecules (≤ 600 Da).

In vitro liposome swelling assays (LSA; see Figure 1.6) and electrophysiology experiments have demonstrated the permeation of β-lactams like penicllins and cephalosporins, and fluoroquinolones through the channels of *E. coli* OmpF/C porins (section 1.5.1). In comparison, antibiotic-related studies with the diffusion porins of *E. cloacae* (OmpE35/E36) and *K. pneumoniae* (OmpK35/K36) and *V. cholerae* (OmpU/T) have been relatively limited (also discussed in sections 1.6.1 and 1.6.2).

This chapter describes the *in vitro* antibiotics uptake assays with OmpE35/E36 and OmpK35/K36 proteins to assess the permeation of different hydrophilic molecules. OmpK35 was expressed (in *E. coli*) and purified by a colleague in the lab for structure determination whilst I performed the *in vitro* antibiotic uptake assays with the isolated pure fractions of the protein. In addition to *in vitro* uptake assays, electrophysiology can reveal information about the kinetic features of the porin channels and helps in gaining a precise knowledge of the functional characteristics of the channel such as conductance and selectivity. We performed functional characterisation of *V. cholerae* porins OmpU/T as well as the deletion mutants (OmpUΔN and OmpTΔL8) using lipid-bilayer electrophysiology experiments. In addition, the single channel electrophysiology and LSA experiments that were performed to study the effect of antibiotics with OmpU/T porins are also discussed in this chapter. The statistical analysis of the data, used for different assays and experiments, has been decribed in the section 2.12 of chapter 2 (also mentioned wherever required).

5.2. Disc diffusion assays

Keeping in mind the size exclusion limit (600 Da) of non-specific porins, we tested the uptake of a wide range of antibiotics with different molecular weights using the disc diffusion assay (see section 2.9.1). The substrates with low molecular weight compounds like fosfomycin (138 Da), trimethoprim (290 Da), ciprofloxacin (331 Da), meropenem (383 Da), gentamycin (477 Da), chlortetracycline (478 Da), ceftazidime (546 Da) and high molecular weights like erythromycin (733 Da), rifampicin (822 Da) were selected for the assay. The proteins OmpE36 (of *E. cloacae*), OmpK36 (of *K. pneumoniae*) and OmpU (of *V. cholerae*) were used for the assay (at 8 mg/ml). *E. coli* cells of omp8 (Bl21) strain were transformed with an "empty" pBAD24 plasmid and used as a negative control for the assay (referred to as pBAD; Kan^r). The data in figure 5.1 displays the cumulative result of the radii of the lytic zones obtained for each antibiotic, averaged from three different experiments (n=3, also described in section 2.12).

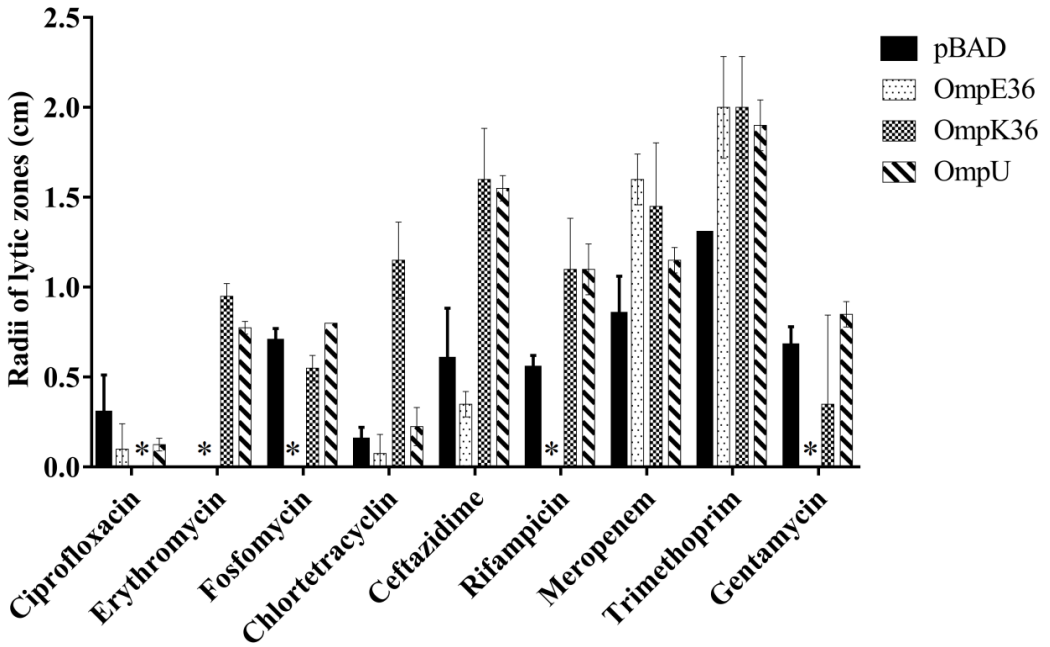

Figure 5.1. Disc diffusion assay of selected antibiotics with porins.
The plot depicts the radii of lytic zones (in centimetres) caused by the diffusion of selected antibiotic (8 mg/ml) through the porin channels of OmpE36, OmpK36 and OmpU. The averaged data is obtained from three separate experiments (n=3; also see section 2.12). * represents no data detected.

Overall, trimethoprim showed maximum diffusion for the three proteins, even higher than the smallest antibiotic fosfomycin. Surprisingly, small-sized ciprofloxacin did not permeate through any of the porins but the high molecular weight compounds like erythromycin and rifampicin (larger than 600 Da) also showed significant uptake through OmpK36 and OmpU

porins. Among the three porins, OmpE36 was the least permeable channel and showed (almost) zero uptake of all antibiotics (except for meropenem and trimethoprim). However apparently, the data displayed an odd behaviour for the negative control (pBAD) by showing significant diffusion for majority of the compounds (Figure 5.2). This suggests that the omp8 (Bl21) cells, despite being devoid of major porins (OmpF/C), expressed some another porin (or porins such as OmpN) that might have allowed the permeation of the substrates. As a result, the results of the disc diffusion data could not be considered reliable.

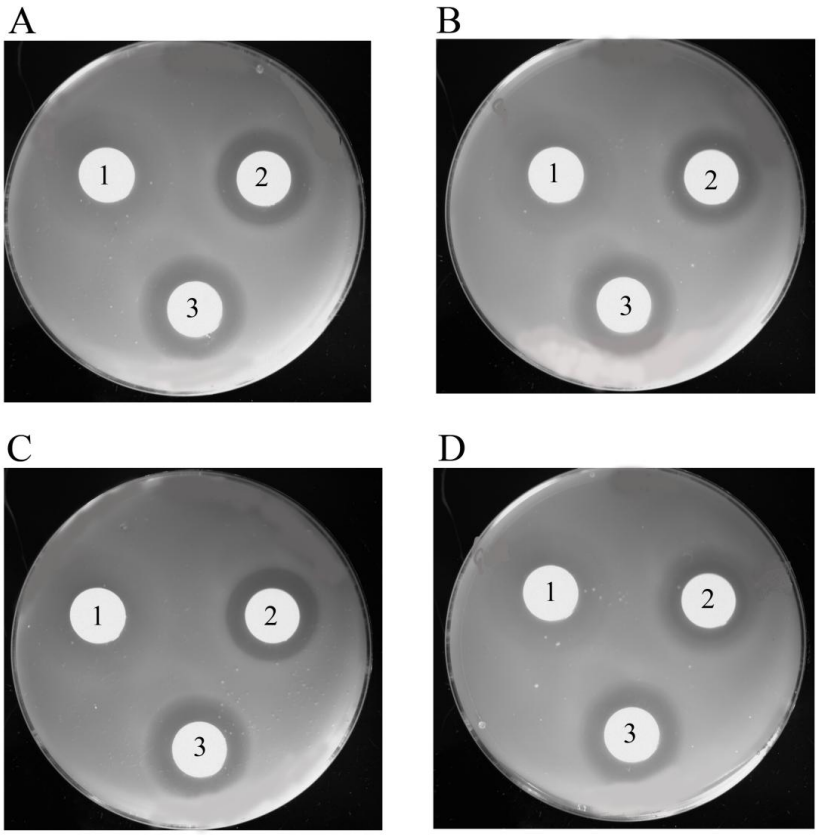

Figure 5.2. Antibiotic lytic zones by porins and negative control.
LB agar plates (Kan^r; supplemented with 0.1% arabinose) display the zones of lysis for gentamycin (1), chlorotetracycline (2) and ceftazidime (3) caused by the cells expressing porin channels of (A) OmpK36, (B) OmpE36, (C) OmpU and (D) negative control omp8 cells.

5.3. Growth assays

The growth assays (see section 2.9.2) were carried out with *E. cloacae* porins OmpE35/E36 and *V. cholerae* OmpU. The two compounds, meropenem (383 Da) and ceftazidime (546 Da) that showed high diffusion rates in the disc diffusion assay (section 5.2) were chosen for the assay. The omp8 (Bl21) cells (Kan^r) were used to express the target proteins and functioned as the negative control in the assay. The growth curves in Figure 5.3 display the effect observed in the cell OD expressed with the target proteins after the addition of meropenem

(0.02/0.04 µg/ml) or ceftazidime (0.08/0.10/0.12 µg/ml). However yet again, the negative control omp8 cells interfered with the cumulative result by showing the same pattern for the growth curves as observed for others (Figure 5.3). As a result, the results of the growth assays remained inconclusive.

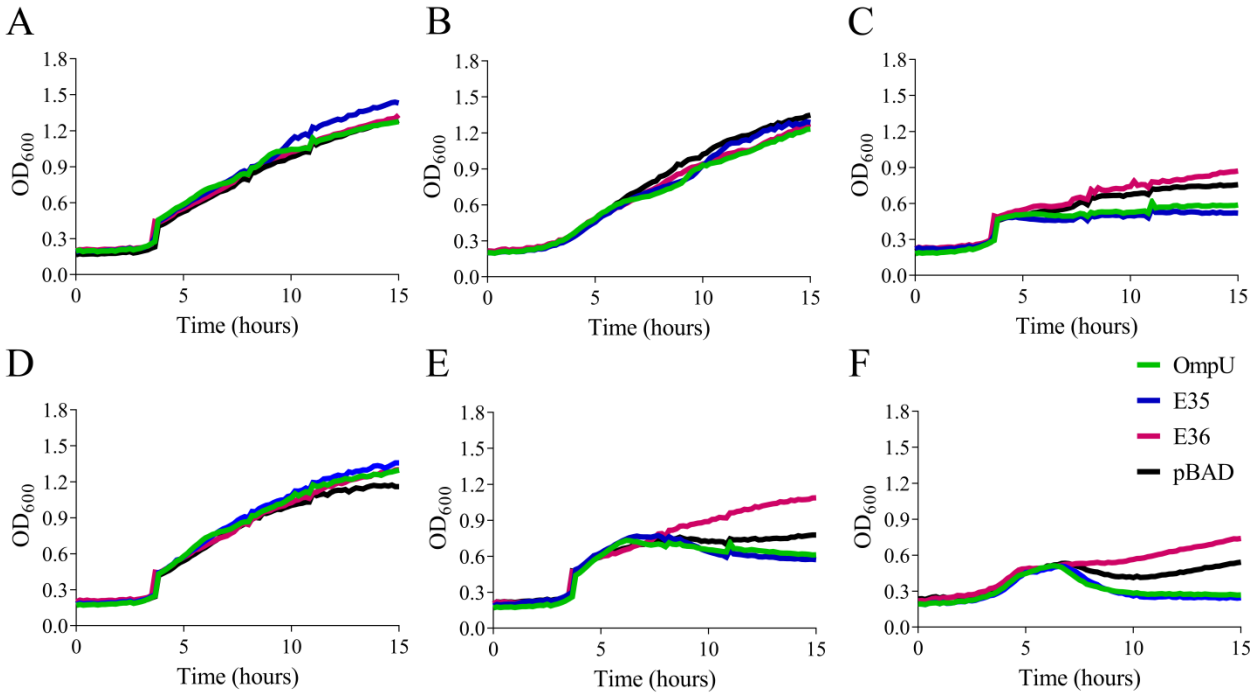

Figure 5.3. Growth assay of OmpE35/E36 and OmpU in presence of antibiotics.
(A) The standard growth rates of cells expressed with OmpE35/E36 and OmpU proteins without the addition of antibiotic. The growth rate of the cells upon addition of (B) 0.02 µg/ml meropenem, (C) 0.04 µg/ml meropenem, (D) 0.08 µg/ml ceftazidime, (E) 0.1 µg/ml ceftazidime and (F) 0.12 µg/ml ceftazidime are also shown. The figure is a representative result of the assay.

5.4. Liposome swelling assay for OMPs of *E. cloacae* and *K. pneumoniae*

Since the *in vivo* assays (sections 5.2 and 5.3) were inconclusive because of the lack of a proper negative background we decided to conduct *in vitro* experiments for testing the antibiotic uptake. To compare the uptake rates of different classes of antibiotics between the OMPs of *E. cloacae* and *K. pneumoniae*, the purified samples of OmpE35, OmpE36, OmpK35 and OmpK36 proteins were used for the preparation of liposomes for the liposome swelling assay (LSA; see section 2.9.3). The proteins of *E. cloacae* (OmpE35/E36) and *K. pneumoniae* (OmpK35/K36) were reconstituted into proteoliposomes along with *E. coli* OmpF (used as positive control) to compare and analyse the relative permeation rates of small hydrophilic solutes. The substrates employed for LSA included glucose, amino acids (glycine, glutamate, arginine) and different antibiotics (ampicillin, meropenem, imipenem, ceftazidime, ertapenem, cefepime, cefotaxime,

ticarcillin and piperacillin) (also see Appendix Figure 4). For analysis, the uptake rate of glycine through each protein was normalised to 100% and used as a reference to calculate the permeation rates for the rest of the substrates through the same protein (also described in section 2.12). The protein levels in the proteoliposome mixtures of OmpF, OmpE35, OmpE36, OmpK35 and OmpK36 were assessed through SDS-PAGE (Figure 5.4). The SDS-PAGE gel depicts almost identical band intensities for the target proteins (Figure 5.4) implying equimolar protein amounts used for the LSA.

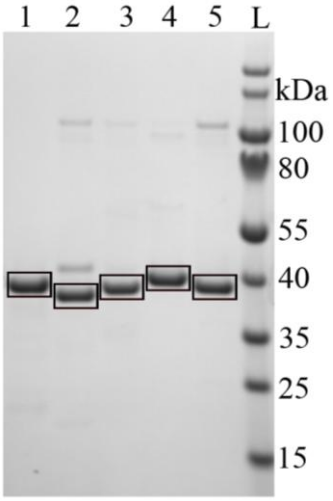

Figure 5.4. SDS-PAGE of proteins from liposome preparations.
Coomassie-stained gel shows the proteins bands (indicated by the boxes in black) for OmpF (Lane 1), OmpE35 (Lane 2), OmpE36 (Lane 3), OmpK35 (Lane 4) and OmpK36 (Lane 5). An equal volume (~10 µl) of proteoliposome mixtures was loaded on the SDS-PAGE. L represents the molecular weight marker.

The LSA data in Figure 5.5 (also see section 2.12) shows faster uptake of glutamate (147 Da) than arginine (174 Da) through OmpF which is expected considering the weak cation-selective nature of the channel. Accordingly, OmpE35 and OmpK35 (OmpF orthologs) are assumed to be less cation selective than OmpE36 and OmpK36 (OmpC orthologs) respectively, and are expected to reproduce OmpF-like uptake patterns for the charged amino acids. However, the uptake of charged molecules through the target porins was slightly different than expected. OmpE35 showed slightly higher uptake of glutamate (~78%) than arginine (~72%) but OmpE36 allowed almost equal uptake of both substrates (~ 61%). Likewise, OmpK36 showed higher uptake of arginine (~ 87%) than glutamate (~ 82%) but OmpK35 showed no particular preference (~ 86% for both glutamate and arginine).

Among the zwitterionic carbapenems, each antibiotic showed similar permeation profile through all proteins except for ertapenem. Ertapenem (475 Da) diffused more rapidly through OmpF orthologs (71% through OmpK35 and 30% through OmpE35) than OmpC counterparts (16% through OmpK36 and none through OmpE36). In contrast, other carbapenems like imipenem and meropenem, showed faster permeation rates than other zwitterionic compounds through all porin channels. The uptake of imipenem (299 Da, ~ 50%) was less than meropenem (~383 Da) and each channel showed more than 70% translocation efficiency for meropenem (highest among the antibiotics and comparable to the amino acids).

A large variation was observed for the uptake of anionic compounds. The only di-anionic compound, ticarcillin (384 Da), failed to permeate through any porin (except for OmpK35). Among the mono-anionic compounds, ceftazidime (546 Da) showed a significant permeation rate of ~ 20% through all the proteins while cefotaxime and piperacillin showed extremely low uptake (≤ 10%). The zwitterions of ampicillin (349 Da) permeated more swiftly through OmpF orthologs than the OmpC orthologs. The maximum uptake of ampicillin (~ 47%) was noted for OmpE35 channel. However, another zwitterionic compound, cefepime (480 Da), showed faster permeation through OmpC orthologs than OmpF orthologs. The highest uptake of cefepime was observed for OmpE36 (66%).

Very recently, after a comprehensive analysis on a large number of compounds, a report suggested certain factors like presence of an amine group, rigidity and low globularity of a small molecule contribute towards its accumulation inside the cells of Gram-negative bacteria (Richter et al., 2017). The compounds containing ionisable nitrogen atoms (amine group) are more likely to pass through cation-selective channels of porins (like OmpF/C) than the molecules with carboxylate-groups. Other factors like rigidity and globularity, contributing towards the molecule conformation, are crucial to overcome the energy barrier at the CR of porins. According to these criteria, the low uptake of piperacillin can be explained due its globular shape while the rest of the molecules adopt linear conformation (Appendix Figure 4). In comparison, despite the linear shape, the low uptake for cefotaxime (8 rotating bonds) is probably because of its lower rigidity than piperacillin (6 rotating bonds). Among the zwitterions, cefepime possesses two additional ionisable nitrogen atoms than ampicillin which may explain its higher translocation rate through all the porins (Richter et al., 2017).

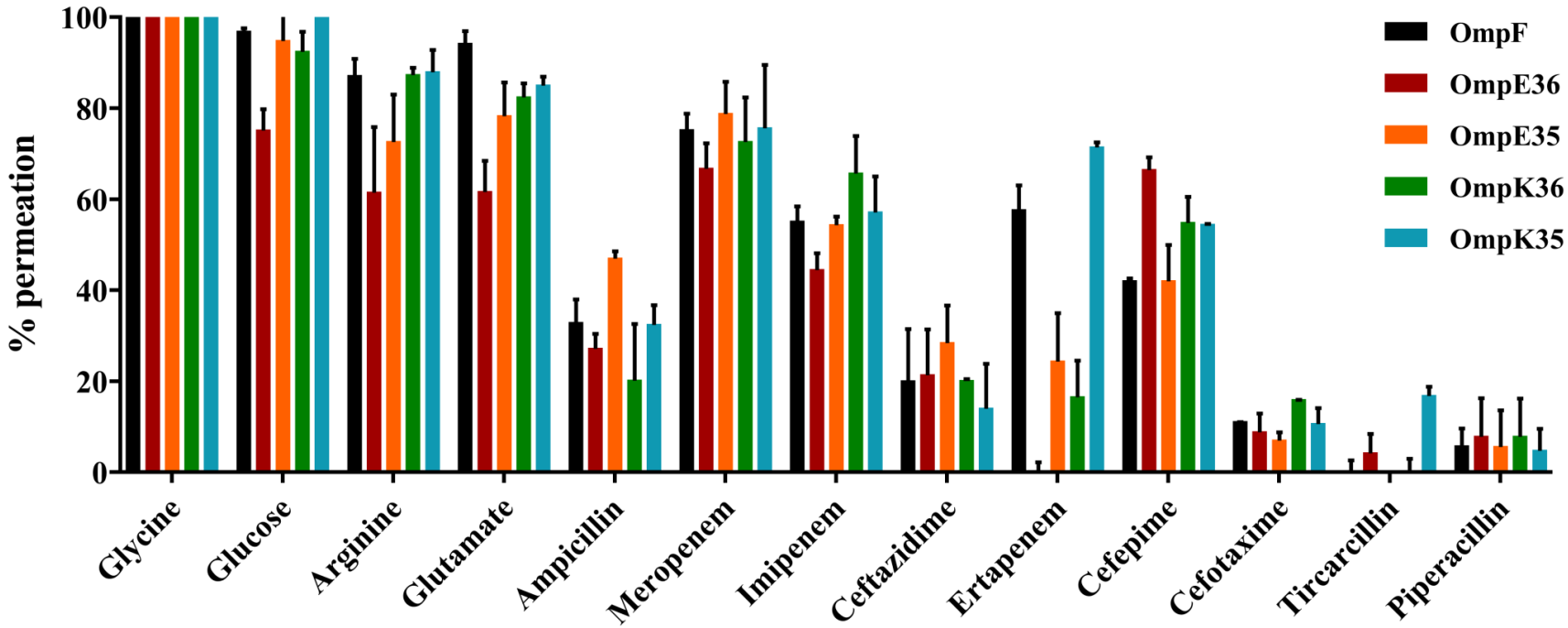

Figure 5.5. Liposome swelling data for OMPs of *E. cloacae* and *K. pneumoniae*.
The figure depicts the permeation rates of various substrates through the proteoliposomes of OmpF, OmpE35/E36 and OmpK35/K36. The substrates include a sugar (glucose), 3 amino acids (glycine, arginine and glutamate) and 9 antibiotics (ampicillin, meropenem, imipenem, ceftazidime, ertapenem, cefepime, cefotaxime, ticarcillin and piperacillin). The substrate uptake rates were averaged from triplicates measured from three different liposome samples prepared on different days. The values shown correspond to averages and their standard deviations (n = 9, also see section 2.12). For each protein, the uptake rate of glycine (0.83) was set to 100% and used as a reference for calculating the permeation of other substrates.

5.5. Single channel electrophysiology studies of OmpU and OmpT proteins

Single channel electrophysiology was used to investigate the channel properties of *V. cholerae* porins OmpU and OmpT (see section 2.10).

5.5.1. *Single channel properties of OmpU and OmpUΔN*

The conductance values for OmpU and OmpUΔN in 1 M KCl (solubilised in 10 mM HEPES, pH 7.5) were recorded as 1.0 ± 0.04 nS and 1.4 ± 0.03 nS respectively (n=3). The higher conductance of OmpUΔN is explained qualitatively by its shorter constriction and larger pore diameter, facilitating higher flow of ions than OmpU. A main point to be noted here is under the conditions of high salt (1 M KCl), the current traces of OmpU and OmpUΔN showed no evidence of trimeric states (evident in the form of trimeric gating). Another notable feature apparent from the current traces of OmpU was the pronounced gating of the channel at positive voltages. As a result, the ion-fluctuation created a subconductance state resulting in a small peak of current obtained for the histogram plot of OmpU channel, in addition to the main current peak (as indicated with an arrow in Figure 5.6 A). However, the ion-current fluctuations were much less pronounced in the traces of OmpUΔN (Figure 5.6 B), which may implicate the role of N-terminus in causing the gating behaviour of OmpU.

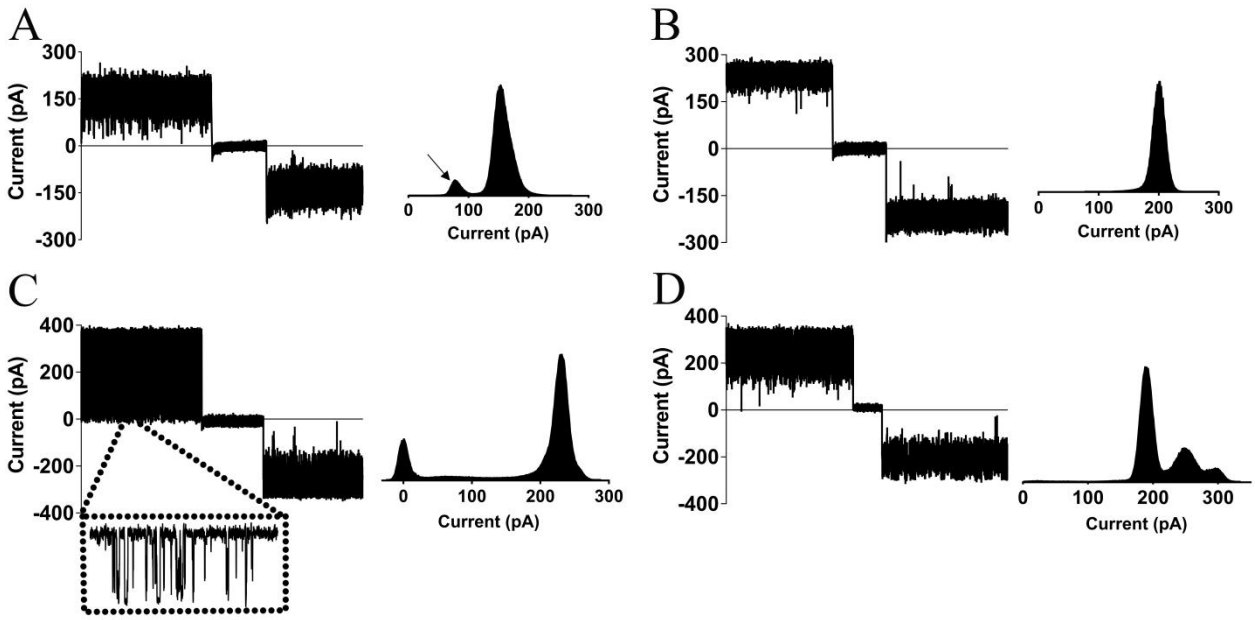

Figure 5.6. C**haracterisation of *V. cholerae* porin channels.**
Single channel current traces for (A) OmpU, (B) OmpUΔN, (C) OmpT and (D) OmpTΔL8. All-point histograms shown on the right side of the traces correspond to the positive voltages only (time period of 5 seconds). Traces were recorded in 1 M KCl (10 mM Hepes pH 7.5) with a potential of 150 mV.

5.5.2. *Single channel properties of OmpT and OmpTΔL8*

The single channel conductances recorded for OmpT and OmpTΔL8 were 2.0 ± 0.17 nS and 2.0 ± 0.11 nS respectively, in 1M KCl (in buffer 10 mM HEPES, pH 7.5). Like OmpU (or OmpUΔN), both OmpT and OmpTΔL8 showed no trimeric traces in 1M KCl, suggesting only monomeric channels are inserted into the lipid bilayer under high ionic strength conditions. The similar conductance values for OmpT and the L8 deletion mutant are surprising, given the much larger pore in the crystal structure of the deletion mutant. The single channel traces of OmpTΔL8 showed 2-3 subconductance states, which were absent in OmpT, suggesting that the lack of L8 causes other extracellular loops to move and partially block the ion current. Frequent gating in the form of transient current blockages was observed for OmpT at positive voltages (Figure 5.6 C). As for OmpU, the traces of the loop deletion mutant OmpTΔL8 showed less pronounced gating behaviour (Figure 5.6 D), and the data therefore suggest that the gating in WT OmpT results from movements of loop L8 within the pore constriction.

5.5.3. Trimeric traces of OmpU and OmpT at low ionic strength

We also made the single channel measurements for OmpU and OmpT in low salt buffer (150 mM KCl, 10 mM HEPES, pH 7.5). In contrast to the high salt data, the low salt recordings showed clear evidence for trimerisation. The trimeric conductances for OmpU and OmpT were determined to be 0.7 nS and 1.1 nS respectively (Figure 5.7 A). These values are similar to earlier published data from proteins purified from *V. cholerae* (Delcour 2003) where trimeric conductances of OmpU and OmpT were reported to be 0.9 nS and 1.3 nS respectively. The comparison of OmpU and OmpT traces in 1 M and 150 mM KCl demonstrates that the trimeric states of these proteins are destabilised in detergent in the presence of high salt concentrations. Such behaviour contrasts with the porins of Enterobacteria, which form stable trimers independent of ionic strength. Analysis of OmpU and OmpT in blue-native PAGE confirms the relatively low stability of the *V. cholerae* porins (Figure 5.7 B), since both proteins produced three bands corresponding to their monomeric, dimeric and trimeric states. A closer look at the gel shows the intensity of trimeric band for OmpT is very weak, implying that the trimer of OmpT is less stable than that of OmpU.

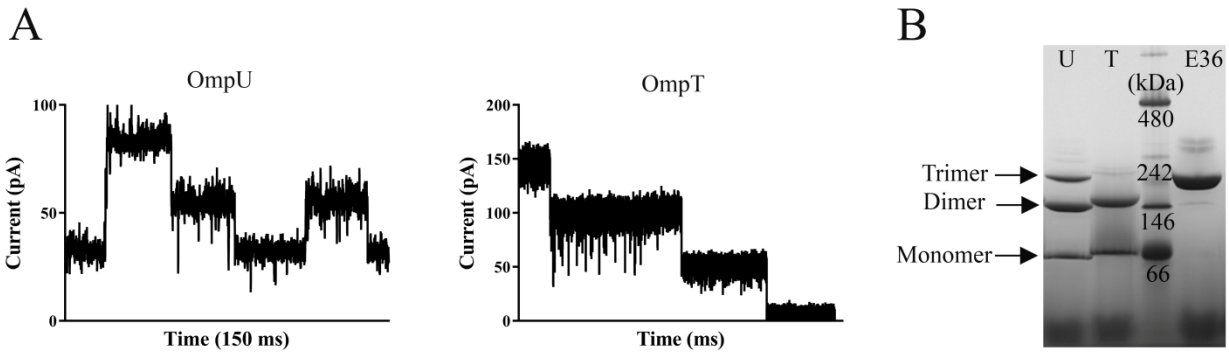

Figure 5.7. Oligomerisation of *V. cholerae* porins OmpU and OmpT.
(A) Single channel traces obtained in 150 mM NaCl (10 mM Hepes pH 7.5; 150 mV), showing trimerisation for both OmpU and OmpT. (B) Blue native-PAGE of OmpU and OmpT. As a control, the OmpF ortholog of *Enterobacter cloacae* (OmpE36) is included as a stable trimer. Molecular weight marker positions are indicated.

5.6. Multichannel electrophysiology studies of OmpU and OmpT

Multiple porin channels of OmpU (and OmpUΔN) and OmpT (and OmpTΔL8) were allowed to insert in a black lipid membrane to corroborate the conductance properties of these channels as revealed from the single channel analysis. As shown in figure 5.8, the conductance values recorded from multichannel bilayer experiments for OmpU, OmpUΔN, OmpT and OmpTΔL8 in 1 M KCl buffer solution (10 mM HEPES, pH 7.0) are in good agreement with the single channel recordings. The maximum number of channels for OmpU and OmpUΔN in 1 M KCl recorded the conductances of 800 pS and 1200 pS respectively. For OmpT and OmpTΔL8, the conductance recorded for maximum number of channels approximated to 1700 pS and 1400 pS respectively. These values are in accordance with the conductances derived from single channel studies except for OmpTΔL8. The deviation of multi-channel conductance of OmpTΔL8 (~ 1.4 nS) from its single channel conductance (2.0 nS) is unusual and may be explained by the fact that the multi-channel measurement is a crude method to estimate the conductance and cannot be considered a robust tool for determining ion-channel properties.

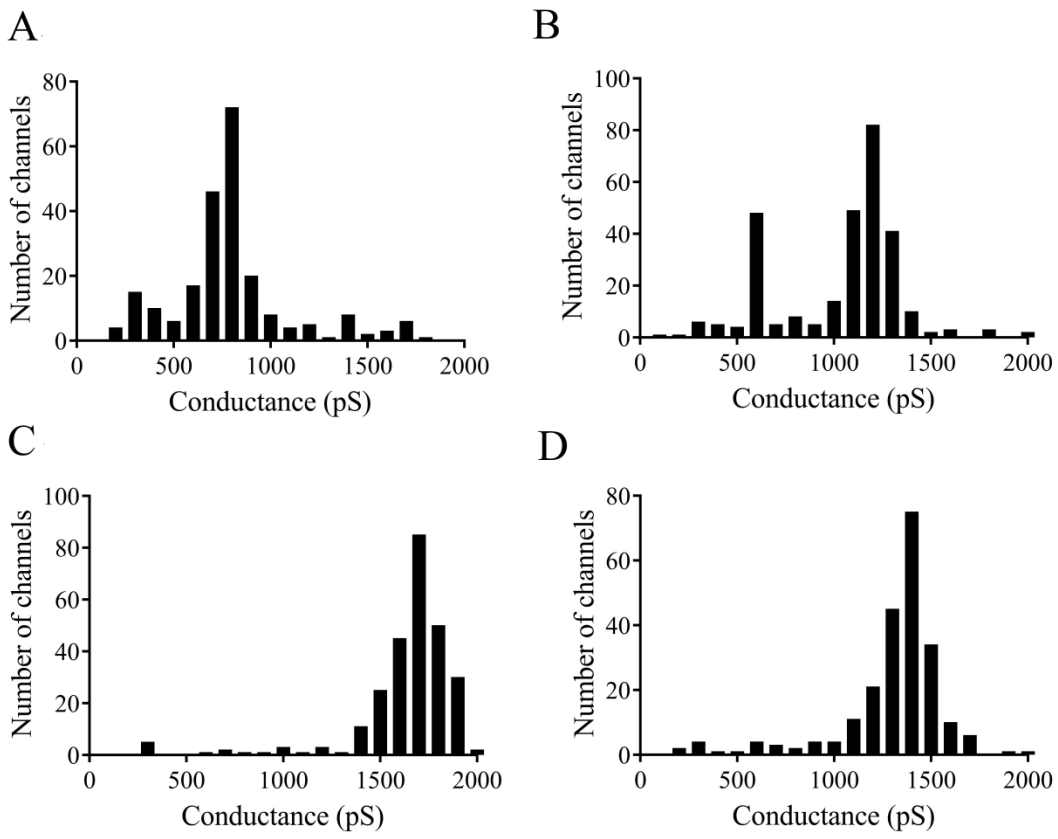

Figure 5.8. Multichannel data for OmpU (/OmpUΔN) and OmpT (/OmpTΔL8). Conductance values (in Siemens) recorded from multichannel (80-100) insertions of (A) OmpU, (B) OmpUΔN, (C) OmpT and (D) OmpTΔL8 in 1 M KCl buffer (10 mM Hepes, pH 7.0.). The data is a mean of three independent measurements (also described in section 2.12).

5.7. Ion-selectivity of OmpU and OmpT

To probe the ion selectivity of the channels, multichannel lipid bilayer experiments for OmpU and OmpT were conducted in three different salt buffers (KCl, LiCl and K^+-acetate) at high ionic strength. The resting membrane potentials recorded in KCl buffer (and in LiCl and K^+-acetate buffers) showed a cation-selective nature for both channels. The electrophoretic mobilities of the charged ions of KCl solution are equal ($K^+ = Cl^-$) but are different for the ions of LiCl and K^+-acetate solutions. As a result and in comparison to the selectivity data in KCl solution, the selectivity for cations is reduced in the LiCl solution because of lower mobility of Li^+ compared to Cl^- ions, but is increased in the K^+-acetate solution because of the higher mobility of K^+ compared to CH_3COO^- ions (Figure 5.9).

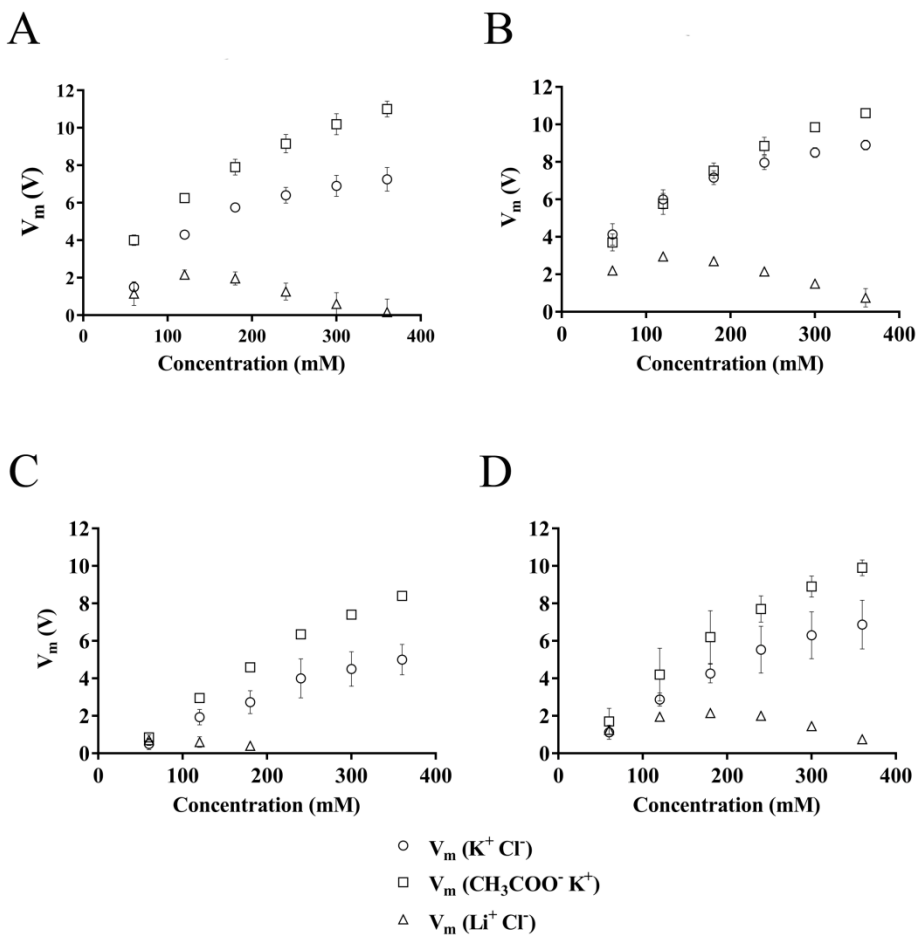

Figure 5.9. Cation selectivity revealed for *V. cholerae* porins.
The multichannel data of (A) OmpU, (B) OmpUΔN, (C) OmpT and (D) OmpTΔL8 show the resting membrane potentials achieved in KCl, LiCl and CH_3COOK solutions. The data shown is a mean of three independent measurements (also described in section 2.12). Some of the error bars are too small to be visible and are hidden behind the data labels.

The ion selectivity measurements of OmpU and OmpT were also conducted under low ionic strength conditions (0.01 M to 0.1 M KCl) for comparison with those done in high ionic strength (0.1 M to 1 M KCl). With ion-selectivity being strongly dependent on the salt concentrations, the cation selectivity difference between OmpU and OmpT was more evident under conditions of low ionic strength (Figure 5.10). The zero-current membrane potentials at 10-fold salt gradient were used to derive the cation to anion permeability ratios (P_k/P_{cl}) via the Goldman–Hodgkin–Katz voltage equation (Hodgkin and Katz, 1949). The permeability ratios were calculated as ~3.8 (OmpU) and ~2.8 (OmpT) and are comparable to OmpF (~3.9) in similar salt conditions (Benz et al., 1985). Contrary to the present study, an earlier paper (Simonet et al., 2003) reported comparatively high P_k/P_{cl} values for OmpU (~14) and OmpT (~4), showing much higher cation selectivity for OmpU for reasons that are unclear.

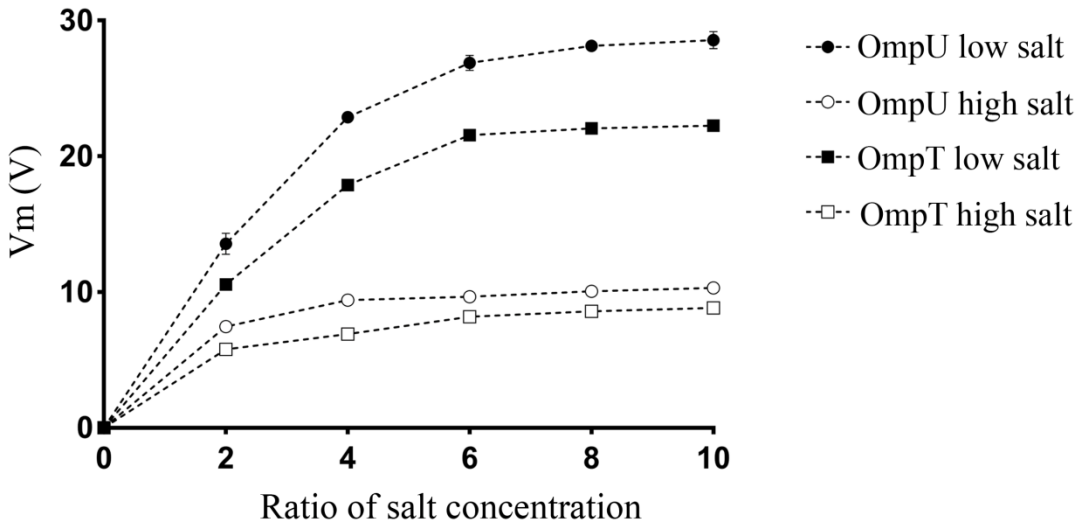

Figure 5.10. Cation selectivity of OmpU and OmpT channels in high vs low salt buffers.

The porin channels of OmpU and OmpT show higher resting membrane potential (V_m) in 10-fold salt gradient of low salt solution (0.01 M – 0.1 M KCl) than for the same gradient of high salt solution (0.1 M – 1 M KCl). The data shown is a mean of three independent measurements (also see section 2.12).

5.8. Single channel analysis of OmpU(/UΔN) and OmpT(/TΔL8) with substrates

Cholera infection is treated most commonly with antibiotics from the tetracycline family (e.g. tetracycline, doxycycline). Unfortunately, the addition of tetracycline or doxycycline did not affect the single channel traces of OmpU/T, which is mostly explained by the limited solubility of those compounds in aqueous buffers (~ 1-2 mM). Moreover, the addition of other, water-soluble β-lactam antibiotics (ampicillin, piperacillin and ticarcillin) showed no effects, even at concentrations of up to 20 mM. However, the addition of two carbapenem antibiotics (imipenem and meropenem), generated interesting features in the single channel current traces that are discussed in the following sections (Figure 5.11). Using proteins purified from *V. cholerae*, it was previously reported that the physiologically important bile component deoxycholate interacts with OmpT and not with OmpU (Duret and Delcour, 2006 and Duret and Delcour 2010). We repeated these experiments with our *E. coli*-expressed proteins to verify those results by testing the effect of deoxycholic acid on OmpU and OmpT traces (Figure 5.11).

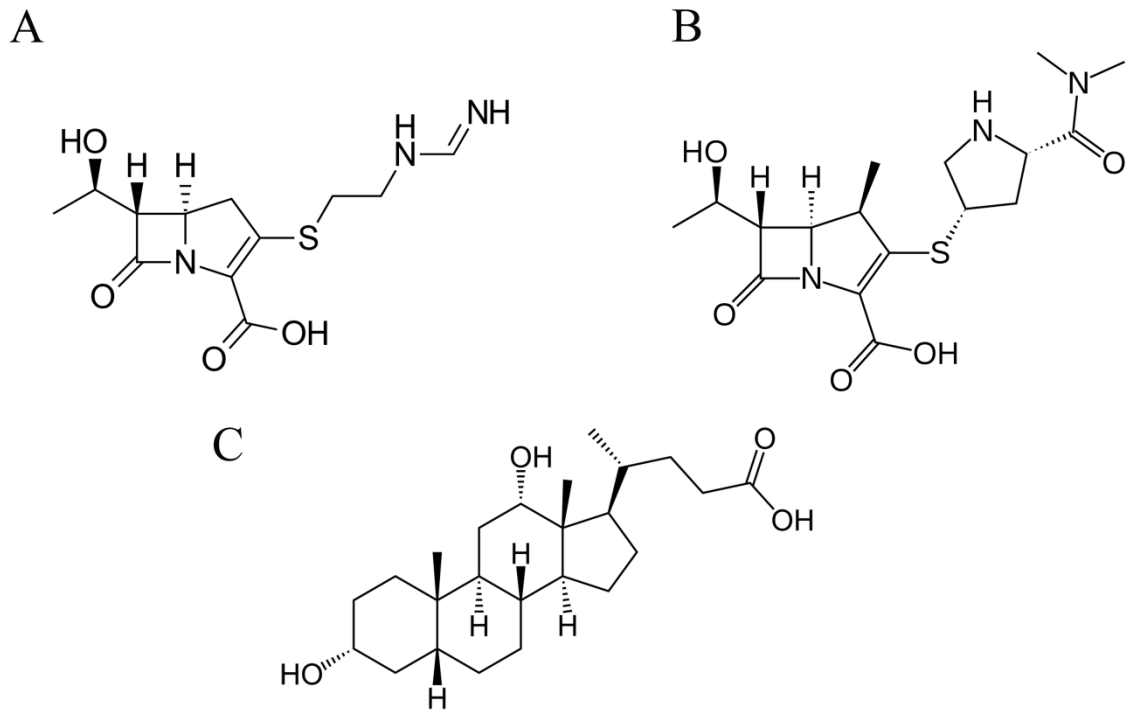

Figure 5.11. Chemical structures of substrates.
Chemical representations of different substrates, (A) meropenem (383 Da), (B) imipenem (299 Da) and (C) deoxycholate (392 Da) which were studied with the single channels of *V. cholerae* porins.

5.8.1. *Imipenem effect on OmpU/T traces*

Imipenem addition to the single channels of OmpU, OmpUΔN, OmpT and OmpTΔL8 generated the following features: increase in the ion-current noise, decrease in the average current and most importantly, transient current blockage events (Figures 5.12 and 5.13). These reversible blockages of current are caused by the entry of a single substrate molecule into the channel. The single step downward transitions of complete closures in the current traces illustrate that monomers of OmpU (and OmpT) are blocked by the antibiotic molecule, further supporting our notion that only monomeric insertions of these porins occur in 1 M KCl. Since, similar effects of imipenem were observed with the traces of the deletion mutants, OmpUΔN and OmpTΔL8, it may indicate that these constriction elements might not be directly (but indirectly) involved in the substrate binding. The measurements for all four channels were performed with cis and trans addition of imipenem (to be noted that the ground and live states of the single channel are referred to as cis and trans states respectively). For OmpU and OmpUΔN, both cis and trans

addition of imipenem generated binding events and hence two association rate constants can be calculated (k_{on}^{cis} and k_{on}^{trans}; $M^{-1}s^{-1}$) for 2.5 mM imipenem at 75 mV along with the dissociation rate constant (k_{off}, s^{-1}) (Table 5.1). The data show that both binding constants of OmpU are similar and very low, indicating that the interaction of imipenem with the OmpU is inefficient. In comparison to OmpU, the binding constants of imipenem with OmpUΔN are slightly higher for both cis and trans sides (Table 5.1). The difference between the two channels caused by meropenem is further illuminated by the current traces and histograms presented in Figure 5.12. An equal concentration of meropenem (2.5 mM) induces less current blockages in OmpU than OmpUΔN resulting in reduced current flow through OmpUΔN channel. This suggests that the deletion of N-terminus in OmpUΔN, by providing a larger pore diameter, may allow better access of imipenem as compared to OmpU.

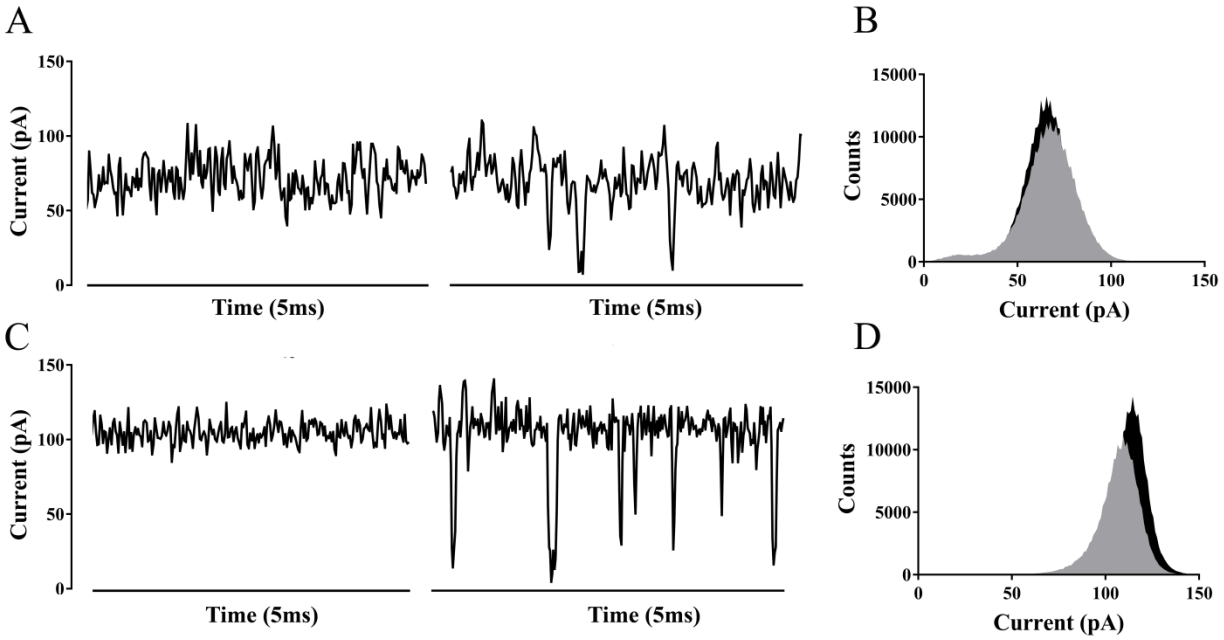

Figure 5.12. Imipenem effect on current traces of OmpU and OmpUΔN channels. Current traces of (A) OmpU and (C) OmpUΔN without imipenem (left panels), display current blockages upon addition of 2.5 mM imipenem (right panels). (B, D) Current histograms (recorded for 10 seconds interval) of (B) OmpU and (B) OmpUΔN with 2.5 mM imipenem (gray) as compared to the current flow without imipenem (black as control). The data shown was recorded at 75 mV in 1 M KCl solution (10 mM HEPES, pH 7.0).

For OmpT, since the channel showed spontaneous gating events at positive voltages (Figure 5.6 C) it became difficult to differentiate the interaction of imipenem from the trans side. Thus, for comparison with OmpU, the k_{on} and k_{off} values for OmpT were calculated only for the cis side with 2.5 mM imipenem at 75 mV (Table 5.1).

Table 5.1. Association (k_{on}) and dissociation (k_{off}) rate constants of imipenem.
The single channels recordings of OmpU/T and their mutants in 1 M KCl, 10 mM Hepes, pH 7.0 with 2.5 mM imipenem at 75 mV. The calculated data is a mean of three independent measurements.

	Protein	k_{on}^{cis} (10^3) (M^{-1} s^{-1})	k_{on}^{trans} (10^3) (M^{-1} s^{-1})	k_{off} (s^{-1})
Imipenem	OmpU	72 ± 20	122 ± 30	18180
	OmpUΔN	90 ± 13	272 ± 40	25000
	OmpT	320 ± 90	-	10000
	OmpTΔL8	411 ± 78	-	9500

- The events for OmpT were not calculated for trans side due to spontaneous gating of the channel.

For OmpTΔL8, the k_{on} and k_{off} values were also calculated for only cis side with 2.5 mM imipenem at 75 mV (Table 5.1). The data shows a ~10-fold higher binding affinity of imipenem for OmpT as evident from the higher association rate (k_{on}^{cis} = 320 × 10^3 $M^{-1}s^{-1}$) compared to OmpU (k_{on}^{trans} = 122 × 10^3 $M^{-1}s^{-1}$). This is further supported by the dissociation rate constants of imipenem, which for OmpT are almost 2-fold lower than those for OmpU (Table 5.1.). Moreover, as compared to OmpU (or OmpUΔN in Figure 5.12), OmpT (or OmpTΔL8) current traces (Figure 5.13) showed higher numbers of blocking events upon addition of 2.5 mM imipenem.

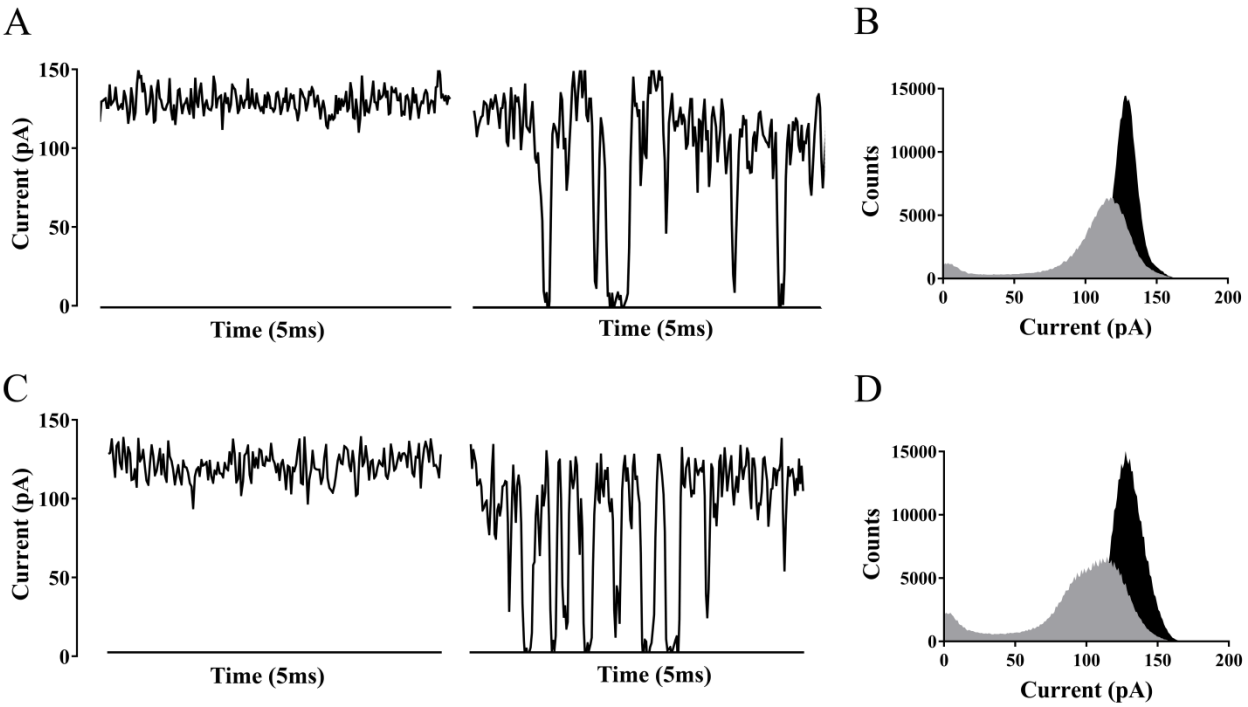

Figure 5.13. Imipenem effect on current traces of OmpT and OmpTΔL8 channels.
The current traces of (A) OmpT and (C) OmpTΔL8 without imipenem (left panels), display current blockages upon addition of 2.5 mM imipenem (right panels). (B,D) Current histograms (recorded for 10 seconds interval) of (B) OmpT and (D) OmpTΔL8 (D) with 2.5 mM imipenem (gray) and without imipenem (black as control). The data shown was recorded at 75 mV in 1 M KCl solution (10 mM HEPES, pH 7.0).

The addition of imipenem causes almost 50% reduction in the current flow through the channels of OmpT and OmpTΔL8 than the control traces without the antibiotic (Figure 5.13 B and D). Like OmpU and OmpUΔN, the deletion mutant of OmpT also showed a higher binding affinity for imipenem than OmpT (Table 5.1).

5.8.2. *Meropenem effect on OmpU/T traces*

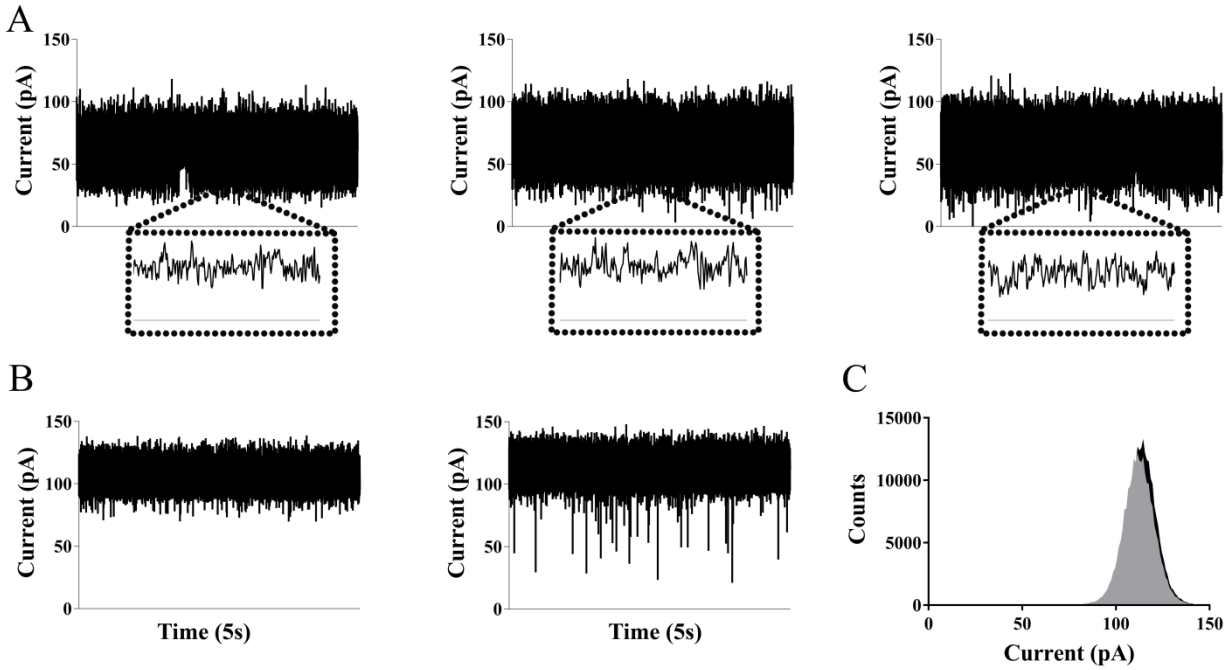

Figure 5.14. Meropenem effect on current traces of OmpU and OmpUΔN channels. (A) The current traces (5 seconds) of OmpU without meropenem (left panel), with 5 mM meropenem (middle panel) and 15 mM meropenem (right panel). The boxed regions show zoomed in 5 ms traces of each OmpU trace. (B) The ion-current traces of OmpUΔN without antibiotic (left panel) and upon addition of 5 mM meropenem (right panel). (C) Histogram representation (recorded for 10 seconds interval) of current for OmpUΔN without meropenem (control in black) and with the addition of 5 mM meropenem (gray). The data shown was recorded at 75 mV in 1 M KCl solution (10 mM HEPES, pH 7.0).

The addition of another carbapenem, meropenem, did not show binding events in the single channel traces of OmpU nor did it lead to a decrease in current (Figure 5.14 A). This could be explained by two extreme possibilities: (i) either meropenem does not permeate through OmpU or (ii) permeation is extremely fast (< 50 μs) and cannot be recorded by the amplifier. However, meropenem reduced the current flow in the traces of OmpUΔN. Although no binding events were observed for OmpUΔN, meropenem addition increased the ion-current noise as well as very slight reduction in the average current flow was also observed (Figure 5.14 B and C).

However, the association or dissociation rates were not calculated for OmpUΔN since no binding events could be recorded upon meropenem addition.

Table 5.2. Association (k_{on}) and dissociation (k_{off}) rate constants of meropenem.
The single channels recordings of OmpU/T and their mutants in 1 M KCl, 10 mM Hepes, pH 7.0 with 2.5 mM meropenem at 75 mV. The data shown is averaged (mean) from three independent measurements.

	Protein	k_{on}^{cis} (10^3) (M^{-1} s^{-1})	k_{on}^{trans} (10^3) (M^{-1} s^{-1})	k_{off} (s^{-1})
Meropenem	OmpU	ND*	ND*	ND*
	OmpUΔN	ND*	ND*	ND*
	OmpT	43 ± 15	-	28570
	OmpTΔL8	52 ± 15	-	14285

*ND Not Detected
- The events for OmpT were not calculated for trans side due to vigorous flickering of the channel.

In contrast to OmpU, meropenem addition to OmpT and OmpTΔL8 showed an increase in the ion-current noise accompanied by a reduction in average current. Compared to imipenem addition, very few discrete binding events were recorded with meropenem (Figure 5.15), giving a binding constant ($K= k_{on}/k_{off}$) of 1.5 M^{-1} for OmpT and 3.6 M^{-1} for OmpTΔL8 at 75 mV (Table 5.2). The data suggests lower binding affinity of meropenem for OmpT (or OmpTΔL8) than imipenem. However, since binding and permeation are two independent aspects and are not necessarily related, the single channel measurements alone do not inform on the permeation rates of meropenem and imipenem.

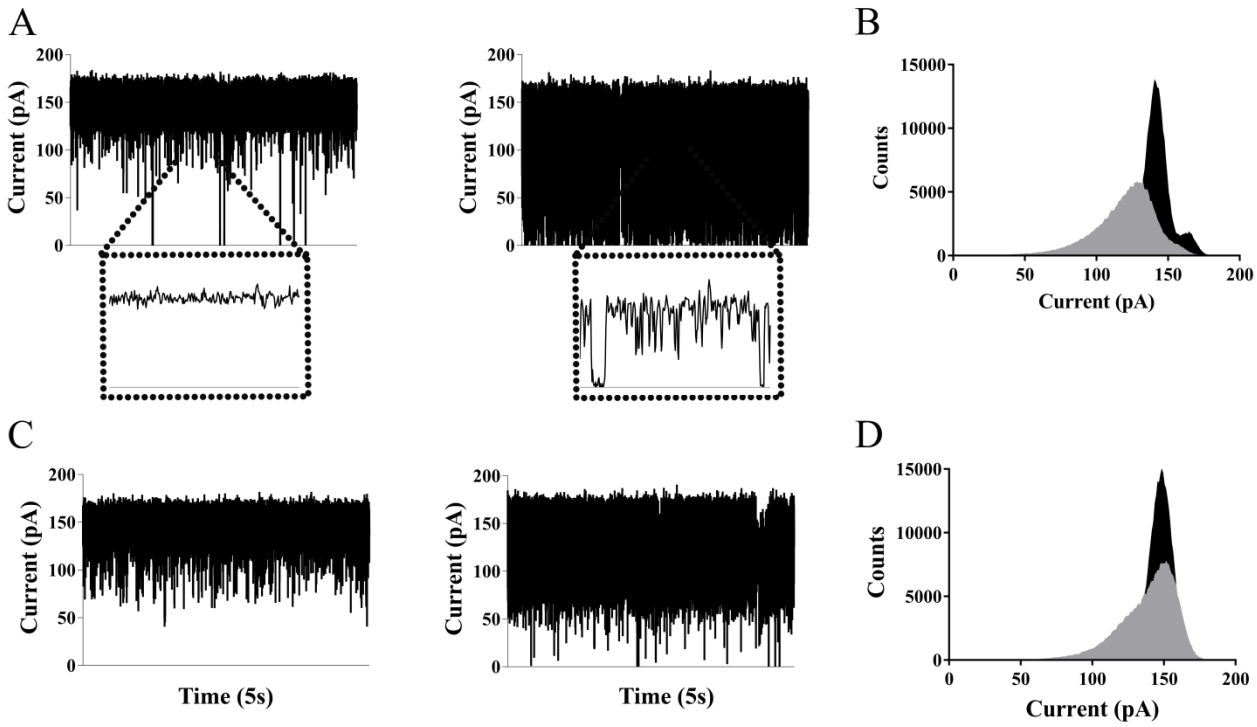

Figure 5.15. Meropenem effect on current traces of OmpT and OmpTΔL8 channels.
A, C) The comparison of the current traces (5 s) of (A) OmpT and (C) OmpTΔL8 without antibiotic (left panels) and with 5 mM meropenem (right panels). The boxed regions are zoomed in (5 ms) for OmpT traces to show current blockages induced by meropenem. (B, D) The histogram (recorded for 10 seconds interval) representation of current flow through (B) OmpT and (D) OmpTΔL8 without meropenem (control in black) and with 5 mM meropenem (gray). The data presented was recorded at 75 mV in 1 M KCl solution (10 mM HEPES, pH 7.0).

5.8.3. *Deoxycholate effect on OmpU/T traces*

Earlier studies on *V. cholerae* porins implicated OmpU to play a crucial role in the colonisation of the human intestine by bacterial cells by generating resistance to bile (also see section 1.6.1.2). Electrophysiological studies on *V. cholerae* porins demonstrated that the addition of deoxycholate causes single step closures in the ion-current traces of OmpT but not with OmpU (Duret and Delcour 2006). In our work, we replicated the study to confirm these findings for our proteins and obtained data that agree well with the previous results. OmpT traces showed single step closures (SSCs) upon the addition of deoxycholate (Figure 5.16). The frequency of SSCs increased with the increase in the concentration of added deoxycholate. However, addition of substrate beyond 250 µM resulted in rupture of the lipid membrane due to the fact that DOC is a detergent.

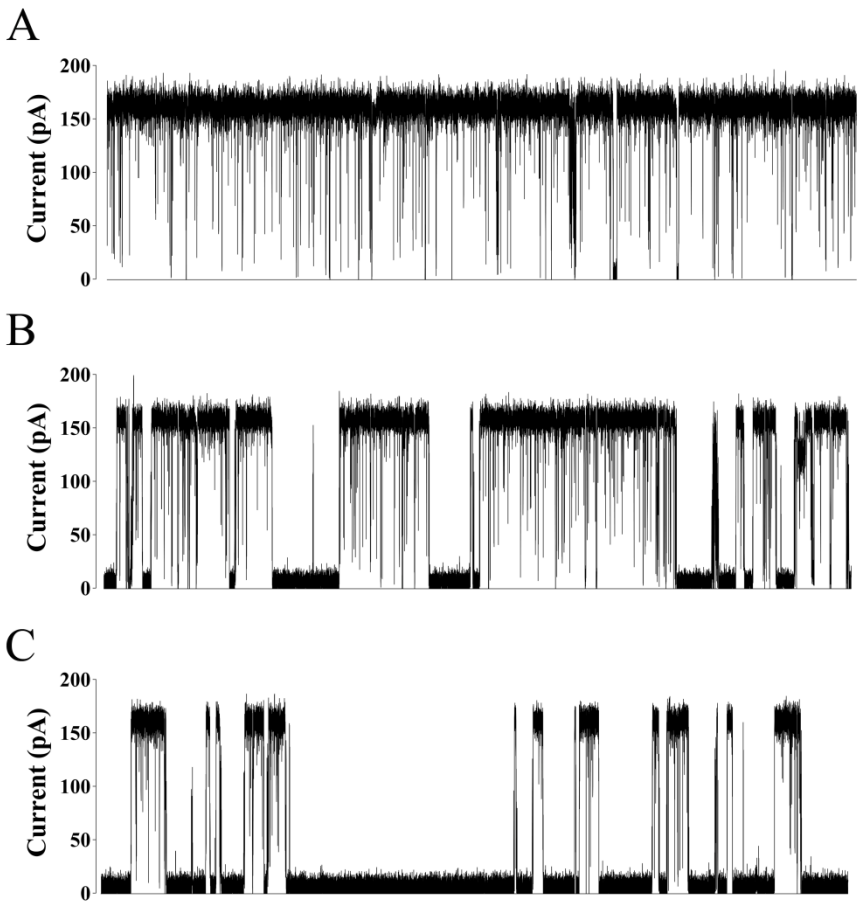

Figure 5.16. Deoxycholate effect on single channel traces of OmpT.
(A) Standard ion-current traces of OmpT. (B, C) The single step closures in the ion-current traces of OmpT with the addition of (B) 100 µM deoxycholate and (C) 200 µM deoxycholate.

In contrast to OmpT, the OmpU traces were completely unaffected by deoxycholate addition (Figure 5.17). The effect of deoxycholate (if any) on OmpU could only be recorded with a maximum concentration of up to 200 µM, since the use of 250 µM or above interfered with the membrane stability of the lipid bilayer and resulted in membrane rupture.

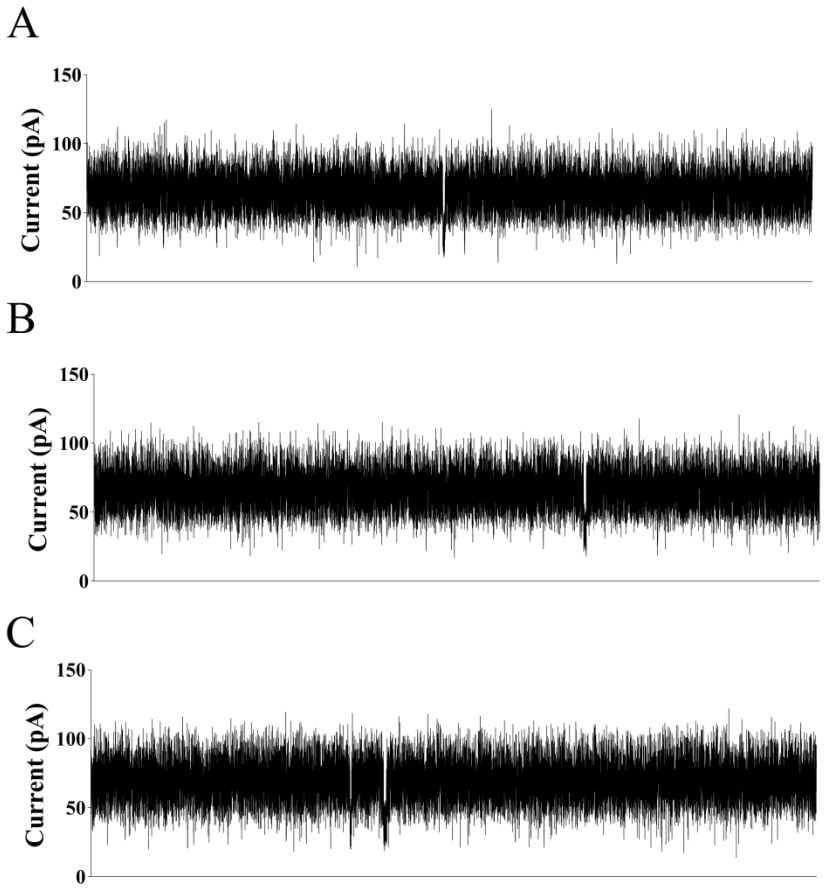

Figure 5.17. Deoxycholate effect on single channel traces of OmpU.
(A) Standard ion-current traces of OmpU which remain uneffaected by the addition of (B) 100 µM deoxycholate and (C) 200 µM deoxycholate.

5.9. Liposome swelling assays for OmpU and OmpT

The electrophysiological studies revealed the interaction of two antibiotics, meropenem and imipenem, with the porins of *V. cholerae*. To corroborate the results of the single channel studies, we carried out LSA for an initial characterisation of small-molecule transport through OmpU and OmpT (Figure 5.18). For comparison, we assessed uptake by *E. coli* OmpF as well. The uptake of glycine through OmpF channel was set to 100% to be used as a reference for calculating the uptake rates of other substrates through OmpF and OmpU/T porins. Overall, uptake rates were roughly proportional to the diameter of the channels, with the highest rates observed for OmpF and the lowest rates for OmpT. The uptake rates for glutamate were slightly higher than those for arginine, despite the cation selectivity of all three channels (Danelon et al., 2003) Possible reasons for this are the slightly higher substrate concentrations used for glutamate (9 mM versus 7 mM for arginine) as well as the higher molecular weight for arginine (174 Da

versus 147 Da for glutamate). Interestingly, the data (Figure 5.18) also show that meropenem is taken up faster than imipenem by both OmpU and OmpT, despite meropenem being substantially larger (383 Da) than imipenem (299 Da). The liposome swelling experiments agree qualitatively with the electrophysiological data, in the sense that imipenem showed stronger and more pronounced interactions with OmpU and OmpT compared to meropenem, likely making uptake of the smaller antibiotic less efficient.

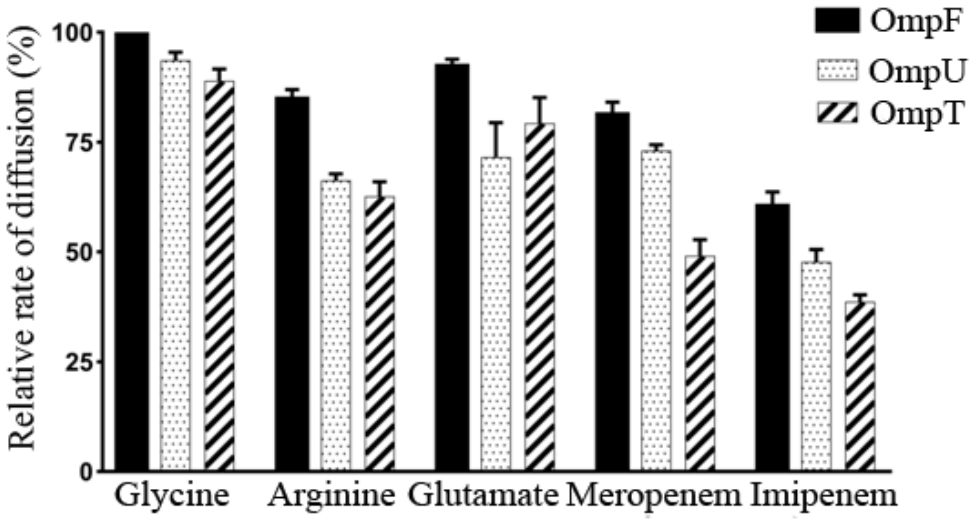

Figure 5.18. LSA data for *V. cholerae* porins.
Liposome swelling data for the substrates glycine (16 mM), glutamate (9 mM), arginine (7 mM), imipenem (16 mM) and meropenem (12 mM). Transport of glycine through OmpF is set to 100% for standardisation. The values shown correspond to the averages and their standard deviations (n = 9, also see section 2.12).

5.10. Discussion

E. coli porins have been extensively explored to provide a plethora of structural (Lou et al., 2011 and Ziervogel and Roux, 2013) and electrophysiological (Hajjar et al., 2010, Mahendran et al., 2009 and Cama et al., 2015) information on the interaction of antibiotics with OmpF/C. This chapter is aimed to investigate the interaction of other Gram-negative porins with antibiotics. The LSA with the porins of *E. cloacae* and *K. pneumoniae* have allowed us to quantify the uptake rates of different compounds and compare the permeation levels with respect to the OmpF channel. Each substrate exhibited similar permeation rates (± 20%) through the diffusion porins targeted for LSA, suggesting an analogy between the uptake mechanisms for hydrophilic solutes by such non-specific channels. This doesn't seem surprising given the structural knowledge of the porins that the channels of OmpE35/E36, OmpK36 (as discussed in section 4.13) and OmpF (Cowan et al., 1992) have equivalent pore sizes. The structure of OmpK35 (determined by another member of the lab) revealed similar pore dimensions as OmpK36. A few substrates however displayed slightly unexpected uptake patterns through these

porins in LSA (Figure 5.5). For instance, the high permeation of ertapenem (zwitterionic; 475 Da) through OmpF orthologs is probably owed to their larger pore sizes than OmpC orthologs. On the other hand, no uptake of small-sized ticarcillin (dianionic; 384 Da) through any porin channel, except for OmpK35, certainly suggests that not only size but the charge of a solute also plays a crucial role in determining its passage through the porin channel (as discussed in section 1.3.1.3). Nonetheless, another equally important factor like electrostatics and charged environment of the channel also affect the translocation of different substrates (Nestorovich et al., 2003, Aguilella-Arzo et al., 2007 and Bajaj et al., 2017). This is best exemplified by the channel of OmpK35 porin (OmpF ortholog) that allows higher uptake of ticarcillin than the porins of OmpF and OmpE35 (another OmpF ortholog). The electrostatics of the three channels differ with respect to their surface charges at the extracellular top (Figure 5.19). The net positive charge of OmpK35 is higher than OmpE35 and OmpF, which may explain the diffusion of the anionic compound (ticarcillin) through OmpK35.

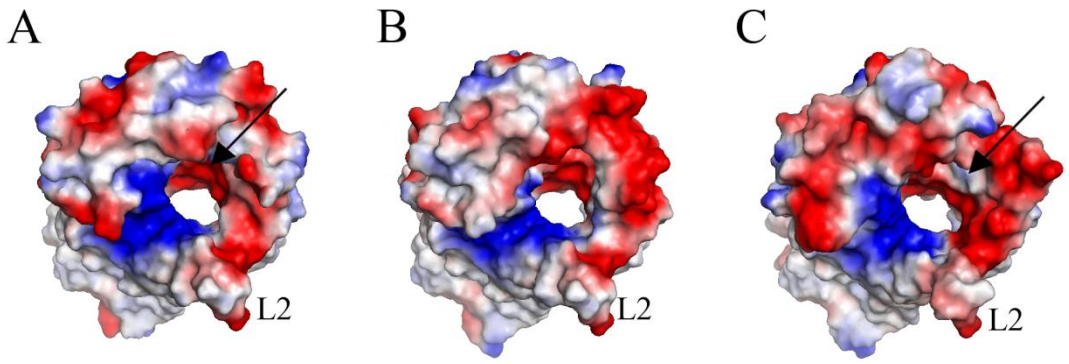

Figure 5.19. Surface electrostatics of OmpF ortholgues.
The figure displays electrostatic surface charges of (A) OmpF, (B) OmpE35 and (C) OmpK35 from the extracellular side. The arrows indicate the difference in the negative charged regions of OmpF and OmpK35.

Single channel electrophysiology experiments show higher single channel conductance of OmpUΔN than OmpU, which is expected due to the short constriction and large pore diameter of OmpUΔN. However, the similar conductance values for OmpT and the L8 deletion mutant are surprising, given the much larger pore in the crystal structure of the deletion mutant (Chapter 4). A possible explanation could be that the electrostatic properties of the two channel constrictions are quite different, with OmpT being negatively charged and the deletion mutant having a more typical "positive-negative" charge distribution due to the lack of loop L8.

V. cholerae porins, to our knowledge, have not yet been scrutinised at the single channel level for the effect of antibiotics. The ion current fluctuations observed upon the addition of

carbapenems report for the first time on the interaction of an antibiotic with OmpU/T porins at the single channel level. The time-resolved current blockages caused by meropenem and imipenem in the traces of OmpT and OmpU/T respectively represent the reversible positioning of antibiotic at the constriction zone such that the flow of ions is completely obstructed. OmpF has been shown previously (Nestorovich et al., 2002) to generate similar current blocking events with the addition of ampicillin (zwitterionic penicillin) and subsequent research has suggested that such events possibly result in the translocation of drug through the channel (Danelon et al., 2006). We anticipated similar behaviour for OmpU/T traces with ampicillin due to the structural homology between their structures and OmpF (section 4.13). Unexpectedly however, ampicillin addition displayed no visible affects in the ion current traces of OmpU/T. As argued before, this does not necessarily reflect an inability to bind or permeate but means that the binding (or translocation) of the compound does not alter the ionic flow of current (Danelon et al., 2006 and Ziervogel and Roux 2013). The zwitterionic carbapenems were recently investigated at the single channel level for their translocation though OmpF (Bodrenko et al., 2015) and OmpC (Bajaj et al., 2016). OmpC revealed binding events with imipenem with lower association rate constant ($k_{on} = 34 \times 10^3\ M^{-1}$) and higher dissociation rate constant ($k_{off} = 25000\ s^{-1}$) than we obtain for OmpU ($k_{on} = 122 \times 10^3\ M^{-1}$; $k_{off} = 18180\ s^{-1}$) and OmpT ($k_{on} = 322 \times 10^3\ M^{-1}$; $k_{off} = 10000\ s^{-1}$) channels. The addition of meropenem (10 mM) to OmpF revealed no such binding events but showed an average current reduction in the ion current traces (Bodrenko et al., 2015) that are similar to the current histograms of OmpT upon addition of 2.5 mM meropenem (Figure 5.15 B). Together, the electrophysiology data suggest that imipenem and meropenem have higher affinities for OmpU/T than for OmpF/C. However, this does not mean that those compounds translocate faster via OmpU/T than via OmpF, as noted above and demonstrated by the liposome swelling assays that show faster permeation via OmpF (Figure 5.18). However, given that the liposome swelling assay reports indirectly on substrate permeation it remains necessary to develop assays that monitor translocation (as opposed to interactions) of small molecules such as antibiotics through OM channels in real time.

Chapter 6. Final Discussion

Multi-drug resistance in Gram-negative bacteria is a consequence of three primary factors (Pages et al., 2008), one of which is the inability of the drugs to permeate the asymmetric OM interface. The diffusion channels present across the OM provide the porin-mediated pathway for the translocation of hydrophilic compounds (≤ 600 Da). An overall aim of the current study is to decipher the mechanism for the small molecule transport through water-filled channels of porins in order to contribute to drug-discovery strategies. Towards this, the goals achieved in this study include the structure determination of *V. cholerae* major porins (and *E. cloacae* and *K. pneumoniae* porins) followed by functional characterisation of porins through electrophysiology and *in vitro* antibiotic uptake assays.

6.1. Structure and Function of Enterobacterial porins

The recombinant OM expression of OmpE35/E36/K36 porins produced more than ~ 5 mg of proteins per litre of cells. The proteins withstood multiple rounds of purification and were purified as trimers through SEC column (unlike *V. cholerae* porins that were eluted as monomers), indicating the robust nature of their oligomerised states. Furthermore, the 3D structures of Enterobacterial porins were crystallised as trimers of 16-stranded β-barrels (Chapter 4). The sequence alignment of *E. cloacae* (OmpE35/E36), *K. pneumoniae* (OmpK35/K36) and *E. coli* (OmpF/C) proteins shows more than 70% sequence identity between the proteins (Appendix Figure 1). In addition, a striking similarity observed on the superposition of the protein folds of Enterobacterial porins and the structural differences are interesting (Figure 6.1 and see section 4.7). The structural superposition shows conservation of more than 50% of the pore-lining residues and the porins also match each other with the positions of the critical charged residues in the constriction region (Chapter 4).

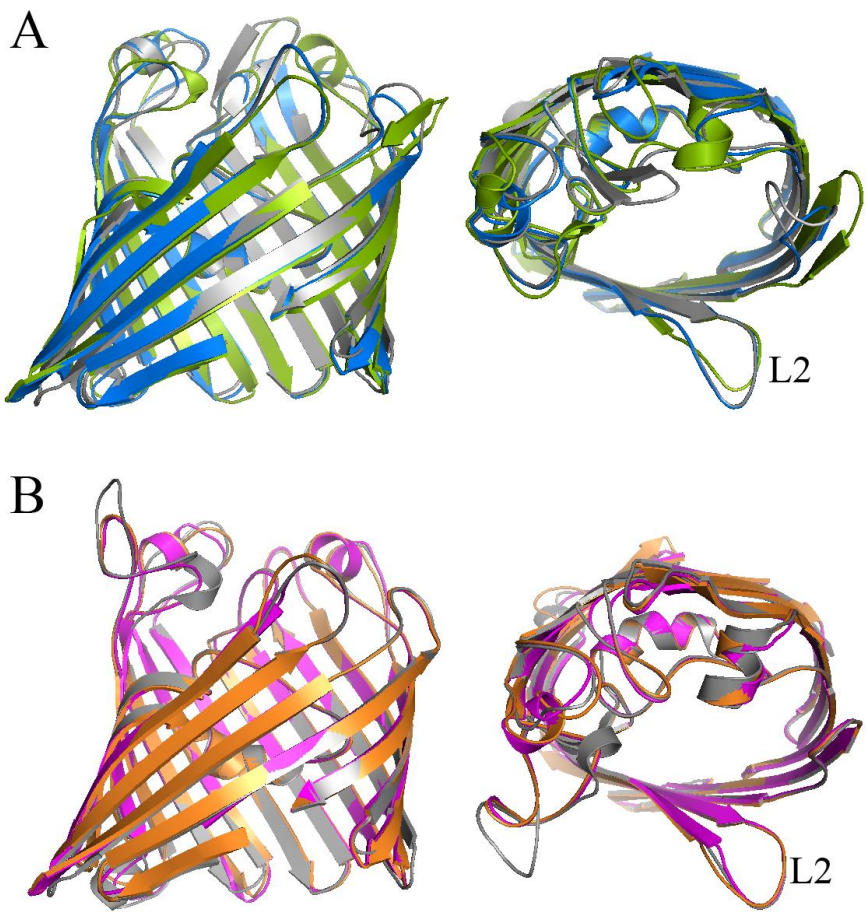

Figure 6.1. Structural superposition of OmpF/C orthologs.
(A) Side and extracellular views of OmpF (gray) superposed on OmpE35 (blue) and OmpK35* (green). (B) Side and extracellular views of OmpC (gray) superposed on OmpE36 (magenta) and OmpK36 (orange).
*Also see Appendix figure 5 for OmpK35 structure.

Small molecule permeation studies with Gram-negative porins have indicated molecular weight, polarity, shape, charge and rigidity as the key factors for determining permeation (Aguilella et al., 2015, Richter et al., 2017 and see section 1.3.1.3). Nonetheless, the charged environment inside a channel is an equally important factor playing a critical role in shaping the channel electrostatics to allow or restrict the passage of a molecule (Bajaj et al., 2017 and Acosta-Gutierrez et al., 2015). For instance, based on the antibiotic flux measurements, the porin channels of OmpE35 and OmpK35 show different uptakes for zwitterions of ampicillin and cefepime (see section 5.4 and figure 5.5). Since the two channels have similar pore-size dimensions, it may be possible that the interior electrostatics of OmpE35 and OmpK35 channels affect the permeation of the same molecule in different ways. The current ortholog paper that we

are working on defines a molecular mechanism which can be used for the prediction of the permeability of compounds through porins. Based on the single channel data and *in vitro* as well as *in vivo* data, we have devised a scoring function to predict a molecule permeability through a specific porin. This in turn depends on avaerge sizes of the molecule and the porin channel, and the electrostatic interactions between the molecule (charge and dipole) and porin (electrostatic potential and electric field).

6.2. Structure and Function of *V. cholerae* porins

The single channel studies under low salt conditions verify the trimeric states of OmpU and OmpT, which dissociate into monomers in high salt conditions. Since OmpF/C porins are trimeric even in high salt conditions, the trimers of OmpU and OmpT are relatively unstable, a finding that is confirmed further by Native-PAGE. Moreover, the two proteins were purified as monomers during purification through SEC. The crystal structures aid in explaining the observed difference in trimer stability. The OmpU structure shows that the L2 loop (~15 residues) latches from one monomer into a groove of the other as observed for OmpF/C porins (Figure 6.2). An interaction analysis with PISA (Krissinel and Hendrick, 2007) shows that OmpF has a more extensive network of salt bridges compared to OmpU, all mediated by loop L2 (Appendix Table 1). However, OmpU makes more hydrogen bonds with the neighbouring monomer compared to OmpF, making a qualitative explanation for the higher trimer stability of OmpF difficult. For OmpT, however, the difference with both OmpF and OmpU is pronounced. The short L2 loop doesn't mediate any electrostatic interactions with the adjacent monomer and the number of hydrogen bonds is low, compared with both OmpF and OmpU. The OmpT structure therefore provides a clear explanation for the low stability of the OmpT trimer in detergent solution.

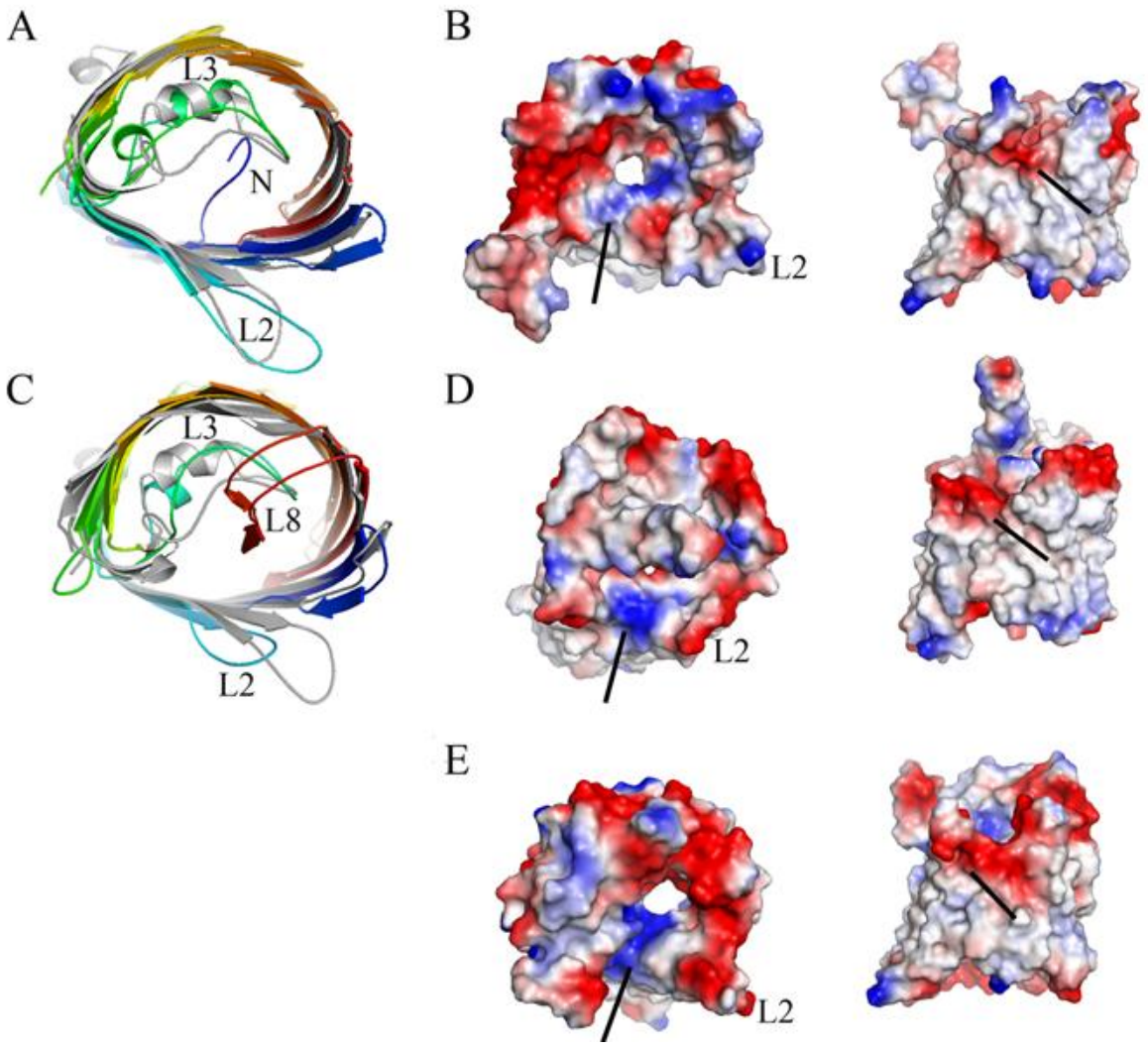

Figure 6.2. **Structural comparison of the L2 loop between OmpU, OmpT and OmpF.** The structural superpositions of rainbow colored cartoons of (A) OmpU and (C) OmpT with OmpF (in gray) show the differences in the lengths of loop L2. Electrostatic representations from the top and side views of OmpU, OmpT and OmpF are shown in B, D and E respectively. The L2-groove interface is indicated by the arrows, showing the positively charged groove (in top views) and negatively charged L2 loop (in side views). Surface potentials vary from -69.8 kT/e to 69.8 kT/e (for OmpU), -76.4 kT/e to 76.4 kT/e (for OmpT) and -63.5 kT/e to 63.5 kT/e (for OmpF).

The crystal structures of general porins like *E. coli* OmpF and OmpC display a classical hourglass shape formed by 16-stranded β-barrel in which the inward-folded L3 loop together with opposing barrel wall residues forms the constriction eyelet. Our structures reveal a similar porin architecture for *V. cholerae* OmpU and OmpT. However, a closer inspection of loop L3 for both OmpU and OmpT shows that its conformation is different from that in OmpF and OmpC. In OmpU and OmpT, the C-terminal part of L3 is located much closer to the barrel wall (Figure

6.2), and this would create a much larger pore without the additional constriction elements (i.e. in OmpUΔN and OmpTΔL8). Crucially, and contrasting with earlier predictions (Nikaido, 2003), L3 is one residue shorter in OmpU and OmpT compared to OmpF/C (Appendix Figures 2 and 3), and it is tempting to speculate that the 1-residue deletion is (partly) responsible for the different conformation of L3 in the barrel lumen, enlarging the channel. From an evolutionary perspective, the deletion may have facilitated subsequent insertion of the additional constriction elements (N-terminus in OmpU; L8 loop in OmpT) to generate channels with smaller pores. An intriguing question is why these structural features have evolved in at least some Vibrio porins. We speculate that the environmental conditions in which many Vibrio species are encountered (high osmolarity, low pH, presence of bile salts) might necessitate small pores for protection of the cell. This notion has precedence, since the expression of the smaller-pore OmpC from Enterobacteria is favoured under conditions of high osmolarity (Pratt et al., 1996).

Comparison of *V. cholerae* porins with OmpU/T orthologs of Vibrionaceae like the OmpL/H porins of Photobacterium profundum (Li et al., 2000) and OmpF/C of *E. coli* show a high conservation of several pore-lining charged residues (Appendix Figures 2 and 3). Strikingly, the N-terminal extension forming the additional constriction element in OmpU of *V. cholerae* is also present in *V. mimicus* but not in other OmpU proteins, raising the possibility that the other OmpU orthologs have different constriction elements that (like the one in *V. cholerae*) are not obvious from sequence alignment. The OmpT alignment, on the other hand, shows that the L8 constriction element is likely present in many other OmpT orthologs but not, for example, in *P. profundum* OmpH. Structural analysis of other OmpU/T porins from Vibrionaceae will be required to establish whether additional constriction elements as present in the *V. cholerae* channels are widespread.

In addition to decreasing the channel size, the additional constriction elements in OmpU and OmpT also affect the internal channel electrostatics. In the case of OmpU, the internal electric field is screened by the N-terminus linking two negative residues of the loop L3 and a positive residue from the basic ladder. In OmpT, the effect of the L8 loop on the channel electrostatics is dramatic. The charge segregation in the constriction region of OmpTΔL8 resembles that in previously studied general porins, but the L8 insertion neutralises it to the extent that the transversal component becomes smaller than the longitudinal one. This unusual

characteristic might make the OmpT channel suitable for the uptake of more hydrophobic compounds (e.g. deoxycholate) that do not readily permeate through general porins due to the strong transversal electric field (Im and Roux 2002a, Im and Roux 2002b).

The N-terminal extension of OmpU was previously implicated to be involved in adhesion during the intestinal colonization of *V. cholerae* (Sperandio et al., 1995), partly based on sequence similarities with a region in the adhesins HMW1 and HMW2 of Haemophilus influenzae. Another report claiming that the N-terminus of Vibrio mimicus OmpU is a motif required for bacterial adhesion (Liu et al., 2015) identified an immunogenic epitope with the sequence NQSGDKAGS (4 - 12 residues of the mature protein), which is identical to the corresponding sequence in *V. cholerae*. However, our structural data clearly shows that this sequence (residues 4 - 12 residues mature OmpU) is periplasmic and folded into the lumen of the channel. Thus, based on our findings, the N-terminus of OmpU in *V. cholerae* is very unlikely to be involved in adhesion.

6.3. Future Work

The structures of OmpF/C orthologs in *E. clocacae* and *K. pneumoniae* display identical protein folds but the presence of unusual constriction elements in the channels of *V. cholerae* porins poses an interesting question on the evolutionary aspect of Gram-negative bacterial porins. In comparsion to Enterobacterial porins, it will be interesting to know if the additional constriction elements are restricted to Vibrionaceae family by determining the structures of porins from other Vibrio species (and other genera of the family). To test if the conformation of L8 loop in OmpT is physiological, the experiments can be carried out by crosslinking loop L8 to the pore via making a double cysteine mutant and analyse the same through electrophysiology experiments.

As seen during single channel study, deoxycholate causes SSCs in the OmpT traces but not in OmpU. Although this implies that DOC either binds or blocks the OmpT pore but doesn't provide an information on its transport. Electrophysiology experiments like reverse potential can be used to analyse if DOC is uptaken by OmpT and not through OmpU. Docking experiments with DOC through molecuar simulation studies can also be used to determine its binding to the pore.

In single channel studies, the reversible blockages indicate that imipenem must have a common binding site within the CR (or inside the pore) of OmpU (or OmpT) and its deletion mutant OmpUΔN (or OmpTΔL8). The cocrystal structures of imipenem with these porin channels using X-ray crystallography may reveal the binding sites of the antibiotic in the pore. Alternatively, the construction of single mutants of the charged residues in the CR (of OmpU/T) and the subsequent analysis through electrophysiology can provide some input on imipenem binding residues of the porins. In addition, meropenem addition doesn't affect OmpU single-channel traces but shows high diffusion rate through OmpU in LSA. Does meropenem get translocated at a faster rate through OmpU than OmpT? Besides obtaining co-crystal structures, the effects of meropenem on OmpU can also be analysed by performing single-channel electrophysiology at low-temperatures (≤ 4°C), which will slow down the diffusion of the molecule and enable us to detect the interaction (if any).

Appendix Figure 1

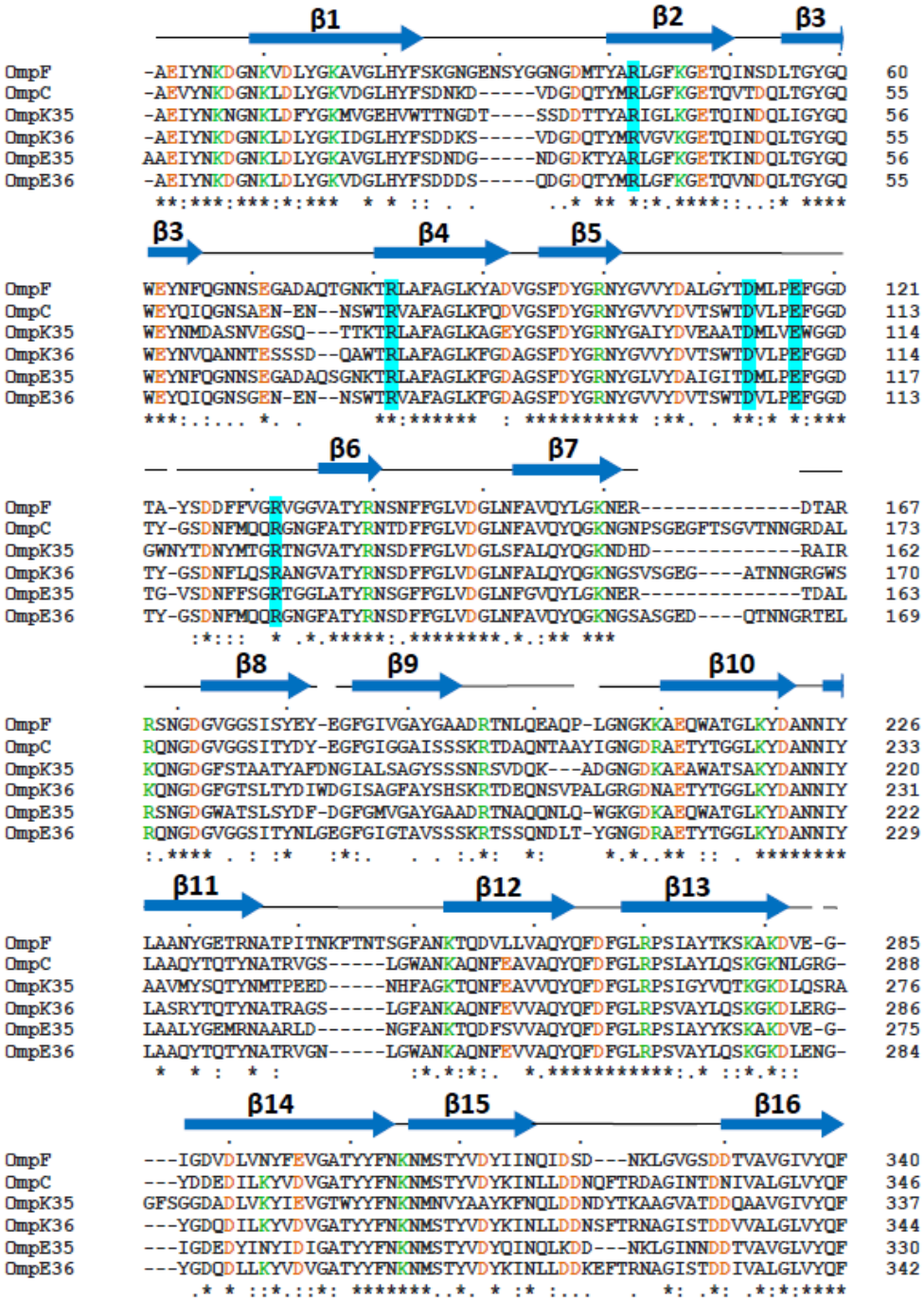

Appendix Figure 1. Sequence alignment of OmpF/C orthologs.
E. coli OmpF and OmpC protein sequences were aligned with the sequences of OmpE35/OmpE36 from *Enterobacter cloacae* and OmpK35/OmpK36 from *Klebsiella pneumoniae*. The charged residues in the CR are highlighted in cyan. Aligned positive and negative charged residues of the protein sequences are colored in orange and green respectively. Conservation symbols (* / . / :) were assigned by Clustal Omega (Sievers et al., 2011).

Appendix Figure 2

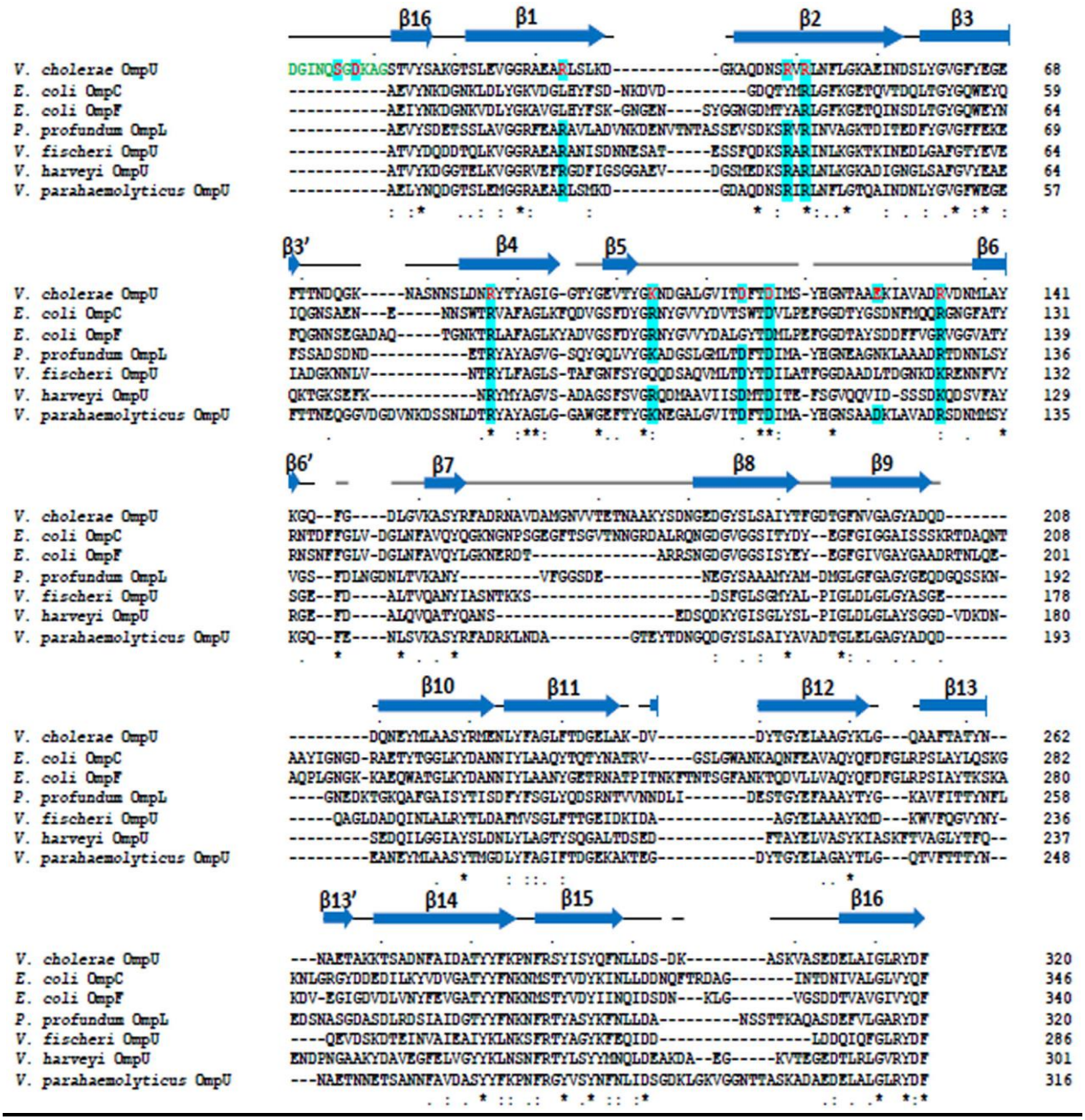

Appendix Figure 2. Sequence alignment of OmpU.
OmpU was aligned with the sequences of OmpF/C porins from E. coli and OmpU homologs in *Photobacterium profundum* (OmpL), *Vibrio fischeri* (OmpU), *Vibrio harveyi* (OmpU) and *Vibrio parahaemolyticus* (OmpU). The N-terminal constriction element of OmpU is shown in green. The amino acids in red are the pore-lining charged residues (except Ser6) of OmpU and equivalent identical residues are highlighted in cyan in the other sequences. Conservation symbols (* / . / :) were assigned by Clustal Omega (Sievers et al., 2011).

Appendix Figure 3

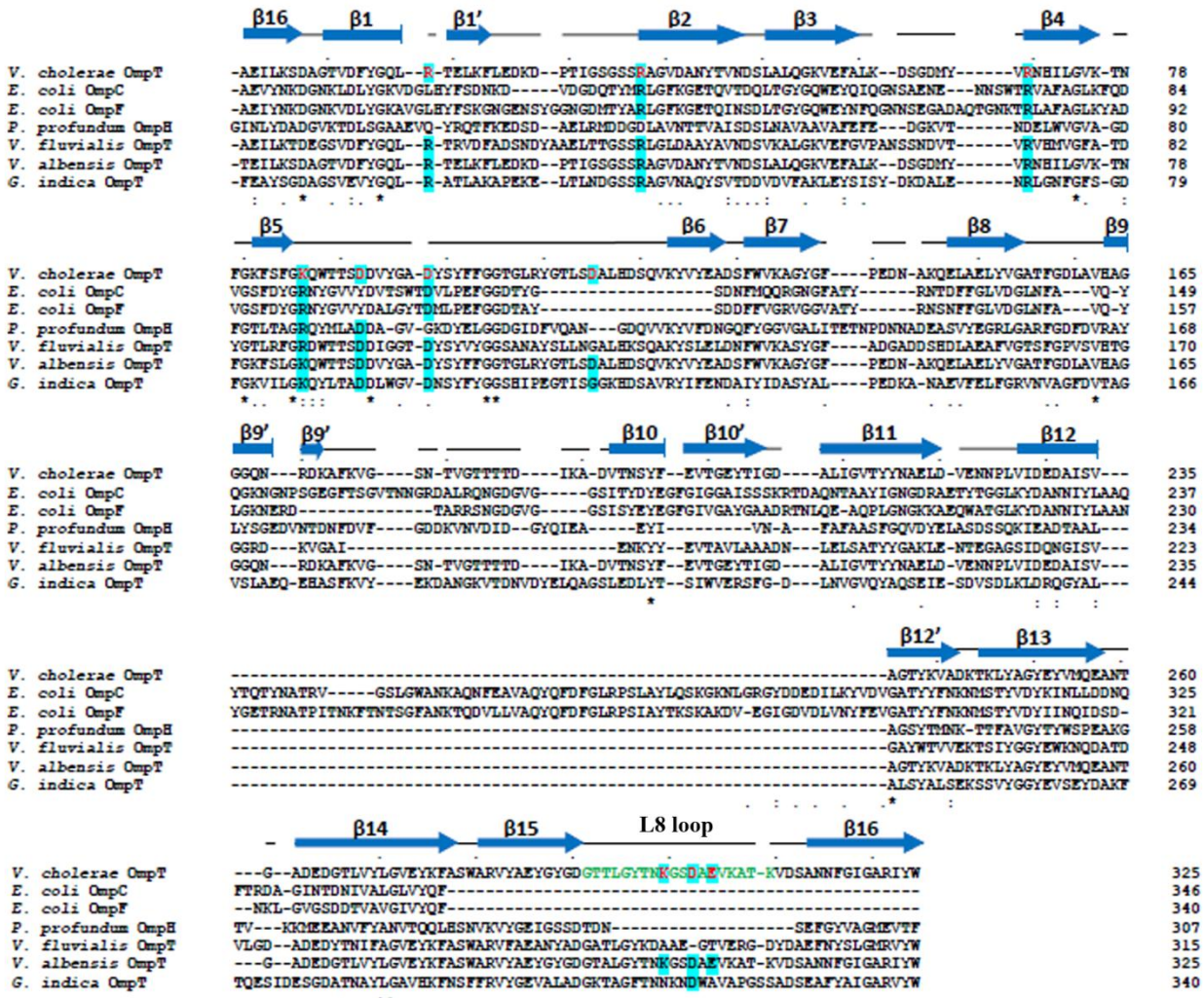

Appendix Figure 3. Sequence alignment of OmpT.
OmpT was aligned with the sequences of OmpF/C porins from *E. coli* and OmpT homologs from *Photobacterium profundum* (OmpH), *Vibrio fluvialis* (OmpU), *Vibrio albensis* (OmpU) and *Grimontia indica* (OmpU). The L8 constriction loop region of OmpT is shown in green. The amino acids in red are the pore-lining charged residues of OmpT and equivalent identical residues are highlighted in cyan in other sequences. Conservation symbols (* / . / :) were assigned by Clustal Omega (Sievers et al., 2011).

Appendix Figure 4

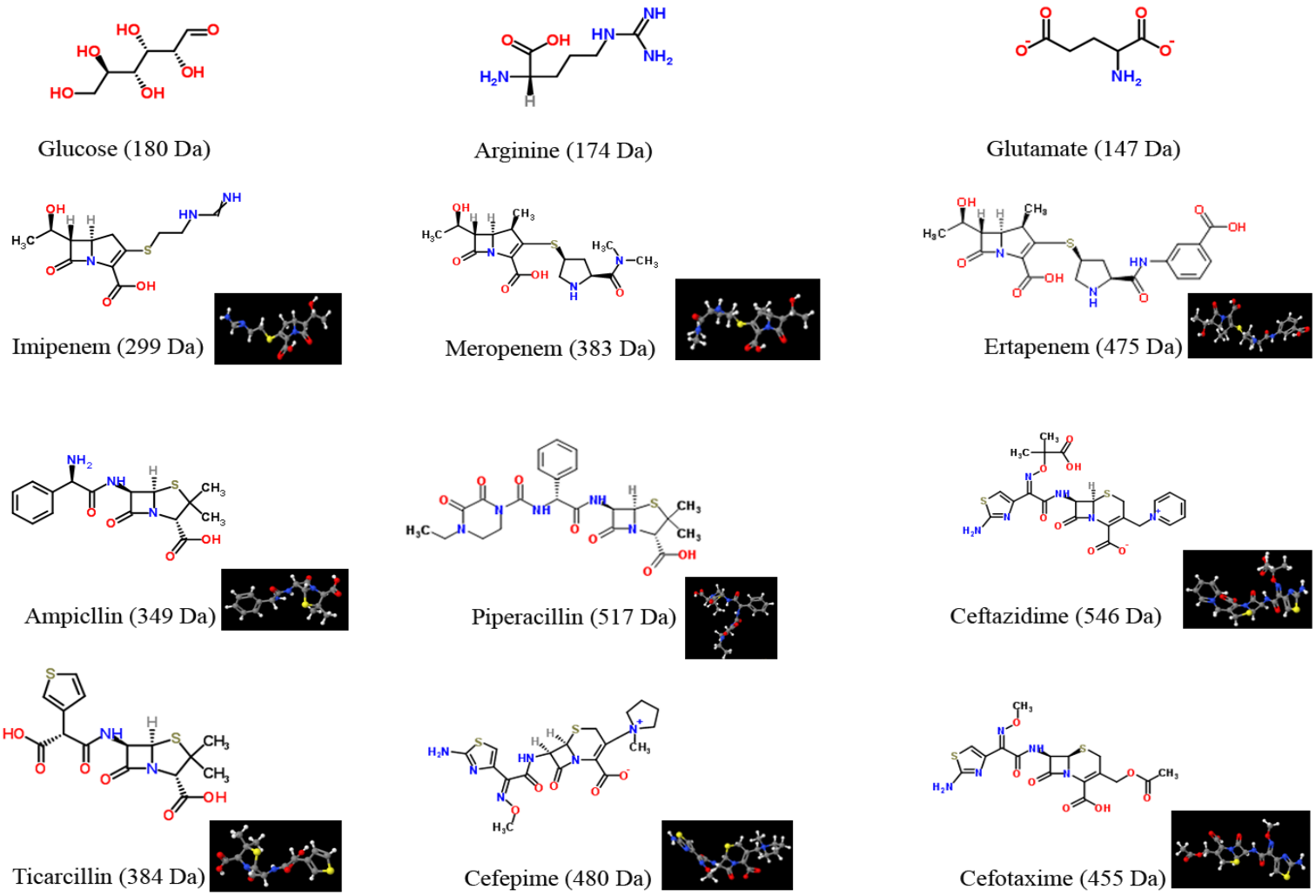

Appendix Figure 4. Chemical structures of the compounds used in this study.
The molecular weights of the compounds are listed in parentheses.

Appendix Figure 5

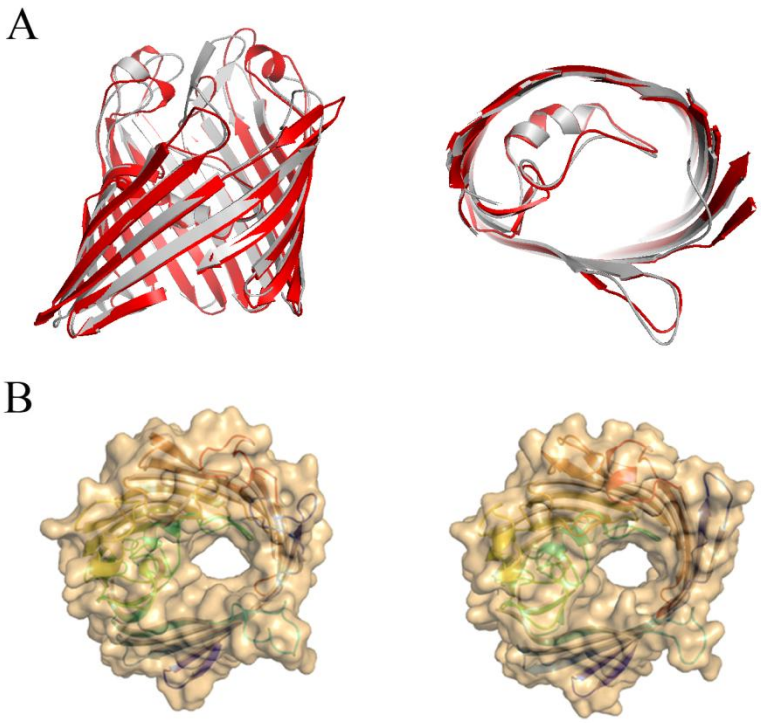

Appendix Figure 5. Structure of *K. pneumoniae* OmpK35.
(A) Extracellular side (left panel) and OM plane (right panel) views for the cartoon presentation of the superposition of OmpK35 (red) to *E. coli* OmpF (grey). (B) Surface presentation of OmpF (left panel) and OmpK35 (right panel) viewed from the top of the barrel.

Appendix Table 1

Protein-protein interface interactions in the trimers of OmpF, OmpT and OmpU. Interface interactions (by salt bridges and hydrogen-bonds) between the subunits of OmpF, OmpT and OmpU trimers, as analysed by PDBePISA (Krissinel and Henrick 2007). L2 loop residues and their interactions are indicated in bold for each protein.

Monomer 1	Distance (Å)	Monomer 2
Salt bridges (OmpF**)**		
Glu71 (OE1)	**2.98**	Arg132 (NH2)
Glu71 (OE1)	**3.84**	Arg132 (NE)
Glu71 (OE2)	**3.52**	Arg132 (NE)
Glu71 (OE2)	**2.80**	Arg132 (NH2)
Glu71 (OE2)	**3.38**	Arg132 (NH2)
Glu71 (OE2)	**2.80**	Arg132 (NE)
Asp74 (OD2)	**3.96**	Arg163 (NH1)
Hydrogen bonds (OmpF**)**		
His21 (ND1)	2.86	Tyr98 (OH)
Glu 71 (N)	**2.77**	Asp126 (OD2)
Gln76 (NE2)	**3.07**	**Asn79 (O)**
Gln76 (NE2)	**2.81**	Tyr63 (OH)
Asn304 (ND2)	2.90	Thr49 (OG1)
Tyr338 (OH)	2.65	Asn9 (OD1)
Leu20 (O)	3.87	Tyr98 (OH)
Asp37 (OD1)	2.85	Tyr98 (OH)
Asn68 (O)	**2.82**	Arg163 (NH1)
Asn69 (O)	**3.36**	Arg100 (NH1)
Glu71 (OE1)	**3.80**	Ser125 (OG)
Glu71 (OE1)	**2.98**	Arg132 (NH2)
Glu71 (OE1)	**2.80**	Arg100 (NH2)
Glu71 (OE1)	**2.80**	Arg132 (NE)
Asn306 (OD1)	3.88	Thr49 (OG1)
Met307 (SD)	3.72	Tyr58 (N)
Tyr338 (OH)	3.54	Glu48 (N)

Monomer 1	Distance (Å)	Monomer 2
Hydrogen bonds (OmpT**)**		
Asp28 (N)	3.00	Asp142 (OD1)
Ile31 (N)	3.16	Glu141 (OE1)
Met66 (N)	**3.13**	**Met66 (O)**
Ser36 (OG)	2.72	His71 (NE2)
Asp62 (O)	**2.97**	Lys86 (NZ)
Asp28 (OD2)	3.33	Asp142 (N)

Monomer 1	Distance (Å)	Monomer 2
Hydrogen bonds (OmpU**)**		
Asp73 (OD1)	**2.80**	Lys103 (NZ)
Asp73 (OD2)	**2.77**	Asp136 (N)
Gln74 (OE1)	**3.42**	Asn180 (ND2)
Gln74 (O)	**3.45**	Asn180 (ND2)
Gly75 (O)	**2.93**	Gln207 (NE2)
Asn77 (OD1)	**3.58**	Arg134 (NH1)
Asn77 (OD2)	**2.86**	Lys103 (NZ)
Ala78 (O)	**3.00**	Lys103 (NZ)
Asn80 (O)	**2.76**	Asn85 (N)
Ser82 (O)	**2.90**	Asn85 (ND2)
Tyr318 (OH)	3.11	Lys52 (N)
Lys35 (NZ)	3.48	Tyr177 (OH)
Thr71 (OG1)	**2.70**	Asp136 (OD2)
Asp73 (N)	**2.87**	Asp136 (OD2)
Gly75 (N)	**3.35**	Asp158 (OD2)
Asn77 (ND2)	**2.90**	Asp133 (OD2)
Asn80 (N)	**2.82**	Asp84 (OD1)
Asn81 (ND2)	**3.56**	**Asn81 (OD1)**
Asn81 (ND2)	**3.14**	**Asn81 (O)**
Asn286 (ND2)	3.40	Thr20 (OG1)
Tyr318 (OH)	3.68	Ser21 (O)

Monomer 1	Distance (Å)	Monomer 2
Salt bridges (OmpU**)**		
Asp73 **(OD1)**	**2.80**	Lys103 (NZ)
Asp73 **(OD2)**	**3.24**	Lys103 (NZ)
Hydrogen bonds (OmpU**)**		
Ser33 (OG)	3.04	Arg159 (NH1)
Ser33 (OG)	3.08	Arg159 (NH2)
Ser33 (O)	3.03	Arg159 (NH1)
Lys38 (O)	3.00	Arg159 (NH1)
Ala39 (O)	3.38	Asn137 (ND2)
Als39 (O)	2.82	Arg159 (N)
Asp41 (OD2)	2.86	Arg137 (N)
Thr70 (O)	**2.93**	Asn85 (ND2)

References

Acosta-Gutiérrez, S., Bodrenko, I., Scorciapino, M. A. and Ceccarelli, M. (2016) Macroscopic electric field inside water-filled biological nanopores. Phys. Chem. Chem. Phys. 18, 8855–8864.

Acosta-Gutierrez, S., Scorciapino, M.A., Bodrenko, I. and Ceccarelli, M. (2015) Filtering with Electric Field: The Case of *E. coli* Porins. J Phys Chem Lett. 6, 1807-12.

Adams, P.D. et al. (2010) PHENIX: a comprehensive Python-based system for macromolecular structure solution. Acta Cryst. D66, 213-221.

Aguilella, V.M., Queralt-Mart, M. and Alcaraz, A (2015) Bacterial porins in Electrophysiology of Unconventional Channels and Pores. Springer Series in Biophysics. Delcour, A. (ed) (Springer series in Biophysics) pp. 101-121.

Aguilella-Arzo, M., García-Celma, J.J., Cervera, J., Alcaraz, A. and Aguilella, V.M. (2007) Electrostatic properties and macroscopic electrodiffusion in OmpF porin and mutants. Bioelectrochemistry 70, 320–327.

Akama, H., Kanemaki, M., Yoshimura, M., Tsukihara, T., Kashiwagi, T., Yoneyama, H., Narita, S., Nakagawa, A., and Nakae, T. (2004). Crystal structure of the drug discharge outer membrane protein, OprM, of Pseudomonas aeruginosa: dual modes of membrane anchoring and occluded cavity end. J. Biol. Chem. 279, 52816–52819.

Albertí, S., Rodríquez-Quiñones, F., Schirmer, T., Rummel, G., Tomás, J.M., Rosenbusch, J.P. and Benedí, V.J. (1995) A porin from *Klebsiella pneumoniae*: sequence homology, three-dimensional model, and complement binding. Infect Immun. 63, 903-10.

Alcaraz, A., Nestorovich, E.M., López, M.L., García-Giménez, E., Bezrukov, S.M., Aguilella, V.M. (2009) Diffusion, exclusion, and specific binding in a large channel: a study of OmpF selectivity inversion. Biophys J. 96, 56-66.

Alexander, C., Rietschel. ET. (2001) Bacterial lipopolysaccharides and innate immunity. J. Endotoxin Res 7, 167–202.

Ali, M., Nelson, A.R., Lopez, A.L. and Sack, D.A. (2015) Updated global burden of cholera in endemic countries. PLoS Negl Trop Dis. 9, e0003832.

Altschul, S.F., Gish, W., Miller, W., Myers, E.W. and Lipman, D.J. (1990) Basic local alignment search tool. J Mol Biol. 215, 403-10.

Arunmanee, W., Pathania, M., Solovyova, A.S., Le Brun, A.P., Ridley, H., Baslé, A., van den Berg, B., Lakey J.H. (2016) Gram-negative trimeric porins have specific LPS binding sites that are essential for porin biogenesis. Proc Natl Acad Sci U S A. 113, E5034-43.

Bajaj, H., Acosta Gutierrez, S., Bodrenko, I., Malloci, G., Scorciapino, M.A., Winterhalter, M. and Ceccarelli, M. (2017) Bacterial Outer Membrane Porins as Electrostatic Nanosieves: Exploring Transport Rules of Small Polar Molecules. ACS Nano. 11, 5465-5473.

Bajaj, H., Scorciapino, M.A., Moynié, L., Page, M.G., Naismith, J.H., Ceccarelli, M. and Winterhalter, M. (2016) Molecular Basis of Filtering Carbapenems by Porins from β-Lactam-resistant Clinical Strains of *Escherichia coli*. J Biol Chem. 291, 2837-47.

Basle, A., Rummel, G., Storici, P., Rosenbusch, J.P., and Schirmer, T. (2006) Crystal Structure of Osmoporin OmpC from *E. coli* at 2.0 Å. J.Mol.Biol. 362, 933.

Batchelor, E., Walthers, D., Kenney, L.J. and Goulian, M. (2005) The *Escherichia coli* CpxA-CpxR envelope stress response system regulates expression of the porins ompF and ompC. J Bacteriol. 187(16), 5723-31.

Begic, S. and Worobec, E.A. (2006) Regulation of *Serratia marcescens* ompF and ompC porin genes in response to osmotic stress, salicylate, temperature and pH. Microbiology. 152, 485-91.

Beher, M.G., Schnaitman, C.A. and Pugsley, A.P. (1980) 'Major heat-modifiable outer membrane protein in gram-negative bacteria: comparison with the ompA protein of *Escherichia coli*', Journal of Bacteriology, 143, 906-913.

Benz, R., Schmid, A. and Hancock, R.E. (1985) Ion selectivity of gram-negative bacterial porins. J Bacteriol. 162, 722-7.

Beutler, B., and Rietschel, E.T. (2003) Innate immune sensing and its roots: the story of endotoxin. Nat Rev Immunol 3, 169-76.

Birch RG1, Pemberton JM, Basnayake WV. (1990) Stable albicidin resistance in *Escherichia coli* involves an altered outer-membrane nucleoside uptake system. J Gen Microbiol. 136, 51-8.

Blanvillain, S. et al. (2007) Plant carbohydrate scavenging through tonb-dependent receptors: a feature shared by phytopathogenic and aquatic bacteria. PLoS ONE 2, e224.

Bodrenko, I., Bajaj, H., Ruggerone, P., Winterhalter, M. and Ceccarelli, M. (2015) Analysis of fast channel blockage: revealing substrate binding in the microsecond range. Analyst. 140, 4820-7.

Bornet, C., Saint, N., Fetnaci, L., Dupont, M., Davin-Régli, A., Bollet, C. and Pagès, J.M. (2004) Omp35, a new *Enterobacter aerogenes* porin involved in selective susceptibility to cephalosporins. Antimicrob Agents Chemother. 48, 2153-8.

Bosch, D., Voorhout, W. and Tommassen, J. (1988) Export and Localization of N-terminally Truncated Derivatives of *Escherichia coli* K-12 Outer Membrane Protein PhoE*. Journal of Biological chemistry, 263, 9952-9957.

Bremer E ., Middendorf A. , Martinussen J. and Valentin-Hansen, P. (1990) Analysis of the tsx gene, which encodes a nucleoside-specific channel-forming protein (Tsx) in the outer membrane of *Escherichia coli*. Gene 96, 59-65.

Broennimann, Ch., Eikenberry, E.F., Henrich, B., Horisberger, R., Huelsen, G., Pohl, E., Schmitt, B., Schulze-Briese, C., Suzuki, M., Tomizaki, T., Toyokawa, H. and Wagner, A. (2006) The PILATUS 1M detector. J Synchrotron Radiat. 13, 120-30.

Brünger A.T. (1992) Free R value: a novel statistical quantity for assessing the accuracy of crystal structures. Nature. 355, 472-5.

Buchanan, S.K, Lukacik, P., Grizot, S., Ghirlando, R., Ali MM, et al. (2007) Structure of colicin I receptor bound to the R-domain of colicin Ia: implications for protein import. EMBO J. 26:2594–604.

Buchanan, S.K., Smith, B.S., Venkatramani, L, Xia, D., Esser, L., et al. (1999) Crystal structure of the outer membrane active transporter FepA from *Escherichia coli*. Nat Struct Biol. 6:56–63.

Bystritskaya, E., Stenkova, A., Chistuylin, D., Chernysheva, N., Khomenko, V., Anastyuk, S., Novikova, O., Rakin, A. and Isaeva, M. (2016) Adaptive responses of outer membrane porin balance of *Yersinia ruckeri* under different incubation temperature, osmolarity, and oxygen availability. Microbiologyopen. 5, 597-603.

Cai, S.J. and Inouye, M. (2002) EnvZ-OmpR interaction and osmoregulation in *Escherichia coli*. J Biol Chem. 277 (27), 24155-61.

Chakrabarti, S.R., Chaudhuri, K., Sen, K. and Das, J. (1996) Porins of *Vibrio cholerae*: purification and characterization of OmpU. J Bacteriol. 178, 524-30.

Chen et al. (2010) MolProbity: all-atom structure validation for macromolecular crystallography. Acta Crystallographica D66:12-21.

Cherezov, V., Yamashita, E., Liu, W., Zhalnina, M., Cramer, WA., and Caffrey, M. (2006) In meso structure of the cobalamin transporter, BtuB, at 1.95 A resolution. J Mol Biol. 364:716–34.

Childers, B.M., Klose, K.E. (2007) Regulation of virulence in Vibrio cholerae: the ToxR regulon. Future Microbiol. 2, 335-44.

Cowan, S. W., Schirmer, T., Rummel, G., Steiert, M., Ghosh, R., Pauptit, R. A., Jansonius, J. N. and Rosenbusch, J. P. (1992) Crystal structures explain functional properties of two *Escherichia coli* porins. Nature 358:727–733.

Crawford, J.A., Kaper, J.B. and DiRita, V.J. (1998) Analysis of ToxR-dependent transcription activation of ompU, the gene encoding a major envelope protein in *Vibrio cholerae*. Mol Microbiol. 29, 235-46.

Dalbey, R.E., Wang, P. and Kuhn, A. (2011) Assembly of bacterial inner membrane proteins. Annu Rev Biochem. 80, 161-87.

Danelon, C., Nestorovich, E.M., Winterhalter, M., Ceccarelli, M., and Bezrukov, SM. (2006) Interaction of zwitterionic penicillins with the OmpF channel facilitates their translocation. Biophys J. 90, 1617-27.

Danelon, C., Suenaga, A., Winterhalter, M. and Yamato, I., (2003) Molecular origin of the cation selectivity in OmpF porin: single channel conductances vs. free energy calculation. Biophys Chem. 104, 591-603.

Davin-Regli, A. and Pagès, J.M. (2015) *Enterobacter aerogenes* and *Enterobacter cloacae*; versatile bacterial pathogens confronting antibiotic treatment. Front Microbiol. 6, 392.

Delcour A.H. (2003) Solute uptake through general porins. Front Biosci. 8, 1055-71.

Delcour, A.H. (2002) Structure and function of pore-forming β-barrels from bacteria. Mol. Microbiol. Biotechnol. 4,1-10.

Delcour, A.H. (1997) Function and modulation of bacterial porins: insights from electrophysiology. FEMS Microbiol Lett. 151, 115-23.

Delcour, A.H. (2009) Outer membrane permeability and antibiotic resistance. Biochim Biophys Acta. 1794, 808-16.

Delihas, N. (1995). Regulation of gene expression by trans-encoded antisense RNAs. Mol. Microbiol. 15, 411–414.

Devanathan, S. and Postle, K. (2007) Studies on colicin B translocation: FepA is gated by TonB. Mol. Microbiol. 65, 441–453.

Domenech-Sanchez, A., Hernandez-Alles, S., Martinez-Martinez, L., Benedi, V.J. and Alberti, S. (1999) Identification and characterization of a new porin gene of *Klebsiella pneumoniae*: its role in beta-lactam antibiotic resistance. J Bacteriol.181, 2726–2732.

Doménech-Sánchez, A., Martínez-Martínez, L., Hernández-Allés, S., del Carmen Conejo, M., Pascual, A., Tomás, J.M., Albertí, S., Benedí, V.J. (2003) Role of *Klebsiella pneumoniae* OmpK35 porin in antimicrobial resistance. Antimicrob Agents Chemother. 47, 3332-5.

Dong, C., Beis, K., Nesper, J., Brunkan-Lamontagne, A.L., Clarke, B.R., Whitfield, C. and Naismith. J.H. (2006) Wza the translocon for *E. coli* capsular polysaccharides defines a new class of membrane protein. Nature. 444, 226-9.

Duret, G. and Delcour, A.H. (2006) Deoxycholic acid blocks *Vibrio cholerae* OmpT but not OmpU porin. J Biol Chem. 281, 19899-905.

Duret, G. and Delcour, A.H. (2010) Size and dynamics of the *Vibrio cholerae* porins OmpU and OmpT probed by polymer exclusion. Biophys J. 98(9), 1820-9.

Dutzler, R., Rummel, G., Alberti, S., Hernandez-Alles, S., Phale, P., Rosenbusch, J., Benedi, V., Schirmer, T. (1999) Crystal structure and functional characterization of OmpK36, the osmoporin of *Klebsiella pneumoniae*. Structure Fold.Des. 7: 425-434.

Emsley, P. and Cowtan, K. (2004) Coot: Model-building tools for molecular graphics. Acta Crystallogr D Biol Crystallogr 60(Pt 12 Pt 1), 2126–2132.

Eren E., Vijayaraghavan, J., Liu J., Cheneke B.R., Touw, D.S., Lepore, B.W., Indic, M., Movileanu, L. and Van den berg, B. (2012) Substrate specificity within a family of outer membrane carboxylate channels. PLoS Biol. 10, e1001242.

Evans, P.R. and Murshudov, G.N. (2013) How good are my data and what is the resolution? Acta Crystallogr D Biol Crystallogr. 69, 1204-14.

Federici, L., Du, D., Walas, F., Matsumura, H., Fernandez-Recio, J., McKeegan, K. S., Borges-Walmsley, M. I., Luisi, B. F., and Walmsley, A. R. (2005). The crystal structure of the outer membrane

protein VceC from the bacterial pathogen *Vibrio cholerae* at 1.8 A resolution. J. Biol. Chem. 280, 15307–15314.

Ferguson, A.D., Hofmann, E., Coulton, J.W., Diederichs, K. and Welte W (1998) Siderophoremediated iron transport: Crystal structure of FhuA with bound lipopolysaccharide. Science 282, 2215–2220.

Fiedler S., Broecker J. and Keller S. (2010) Protein folding in membranes, Cell Mol Life Sci. 67, 1779-98.

Fiedler, G., Pajatsch, M., and Boeck, A. (1996) Genetics of a novel starch utilisation pathway present in *Klebsiella oxytoca*. J. Mol. Biol. 256, 279–291.

Forst, D., Welte, W., Wacker, T., Diederichs, K. (1998) Structure of the sucrose-specific porin ScrY from *Salmonella typhimurium* and its complex with sucrose. Nat.Struct.Biol. 5: 37-46.

Galdiero, S., Falanga, A., Cantisani, M., Tarallo, R., Della Pepa, M.E., D'Oriano, V. and Galdiero, M. (2012) Microbe-host interactions: structure and role of Gram-negative bacterial porins. Curr Protein Pept Sci. 13, 843-54.

Gao, H., Zhang, Y., Han, Y., Yang, L., Liu, X., Guo, Z., et al. (2011) Phenotypic and transcriptional analysis of the osmotic regulator OmpR in *Yersinia pestis*. BMC Microbiol. 11, 39.

Garavito, R.M. and Ferguson-Miller, S. (2001) Detergents as tools in membrane biochemistryJ Biol Chem. 2001 Aug 31;276(35), 32403-6.

Gorrec, F. (2015) The MORPHEUS II protein crystallization screen. Acta Crystallogr F Struct Biol Commun. 71, 831-7.

Gu, W., Wang, X., Qiu, H., Luo, X., Xiao, D., Xiao, Y., et al. (2012) Comparative antigenic proteins and proteomics of pathogenic *Yersinia enterocolitica* bio-serotypes 1B/O:8 and 2/O:9 cultured at 25°C and 37°C. Microbiol. Immunol. 56, 583–594.

Gumbart, J., Wiener, M.C., and Tajkhorshid, E. (2007) Mechanics of force propagation in TonB-dependent outer membrane transport. Biophys J. 93, 496-504.

Guzman, L.M., Belin, D., Carson, M.J. and Beckwith, J. (1995) Tight Regulation, Modulation, and High-Level Expression by Vectors Containing the Arabinose PBAD Promoter. Journal of Bacteriology, 4121-4130.

Hajjar, E., Mahendran, K.R., Kumar, A., Bessonov, A., Petrescu, M., Weingart, H., Ruggerone, P., Winterhalter, M. and Ceccarell, M. (2010) Bridging timescales and length scales: from macroscopic flux to the molecular mechanism of antibiotic diffusion through porins. Biophys J. 98, 569-75.

Hanahan, D. (1983) Studies on transformation of *Escherichia coli* with plasmids. Journal of Molecular Biology, 166: 557-580.

Hantke K. (1976) Phage T6--colicin K receptor and nucleoside transport in *Escherichia coli*. 70, 109-12.

Hayat, S. and Elofsson, A. (2012) BOCTOPUS: improved topology prediction of transmembrane β barrel proteins. Bioinformatics. 28, 516-22.

Hearn, E.M., Patel, D.R., Lepore, B.W., Indic, M. and Van den Berg, B., (2009) Transmembrane passage of hydrophobic compounds through a protein channel wall. Nature 458, 367–370.

Hendrickson, W.A. (2014) Anomalous diffraction in crystallographic phase evaluation. Q Rev Biophys. 47, 49-93.

Herath, T.D., Darveau, R.P., Seneviratne, C.J., Wang. C.Y., Wang, Y., and Jin, L., (2013) Tetra- and Penta-Acylated Lipid A Structures of Porphyromonas gingivalis LPS Differentially Activate TLR4-Mediated NF-κB Signal Transduction Cascade and Immuno-Inflammatory Response in Human Gingival Fibroblasts, PLoS One. 8, e58496.

Hille, B. (2001) Ion Channels of Excitable Membranes, 3rd ed. Sinauer, Sunderland, MA.

Hodgkin, A. L. and Katz, B. (1949) The effect of sodium ions on the electrical activity of the giant axon of the squid. J Physiol, 108, 37–77.

Holm, L. and Laakso L. M. (2016) Dali server update. Nucleic acids research 44 (W1), W351-W355.

Joseph, J. and Rodvold, K.A. (2008) The role of carbapenems in the treatment of severe nosocomial respiratory tract infections. Expert Opin Pharmacother, 9, 561-75.

Kamio, Y., and Nikaido H. (1976) Outer membrane of *Salmonella* typhimurium: accessibility of phospholipid head groups to phospholipase c and cyanogen bromide activated dextran in the external medium. Biochemistry 15, 2561-70.

Kanehisa, M. and Goto, S. (2000) KEGG: kyoto encyclopedia of genes and genomes. Nucleic Acids Res. 28, 27-30.

Karshikoff, A., Spassov, V., Cowan, S.W., Ladenstein, R. and Schirmer, T. (1994) Electrostatic properties of two porin channels from *Escherichia coli*. J Mol Biol. 240, 372-84.

Keegan, R.M. and Winn, M.D. (2007) Mr BUMP: Automated search-model discovery and preparation for structure solution by molecular replacement Acta Cryst. D63, 447 – 457.

Khan, J., Gupta, S., Chattopadhyay, K. and Mukhopadhaya and Refolding, A. (2012) Functional Assembly of the *Vibrio cholerae* Porin OmpU Recombinantly Expressed in the Cytoplasm of Escherichia Coli. Protein Expr Purif 85, 204-210.

Kibbe, W.A. (2007) OligoCalc: an online oligonucleotide properties calculator. Nucleic Acids Res. 35(Web Server issue):W43-6.

Kitaoka, M., Miyata, S.T., Unterweger, D. and Pukatzki, S. (2011) Antibiotic resistance mechanisms of *Vibrio cholerae*. J Med Microbiol. 60, 397-407.

Klebba, P.E. and Newton, S.M. (1998) Mechanisms of solute transport through outer membrane porins: burning down the house. Curr Opin Microbiol. 1, 238-47.

Koebnik, R., Locher, K.P. and Van Gelder, P. (2000) Structure and function of bacterial outer membrane proteins: barrels in a nutshell. Mol Microbiol. 37, 239-53.

Koronakis, V., Sharff, A., Koronakis, E., Luisi, B., and Hughes, C. (2000). Crystal structure of the bacterial membrane protein TolC central to multidrug efflux and protein export. Nature 405, 914–919.

Kovacs-Simon, A., Titball, R. W., and Michell, S. L. (2011) Lipoproteins of Bacterial Pathogens Infect Immun. 79, 548–561.

Lee, E.H., Collatz, E., Trias, J. and Gutmann, L. (1992) Diffusion of beta-lactam antibiotics into proteoliposomes reconstituted with outer membranes of isogenic imipenem-susceptible and -resistant strains of *Enterobacter cloacae*. J Gen Microbiol. 138, 2347-51.

Lee, Y., Choi, H., Yum, J.H., Kang, G., Bae, I.K., Jeong, S.H. and Lee, K. (2012) Molecular mechanisms of carbapenem resistance in *Enterobacter cloacae* clinical isolates from Korea and clinical outcome. Ann Clin Lab Sci. 42, 281-6.

Lepore, B.W., Indic, M., Pham, H., Hearn, E.M., Patel, D.R., van den Berg, B. (2011) From the Cover: Ligand-gated diffusion across the bacterial outer membrane. Proc.Natl.Acad.Sci.USA 108: 10121-10126.

Lerouge, I. and Vanderleyden, J. (2002) O-antigen structural variation: mechanisms and possible roles in animal/plant–microbe interactions. FEMS Microbiology Reviews, 26: 17–47.

Leslie, A.G. (2006) The integration of macromolecular diffraction data. Acta Crystallogr D Biol Crystallogr. 62, 48-57.

Li, C.C., Crawford, J.A., DiRita, V.J. and Kaper, J.B. (2000) Molecular cloning and transcriptional regulation of ompT, a ToxR-repressed gene in *Vibrio cholerae*. Mol Microbiol. 35, 189-203.

Li, C.C., Merrell, D.S., Camilli, A. and Kaper, J.B (2002) ToxR interferes with CRP-dependent transcriptional activation of ompT in *Vibrio cholerae*. Mol Microbiol.;43(6), 1577-89.

Liu, X. and Ferenci T. (2001) An analysis of multifactorial influences on the transcriptional control of ompF and ompC porin expression under nutrient limitation. *Microbiology*, 147, 2981–2989.

Locher, K.P., Rees, B., Koebnik, R., Mitschler, A., Moulinier, L., et al. (1998) Transmembrane signaling across the ligand-gated FhuA receptor: crystal structures of free and ferrichrome-bound states reveal allosteric changes. *Cell.* 95:771–8.

Long, F., Vagin, A.A., Young, P. And Murshudov, G.N. (2008) BALBES: a molecular-replacement pipeline. Acta Crystallogr D Biol Crystallogr. 64 (Pt 1), 125-32.

Loppnow, H., Brade, H., Dürrbaum, I., Dinarello, C.A., Kusumoto, S., Rietschel, E.T., Flad, H.D. (1989) IL-1 induction-capacity of defined lipopolysaccharide partial structures. *J Immunol.* 142, 3229-38.

Ma, L. et al. (2007) Evidence of ball-and-chain transport of ferric enterobactin through FepA. *J. Biol. Chem.* 282, 397–406.

Magalhães, P.O., Lopes A.M., Mazzola P.G., Rangel-Yagui C., Penna T.C., Pessoa A.Jr. (2007) Methods of endotoxin removal from biological preparations: *a review. J Pharm Pharm Sci.* 10, 388-404.

Mahendran, K.R., Hajjar, E., Mach, T., Lovelle, M., Kumar, A., Sousa, I., Spiga, E., Weingart, H., Gameiro, P., Winterhalter, M. and Ceccarelli, M. (2010) Molecular basis of enrofloxacin translocation through OmpF, an outer membrane channel of *Escherichia coli*--when binding does not imply translocation. J Phys Chem B. 114, 5170-9.

Mahendran, K.R., Kreir, M., Weingart, H., Fertig, N. and Winterhalter, M. (2010) Permeation of antibiotics through *Escherichia coli* OmpF and OmpC porins: screening for influx on a single-molecule level. J Biomol Screen. 15, 302-7.

Manning P.A., Reeves, P. (1976) Outer membrane of *Escherichia coli* K-12: Tsx mutants (resistant to bacteriophage T6 and colicin K) lack an outer membrane protein. 71, 466-471.

Mathur, J. and Waldor, M.K. (2004) The *Vibrio cholerae* ToxR-regulated porin OmpU confers resistance to antimicrobial peptides. Infect Immun. 72, 3577-83.

Matsubara, M., Kitaoka, S.I., Takeda, S.I. and Mizuno, T. (2000) Tuning of the porin expression under anaerobic growth conditions by His-to-Asp cross-phosphorelay through both the EnvZ-osmosensor and ArcB-anaerosensor in *Escherichia coli*. Genes Cells. 5, 555-69.

McCoy, A.J., Grosse-Kunstleve, R.W., Adams, P.D., Winn, M.D., Storoni, L.C. and Read, R.J. (2007) Phaser crystallographic software. J. Appl. Cryst. 40, 658-674.

McCoy, A.J., Grosse-Kunstleve, R.W., Adams, P.D., Winn, M.D., Storoni, L.C. and Read, R.J. (2007) Phaser crystallographic software, *J. Appl. Cryst.* 40**,** 658-674.

Mecsas, J., Welch, R., Erickson, J.W., and Gross, C.A.J. (1995) Identification and characterization of an outer membrane protein, OmpX, in *Escherichia coli* that is homologous to a family of outer membrane proteins including Ail of *Yersinia enterocolitica*. Bacteriol, 177, 799–804.

Merrell, D.S., Bailey, C., Kaper, J.B. and Camilli, A. (2001) The ToxR-mediated organic acid tolerance response of *Vibrio cholerae* requires OmpU. J Bacteriol. 183, 2746-54.

Miller, V. L., Taylor, R. K. and Mekalanos, J. J. (1987) Cholera toxin transcriptional activator ToxR is a transmembrane DNA binding protein. Cell 48, 271–279.

Miller, V.L. and Mekalanos, J.J. (1988) A novel suicide vector and its use in construction of insertion mutations: osmoregulation of outer membrane proteins and virulence determinants in *Vibrio cholerae* requires toxR. J Bacteriol. 170, 2575-83.

Mittal, R., Krishnan, S., Gonzalez-Gomez, I., Prasadarao, N.V. (2011) Deciphering the roles of outer membrane protein A extracellular loops in the pathogenesis of *Escherichia coli* K1 meningitis. *J Biol Chem.* 286, 2183–2193.

Mizuno, T. (1998) His-Asp Phosphotransfer Signal Transduction. J. Biochem. 123, 555-56.

Mizuno, T. and Tanaka, I. (1997) Structure of the DNA-binding domain of the OmpR family of response regulators. Mol. Microbiol. 24, 665–667.

Montminy, S.W., Khan, N., McGrath, S., Walkowicz, M.J., Sharp, F., Conlon, J.E., et al. (2006) Virulence factors of *Yersinia pestis* are overcome by a strong lipopolysaccharide response. Nat Immunol 7, 1066-1073.

Moraes, T.F., Bains, M., Hancock, R.E. and Strynadka, N.C. (2007) An arginine ladder in OprP mediates phosphate specific transfer across the outer membrane. Nat Struct Mol Biol 14 85-87.

Morona, R., Klose, M., Henning, U., (1984) *Escherichia coli* K-12 outer membrane protein (OmpA) as a bacteriophage receptor: analysis of mutant genes expressing altered proteins. *J Bacteriol*.159:570–578.

Mullis, K., Faloona, F., Scharf, S., Saiki, R., Horn, G. and Erlich, H. (1986) 'Specific enzymatic amplification of DNA in vitro: the polymerase chain reaction', Cold Spring Harb Symp Quant Biol, 51, 263-73.

Nakasone, N. and Iwanaga, M. (1998) Characterization of outer membrane protein OmpU of *Vibrio cholerae* O1. Infect Immun. 66, 4726-8.

Nandi, B., Nandy, R.K., Sarkar, A. and Ghose, A.C. (2005) Structural features, properties and regulation of the outer-membrane protein W (OmpW) of *Vibrio cholerae*. Microbiology. 151, 2975-86.

Nestorovich EM, Rostovtseva TK, Bezrukov SM (2003) Residue ionization and ion transport through OmpF channels. Biophys J 85, 3718–3729.

Neugebauer, H. et al. (2005) ExbBD-dependent transport of maltodextrins through the novel MalA protein across the outer membrane of *Caulobacter crescentus*. *J. Bacteriol*. 187, 8300–8311.

Newstead S., Ferrandon S. and Iwata S. (2008) Rationalizing alpha-helical membrane protein crystallization. Protein Sci. 17(3):466-72.

Nikaido H, Vaara M. (1985) Molecular basis of bacterial outer membrane permeability. Microbiol Rev. 49, 1-32.

Nikaido H. (2011) Structure and mechanism of RND-type multidrug efflux pumps. Adv Enzymol Relat Areas Mol Biol. 77, 1-60.

Nikaido, H. (2003) Molecular basis of Outer Membrane Permeability Revisited. Microbiol Mol Biol Rev. 67, 593-656.

Nikaido, H., and Rosenberg, E. Y. (1981) Effect on solute size on diffusion rates through the transmembrane pores of the outer membrane of *Escherichia coli*. J. Gen. Physiol. 77, 121–135.

Nikaido, H., and Rosenberg, E. Y. (1983) Porin channels in *Escherichia coli*: studies with liposomes reconstituted from purified proteins. J. Bacteriol. 153, 241–252.

Noinaj N., Guillier, M., Barnard, T.J., Buchanan, S.K. (2010) TonB-dependent transporters: regulation, structure, and function. *Annu Rev Microbiol*. 64, 43-60.

Lüderitz, O., Tanamoto, K., Galanos, C., McKenzie, G. R., Brade, H., Zähringer, U., Rietschel E.T., Kusumoto, S. and Shiba, T. (1984) Lipopolysaccharides: Structural Principles and Biologic Activities, *Reviews of Infectious Diseases*,6, 428–431.

Ottemann, K. M., V. J. DiRita and Mekalanos, J. J. (1992) ToxR proteins with substitutions in residues conserved with OmpR fail to activate transcription from the cholera toxin promoter. J. Bacteriol. 174, 6807–6814.

Pagès, J.M., James, C.E. and Winterhalter, M. (2008) The porin and the permeating antibiotic: a selective diffusion barrier in Gram-negative bacteria. Nat Rev Microbiol.6, 893-903.

Pape, T. and Schneider, T.R. (2004) HKL2MAP: a graphical user interface for phasing with SHELX programs. J. Appl. Cryst. 37:843-844.

Parker, J.L. and Newstead, S. (2012) Current trends in α-helical membrane protein crystallization: an update. Protein Sci.2, 1358-65.

Paterson, D.L. and Bonomo, R.A. (2005) Extended-spectrum beta-lactamases: a clinical update. Clin Microbiol Rev. 18, 657-86.

Pathania, M., Acosta-Gutierrez, S., Baslé, A., Ceccarelli, M., van den Berg, B. (2017) Unusual constriction zones in the major porins OmpU and OmpT from *Vibrio cholera*. submitted to Structure (*under press*).

Pautsch, A., Schulz, G.E. (1998) Structure of the outer membrane protein A transmembrane domain. *Nat.Struct. Biol.* 5: 1013-1017.

Pawelek, P.D., Croteau, N., Ng-Thow-Hing, C., Khursigara, C.M., Moiseeva, N., Allaire, M. and Coulton, J.W. (2006) Structure of TonB in complex with FhuA, *E. coli* outer membrane receptor. *Science* 312, 1399–1402.

Peterson, K.M. and Mekalanos, J. J. (1988) Characterisation of the *Vibrio cholerae* ToxR regulon: identification of novel genes involved in intestinal colonization. Infect Immun. 1988 Nov; 56(11), 2822–2829.

Phale, P.S., Philippsen, A., Kiefhaber, T., Koebnik. R., Phale, V.P., Schirmer, T. and Rosenbusch, J.P. (1998) Stability of trimeric OmpF porin: the contributions of the latching loop L2. Biochemistry. 37, 15663-70.

Pratt, L.A., Hsing, W., Gibson, K.E. and Silhavy, T.J. (1996) From acids to osmZ: multiple factors influence synthesis of the OmpF and OmpC porins in *Escherichia coli*. Mol Microbiol. 20, 911-7.

Prilipov, A., Phale, P.S., Van Gelder, P., Rosenbusch, J.P. and Koebnik, R. (1998) Coupling site-directed mutagenesis with high-level expression: large scale production of mutant porins from *E. coli*. FEMS Microbiol Lett. 163, 65-72.

Provenzano, D. and Klose, K.E. (2000) Altered expression of the ToxR-regulated porins OmpU and OmpT diminishes *Vibrio cholerae* bile resistance, virulence factor expression, and intestinal colonization. Proc Natl Acad Sci U S A. 97, 10220-4.

Provenzano, D., Schuhmacher, D.A., Barker, J.L. and Klose K.E. (2000) The virulence regulatory protein ToxR mediates enhanced bile resistance in *Vibrio cholerae* and other pathogenic Vibrio species. Infect Immun. 68, 1491-7.

Raetz, C.R.H. and Whitfield, C. (2002) Lipopolysaccharide endotoxins. Annu. Rev. Biochem. 71, 635-700.

Raimondi, A., Traverso, A. and Nikaido, H. (1991) Imipenem- and meropenem-resistant mutants of *Enterobacter cloacae* and *Proteus rettgeri* lack porins. Antimicrob Agents Chemother. 35, 1174-80.

Rasmussen, B.A. and Silhavy, T.J. The first 28 amino acids of mature LamB are required for rapid and efficient export from the cytoplasm. Genes & Dev. 1987. 1, 185-196

Reeves, A.R., D'Elia, J.N., Frias, J. and Salyers, A.A. (1996) A Bacteroides thetaiotaomicron outer membrane protein that is essential for utilization of maltooligosaccharides and starch. J Bacteriol. 178, 823-30.

Rice, L.B. (2009) Federal funding for the study of antimicrobial resistance in nosocomial pathogens: no ESKAPE, J Infect Dis, vol. 197, 1079-81.

Richter, M.F., Drown, B.S., Riley, A.P., Garcia, A., Shirai, T., Svec, R.L. and Hergenrother, P.J. (2017) Predictive compound accumulation rules yield a broad-spectrum antibiotic. Nature. 545, 299-304.

Rietschel, E.T., and Brade H. (1992) Bacterial endotoxins. Sci Am. 267, 54-61.

Robert, V., Volokhina, E.B., Senf, F., Bos, M.P., Van Gelder, P. and Tommassen, J. (2006) Assembly factor Omp85 recognizes its outer membrane protein substrates by a species-specific C-terminal motif. PLoS Biol. 4, e377.

Rollauer, S.E., Sooreshjani, M.A., Noinaj, N. and Buchanan, S.K. (2015) Outer membrane protein biogenesis in Gram-negative bacteria. Philos Trans R Soc Lond B Biol Sci. 370.

Rosenfeld, Y. and Shai, Y. (2006) Lipopolysaccharide (Endotoxin)-host defense antibacterial peptides interactions: Role in bacterial resistance and prevention of sepsis. Biochim Biophys Acta. 1758, 1513-22.

Rostovtseva, T.K., Nestorovich, E.M. and Bezrukov, S.M. (2002) Partitioning of differently sized poly(ethylene glycol)s into OmpF porin. Biophys J. 82,160-9.

Schauer, K., Gouget, B., Carrière, M., Labigne, A., de Reuse, H. (2007) Novel nickel transport mechanism across the bacterial outer membrane energized by the TonB/ExbB/ExbD machinery. Mol Microbiol. 63, 1054-68.

Schauer, K., Rodionov, D.A. and de Reuse, H. (2008) New substrates for TonB-dependent transport: do we only see the 'tip of the iceberg'? Trends Biochem Sci. 33:330–8.

Schirmer, T., Keller, T.A., Wang, Y.F., Rosenbusch, J.P. (1995) Structural basis for sugar translocation through maltoporin channels at 3.1 Å resolution. Science 267, 512-514.

Schrödinger (2010) The PyMOL Molecular Graphics System, Version 1.3r1. www.pymol.org.

Schulz, G.E. (2002) The structure of bacterial outer membrane proteins. Biochimica et Biophysica Acta 1565, 308-317.

Sheldrick, G.M. (2010) Experimental phasing with SHELXC/D/E: combining chain tracing with density modification. Acta Crystallogr D Biol Crystallogr. 66, 479-85.

Shin, S.Y., Bae, I.K., Kim, J., Jeong, S.H., Yong, D., Kim, J.M. and Lee, K. (2012) Resistance to carbapenems in sequence type 11 *Klebsiella pneumoniae* is related to DHA-1 and loss of OmpK35 and/or OmpK36. J Med Microbiol. 61, 239-45.

Shultis, D.D., Purdy, M.D., Banchs, C.N. and Wiener, M.C. (2006) Outer membrane active transport: structure of the BtuB:TonB complex. Science 312, 1396–1399.

Sievers, F., Wilm, A., Dineen, D., Gibson, T.J., Karplus, K., Li, W., Lopez, R., McWilliam, H., Remmert, M., Söding, J., Thompson, J.D. and Higgins, D.G. (2011) Fast, scalable generation of high-quality protein multiple sequence alignments using Clustal Omega. Mol Syst Biol. 7, 539.

Simonet, V.C., Baslé, A., Klose, K.E. and Delcour, A.H. (2003) The *Vibrio cholerae* porins OmpU and OmpT have distinct channel properties. J Biol Chem. 278, 17539-45.

Smart, O.S., Goodfellow, J.M. and Wallace, B.A. (1993) The Pore Dimensions of Gramicidin Biophysical Journal. 65, 2455-2460.

Snijder, H.J., Ubarretxena-Belandia, I., Blaauw, M., Kalk, K.H., Verheij, H.M., Egmond, M.R., Dekker, N., Dijkstra, B.W. (1999) Structural evidence for dimerization-regulated activation of an integral membrane phospholipase. Nature 401: 717-721.

Sperandio, V., Girón, J.A., Silveira, W.D. and Kaper, J.B. (1995) The OmpU outer membrane protein, a potential adherence factor of *Vibrio cholerae*. Infect Immun. 63, 4433-8.

Stavenger, R.A. and Winterhalter, M. (2014) TRANSLOCATION project: how to get good drugs into bad bugs. Sci Transl Med. 6, 228ed7.

Stevenson, G., Neal, B., Liu, D., Hobbs, M., Packer, N.H., Batley, M., Redmond, J.W., Lindquist, L., Reeves, P. (1994) Structure of the O antigen of *Escherichia coli* K-12 and the sequence of its rfb gene cluster, J. Bacteriol. 176, 4144–4156.

Stierand, K. and Rarey, M. (2010) Drawing the PDB: Protein-ligand complexes in two dimensions. ACS Med Chem Lett 1(9), 540–545.

Strong, M., Sawaya, M.R., Wang, S., Phillips, M., Cascio, D. and Eisenberg, D. (2006) Toward the structural genomics of complexes: Crystal structure of a PE/PPE protein complex from *Mycobacterium tuberculosis*. Proc Natl Acad Sci USA. 103, 8060-8-65.

Sugawara, E., Kojima, S. and Nikaido, H. (2016) *Klebsiella pneumoniae* major Porins OmpK35 and OmpK36 Allow More Efficient Diffusion of β-Lactams than Their Escherichia coli Homologs OmpF and OmpC. J Bacteriol. 198, 3200-3208.

Teng, T.-Y. (1990).Mounting of crystals for macromolecular crystallography in a free-standing thin film. J. Appl. Cryst. 23, 387–391.

Terwilliger, T.C., Adams, P.D., Read, R.J., McCoy, A.J., Moriarty, N.W., Grosse-Kunstleve, R.W., Afonine, P.V., Zwart, P.H. and Hung, L.W. (2009) Decision-making in structure solution using Bayesian estimates of map quality: the PHENIX AutoSol wizard. Acta Crystallogr D Biol Crystallogr 65, 582-601.

Thomas, A.D. and Booth, I.R. (1992) The regulation of expression of the porin gene ompC by acid pH. Journal of General Microbiology, 138, 1829-1835.

Thorn, A. and Sheldrick, G.M. (2013) Extending molecular-replacement solutions with SHELXE. Acta Crystallogr D Biol Crystallogr. 69, 2251-6.

Tommassen, J. (2010) Assembly of outer-membrane proteins in bacteria and mitochondria. Microbiology, 156, 2587–2596.

Tsai, Y.K., Fung, C.P., Lin, J.C., Chen, J.H., Chang, F.Y., Chen, T.L. and Siu, L.K. (2011) *Klebsiella pneumoniae* outer membrane porins OmpK35 and OmpK36 play roles in both antimicrobial resistance and virulence. Antimicrob Agents Chemother. 55, 1485-93.

Vagin, A. and Teplyakov, A. (1997) MOLREP: an automated program for molecular replacement. J. Appl. Cryst. 30, 1022-1025.

Van den Berg B, Black PN, Clemons WM Jr, Rapoport TM. (2004) Crystal structure of the long-chain fatty acid transporter FadL. Science 304, 1506–1509.

Van den Berg B., (2012) Structural Basis for Outer Membrane Sugar Uptake in Pseudomonads. J Biol Chem. 287, 41044-52.

Van Den Berg, B., P Bhamidimarri, S., Prajapati, J.D., Kleinekathoefer, U., Winterhalter, M. (2015) Outer Membrane Translocation of Bulky Small Molecules by Passive Diffusion Proc.Natl.Acad.Sci.USA 112, E2991.

Van Duyne, G.D., Standaert, R.F., Karplus, P.A., Schreiber, S.L. and Clardy, J. (1993) 'Atomic structures of the human immunophilin FKBP-12 complexes with FK506 and rapamycin', J Mol Biol, 229, 105-24.

Vandeputte-Rutten L., Kramer R.A., Kroon J., Dekker N., Egmond M.R., Gros P. (2001) Crystal structure of the outer membrane protease OmpT from *Escherichia coli* suggests a novel catalytic site. EMBO J. 20, 5033-9.

Vidal, S., Bredin, J., Pagès, J.M. and Barbe, J. (2005) Beta-lactam screening by specific residues of the OmpF eyelet. J Med Chem. 48, 1395–1400.

Vincze, T., Posfai, J. and Roberts, R.J. (2003) NEBcutter: A program to cleave DNA with restriction enzymes. Nucleic Acids Res. 31, 3688-91.

Viveiros, M., Dupont, M., Rodrigues, L., Couto, I., Davin-Regli, A., Martins, M., Pages, J.M. and Amaral, L. (2007) Antibiotic stress, genetic response and altered permeability of *E. coli.* PLoS ONE. 2, e365.

Vogt, J., Schulz, G.E. (1999) The structure of the outer membrane protein OmpX from *Escherichia coli* reveals possible mechanisms of virulence. Structure. 7(10):1301-9.

Wang, X. and Quinn, P.J. (2010) Lipopolysaccharide: Biosynthetic pathway and strucuture modification.

Wang, Y.F., Dutzler, R., Rizkallah, P.J., Rosenbusch, J.P., Schirmer, T. (1997) Channel specificity: structural basis for sugar discrimination and differential flux rates in maltoporin. J.Mol.Biol. 272: 56-63.

Webb, M. (1949) The Influence of Magnesium on Cell Division. J Gen Microbiol. 5, 480-4.

Weiss, M. S., Kreusch, A., Schiltz, E., Nestel, U., Welte, W., Weckesser, J. and Schulz., G.E. (1991) The structure of porin from *Rhodobacter capsulatus* at 1.8 Å resolution. FEBS Lett. 280, 379–382.

White, S.H. and Wimley, W.C. (1999) Membrane protein folding and stability: physical principles. Annu Rev Biophys Biomol Struct. 28, 319-65.

White, S.H., Ladokhin, A.S., Jayasinghe, S. and Hristova, K. (2001) How Membranes Shape Protein Structure. J Biol Chem. 276, 32395-8.

Wibbenmeyer, J.A., Provenzano, D., Landry, C.F., Klose, K.E. and Delcour, A.H. (2002) *Vibrio cholerae* OmpU and OmpT porins are differentially affected by bile. Infect Immun. 70, 121-6.

Wilkinson, S.G. (1996) Bacterial lipopolysaccharides- themes and variations. Prog. Lipid. Res. 35, 283-343.

Winn, M. D. et al. (2011) "Overview of the CCP4 suite and current developments". Acta. Cryst. D67, 235-242.

Winter, G. (2010) xia2: an expert system for macromolecular crystallography data reduction. J. Appl. Cryst. 43, 186-190.

Wu, M.C. and Health, E.C. (1973) Isolation and Characterization of Lipopolysaccharide Protein from *Escherichia coli*. Proc. Nat. Acad. Sci. USA, 70, pp. 2572-2576.

Yamaguchi, A., Nakashima, R. and Sakurai, K. (2015) Structural basis of RND-type multidrug exporters. Front Microbiol. 6, 327.

Yamashita, E., Zhalnina, M.V., Zakharov, S.D., Sharma, O., Cramer, W.A. (2008) Crystal structures of the OmpF porin: function in a colicin translocon. EMBO J. 27:2171-80.

Ye J1, van den Berg B. (2004) Crystal structure of the bacterial nucleoside transporter Tsx. EMBO J. 23, 3187-95.

Yoshimura, F. and Nikaido, H. (1985) Diffusion of beta-lactam antibiotics through the porin channels of *Escherichia coli* K-12. Antimicrob Agents Chemother. 27, 84–92.

Zahn, M., D'Agostino, T., Eren, E., Baslé, A., Ceccarelli, M. and Van den Berg, B. (2015) Small-Molecule Transport by CarO, an Abundant Eight-Stranded β-Barrel Outer Membrane Protein from *Acinetobacter baumannii*. J Mol Biol. 427, 2329-39.

Zeth, K., Diederichs, K., Welte, W. and Engelhardt, H. (2000) Crystal structure of Omp32, the anion-selective porin from *Comamonas acidovorans*, in complex with a periplasmic peptide at 2.1 A resolution. Structure. 8, 981-92.

Zgurskaya H.I., Krishnamoorthy G., Ntreh A. and Lu S. (2011) Mechanism and Function of the Outer Membrane Channel TolC in Multidrug Resistance and Physiology of Enterobacteria. Front Microbiol. 2, 189.

Zhang, Y., Jiang, X., Wang, Y., Li, G., Tian, Y., Liu, H., Ai, F., Ma, Y., Wang, B., Ruan, F. and Rajakumar, K. (2014) Contribution of β-lactamases and porin proteins OmpK35 and OmpK36 to carbapenem resistance in clinical isolates of KPC-2-producing *Klebsiella pneumoniae*. Antimicrob Agents Chemother.58, 1214-7.

Zheng, H., Cooper, D.R., Porebski, P.J., Shabalin, I.G., Handing, K.B., and Minor, W. (2017) CheckMyMetal: a macromolecular metal-binding validation tool. Acta crystallographica. Section D, Structural biology, 73, 223-233.

Ziegler, K., Benz, R. and Schulz, G.E. (2008) A putative alpha-helical porin from *Corynebacterium glutamicum*. J Mol Biol. 379, 482-91.

Ziervogel, B.K. and Roux, B. (2013) The binding of antibiotics in OmpF porin. Structure. 21, 76-87.